THE UNIVERSITY OF MICHIGAN SPACE SYSTEM DESIGN

GRYPHON

Air Launched Space Booster

NASA ★ USRA

ADVANCED SPACE SYSTEM DESIGN

The University of Michigan

Aerospace 483 Space System Design

PRESENTS

GRYPHON

Air Launched Space Booster

June, 1993

NASA/USRA

Table of Contents

Foreword

The project chosen for the winter semester Aero 483 class was the design of a next generation Air Launched Space Booster. Based on Orbital Sciences Corporation's Pegasus concept, the goal of Aero 483 was to design a 500,000 pound air launched space booster capable of delivering 17,000 pounds of payload to Low Earth Orbit and 8,000 pounds of payload to Geosynchronous Earth Orbit. The resulting launch vehicle was named the Gryphon. The class was led by Project Manager Brad King and Assistant Manager Mike Fisher. The class of forty senior aerospace engineering students was broken down into eight interdependent groups. Each group was assigned a subsystem or responsibility which then became their field of specialization.

Spacecraft Integration was responsible for ensuring compatibility between subsystems. This group kept up to date on subsystem redesigns and informed those parties affected by the changes, monitored the vehicle's overall weight and dimensions, and calculated the mass properties of the booster. This group also performed the cost/profitability analysis of the Gryphon and obtained cost data for competing launch systems.

The Mission Analysis Group was assigned the task of determining proper orbits, calculating the vehicle's flight trajectory for those orbits, and determining the aerodynamic characteristics of the vehicle.

The Propulsion Group chose the engines that were best suited to the mission. This group also set the staging configurations for those engines and designed the tanks and fuel feed system.

The commercial satellite market, dimensions and weights of typical satellites, and method of deploying satellites was determined by the Payloads Group. In addition, Payloads identified possible resupply packages for Space Station Freedom and identified those packages that were compatible with the Gryphon.

The guidance, navigation, and control subsystems were designed by the Mission Control Group. This group identified required tracking hardware, communications hardware, telemetry systems, and ground sites for the location of the Gryphon's mission control center.

The Structures group was responsible for ensuring the structural integrity of the vehicle. Their designs included the payload shroud, payload support structure, exterior hull, and engine support struts.

The Gryphon's power requirements were determined by the Power/Thermal/Attitude Control Group. This group then selected suitable batteries and other components to meet these requirements. The group also designed heat shielding and cooling systems to ensure subsystem performance. In addition to these responsibilities this group designed the attitude control methods and RCS components for the vehicle.

The Aircraft Integration Group was responsible for all aspects of the booster-aircraft connection. This included the design of the connection structure and the drop mechanism. This group also designed the vehicle assembly facility and identified possible ground bases for the plane.

Preface - **Class Organization Structure**

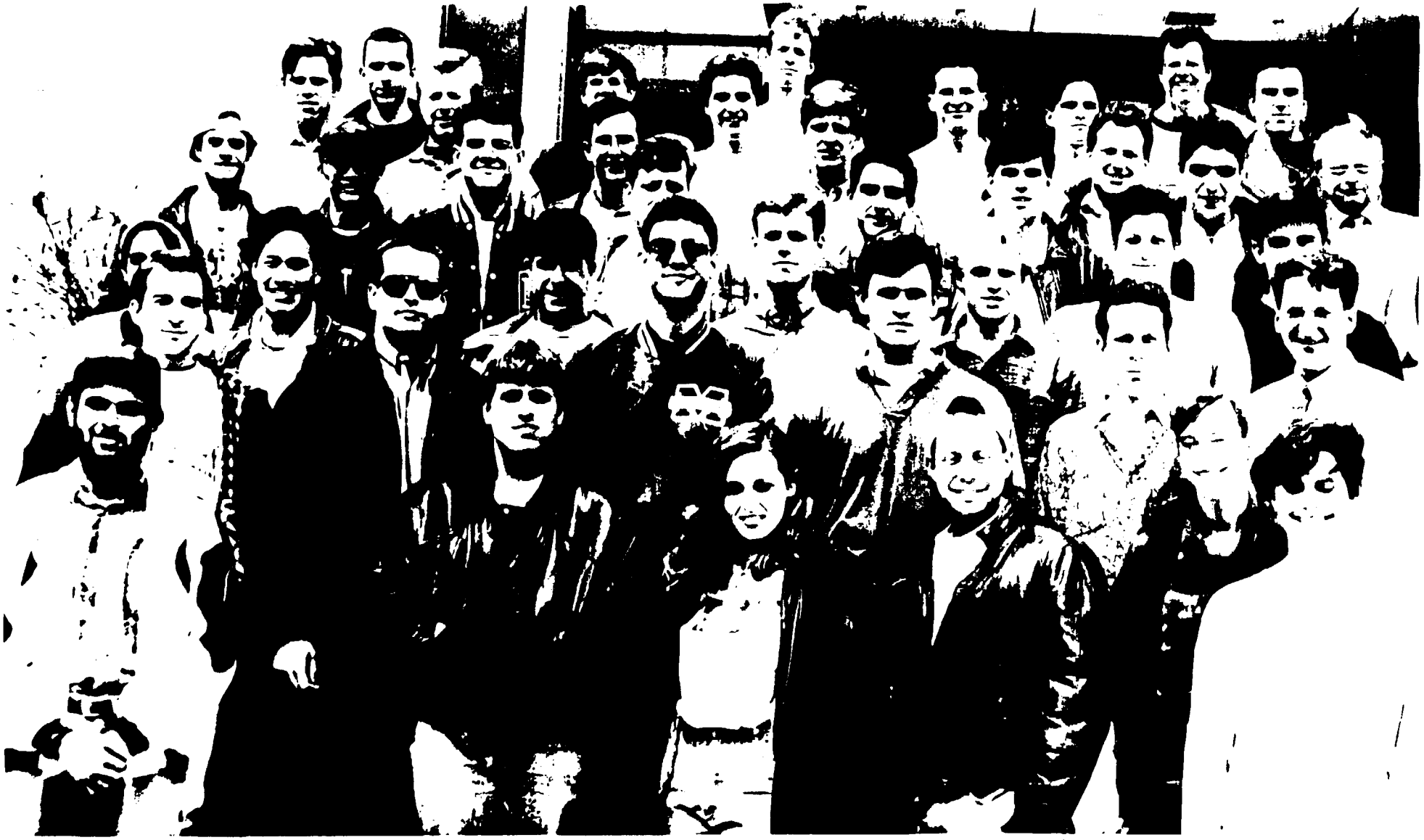

Back Row: Mike Fisher, Mike Hindley, Scott Mullinson, Brian Smith, Jon Albert, Alan Ristow, James Akers, Brad King

Fourth Row: Tom Godfroy, Kah-Wai Aw, Dave Cortright, James Dice, Dan Potter, Joe Ruddy, Adam Koziel, Ron Shimshock, Prof. Joe Eisley

Second Row: Chris Bernard, John Vandenberg, Scott Egbert, Phil Wojcik, Kevin Kilburn, Joe Regner

Fifth Row: Wolfgang Schubert, Vince Wiltse Adam Nagaj, Chris Vegter

Third Row: Romy Sharieff, Chris Yee, Tim Baffew Todd Mueller, Josh Baron, Chad Hoggard

First Row: Bilal Rathur, Rick Draper, Krista Campbell, Kevin Whalen, Elizabeth Hilbert, Karina Jacobson

The following lists each member's area of technical expertise within the University of Michigan's Aerospace Space System Design Project Gryphon.

Project Manager	
Brad King	Daily Agenda
Assistant Project Manager	
Mike Fisher	Administration
Spacecraft Integration	
Leader - Elizabeth Hilbert	Overall Configuration
Tim Ballew	Cost and Financing
David Cortright	Saftey
Todd Mueller	Cost and Financing
Dan Potter	Axis System
Mission Analysis	
Leader - Alan Ristow	Trajectory
Rick Draper	Mission Timeline
Sean Fifield	Orbits
Scott Mullison	Spin Rates
Vince Wiltse	Aerodynamics
Propulsion	
Leader - Krista Campbell	Solid Fuel Engines
Chad Hoggard	Cryogenic Fuels
Adam Nagaj	Tank/Staging Design
Bilal Rathur	LR91s/Storable Fuels
John Vandenberg	Stage Optimization
Payloads	
Leader - Kari Jacobson	Space Station Options
Chris Bernard	Weights and Sizing
James Dice	Market
Kevin Whalen	Payload Limitations
Craig Litherland	Structural Aspects
Mission Control	
Leader - Scott Egbert	GPS/Air Support
Kah-Wai Aw	On-board Computer
Brian Smith	Inertial Guidance
Chris Yee	Communications

Structures

Leader - Joe Ruddy	Shroud Design
Scott Huggins	Interstage Design
Wolfgang Schubert	Dynamic Analysis
Ron Shimshock	Fairing Analysis
Phil Wojcik	Payload Interface

Power/Thermal/Attitude

Leader - Joe Regner	Release Analysis
Josh Baron	Power Systems
Tom Godfroy	Venting System
Kevin Kilburn	Thermal Control
Romy Sharieff	Attitude Control

Aircraft Integration

Leader - Mike Hindley	Aircraft Interface
Jon Albert	Auxillary Connections
Adam Koziel	Attachment Design
Chris Vegter	Production Site

Wind Tunnel Model

Leader - Chad Hoggard	Flow Visualization
Tom Godfroy	Model Construction
Chris Yee	Technical Presentation
Mike Hindley	Data Recording

CAD

Leader - Mike Fisher	System Coordination
Kevin Whalen	Integration
Adam Koziel	Attachment Structure
Joe Ruddy	Shroud & Fairings
Adam Nagaj	Propulsion System

Display Model

Leader - Mike Fisher	Component Integration
Lee Ann Bird	Detailing
Elizabeth Hilbert	Technical Support

Final Report Publication

Leader - Mike Fisher	Editor in Chief
Krista Campbell	Technical Integration
Elizabeth Hilbert	Technical Editing
Scott Egbert	Processing Support
Vince Wiltse	Technical Editing

Symbol List

$	Dollar
A	Area
α	Angle of attack
a	Speed of sound
AC	Alternating Current
A_{cl}	Area of clean room
AKM	Apogee Kick Motor
A_l	Launch azimuth angle
ANC	Aft Nozzle Cover
a_s	Orbit semi-major axis
A_{sa}	Area of stage assembly room
A_{si}	Area of Stage Integration room
β	Yaw angle
BER	Bit Rate Error
c	Speed of light
CAD	Computer Aided Design
C_{cl}	Cost of clean room
C_D	Coefficient of drag
Cdo	Zero lift coefficient of drag
CG	Center of gravity
C_L	Coefficient of lift
CM	Center of Mass
Cm	Coefficient of pitching moment
Cn	Coefficient of yaw moment
CP	Center of pressure
Cp	Coefficient of sideforce
CPU	Central Processing Unit
Cr	Coefficient of rolling moment
C_s	Cost of stage room
D	Drag
d	Diameter
d_{arm}	Distance of lever arm
dB	Decible
DC	Direct Current
D_c	Drag at cruise launch
d_{com}	Distance of connectors on lever arm
DDAS	Digital Data Acquisition System
D_f	Diameter of Fireball
d_T	Fuel tank diameter
ΔV	Change in velocity
E	Modulus of elasticity
ε	Emissivity
e	Orbit eccentricity
ECEF	Earrth-centered, earth-fixed
E_s	Structural coefficient
°F	Degrees Fahrenheit
ϕ	Angle between body and inertial axis
f	Frequency of signal

FCC	Federal Communications Commision
FCS	Flight Control System
$F_{hydraulic}$	Hydraulic force
F_{pin}	Forces on a pin
f_s	Sample rate
F_T	Thrust
ft	Foot
FTS	Flight Termination System
F_x	Aerodynamic force on booster in horizontal direction
F_y	Aerodynamic force on booster in vertical direction
g	Acceleration due to gravity
γ	Flight path angle
GAB	Gryphon Assembly Building
GEO	Geosynchronous Earth Orbit
GNC	Guidance, Navigation, and Control
g_o	Acceleration due to gravity evaluated at sea level
GPS	Global Positioning System
GTO	Geostationary Transfer Orbit
GTT	Gryphon Transportaion Trailer
h	Altitude
Hz	Hertz
I	Current
i	Orbit inclination
I_{axx}	Area moment of inertia about roll axis
I_{ayy}	Area moment of inertial about pitch axis
I_{azz}	Area moment of inertia about yaw axis
ICS	Inertial Instrument Control and Sensing
IMU	Inertial Measurement Unit
I_{mxx}	Mass moment of inertia of booster about roll axis
I_{myy}	Mass moment of inertia of booster about pitch axis
I_{mzz}	Mass moment of inertia of booster about yaw axis
in	Inch
I_{sp}	Specific impulse
K	Thermal conductivity
k	Factor of safety
KIPS	Kilo Instruction Per Second
L	Lift force
λ	Wavelength of signal
LCD	Liquid Crystal Display
LEO	Low Earth Orbit
λ_l	Latitude
LPC	Launch Panel Console
LPO	Launch Panel Operator
M	Mach number
μ	Earth's gravitational constant
m	Mass
M_A	Moment applied by aeodynamic loads during freefall about pitch axis
M_c	Moment applied by control mechanisms during freefall about pitch axis
M_f	Static coefficient of friciton for steel on steel
MI	Moments of inertia
MIPS	Mega Instruction Per Second
mph	Miles per hour

μ_{st}	Friction coefficient of steel
MUX	Multiplexer
μ_v	Coefficient of Viscosity
MW	Mega Words
n	Number of samples
NPC	Navigation Processor Card
OMV	Orbital Maneuvering Vehicle
OSC	Orbital Sciences Corporation
P	Power
PAM	Payload Assist Module
$P_{hydraulic}$	Hydraulic Pressure
PKM	Perigee Kick Motor
PLM	Pressurized Logistics Module
p_T	Fuel tank pressure
θ	Angle between booster's axis and horizontal
q	Dynamic pressure
$\dot{\theta}$	Angular velocity of booster about pitch axis
$\ddot{\theta}$	Angular accel. of booster about pitch axis
θ_c	Coning angle
θ_g	Engine gimbal angle
q_h	Rate of heat transfer
°R	Degrees Rankine
R	Resistance
ρ	Density of air
r	Sampling rate
ρ_c	Density at cruise launch
RCS	Roll Control System
Rd	Data rate
R_e	Earth radius
Re	Reynold's number
RF	Radio frequency
R_{pin}	Pin Force
R_T	Radius of fuel tank
S	Surface area
σ	Stress
s	Yield stress in shear
SA	Selective Availability
s_b	Boltzman's constant
SNR	Signal-to-noise ratio
SPS	Standard Positioning Service
s_u	Ultimate stress
s_{yt}	Yield stress in tension
T_s	Sampling period
T	Temperature
t	Time after drop
T_b	Beam width
t_b	Burn time
τ_{max}	Shear
TTC	Tracking Telemetry and Command
t_w	Fuel tank wall thickness

ULC	Unpressurized Logistics Carrier
V	Voltage
V_c	Cruise velocity at launch
V_{oo}	Magnitude of booster velocity
V_w	Wind velocity
V_x	Booster's velocity in horizontal direction
V_y	Booster's velocity in vertical direction
W-h	Watt-hours
W-h/kg	Specific energy density
W_B	Weight of booster
W_f	Final gross weight
W_o	Initial gross weight
ω_z	Spin rate
W_{st}	Total stage weight
Ξ	Speed in x-inertial direction
x	Speed in x-body direction
X_B	Booster's horizontal position with respect to drop point
x_{cm}	Location of center of mass
x_{cp}	Location of center of pressure
Ψ	Speed in y-inertial direction
y	Speed in y-body direction
Y_B	Booster's vertical postition with respect to drop point

References

1. _____, Aerospace America, "A Letter from Orbital Science" Oct 1992
2. _____, Aviation & Space Technology, "Lockheed Renovates Clean Room for Work on Large Satellites", June 12, 1989
3. _____, Aviation Week and Space Technology, Aug 14, 1989
4. _____, Aviation Week and Space Technology, Aug 24, 1992
5. _____, Aviation Week and Space Technology, "Commercial Winged Booster to Launch Satellites from B-52", June 6,1988
6. _____, Aviation Week and Space Technology, Feb 11, 1991
7. _____, Aviation Week and Space Technology, June 27, 1988
8. _____, Aviation Week and Space Technology, Oct 28, 1991
9. _____, Aviation Week and Space Technology, "Orbital Sciences Charts Rapid Growth with Reduced Risk for Pegasus Investment", June 27,1988
10. _____, Aviation Week and Space Technology, "Relay Satellite, Gas Release Payload Scheduled for Pegasus Winged Booster" Jan 9, 1989
11. _____, Design of Liquid Propellant Rocket Engines, NASA SP-125
12. _____, Engineering Materials Handbook: Volume 1: Composites, ASM International, 1987
13. _____, Handbook of Pyrotechnics
14. _____, "Launch Vehicles-Specifications", Aviation Week and Space Technology, March 18, 1991, pg 131-132
15. _____, Liquid Propellant Rockets, Princeton University Press, 1960
16. _____, Machine Design, "Space launch vehicle gets jump start", March 22, 1990
17. _____, Metals Handbook, Tenth Ed., Volume 1: Properties Selection: Irons, Steels and High Performance Alloys, ASM International, 1990
18. _____, Metals Handbook, Tenth Ed., Volume 2: Properties Selection: Nonferrous Alloys and Pure Metals, ASM International, 1990
19. _____, Small-Satellite Technology and Applications
20. _____, Space, December 1992 - February 1993
21. 36th International SAMPE Symposium, "Design, Fabrication and Testing of the Pegasus Composite Payload Fairing", April 15-18, 1991

22. Aerojet Systems Company, Titan III Propulsion System, Propulsion Engineering Division, 1988

23. Aerospace 483 Aerospace System Design, Project APEX, University of Michigan, 1992

24. Aerospace 483 Aerospace System Design, Project Egress, University of Michigan, 1990

25. Aerospace 483 Aerospace System Design, Project UMHaul, University of Michigan, 1991

26. Anderson, J.D., Introduction to Flight, McGraw-Hill, New York, 1989

27. Argrawal, Brij N., Design of Geosynchronous Spacecraft

28. Atley, Gail M., Program Manager LN-81/LN-81, Litton Guidance and Control Systems

29. Barbour, Richard T., Pyrotechnics in Industry, McGraw-Hil Book Company, 1981

30. Barrere, M. et al., Rocket Propulsion, Elsevier Publishing Company, New York, 1960

31. Beer, Ferdinand P. and Johnston, E. Russel Jr., Mechanics of Materials, McGraw-Hill, 1981

32. Berlin, Peter, Cambridge Aerospace Series, The Geostationary Applications Satellite, Cambridge University Press, 1988

33. Brunschwayler, John, Orbital Sciences Corporation

34. Burton, R. G., Inertial Sensing, Ithaco Inc.

35. Chetty, Satellite Technology and it's Applications, 1988, Tab Books inc

36. Chobotov, Vladimir A., SpaceCraft Attitude Dynamics and Control, Krieger Co, Malabar, 1991

37. Colucci, Frank, "Taurus Technology", Space, Vol 6, Dec 92 - Jan 93

38. Crompton, T.R., Small Batteries, John Wiley & Sons, New York, 1982

39. Crotty, Mark, Tracking Engineer, Trimble

40. Curtis, Anthony, R., Space Almanac, 2nd ed., 1990

41. Department of Aerospace Engineeringand Engineering Mechanics, The University of Texas at Austin, Spacecraft Subsystems, January 1992

42. Director of Defense Research and Engineering, Handling and Storage of Liquid Propellants, U.S. Government Printing Office, Washington DC, 1963

43. Dunn, Barrie D., Mettallurgical Assesment of Spacecraft Parts and Materials, Wiley & Sons, 1989

44. Fries, Capt. Doug, Air Force Magazine, "The BUFF at War", June 1992, Vol 75, No. 6, pg 44-52

45. Galbano, Jean-Paul, Lithium Batteries, Academic Press, London, 1983

46. Gallimore, Prof., University of Michigan, Department of Aerospace Engineering

47. Gary, Vyhnalek, LPO Design Manager, Orbital Sciences Corporation

48. Gayle, J.B. and Bransford, Size and Duration of Fireballs From Propellant Explosions, NASA TM X-53314, Aug 4, 1965

49. Gayle, J.B., Investigation of S-IV All Systems Vehicle Explosions, NASA TM X-53039, NASA Marshall Space Flight Center, April 27, 1964

50. Gibson, Lorna J. and Ashby, Michael F., Cellular Solids Structures and Properties, Pergammon Press, New York, 1988

51. Gieck, Kurt and Gieck, Reiner, Engineering Formulas, 6th ed., McGraw-Hill, New York, 1989

52. Greenberg, Joel S. and Hertzfeild, Henry R., Space Economics, AIAA, Washington DC, 1992

53. Grey, Jerry, Aerospace Magazine, "Ups and Downs of New Space Launcer", June 1992, Vol 32, No. 6, pg 26-31

54. Griffin, M and French, J., Space Vehicle Design, AIAA Washington DC, 1991

55. Griffin, Michael D and French, James R., Space Vehicle Design

56. Henry F. Lemieux, Marketing Manager, Orbital Sciences Corporatio

57. Henry, Lt. Gen Richard C., "Launches into Low-Earth Orbit Should be Economical, Routine," Aviation Week and Space Technology, Nove 1989, pg 93-96

58. Hill, Phillip G. and Peterson, Carl R., Mechanics and Thermodynamics of Propulsion, 2nd ed., Addison-Wesley Publication Company Inc., 1992

59. Hoskins, W. Andrew, Rocket Research Company

60. Hughes Aircraft Company, Hughes Aircraft Company Geosynchronous Spacecraft Case Histories, vol I-III', Jan. 1981

61. Huzel and Huang, Design of Liquid Propellant Rocket Engines, NASA SP-125, National Aeronautics and Space Administration, Washington DC, 1971

62. Jerrel, Dan, University of Michigan Solid State Electronics Laboratory

63. John R. Brunschwyler, Pegasus Mission Manager, Orbital Sciences Corporation

64. Kauffman, Prof., University of Michigan, Department of Aerospace Engineering

65. Kendal, Brian, Manual of Avionics, Granada Publishing Limited 1979

66. Kyle Chanet, Co-Op Student, Orbital Sciences Corporation

67. Laporte-Weywada, H. and Rallion, E., "Ariane 5 - A New Launcher For Europe", Advances in the Aeronautical Sciences, American Astronautical Society, Vol 61, 1984, pg 389-404

68. Lawrence J. Mauch, Flight Assur. Manager, Orbital Sciences Corporation

69. Leith, Kevin, Orbital Sciences Corporation

70. Long, Mark, World Satellite Almanac, 2nd. ed., Howard W. Sams & Company, 1987, Indianapolis

71. Lubin, George (ed), Handbook of Composites, Van Nostrand Reinhold, New York, 1982

72. Martin, Donald H., "Communications Satellites" 1958-72

73. Mihara, S.K., "Delta II Launch Service and Flight Results", Advances in the Aeronautical Sciences, American Astronautical Society, Vol 73, 1984, pg 645-656

74. Morrison, R., Design Data for Aeronautics and Astronautics: A Compilation of Existing Data, John Wiley & Sons, New York, 1962

75. NASA Conference Publication 3112, vol. 2, Space Transportation Propulsion Technology Symposium, Volume 2-Symposium Proceedings, June 25-29, 1989

76. NASA Johnson Space Center, "Shuttle Vehicle Mold Lines and Protuberances, ICD-2-00001"

77. Neighbors, Joyce and Ryan, Robert S., Aerospace America, "Structural Dynamics for New Launch Vehicles", Sept 1992, Vol 30, No. 9, pg 26-32

78. Neil E. Holben, L-1011 Project Manager, Orbital Sciences Corporation

79. Office of Directorate of Defense Research and Engineering, The Handling and Storage of Liquid Propellants, U.S. Government Printing Office, Washington DC, 1963

80. Orbital Sciences Corporation, Pegasus Payload User's Guide

81. Orbital Sciences Corporation, Pegasus User's Manual

82. Osgood, Charles, Spacecraft Structures, Prentice Hall, New York, 1986

83. Otto, Al, Rockwell International

84. Parks, Howard, Engineer, Motorola

85. Peery, D.J. and Azar, J.J., Aircraft Structures, McGraw-Hill, New York, 1982

86. Pitts, Andrew W., Aviation Ordinanceman, 1990 Edition prepared by AOCS

87. Portney, Joel, Manager, Advanced Programs, Litton Guidance and Control Systems

88. Ring, Elliot, Rocket Propellant and Pressurization Systems, Prentice Hall, Englewood Cliffs, NJ, 1964

89. Roark, Raymond J. and Young, Warren C., Roark's Formulas for Stress and Strain, 6th ed., McGraw-Hill, New York, 1989

90. Romere, Paul, NASA Engineer, Johnson Space Center

91. Roskham, Jan, Airplane Design, Vol . 6

92. Schade, C., Pegasus, Taurus, and Glimpses of the Future, AIAA 90-3573

93. Shen, Frank and Pope, Dennis, "Design & Development of Composite Fairing Structures for Space Launcd Vehicles", SAE Technical Paper 901836

94. Sheppardson, Ken, Lecture: "Space Station Freedom Post PMC Logistic Requirements", February 1, 1993

95. Smith, Bruce A., "Pegasus Air Launched Test Vehicle is Rolled Out", Aviation Week & Space Technology, Aug 14, 1989, McGraw-Hill, pg 36-41

96. Sonntag and Van Wylen, Introduction to Thermodynamics: Classical and Statistical, 2nd ed., John Wiley & Sons, New York, 1989

97. Steven L. Olsen, Sr. Mechanical Engineer, Orbital Sciences Corporation

98. Stowers, James E., Sr. Systems Engineer, Orbital Sciences Corporation

99. Sutton G., Rocket Propulsion Elements: An Introduction to the Engineering of Rockets, John Wiley & Sons, New York, 1976

100. The Boeing Company, received from NASAJohnson Space Center, "Structure Analysis", Document # D180-18404-1, Controlled By 747 CAM Structures Staff Group

101. Tuck, Clive D.S., Modern Battery Technology, Ellis Horwood, New York, 1991

102. Vegter, Albert J., Daniels & Zermack Assoc., Architect

103. Venkatasetty, H.V., Lithium Battery Technology, John Wiley & Sons, New York, 1984

104. Vinson, J.R. and Sierakowski, The Behavior of Structures Composed of Composite Materials, Martinus Nijhoff Publishers, Dordrecht

105. Wafer, Phillip R., "Means Building Construction Cost Data", R.S. Means Co., Kingston MA

106. Wafer, Phillip R., "Means Square Foot Costs", R.S. Means Co., Kingston MA

107. Warren E. Frick, Pegasus Project Manager, Orbital Sciences Corporation

108. Wertz, J and Larson, Space Mission Analysis and Design, John Wiley & Sons, Boston, 1991

109. White, J. Frederick, Flight Performance Handbook for Powered Flight Operations, John Wiley & Sons, New York, 1963

110. Whitney, James, Structural Analysis of Laminated Anisotropic Plates, Technomic Publishing Company, Lancater, 1987

111. Wood, K., Aerospace Vehicle Design, Johnson Publishing Co, Boulder, 1963

112. Wurtz, James R. and Larson, Wiley J., Space Mission Analysis and Design

113. Zappe, R.W., Valve Selection Handbook, 3rd ed., Gulf Publishing Company, Houston, 1992

114. RL10 Liquid Rocket Engine Service Manual, United Technologies, Pratt and Whitney, March 30, 1991

115 Comiez, John M.

INTRODUCTION

Chapter One

1.1 HISTORY OF SATELLITE LAUNCH VEHICLES

Man's quest for total access to the universe will one day be realized. Although the distances to cover are vast, they have been greatly reduced since the beginning of the space race on October 4, 1957 with the launch of Sputnik 1.

Manned space missions attract more interest and appeal than their unmanned counterparts. However, automatic probes have contributed immeasurably in the areas of communications, planet exploration, and scientific research. Without the proliferation of satellites orbiting the Earth, life would be drastically different.

1.1.1 The Evolution of Launch Vehicles

The Gryphon Project is a study in the advancement of current space booster technology. This booster is a deviation from conventional booster design; it is a combination of a standard vertical rocket design and a laterally, air launched missile design. Its objective is to minimize the effects of gravity and the lower atmosphere to allow larger payloads to be injected into orbit. The following paragraphs describe the evolution of launch vehicles and how the air launched boosters have capitalized on the evolving technology.

On January 31, 1958 the United States Army Ballistic Missile Agency launched the Explorer 1 satellite aboard a Jupiter C launch vehicle. The Jupiter C was a 4 stage vehicle with 3 solid-fuel stages. Its 69,997 lb of thrust was capable of placing its 30.7 lb satellite into an orbit of 224 nautical miles. Unfortunately, the Jupiter C was not reliable, with two of its five launches resulting in failure.

After the United States entered the satellite business with the Jupiter C, many technological improvements and discoveries were made which enabled enormous and rapid improvement in the ensuing launch vehicles. In 1966, the first operational meteorological satellite for environmental studies was deployed by a Thor-Delta E. It had the capacity to launch 450 lb into a transfer orbit and 1,206 lb into a 230 nautical mile orbit. This 3 stage booster used Castor 1S's in its six year and 26 mission history.

Throughout the 1960's and 70's, launch vehicles became much larger, with an ever increasing payload capacity. The basic configuration of a long, cylindrical vehicle, launched vertically from the ground was the rule for civilian satellite boosters. In 1990, the Orbital Sciences Corporation (OSC) changed that rule.

1.1.2 Pegasus

The Pegasus project was started in 1988. The goal was to develop an air launched orbital transportation system capable of deploying small satellites. The first launch took place on April 16, 1990, and was carried underneath the wing of a B-52. An updated version was dropped by a L1011 in March 1993.

The hypothesis stated that by dropping the Pegasus in the upper atmosphere, the total cost could be dramatically reduced. However, the original versions of the Pegasus are around 40,000 lb and have only been able to carry payloads of approximately 900 lb, making the feasibility of the project questionable. When all of the research and development costs are considered, profitability becomes difficult especially since one cannot charge a large price for small satellites.

1.2 DESIGN OF THE GRYPHON

The goal of the Gyphon Design Team was to develop a 500,000 lb air launched space booster with the capability of delivering 7,900 to Geosynchronous Earth Orbit (GEO) and 17,000 lb to Low Earth Orbit (LEO). These payload goals were determined in order to beat the competition's cost by 50% to insure investor's of a 15% return. The task of designing the Gryphon was daunting. No project of its size and nature had been undertaken. OSC has begun an initial study of a similar sized Pegasus III version, but they have yet to decide whether they will continue. An additional challenge stemmed from the 'real world' application of the Gryphon. Unlike many design projects, there is current commercial interest. This restriction has not allowed for design of components and systems to be developed in the 'future', or no cost restraint. With the added dimension of time limitations, the Gryphon has been designed as efficiently as possible, above and beyond all of the limitations imposed.

1.2.1 Reason for the Configuration

Robert Lovell of OSC presented the idea of a large air launched space booster based on his department's belief in a market opportunity between the Space Station Freedom resupply needs and the commercial communications industry. The 500,000 lb weight suggestion was based on his intuitive knowledge of available engines and their capabilities. Other than his initial weight recommendation and stipulation of a 15% return, the entire project's development was left to the design team.

Unlike the Pegasus, which is carried underneath a L1011, the Gryphon's weight caused an entirely new aircraft to be developed in order to carry it into the upper atmosphere. The Eclipse Design Team, which designed the carrier airplane, specified a drop at approximately 40,000 ft at a speed of 500 mph. With this knowledge, the technical groups proceeded in their research and design. At the start, the Pegasus was used as a baseline and many aspects were designed as larger upgraded versions of those found on the Pegasus. However, it was quickly realized that extrapolating components from a 40,000 lb vehicle to a 500,000 lb vehicle was not always possible. Even though many aspects from the Pegasus could not be used, the Gryphon still resembles current launch vehicles. All the systems and components are currently available. Its final configuration results from a combination of cost, simplicity, and available technology.

1.2.2 Design Considerations

The design process was a Phase I analysis which combined the efforts of the following technical groups:

- Spacecraft Integration
- Mission Analysis
- Propulsion
- Payloads
- Mission Control
- Structures
- Power/Thermal/Attitude Control
- Aircraft Integration

Each of these groups were responsible for individual aspects of the Gryphon. However, many aspects were developed through inter-group cooperation. All of the groups did share a common aspect: keeping costs down. In order to have a successful project, all groups had to adhere to a strict budget. Even though the groups complied with this requirement, some areas did adversely affect the overall cost. These include:

- Eclipse research, development, testing, and operations cost
- Cryogenic fuels and accompanying systems
- Assembly building
- Rocket engines
- Honeycomb aluminum structural shell

Outside of cost considerations, safety precautions were very carefully investigated. Since the Gryphon is carried underneath the Eclipse, which holds four personnel, extra care is necessary. The use of cryogenic and liquid fuels only added to this concern. These fuels also caused increased attention to the fueling and handling of the attachment procedure. Although it would be preferable to use an entirely solid rocket vehicle for additional safety, the design process dictated the use of alternate fuels (See Chapter 4).

Another aspect which arose was the difficulty in controlling the Gryphon after release from the Eclipse. Many different combinations of a Delta wing, canards, and winglets were considered (See Chapter 3). However, the additional weights from these components were too significant. Instead, a vertical tail was used for yaw control. Over the course of the design, it was found that the Gryphon's geometry would orient it in the proper angle for ignition.; therefore, the problem of control was primarily worked out by further investigation, rather than using unnecessary systems.

Finally, the Gryphon must compete with traditional style launch vehicles which are currently on the market. The primary competition is Ariane 44l, Titan 3, and Atlas Centaur. These vehicles have similar capabilities as the Gryphon (See Chapter 2, Table 2.1). Consequently, focus was placed on beating the competition by 50% to insure the 15% return on investment.

The design process included many factors, some of which have been detailed here. For a much more detailed explanation of the technical groups, please consult the specific chapters.

1.3 OVERVIEW OF THE GRYPHON

The final Phase 1 design of the Gryphon points to success. It has a cost per pound of approximately $6200, which beats the competition by the required 50% (See Chapter 2). The major components can be seen in Table 1.1, and general information from all aspects of the Gryphon is in Tables 1.2 - 1.24. The next pages show a solid model transparent view of the major components and a view of the Gryphon and Eclipse while attached.

Table 1.1 Major Components

Stage 1
2 Castor Solid Rocket Motors
LR91-AJ-11 Storable Liquid Rocket Motor
Gryphon-Eclipse Rings 1 & 2
Engine Mount
Plane Attach Ring 1
Interstage Ring
Aft Nozzle Cover
Fairing Attach Rings
Stage 2
2 LR91-AJ-11 Storable Liquid Rocket Motor
Gryphon-Eclipse Rings 3 - 8
Plane Attach Rings 2 & 3
External Skin
Strut Support Ring
Engine Mount
Interstage Ring
Stage 3
1 RL10A-4 Cryogenic Liquid Fuel Rocket Motor
Payload Interface
External Skin
Engine Attach
Power/Avionics Ring
Cabling
Hydrazine/Oxidizer & Tanks
Control Thrusters
Venting System
Thermal Control
Batteries
CPU
Radar Transponder
Telemetry Transmitters
GPS
Inertial Guidance (IMU)

General

Table 1.2 Overall Data

Airplane Cost	$1 billion
Project Costs	$1.062 billion
Vehicle Cost	$27.94 million
Airplane Operations Cost	$2 million
Total Mission Cost	$48.3 million
Total Length w/ ANC (GTO)	124 ft - 3 in
Total Length w/ ANC (LEO)	104 ft - 5 in
Total Length (GTO)	106 ft - 3 in
Total Length (LEO)	86 ft - 5 in
Total Height	30 ft
Total Weight (GTO)	479,056 lb
Total Weight (LEO)	476,368 lb
Center of Mass (GTO)	27.0 ft
Center of Mass (LEO)	26.2 ft

Propulsion

Table 1.3 Individual Engine Data as Configured for the Gryphon

Engine	Stage	ISP	Burn Time (s)	Total Weight (lb)	Propellant Weight (lb)	Length (ft)	Width (ft)	Thrust (lb)
Castor 120	1	292	78	117,687	108,159	30	7.5	403,759
LR91	1	316	78	1,298	8,365	9.2	5.3	105,000
LR91	2	316	239	2,596	29389	9.2	5.3	210,000
RL10	3	449	181	370	9,057	8	4	20,800

Table 1.4 Gross Weights

Stage	Weight (lb)
1	2673,501
2	173,235
3	12,748

Table 1.5 Break Down of Gross Weights by Stage

Stage	Dry Weight (lb)	Propellant (lb)	Total (lb)
1	30,824	242,877	273,501
2	9,235	164,000	173,235
3	4,502	8,246	12,748

Table 1.6 Oxidizer and Fuel Weights

Stage	Oxidizer (lb)	Fuel (lb)
1	15,948	8,574
2	112,057	60,246
3	7,547	1,510

Table 1.7 Volume of Propellant Tanks

Stage	Oxidizer (ft3)	Fuel (ft3)
1	188	161
2	1318	1130
3	110	357

Table 1.8 Thickness and Weight of Propellant Tanks

Stage	Thickness (in)	Weight (lb)
1	0.0486	395
2	0.0486	2,500
3 - Fuel	0.022	350
3 - Oxidixer	0.02	260

Payload

Table 1.9 Payload Weight for Differnt Orbits

Orbit	Weight (lb)
LEO	17,000
GTO	7,900

Table 1.10 Payload Dimensions

Dimension	Length (ft)
Total Height	35
Height at top of Rectangular Area	25
Width at Bottom of Rectangular Area	15.5
Width at Top	3.95

Mission Control

Table 1.11 Major Components Characteristics

Component	Version	Cost ($)	Size (in)	Weight (lb)
IMU	Littion - 81	100,000	6.3 x 2.5 x 3.0	12.8
GPS Receiver	Trimble Quadrex	14,000	7 x 7 x 7	3
On-Board Computer	32 Bit 6800 Motorolla Versa Module Europ Bus	2,000,000	4 x 8 x 8	10

Structures

Table 1.12 Cross Sectional Areas and Weights

Component	Area (in2)	Weight (lb)
Stage 1	36.8	550
Interstage	57.8	485
Stage 2	57.8	1630
Stage 3	36.8	865

Table 1.13 Payload Shroud Characteristics

Thickness	0.948 in
Material	5056 Aluminum Honeycomb
Composition	18 Piles of IM7-8551-7 Carbon Epoxy

Table 1.14 Payload Interface Characteristics

Height	16 ft
Diameter	10 - 14 ft
Total Support Weight	10,000 lb
Material	1/64 in Aluminum Skin
Weight	636 lb

Table 1.15 Engine Mounts Weight and Material

Stage	Weight (lb)	Material
1	349	A333 Steel
2	646	A333 Steel
3	234	Tubular Aluminum

Table 1.16 Interstage Ring Characteristics

Outer Diameter	15.5 ft
Inner Diameter	15.44 ft
Height	0.25 ft
Thickness	3/8 in
Weight	80 lb

Power

Table 1.17 Power Requirements of the On-Board Systems

Component	Power (W)
Flight Computer	250
GPS	305
2 Telemetry Transmitters	98
Radar Transponder	31
Communications	323
Thrusters	200
Inertial Receiver	250
Miscellaneous	250
Total	1356

Table 1.18 Principal Power Sub-System Characteristics

Main Component	4 Li/$SOCl_2$ 8 Cell Modules
Length	21.5 in
Width	11.8 in
Height	9.8 in
Cost	$3000
Weight	250 lb
Power	28 V

Table 1.19 Venting System Characteristics

Number of Units	8
Size	1.33 ft^3
Weight	12 lb
Cost	$800

Table 1.20 Gryphon Assembly Timeline

Step	Time (weeks)
Stage Build Up & Pre-Integration Testing	4
Stage Integration & Vehicle Testing	4
Payload Integration	2
Final Systems Tests	2
Total	12

Table 1.21 Gryphon Assembly Building (GAB) Characteristics

Length	400 ft
Width	160 ft
Height	50 ft
Perimeter Length	1120 ft
Area	64,000 ft2
Total Cost	$3,420,000

Table 1.22 GAB Class 10,000 Clean Room Characteristics

Length	125 ft
Width	160 ft
Height	50 ft
Area	20,000 ft2
Cost	$10,000,000

Table 1.23 Crane Requirements

Size	Cost ($)
2 80 Ton 80 ft Span Overhead	360,000
2 20 Ton 80 ft Span Overhead	120,000

Table 1.24 Aircraft Interface Mechanism Characteristics

Number of Pins	8
Area of each Pin	10.54 in^2
Material	ASTM-A242 Steel Alloy
Hook Area	16 in^2
Max Pin Length	27 in
Total System Weight	1328 lb
Total Cost	$472,163

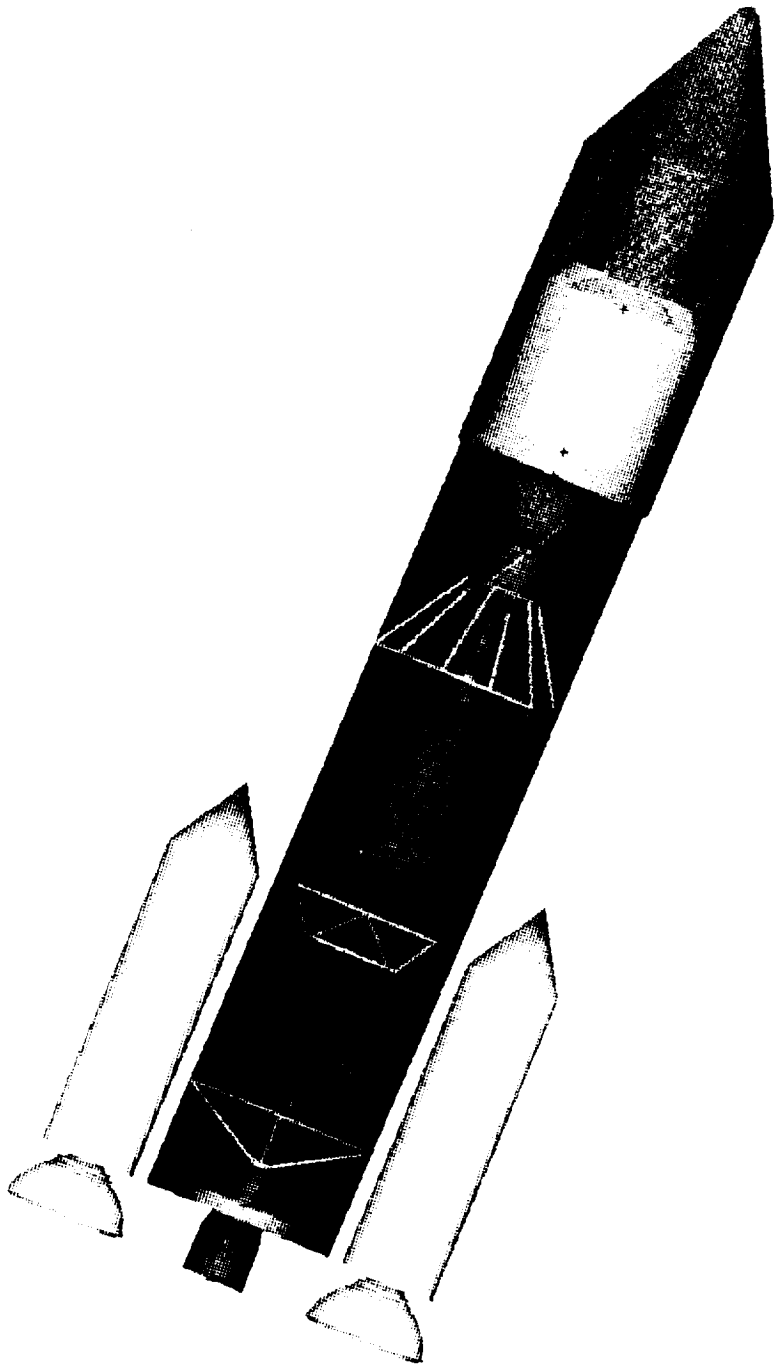

Figure 1.1 Transparent View of the Gryphon

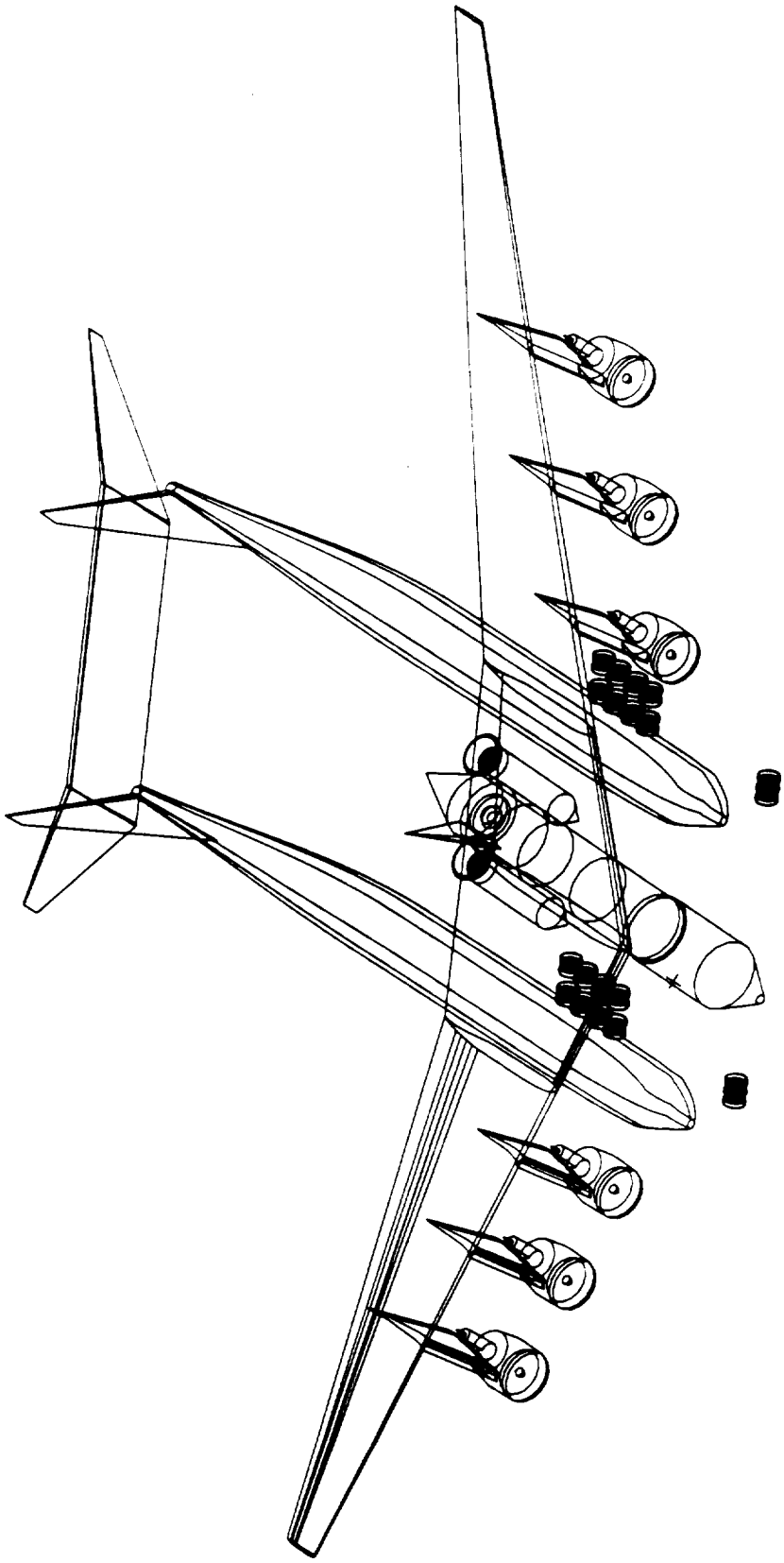

Figure 1.2 Gryphon and Eclipse while attached

SPACECRAFT INTEGRATION

Chapter Two

2.1 INTRODUCTION

The Spacecraft Integration Goup had three major tasks during the design process. These were:

- to complete a budget for the Gryphon and determine the feasibility of this project through cost analysis
- to design the overall layout of the Gryphon and determine the mass, dimensions, moments of inertia, and centers of mass for the Gryphon during all stages of flight
- to determine the air-safety precautions

This group was primarily responsible for compiling the data from the other groups into the final design specifications presented here. The group ensured that all information was kept consistent throughout the project's development. All of the information presented here is in its most general form. Please refer to the other chapters for a more detailed description.

2.2 THE BOTTOM LINE: COST

The most important aspect of this project is to give investors a fifteen percent return on their investments. To achieve this, the cost (per pound of payload) of the Gryphon was determined in order to beat the launch prices (also per pound of payload) of chief competitors by at least fifty percent. This leaves the other fifty percent for financing, insurance, and profits while still having a competitive price.

Gryphon's main competitors in the satellite launch market are the Ariane 4, Atlas Centaur, and Titan 3. The Chinese Long March and the Russian Proton were not considered fair competition because their prices do not reflect real costs. The price data for these and other launchers are listed below in Table 2.1. Note that Ariane prices are in 1990 dollars, Atlas and Titan prices are in 1991 dollars, and numeric figures are averages.

Table 2.1 Launch Prices of the Competition

Launch Vehicle	Payload Size (lb)	Launch Price	Price per Pound
Ariane 40	4,190	$ 65 million	$ 15,513
Ariane 42P	5,730	$ 67 million	$ 11,692
Ariane 44P	6,610	$ 70 million	$ 10,590
Ariane 42L	7,050	$ 90 million	$ 12,766
Ariane 44LP	8,160	$ 95 million	$ 11,642
Ariane 44L	9,260	$ 115 million	$ 12,419
Atlas Centaur	5,148	$ 60 million	$ 11,655
Titan 3	10,978	$ 110 million	$ 10,020

Using the market average price per pound of the competition derived from Table 2.1 and an inflation factor of 4.5% per year, a project goal cost per pound of $ 6,200 was determined. This cost per pound translates into a payload of 7,900 lbs to Geosynchronous Transfer Orbit (GTO) and a per mission cost of $49 million.

2.2.1 Cost Analysis

The cost analysis was a combination of research, teamwork, and to a large extent educated guesswork. Cost data in the launch vehicle business is extremely difficult to obtain. Nevertheless, a detailed expense report has been assembled and all cost goals have been met.

The final cost analysis is given below on Table 2.2. The costs given are high estimates and include a fifty million dollar development cost (which is what OSC used for their Pegasus program).

Table 2.2 Cost Analysis

Airplane Cost	$ 1,000 million
Project Costs	$ 106 million
Vehicle Cost	$ 28 million
Airplane Operating Costs	$ 2 million

The total mission cost was calculated by dividing the one-time costs (the airplane and project costs) by sixty launches and adding the per launch costs for the vehicle and plane operation. Sixty launches was chosen as a realistic estimate for the number of launches that would be performed over ten years. This estimate is based on the recent satellite market. Table 2.3 shows the final mission cost of the Gryphon. It should be noted that this cost estimate meets the project goal of $49 million per launch.

Table 2.3 Cost of Gryphon

Total Mission Cost (60 launches)	$ 48.3 million

Insurance and financing are not included in the above result.

2.2.2 Financial Analysis

The financial analysis of the Gryphon Project includes the determination of the profit margin per launch and a financial loan schedule. The data used for this is the high estimates to provide a conservative evaluation of the project performance.

Eclipse

The Eclipse is the airplane that carries the Gryphon during each launch. Its financing is presented separately by the Eclipse design team. The cost of the airplane does affect the profit margin of the Gryphon. The fixed cost of the Eclipse including financing costs is $1 billion. The fixed cost remains the same regardless of the number of launches over the duration of the project. The per launch cost of the Eclipse is $2 million which occurs with each launch only.

Insurance

In addition, payload launch insurance must be taken into account. Premium rates are currently 16-18% for communication satellite launches to GEO A figure of 18% is used for the Gryphon's analysis.

Per Launch Cost

The per launch cost of the Gryphon is $27.9 million, while the per launch cost of the Eclipse is $2 million. Also the $1 billion fixed cost of the Eclipse must be evenly spread over each launch. For a projected duration of 60 launches, this calculates to a total average cost per launch of $46.6 million. The minimum price that can be charged per launch and still turn a profit in the last year is $65.2 million. This includes the additional 18% for insurance. Disregarding the amount per launch towards insurance premiums, the Gryphon grosses $55.2 million per launch. The net profit is the amount grossed per launch minus the total expenses per launch resulting in a net profit margin of $8.6 million per launch.

Over a projected lifetime of ten years, the conservative estimate of the total number of launches is 60. To allow for complications in the first two years, the assumption was made that only 2 launches occur in the first year of operation, 4 launches in the second, 6 launches in the third and fourth, and an average of 7 launches per year for the remainder of the project.

Facilities and Certification

Two years are initially allowed for facility construction and another one year for space certification prior to the first years of operation. With regard to budget scheduling, the first and second years are assumed to deal with facility construction with the expenses evenly split while the third year consists of obtaining space certification. The industry standard is to allow for two complete launches to obtain space certification. Considering the highly experimental nature of this project, it is assumed that three launches are needed in order to become space certified.

Since Orbital Sciences Corporation (OSC) has specified that its investors want a 15% rate of return on their investment, this is the interest rate that is used in the financial schedule. In addition the standard business venture tax rate is 36% which is what this analysis uses.

Conclusion

Figure 2.4 depicts the projected financial figures for the Gryphon. It assumes a three year start-up period, a ten year operational lifetime, and a total of 60 launches over the ten year period. It accounts for insurance premiums, a 36% tax rate, and a 15% rate of return compounded continually for the investors. The minimum customer price relates to $8,250 per pound. This beats the average competitor's price by 33.5%. The data used in Figure 2.4 is provided in Appendix A.3.

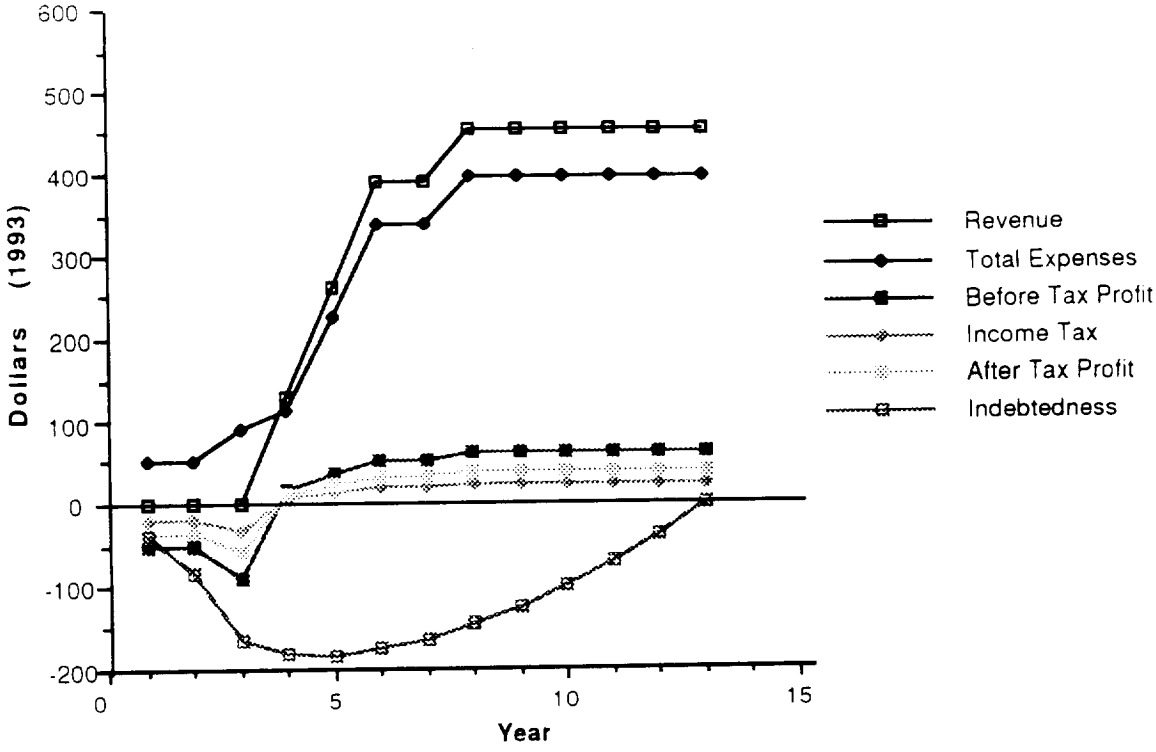

Figure 2.1 Financial Projections

2.2.3 Cost and Financial Conclusion

All of the financial goals set at the beginning of the project were met or even exceeded. The total cost per launch including the fixed costs and per launch costs of the Gryphon and the Eclipse is estimated at $48.3 million. The maximum limit goal set at $6,200 per pound translates to $49.0 million per launch with a 7,900 pound payload. Even after accounting for insurance premiums, government taxes, and a 15% investors rate of return, the Gryphon is still capable of beating the competition by over 33%. In addition, this entire financial analysis is based on a "worst case scenario" using only the most conservative estimates.

Due to the possible financial advantages, this business venture appears to be a worthwhile investment.

2.3 VEHICLE CONFIGURATION

The design project was initiated by determining the major goals of the Gryphon. Of these goals, those applicable to the vehicle configuration are:

- A maximum booster weight of 500,000 lb
- Approximately 8,000 lb of payload to GTO
- Approximately 17,000 lb of payload to Low Earth Orbit (LEO)
- Two independent payloads during one launch to GTO
- A payload envelope diameter of at least 15 ft to accommodate Space Station Freedom modules

Using this as a starting point, each group proceeded to research their designated area. The information that they obtained was then submitted to Spacecraft Integration in order to compile it into the final design. This section highlights the prominent features of the design and layout of the Gryphon. The final vehicle configuration can be seen in Figures 2.2 and 2.3.

2.3.1 Propulsion

The Gryphon consists of three stages for the GTO configuration. For the LEO configuration, the third stage engine and propellant tanks are removed and replaced with pure payload.

The first stage engines include a LR91-AJ-11 mounted in the middle of the main body and two Castor 120 solid rocket boosters attached symmetrically to the sides. The elliptical propellant tanks, containing nitrogen tetroxide for oxidizer and Aerozine-50 for fuel, are mounted just ahead of the LR91. Control of the booster is provided by a vertical tail and gimbaled nozzles on all three engines.

After the Stage One engines and structure have jettisoned and a coast phase is completed, two LR91-AJ-11's ignite for the second stage. The propellants are the same for the first stage LR91 but are contained in two large, nearly cylindrical tanks. Gimbaled nozzles again provide stability.

For a GTO mission, these engines are released and after another coast phase, a RL10A-4 engine ignites and burns cryogenic propellant. Liquid oxygen is supplied from a nearly cylindrical tank just ahead of the engine and liquid hydrogen is supplied from a spherical tank attached in front of the oxidizer tank. The RL10's vectorable nozzle provides control along with RCS thrusters. For a LEO configuration, this stage is not needed and orbit can be established after the second stage. Refer to Figure 2.2 to see the overall configuration.

Figure 2.2 Overall Configuration

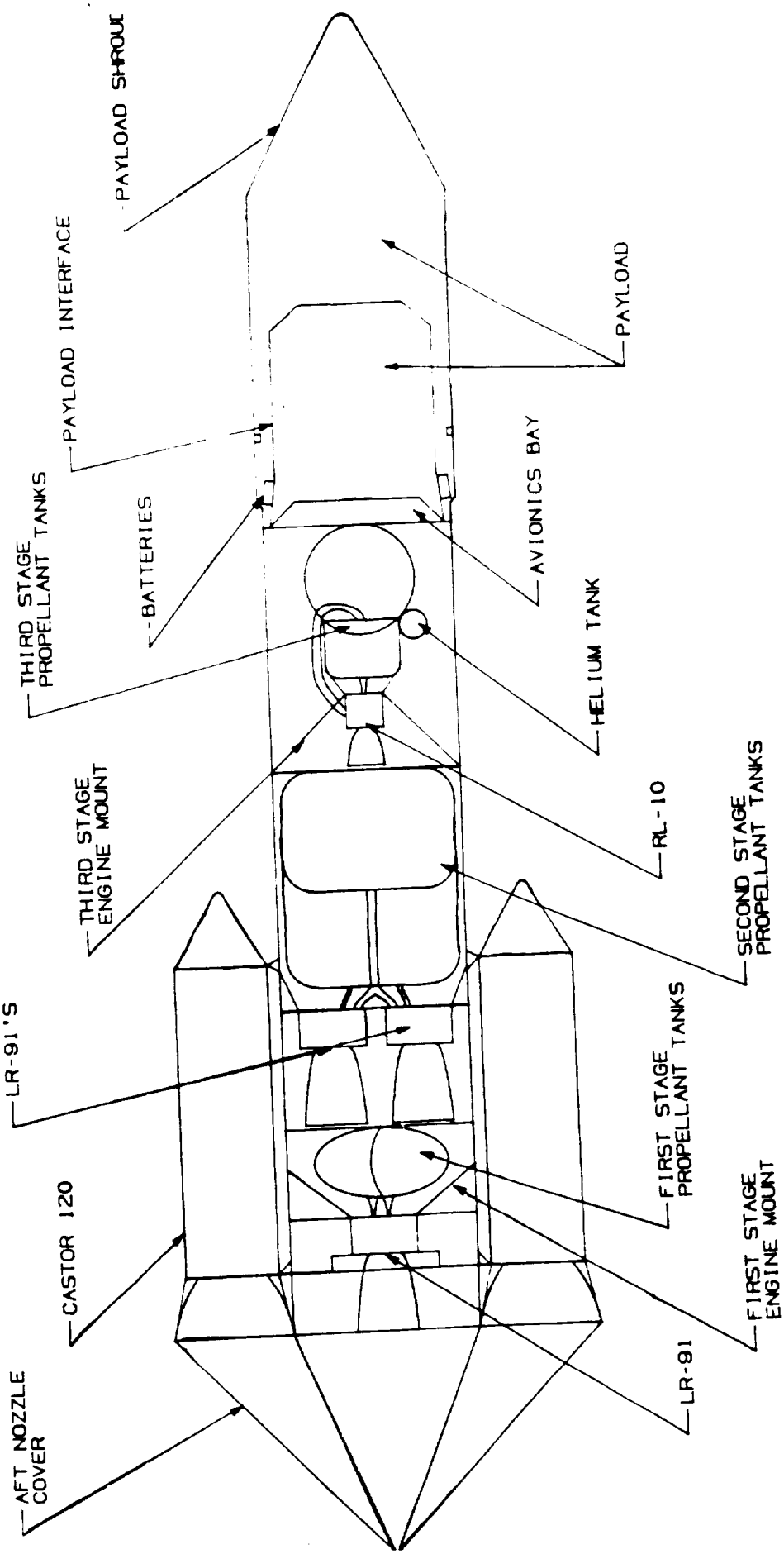

Figure 2.3 Cross-section

2.3.2 Avionics

Most of the navigation and power/thermal components are located in and around the avionics bay. The avionics bay is located just below the power/avionics ring and just above the payload interface attach. It is 14 feet in diameter at the base and 10 feet in diameter at the top with a height of 2 feet. The components located in the avionics bay are as follows:

- Hydrazine Tank
- Oxidizer Tank
- Central Processing Unit (CPU)
- Global Positioning System (GPS)
- Inertial Guidance Systems (Sensors, Electronics, Navigation, Telemetry Transmitter, and Radar Transmitter)
- Cables and Tubing

The hydrazine and oxidizer tanks are located at the base of the avionics bay. See Figure 2.4. The length of the oxidizer tank is 6 feet and the length of the fuel tank is 8 feet. Both tanks are 1 foot in diameter and together weigh about 700 pounds. These tanks supply the propellant necessary for the Roll Control System thrusters needed for a launch to GTO. There are six RCS thrusters spaced evenly about the bottom of the payload interface ring.

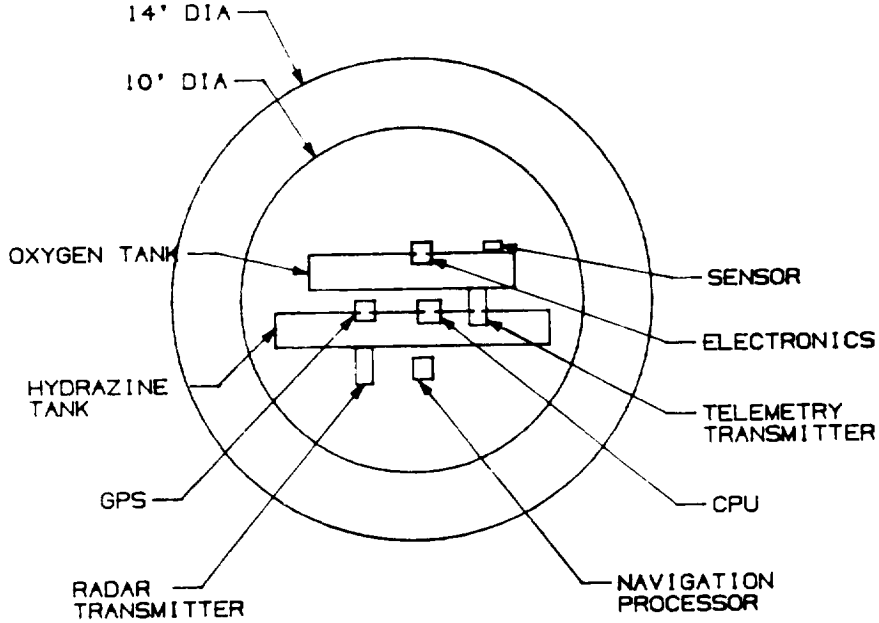

Figure 2.4 Avionics Bay

All of the mission control components (i.e. the CPU, GPS, and Inertial Guidance Systems) are bolted to the top of the avionics bay. They are positioned with their smallest dimension oriented in the x-direction. There are four battery modules located around the payload interface ring and below the RCS thrusters. They are evenly spaced around the ring in order to ensure that enough power will be continuously supplied in case one is disabled during the mission. See Figure 2.5.

All components located in and around the avionics bay must be cooled through out the duration of Gryphon's flight. These components are cooled with helium from a tank located next to the third stage propellant tanks. After the third stage drops, all components, such as the computer, are cooled by a radiator system.

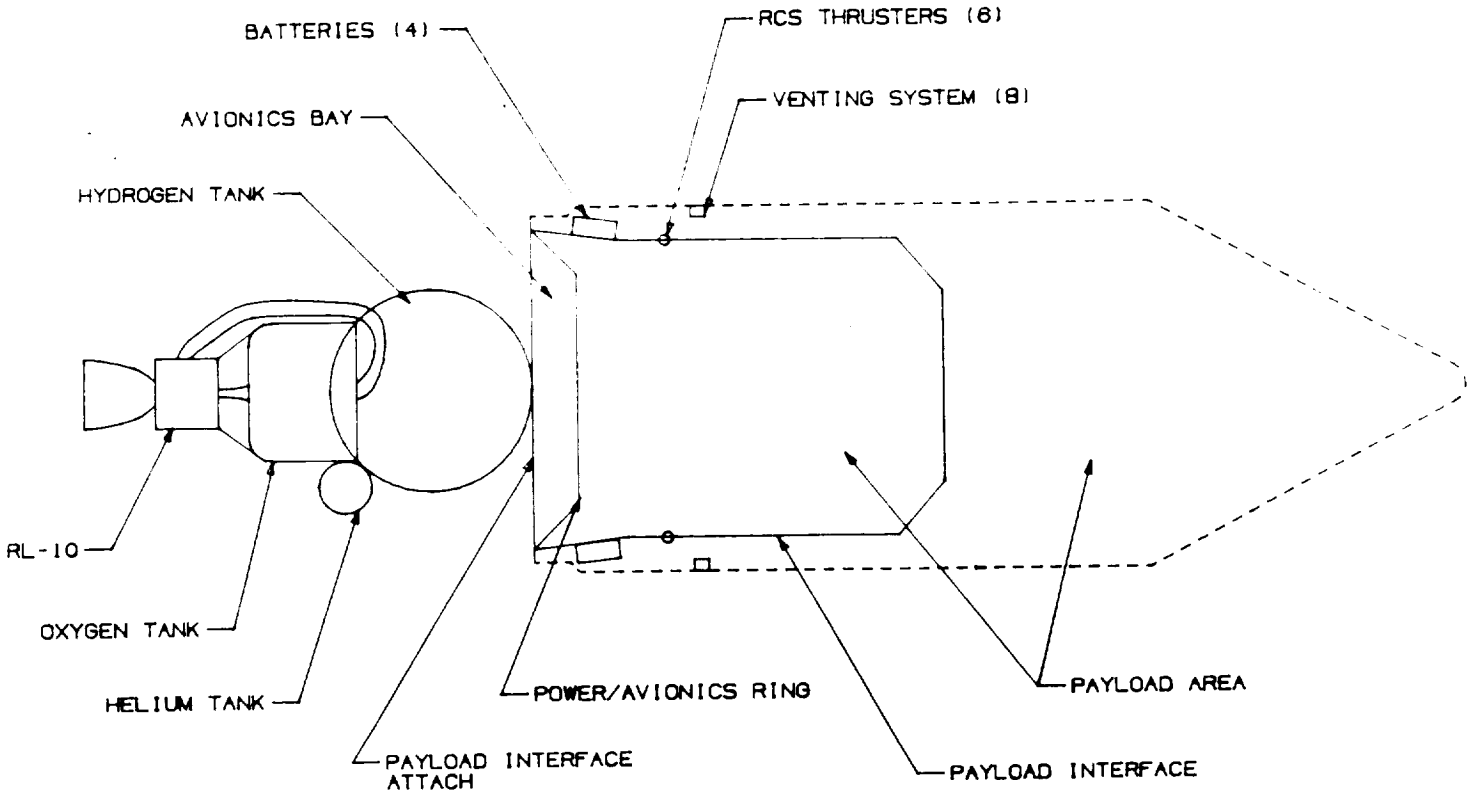

Figure 2.5 Payload Bay

Cables are located in the avionics bay to link the mission control components. Propellant tanks in the avionics bay supply fuel and oxidizer to the RCS thrusters via propellant tubing. Tubes also connect the helium tanks to all of the components that need to be cooled, such as the navigation equipment and the batteries.

2.3.3 Structures

The structural system consists of components that connect and/or support the various subsystems of the Gryphon. These include internal supports, external skin, and aerodynamic surfaces. In general, each stage has the following structures:

- Engine mounts
- Propellant tank supports
- Interstage connections
- External skin with reinforcements

Additionally, the payload and avionics are supported by dedicated support structures. Please see Figures 2.2 and 2.3 for a graphical representation of the structures. For a more complete description of this area, refer to Chapter 7.

In the first stage, each Castor 120 has two sets of two attach struts which connect it to the main body of the Gryphon. Each Castor 120 also has a conical fairing mounted on its top to reduce drag. The LR91 is held in place by an engine mount, and the LR91 and its propellant tanks are encased by a reinforced external skin. An interface ring links the skin with the interstage connector. The interstage connector sheaths the nozzles of the second stage engines. A right triangular vertical tail attached to the skin of this stage provides stability during the drop from the Eclipse. While the Gryphon is being carried by the aircraft, the aft nozzle cover (ANC) envelopes the first stage engine nozzles to reduce drag.

The second stage consists of two LR91's affixed to the Gryphon by means of the second stage engine mount. The engine mount then transfers the thrust produced by the engines to the total vehicle. The reinforced external skin covers the propellant tanks and support structure for this stage. An interface ring connects the skins of the second and third stage.

The third and final stage has an engine attach which unites the RL10 with the propellant tanks. A structure mount supports the engine and fuel tanks which are designed to carry the thrust load while a payload interface attach connects the third stage with the payload area.

The volume between the power/avionics ring and the payload interface attach comprises the avionics bay. Navigational modules are attached to the power/avionics ring via an adapter plate. In the dual-satellite configuration, the first payload is mounted directly to the power/avionics ring, and the second payload is mounted to the payload interface which surrounds the first satellite. A payload shroud encloses the entire payload/avionics area. As with the Castor 120 fairing, the payload shroud conically tapers to a point to reduce drag.

For a LEO launch, the third stage is removed and the second stage interface ring is attached directly to the payload interface attach. All other structures remain the same as for a GTO launch.

2.3.4 Vehicle Configuration Final Results

Figure 2.6 displays the axis systems for the Gryphon for various configurations.

In Table 2.4 below, these axis systems are used for the moments of inertia. The weights, centers of mass (CM) and mass moments of inertia are broken down for the GTO and LEO configurations for full, half full, and empty propellant tanks. This data shows the progression of these values from one configuration to the next as the Gryphon burns propellant and drops stages in flight. The first configuration is for the Gryphon with the aft nozzle cover (ANC) the moment after it is dropped from the Eclip

I_{mxx} = mass moment of inertia about the roll axis
I_{myy} = mass moment of inertia about the pitch axis
I_{mzz} = mass moment of inertia about the yaw axis

Note: Mass moment of inertia given in millions in Table 2.4

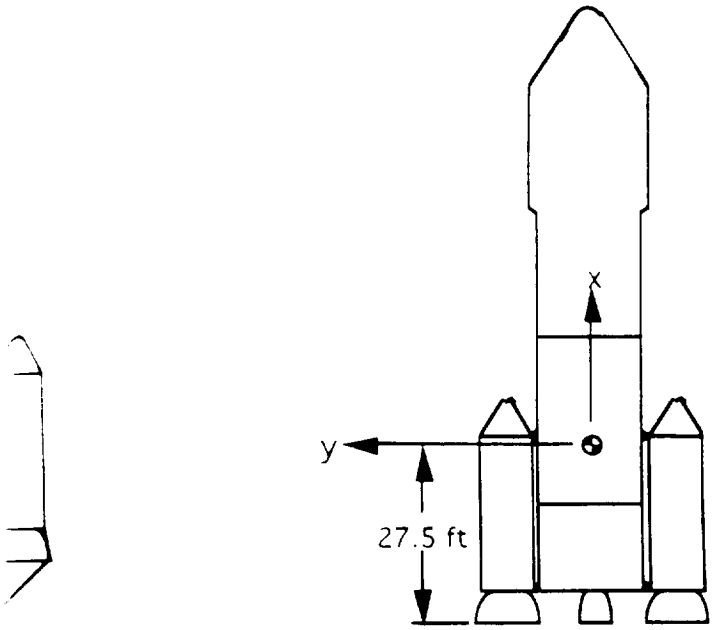

ı ANC

Stages 1, 2 and 3

ıyload

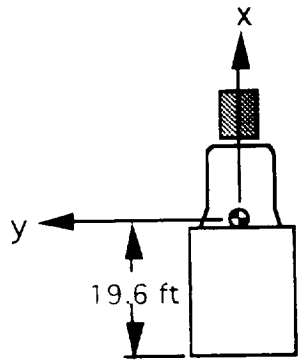

3

Stage 3

Note: The z-axis points out of the page.

Figure 2.6 Gryphon Axis Systems

Table 2.4 Weight, Center of Mass and Inertia for Various Configurations

Stages	Full Propellant Tanks		Half Full PropellantTanks		Empty Propellant Tanks	
1,2,3 and ANC	GTO	LEO	GTO	LEO	GTO	LEO
Weight (lb)	479,056	476,368				
CM (ft)	27.00	26.19				
I_{mxx} (lb ft2)	43.54	43.66				
I_{myy} (lb ft2)	192.8	171.7				
I_{mzz} (lb ft2)	228.6	207.5				
Stages 1,2,3						
Weight (lb)	473,256	470,568	352,294	349,606	231,332	228,644
CM (ft)	27.52	26.70	31.05	29.97	38.39	36.83
I_{mxx} (lb ft2)	43.37	43.49	26.32	26.44	8.658	8.781
I_{myy} (lb ft2)	186.2	165.3	191.4	170.3	207.6	186.1
I_{mzz} (lb ft2)	222.0	201.1	210.5	189.4	210.0	188.6
Stages 2,3						
Weight (lb)	200,467	197,779	116,416	113,678	32,366	29,678
CM (ft)	23.44	22.29	24.04	22.19	37.25	31.34
I_{mxx} (lb ft2)	5.080	5.204	3.324	3.448	0.9616	1.085
I_{myy} (lb ft2)	188.6	179.6	138.8	128.4	97.67	85.18
I_{mzz} (lb ft2)	188.6	179.6	138.8	128.4	97.68	85.19
Stage 3						
Weight (lb)	22,129	19,441	17,601	19,441	13,072	19,441
CM (ft)	19.56	12.08	21.61	12.08	26.12	12.08
I_{mxx} (lb ft2)	0.5943	0.7180	0.5714	0.6952	0.5486	0.6723
I_{myy} (lb ft2)	50.27	43.47	40.40	43.44	29.85	43.42
I_{mzz} (lb ft2)	50.28	43.48	40.41	43.44	29.86	43.43

The weight values above for Sages 1,2,3 and the ANC do not include extra weight that is carried by the aircraft for computers, an operator and Gryphon - Eclipse attachments. Even though these weights are not included in the Gryphon after it is launched, they are technically Gryphon weights that are considered payload to the aircraft. These components add an additional 10,435 pounds. Table 2.5 displays the Gryphon's total weight along with the total length for the GTO and LEO configurations with and without the ANC. It also lists the height including the vertical tail and the body width measured from the outside surfaces of the Castor engines. The Castor nozzles actually extend beyond this length by 2 ft - 2 in.

These total weights are under the 500,000 lb limit. Appendix A.2 lists the individual weights and centers of mass for each component on the Gryphon and describes the method used to calculate centers of mass and moments of inertia. Extra weight is anticipated from rivets, fasteners, etc. However, weight is expected to be trimmed from other components to keep the total weight under the maximum allowable 500,000 lb.

Table 2.5 Overall Gryphon Weights and Dimensions

	GTO	LEO
Stage 1,2,3 and ANC (lb)	479,056	476,368
Components on Eclipse (lb)	10,435	10,435
Total Gryphon Weight (lb)	489,491	486,803
Total Length with ANC	124' - 3"	104' - 5"
Total Length without ANC	106' - 3"	86' - 5"
Width	32' - 2"	32' - 2"
Height	30' - 0"	30' - 0"

2.4 AIR SAFETY PRECAUTIONS

In order to ensure the safety of the Eclipse, the Gryphon must drop about 2,000 feet before the ignition of its first stage engines. The safe drop distance of 2,000 feet was determined by the Fireball Diameter of Gryphon times a factor of safety of 2.67.

The fireball diameter was determined from the following equation:

$$D_f = 10(W)^{1/3} \qquad \text{(Eq 2.1)}$$

D_f = diameter of fireball
W = total propellant weight

With a 420,000 lb total propellant weight, the diameter of the fireball is 750 ft. This assumes that all of the propellant being used in the Gryphon is cryogenic to determine a worst case scenario.

In addition to the above equation, NASA produced a graph that relates fireball diameter vs. total propellant weight in pounds. The fireball diameter taken from this graph is approximately the same.

2.5 CONCLUSION

From the data presented here, it can be concluded that all design goals have been met with the final Gryphon specifications. A summary of the design goals and how they were achieved is provided below. These include:

- Maximum mission cost of $ 48.4 million which is less than the projected 50% undercut cost of $49.0 million per launch
- 15% return to investors. This would result in a cost per launch of $75 million to the customer
- Total booster weight of 489,491 lb which is less than the 500,000 lb maximum

- Payload weight of 7,900 lb GTO which is on the order of the initial 8,000 lb goal
- Payload weight of 17,000 lb to LEO which is the same as the initial 17,000 lb goal
- Two independent payloads delivered during one launch to GTO
- Payload envelope diameter of 15 ft which is capable of accommodating Space Station Freedom modules

Since all project have been met, this project seems to be a worthwhile venture. The recommendation of this design team is that Project Gryphon be implemented.

MISSION ANALYSIS

Chapter Three

3.1 INTRODUCTION

Vehicle aerodynamics, mission planning, the ascent trajectory, and orbital maneuvers fall under the mantle of the Mission Analysis Group. These responsibilities included working with the Power/Thermal/Attitude Control Group to analyze the drop of Gryphon from the Eclipse, and with the Propulsion Group to ensure adequate vehicle sizing.

3.2 MISSION DEFINITION

The primary mission of the Gryphon is delivery of a commercial payload to a Geosynchronous Transfer orbit (GTO), allowing the payload to reach Geosynchronous Earth Orbit (GEO) under its own power. Secondary missions include delivery of scientific payloads to a Low Earth Orbit (LEO) and resupply of Space Station Freedom in LEO.

Each of the missions has several common phases. In all missions, the Gryphon is mounted to the underside of the Eclipse and carried to its launch position. When the correct launch coordinates are reached the Gryphon is dropped from the Eclipse, falling until the vehicles are far enough apart to ignite the rocket engines without endangering the airplane. The aerodynamic design of the Gryphon is such that it will pitch up during the drop phase. The final phase begins when the first stage engines ignite and the Gryphon pulls out of its free fall. It then follows a predetermined ascent trajectory into orbit.

In a mission to GTO, the low earth orbit will be a circular parking orbit approximately 100 nm in altitude. The Eclipse carrier aircraft will typically take off from Vandenburg Air Force Base, allowing the Gryphon to enter an orbit with relatively low inclination of about 12.5°. When the vehicle reaches the correct position relative to the target position in GEO, the third stage will boost the vehicle to GTO. Near the apogee of GTO, the third stage will fire again to establish a zero-inclination, or equatorial, orbit. The payload will then be released from the vehicle and its apogee kick motors will boost it into GEO. If multiple payloads are being delivered to GEO, the Gryphon and the remaining payloads will continue to orbit in GTO until GEO is reached again and the next payload can be deployed.

Missions to LEO depend on the final orbit desired. Scientific missions have a wide variety of target orbits and thus the required orbital maneuvers are mission dependent. A mission to resupply Space Station Freedom is a specific example of a LEO mission.

Currently, the planned orbit strategy for Space Station Freedom is 180 to 150, 2 sigma. This means that its orbit must not decay to an altitude less than 150 nm in 180 days time. Therefore, its nominal orbital altitude will be between 200 nm and 240 nm. For missions to rendezvous with Space Station Freedom, the Gryphon will first reach a parking orbit slightly lower than the station's orbit. This lower position will orbit the Earth more quickly, allowing the Gryphon to chase the station until it reaches the proper position for a final maneuver that will transfer it to the space station's orbit for rendezvous.

3.3 ASCENT TRAJECTORY

The first step in calculating the trajectory is to define the mission the Gryphon will fly. Next, the rocket's ideal ΔV must be calculated, and the losses associated with the ascent to orbit must be estimated. The trajectory is defined and made to fit all of the conditions stipulated by this data. Finally, the trajectory is optimized in order to maximize the weight of the payload carried into orbit.

The initial parameters required to compute an ascent trajectory are shown in Table 3.1. The parameters required for second stage analysis follow in Table 3.2.

Table 3.1 First Stage Parameters

Thrust-to-weight ratio	$\frac{T}{W_o}$	1.93
Initial weight	W_O	473,353 lb
Specific impulse	I_{sp}	295 s
Maximum drag coefficient	C_{dmax}	0.6 (at Mach 2.0)
Burn time	t_b	78 s
Weight ratio	$r = \frac{W_o}{W_{bo}}$	2.144
Reference area	A	278 ft^2

Table 3.2 Second Stage Parameters

Thrust-to-weight ratio	$\frac{T}{W_o}$	1.047
Specific impulse	I_{sp}	316 s
Burn time	t_b	240 s
Weight ratio	r	6.1782
Inverse weight ratio	$P_f = \frac{1}{r}$	0.1619

The ideal velocity the first stage can attain is:

$$\Delta V = g_o I_{sp} \ln r \qquad \text{(Eq 3.1)}$$

Thus, the first stage ideal ΔV, ΔV_{1id}, is 7,246 ft/s.

In order to estimate losses, the trajectory for the first stage must be determined. The first stage burns entirely within the atmosphere, hence there are losses due to drag and thrust atmospheric effects in addition to gravity. Trajectory analysis for the first stage was completed using theory for vertically launched rockets; however, the Gryphon is not a vertically launched rocket. In order to make up for this discrepancy, the first 8 seconds of the first stage burn are devoted to establishing an initial pitch up angle which coincides with the kick angle of a vertically launched rocket. The rocket must pitch up at a rate of 6.25 degrees per second once the first stage engines ignite.

Once the Gryphon has reached the maximum pitch angle of 10 degrees from vertical, it enters a gravity turn , thereby minimizing gravitational losses. The gravity turn trajectory slowly pitches down as the Gryphon approaches the first stage burnout angle β_{bo}. This angle was determined via a burnout angle nomograph from Reference 109, See Figure B.1.

Using the technique outlined by this reference, a burnout angle, β_{bo}, of 70 degrees was determined. With the first stage burnout angle determined, losses for the first stage could be estimated.

3.3.1 Gravitational Losses

The gravitational loss, ΔV_{Lg}, is given by the following equation:

$$\Delta V_{L_g} = \left(gt_b - K_{gg}\right)\left[1 - K_g\left(1 - \frac{1}{r}\right)\left(\frac{\beta_{bo}}{90}\right)^2\right] \qquad \text{(Eq 3.2)}$$

where K_g is an empirical constant which accounts for changes in Earth's gravity as altitude increases, and K_{gg} is an empirical constant accounting for differences in thrust atmospheric effects as altitude increases. Since the Gryphon is launched at an altitude of 43,000 feet, the thrust is very close to vacuum thrust; therefore, K_{gg} is negligible. K_g is found using the nomograph in Figure B.2 and a mass ratio correction factor from Figure B.3.

Figure B.1 yields a K_g of 0.9 while Figure B.2 shows a mass ratio correction factor of 1.2. Thus, K_g is 1.08. Substitution into (Eq 3.2) yields a ΔV_{Lg} of 1,740 ft/s.

3.3.2 Aerodynamic Drag Losses

The drag losses incurred during first stage operation can be estimated using the drag coefficient for the maximum drag force encountered during the flight. This can be determined by finding the Mach number for peak drag, M_{pd}, from first stage parameters and the first stage burnout angle (Figure B.3). The value of C_d at this Mach number, C_{dpd} can then be found from the vehicles supersonic aerodynamics. Next, the empirical constant K_d is found using the same manner used to find M_{pd} (Figure B.4). The ΔV losses due to aerodynamic drag, ΔV_{Ld}, are calculated as follows:

$$\Delta V_{Ld} = K_d \frac{C_{dpd} A}{W_o} \qquad \text{(Eq 3.3)}$$

Using values from Figures B.3 and B.4, K_d is 3.7E+06, M_{pd} is 2.0, and C_{dpd} is 0.6, and ΔV_{Ld} is found to be 1,305 ft/s. However, since a large portion of the atmosphere is already below the Gryphon at first stage ignition, just 20% of this value is used. Therefore, ΔV_{Ld} is 261 ft/s.

The burnout velocity of the first stage can be determined from (Eq 3.4):

$$V_{bo} = \Delta V_{Id} - \Delta V_{Lg} - \Delta V_{Ld} \qquad \text{(Eq 3.4)}$$

This yields a value of 5,245 ft/s.

3.3.3 First Stage Performance

Once the losses have been calculated, the flight performance of the first stage can be analyzed. First, the empirical constant K_h must be found from Figure B.3. Then the following data may be calculated: altitude of first stage burnout, h_i; the range angle, θ_i; the inertial thrust orientation angle, ε_i; the inertial burnout velocity, V_i; the inertial burn out angle, β_i; and the inertial angle of attack, α_i.

$$h_i = \left(\hat{h} - \frac{\Delta V_{Ld} t_b}{2} \right) \left[1 - \left(\frac{\beta_{bo}}{K_h} \right)^2 \right] \qquad \text{(Eq 3.5)}$$

where

$$\hat{h} = g_o I_{sp} t_b \left(1 - \frac{\ln r}{r-1} \right) - \frac{g_o t_b^{\,2}}{2} \qquad \text{(Eq 3.6)}$$

Evaluation of (Eq 3.6) yields an $\hat{h}$ of 142,750 feet, which results in an h_i of 130,397 feet.

Inertial burnout velocity can be computed from the following equation:

$$V_i = \sqrt{\left(V_{bo} + V_{eclipse} \right)^2 + V_{rot}^{\,2} + 2\left(V_{bo} + V_{eclipse} \right) V_{rot} \sin\beta_{bo}} \qquad \text{(Eq 3.7)}$$

where $V_{eclipse}$ is the initial velocity of the Eclipse carrier aircraft and V_{rot} is the rotational velocity of the Earth in the southern United States. Assuming these values are 778 ft/s and 1,340 ft/s, respectively, V_i is 7,297 ft/s.

The angles α, β, ε, and θ are illustrated in Figure 3.1 to allow easier interpretation of the results presented herein.

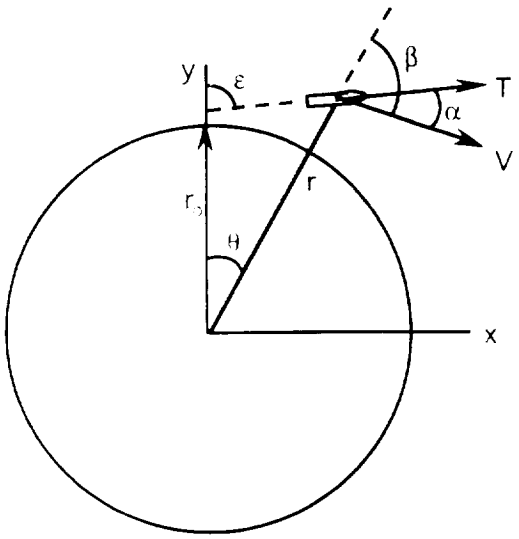

Figure 3.1 Circular Orbit Diagram for Trajectory Analysis [Reference 109]

Figure B.5 yields a range angle, θ_i, of 1 degree. The inertial thrust orientation angle, ε_{bo}, is simply the sum of the range angle and the burnout angle:

$$\varepsilon_{bo} = \theta_i + \beta_{bo} \qquad \text{(Eq 3.8)}$$

Inertial burnout angle, β_i, and inertial angle of attack, α_i, are found from the following equations:

$$\beta_i = \cos^{-1}\left(\frac{\cos\beta_{bo}}{V_{boI}} V_{bo}\right) \qquad \text{(Eq 3.9)}$$

$$\alpha_i = \beta_i - \beta_{bo} \qquad \text{(Eq 3.10)}$$

Thus, β_i is 75.8 degrees and α_i is 5.8 degrees.

3.3.4 Determination of Second Stage Burnout Conditions

The analysis for the second stage assumes that the second stage trajectory is essentially non-atmospheric. A method for modeling low altitude circular orbits with a constant pitch rate was employed for trajectory analysis. This method is outlined in Appendix A of Reference 109. Figure 3.8 depicts a typical trajectory profile generated by this method.

This procedure finds the flight path burnout angle, altitude, and the final burnout velocity for circular orbital insertion by iterating different constant pitch rates. For the Gryphon, a low earth parking orbit (LEO) of 100 nm, or 607,610 feet, is desired. This

requires a final velocity of 25,581 ft/s at an angle of 90.0 degrees. From this parking orbit the Gryphon can enter the elliptical GTO and insert its payload into a GEO.

Required input for the procedure are: the initial thrust acceleration angle, ε_{0i}; the initial inertial velocities, x and y (see Figure 3.1), the initial pitch rate, $\dot{\varepsilon}$, and the initial distance from the center of the Earth, r_i. These values are found using the equations below:

$$\varepsilon_{0i} = \beta_i - \alpha_i \qquad \text{(Eq 3.11)}$$

$$\dot{x} = V_i \sin\beta_i \qquad \text{(Eq 3.12)}$$

$$\dot{y} = V_i \cos\beta_i \qquad \text{(Eq 3.13)}$$

$$\dot{\varepsilon} = 0.075 \qquad \text{(Eq 3.14)}$$

$$r_i = r_e + h_i \qquad \text{(Eq 3.15)}$$

The results obtained with these equations are shown below in Table 3.3. Note also that the value for $\dot{\varepsilon}$ shown in (Eq 3.14) is an initial estimate. Using the method outlined here, this initial value is modified if necessary. In the case of the Gryphon, the value shown in Table 3.3 is sufficient to reach the desired orbit.

Table 3.3 Initial Second Stage Input

ε_{0i}	70°
$\dot{x}_i$	7,074 ft/s
$\dot{y}_i$	1,790 ft/s
$\dot{\varepsilon}$	0.075°/s
r_i	21,033,297 ft

Additional information is needed to proceed with the analysis, however. The effective radial distance from the center of the Earth, r^*, the effective gravitational acceleration, g^*, and the effective exhaust velocity of the rocket engines, c^*, are computed as shown below.

$$r^* = r_i + t_b\left[V_i + g_o I_{sp}\left(1 + \frac{P_f \ln P_f}{1 - P_f}\right) - \frac{g_o t_b}{2}\right]K^* \cos\beta_i \qquad \text{(Eq 3.16)}$$

where

$$K^* = \frac{0.0163(T/W_i)}{P_f\left[1 - P_f(1 - \ln P_f)\right]} \qquad \text{(Eq 3.17)}$$

Using values from Table 3.2 to find K^* yields 0.194. Substitution into (Eq 3.16) results in a value of 21,147,847 ft for r^*. Finally:

$$g^* = g\left(\frac{r_e}{r^*}\right)^2 \qquad \text{(Eq 3.18)}$$

$$c^* = g_o I_{sp} \qquad \text{(Eq 3.19)}$$

yielding values of 31.45 ft/s^2 for g^* and 10,175 ft/s for c^*.

Altitude and velocity are found by solving two equations of motion. They are differential equations derived by assuming circular motion in a plane. Using the coordinate system illustrated in Figure 3.1, the equations of motion are

$$\ddot{y} = \frac{T}{m}\cos\varepsilon - g^*\cos\theta \qquad \text{(Eq 3.20)}$$

$$\ddot{x} = \frac{T}{m}\sin\varepsilon - g^*\sin\theta \qquad \text{(Eq 3.21)}$$

where T is thrust and m is mass. From Figure 3.1:

$$\cos\theta = \frac{y}{r} \qquad \text{(Eq 3.22)}$$

$$\sin\theta = \frac{x}{r} \qquad \text{(Eq 3.23)}$$

where r is the radial distance from the center of the Earth.

Assuming that the variation in r is small compared to its initial value, (Eqs 3.19-20) can now be simplified.

$$\ddot{y} + \frac{g^*}{r^*}y = \frac{T}{m}\cos\varepsilon \qquad \text{(Eq 3.24)}$$

$$\ddot{x} + \frac{g^*}{r^*}x = \frac{T}{m}\sin\varepsilon \qquad \text{(Eq 3.25)}$$

Assuming constant thrust, the generalized thrust to weight equation can be defined and solved:

$$\eta = \left(\frac{T}{W_i}\right)\left(\frac{g_o}{g^*}\right) \qquad \text{(Eq 3.26)}$$

The constant thrust assumption is valid due to the Gryphon's high altitude. Substitution of the appropriate values results in a value of η equal to 1.0578.

Since ε_{oi} denotes the initial thrust attitude, the thrust attitude varies in time as follows:

$$\varepsilon = \varepsilon_{oi} + \dot{\varepsilon} t \qquad \text{(Eq 3.27)}$$

where t is time.

Allowing that $T = \dot{m} c^*$ and substituting into (Eq 3.26), one can show that

$$t = (1 - P_f)\frac{c^*}{\eta g^*} \qquad \text{(Eq 3.28)}$$

Substituting this equation into (Eq 3.27) yields:

$$\varepsilon = \nu + \xi P_f \qquad \text{(Eq 3.29)}$$

where

$$\nu = \varepsilon_{oi} + \frac{c^* \dot{\varepsilon}}{\eta g^*} \qquad \text{(Eq 3.30)}$$

and

$$\xi = -\frac{c^* \dot{\varepsilon}}{\eta g^*} \qquad \text{(Eq 3.31)}$$

Solution of (Eqs 3.30-31) results in ν equal to 1.6220 radians and ξ equal to –0.4003 radians.

At this point, (Eq 3.26) and (Eq 3.29) are substituted into the equations of motion, and the independent variable is changed from t to P_f. The differential equations become

$$y'' + \chi^2 y = \zeta\left[\frac{\cos(\nu + \xi P_f)}{P_f}\right] \qquad \text{(Eq 3.32)}$$

$$x'' + \chi^2 x = \zeta\left[\frac{\sin(\nu + \xi P_f)}{P_f}\right] \qquad \text{(Eq 3.33)}$$

where

$$\zeta = \frac{(c^*)^2}{\eta g^*} \qquad \text{(Eq 3.34)}$$

and

$$\chi = \frac{\zeta}{c^*}\sqrt{\frac{g^*}{r^*}} \qquad \text{(Eq 3.35)}$$

Solution of (Eqs 3.33-34) yields values of ζ equal to 3.1120E+06 and χ equal to 0.3730.

The bracketed portions of (Eqs 3.31-32) are in the form of sine and cosine integrals, defined as follows:

$$S(u) = \int_0^u \frac{\sin\sigma}{\sigma} d\sigma \qquad \text{(Eq 3.36)}$$

$$C(u) = -\int_u^\infty \frac{\cos\sigma}{\sigma} d\sigma \qquad \text{(Eq 3.37)}$$

These integrals were evaluated using MAPLE V. The results are presented in Table 3.4.

Table 3.4 Sine and Cosine Integrals

Function Argument (u)	Cosine Integral $C_i(u)$	Sine Integral $S_i(u)$
$\xi + \chi = -0.02730$	–3.02384	–0.027299
$(\xi + \chi)P_f = -0.0044$	–4.84894	–0.004399
$\xi - \chi = -0.77330$	0.174305	–0.748066
$(\xi - \chi)P_f = -0.1252$	–1.50540	–0.125091

The equations of motion are linear first order differential equations. They are solved using an integrating factor of $e^{-i\chi P_f}$. The actual solution method is too complex for inclusion here (see pages A-15 to A-18 of Reference 109 for details), though it results in two important complex quantities Z and ω that will be used later.

In order to solve the differential equations, several constants whose values were derived during the equations' solution must be found. These constants were evaluated using information from Table 3.4:

$$E = \left[C_i(\xi+\chi)P_f - C_i(\xi+\chi)\right] + \left[C_i(\xi-\chi)P_f - C_i(\xi-\chi)\right] \qquad \text{(Eq 3.38)}$$

$$F = \left[S_i(\xi+\chi)P_f - S_i(\xi+\chi)\right] + \left[S_i(\xi-\chi)P_f - S_i(\xi-\chi)\right] \qquad \text{(Eq 3.39)}$$

$$G = \left[C_i(\xi+\chi)P_f - C_i(\xi+\chi)\right] - \left[C_i(\xi-\chi)P_f - C_i(\xi-\chi)\right] \qquad \text{(Eq 3.40)}$$

$$H = \left[S_i(\xi+\chi)P_f - S_i(\xi+\chi)\right] - \left[S_i(\xi-\chi)P_f - S_i(\xi-\chi)\right] \qquad \text{(Eq 3.41)}$$

The following constants were evaluated using the values of the constants calculated in (Eqs 3.38-41):

$$A = \tfrac{1}{2}(E\cos\nu - F\sin\nu) \qquad \text{(Eq 3.42)}$$

$$B = \tfrac{1}{2}(G\sin\nu + H\cos\nu) \qquad \text{(Eq 3.43)}$$

$$C = \frac{1}{2}(E\sin\nu + F\cos\nu) \qquad \text{(Eq 3.44)}$$

$$D = \frac{1}{2}(-G\cos\nu H\sin\nu) \qquad \text{(Eq 3.45)}$$

The values of these constants are shown in Table 3.5.

Table 3.5 Solution Constants

A	-0.2329
B	-0.0577
C	-1.7662
D	-0.3034
E	-3.5039
F	-0.6459
G	-0.1463
H	-0.6001

Using these constants the real and imaginary parts of Z and ω were computed. Their values are shown in Table 3.6.

$$\mathrm{Im}\,Z = A\sin\chi P_f - B\cos\chi P_f \qquad \text{(Eq 3.46)}$$

$$\mathrm{Re}\,Z = A\cos\chi P_f + B\sin\chi P_f \qquad \text{(Eq 3.47)}$$

$$\mathrm{Im}\,\omega = C\sin\chi P_f - D\cos\chi P_f \qquad \text{(Eq 3.48)}$$

$$\mathrm{Re}\,\omega = C\cos\chi P_f + D\sin\chi P_f \qquad \text{(Eq 3.49)}$$

Evaluation of (Eqs 3.46-49) results in values of 0.0435, -0.2360, 0.1962, and -1.7813, respectively.

With the differential equations solved, the rectangular coordinates and velocities were computed using the following equations:

$$y = \frac{\zeta}{\chi}\left[\mathrm{Im}\,Z + \frac{\dot{x}_i}{c^*}\sin\chi(1-P_f)\right] + r_i\cos\chi(1-P_f) \qquad \text{(Eq 3.50)}$$

$$x = \frac{\zeta}{\chi}\left[\mathrm{Im}\,\omega + \frac{\dot{x}_i}{c^*}\sin\chi(1-P_f)\right] \qquad \text{(Eq 3.51)}$$

$$\dot{y} = -c^*\left[\mathrm{Re}\,Z + \frac{r_i\chi}{\zeta}\sin\chi(1-P_f)\right] + \dot{y}_i\cos\chi(1-P_f) \qquad \text{(Eq 3.52)}$$

$$\dot{x} = -c^*(\mathrm{Re}\,\omega) + \dot{x}_i\cos\chi(1-P_f) \qquad \text{(Eq 3.53)}$$

The solutions of these equations are presented in Table 3.6.

Table 3.6 Solutions to Equations of Motion

y	2.1207E+07 ft
x	3.3936E+06 ft
ẏ	-2,354.5 ft/s
ẋ	24,751 ft/s

Finally, the values of final height, velocity, and flight path angle at second stage burnout were calculated.

$$h_f = \sqrt{x^2 + y^2} - r_e + h_i \qquad \text{(Eq 3.54)}$$

$$V_f = \sqrt{\dot{x}^2 + \dot{y}^2} \qquad \text{(Eq 3.55)}$$

$$\beta_f = \cos^{-1}\left[\frac{x\dot{x} + y\dot{y}}{\sqrt{(x^2 + y^2)(\dot{x}^2 + \dot{y}^2)}}\right] \qquad \text{(Eq 3.56)}$$

From this data the thrust orientation angle, ε_f, the total velocity loss, ΔV_L, the range angle, θ_f, and the final angle of attack, α_f, at burnout of the second stage can be found:

$$\varepsilon_f = \varepsilon_i + \dot{\varepsilon} t_b \qquad \text{(Eq 3.57)}$$

$$\Delta V_L = c^* \ln\frac{1}{P_f} + V_i - V_f \qquad \text{(Eq 3.58)}$$

$$\theta_f = \theta_i + \cos^{-1}\left(\frac{y}{\sqrt{x^2 + y^2}}\right) \qquad \text{(Eq 3.59)}$$

$$\alpha_f = \beta_f + \theta_f - \varepsilon_f \qquad \text{(Eq 3.60)}$$

The results of the evaluation of these equations are presented in Table 3.7, with the exception of ΔV_L, which is 962.3 ft/s. It does not appear in Table 3.7 because it is taken into account in the value for V_f.

Table 3.7 Vehicle Performance Results

First Stage	Second Stage
V_i = 7,297 ft/s	V_f = 24,864 ft/s
β_i = 75.8°	β_f = 86.34°
h_i = 130,397 ft	h_f = 574,240 ft
θ_i = 1°	θ_f = 10.09°
ε_{oi} = 70°	ε_f = 88°
α_i = 5.8°	α_f = 89°
	$\dot{\varepsilon}$ = 0.075°/s

3.4. GEOSYNCHRONOUS MISSIONS

For a mission to GEO, the Gryphon will first launch to a circular LEO and execute a Hohmann transfer as shown in Figure 3.2.

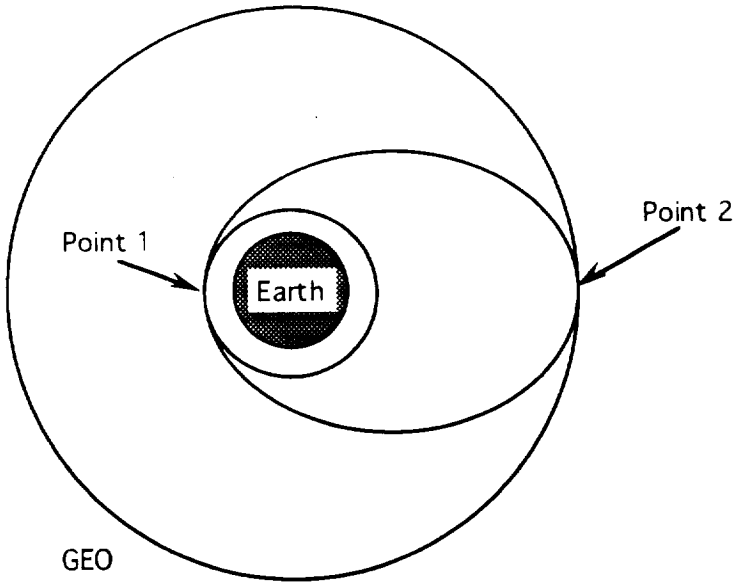

Figure 3.2 Hohmann Transfer

The Hohmann transfer consists of two maneuvers. The first occurs at Point 1, where an impulse increases the orbital velocity of the vehicle, putting it into a geotransfer orbit (GTO). Once the vehicle has reached Point 2, apogee of GTO, the payload is released and another impulse inserts into GEO in an analogous manner.

The first change in velocity, ΔV_1, is the difference between the velocity of the elliptical LEO and the velocity at perigee of GTO. This is:

$$\Delta V_1 = \sqrt{2\mu\left(\frac{1}{r_{LEO}} - \frac{1}{r_{LEO} + r_{GEO}}\right)} - \sqrt{\frac{\mu}{r_{LEO}}} \qquad \text{(Eq 3.61)}$$

where μ is the gravitational constant of the Earth (1.40764E+16 ft^3/s^2), r_{LEO} is the apogee radius of the circular LEO, and r_{GEO} is the orbital radius at GEO (22,766 nm).

The second change in velocity, ΔV_2, will be performed at the apogee of GTO, where it intersects GEO. This is:

$$\Delta V_2 = \sqrt{\frac{\mu}{r_{GEO}}} - \sqrt{2\mu\left(\frac{1}{r_{GEO}} - \frac{1}{r_{LEO} + r_{GEO}}\right)} \qquad \text{(Eq 3.62)}$$

This turns out to be 4,776 ft/s. This is handled by apogee kick motors that are part of the payload.

Since GEO has an inclination of zero, unless the Gryphon can be launched from a point directly over the equator, an inclination change must be performed. The ΔV required is given by equation (3.6).

$$\Delta V = 2\sin\left(\frac{\Delta i}{2}\right)\sqrt{2\mu\left(\frac{1}{R} - \frac{1}{r_{LEO} + r_{GEO}}\right)} \qquad \text{(Eq 3.63)}$$

where R is the distance from the center of the earth at the time the maneuver is performed. Since the minimum ΔV_i is desired, the maneuver should be performed as far away from earth as possible, i.e. as close to GEO as possible.

The required change in inclination will be equal to the latitude at which the Gryphon is launched. The minimum launch latitude depends on both the launch site and the distance it is carried by the Eclipse before launch. Assuming that the inclination change maneuver is performed when R equals r_{GEO} for an inclination of 12.5°, the ΔV required will be 998 ft/s. This can be performed by the remaining fuel in the RL10A-4. The actual R when the maneuver is performed will be less than r_{GEO}, since the payload must separate from the orbiter before rendezvous with GEO. If the maneuver is performed when R is 20,766 nm, or 2,000 nm from GEO, the ΔV_i is 1,300 ft/s.

3.4.1 Phasing for transfer from LEO to GEO

GTO must be phased properly if the orbiter is to deploy its payload at the proper point over the equator. That is, the orbiter must enter GTO at a specific point in space relative to its destination. To do this correctly, the time taken to reach that point must be calculated.

The time taken by the transfer is simply half of the period of the transfer ellipse. The period of an elliptical orbit is given by:

$$T = 2\pi\sqrt{\frac{a^3}{\mu}} \qquad \text{(Eq 3.64)}$$

Thus Δt is:

$$\Delta t = \pi\sqrt{\frac{\left[(a_1 + a_2)/2\right]^3}{\mu}} \qquad \text{(Eq 3.65)}$$

where a_2 is the semimajor axis of the GEO orbit and a_1 is the semimajor axis of the LEO orbit. Note that for a circular orbit, a_1 and a2 are simply equal to their respective orbital radii.

The transfer of the payload from the parking orbit in LEO to GTO must be timed correctly in order for the payload to arrive at the correct position in GEO. Figure 3.3 shows how the payload must be positioned.

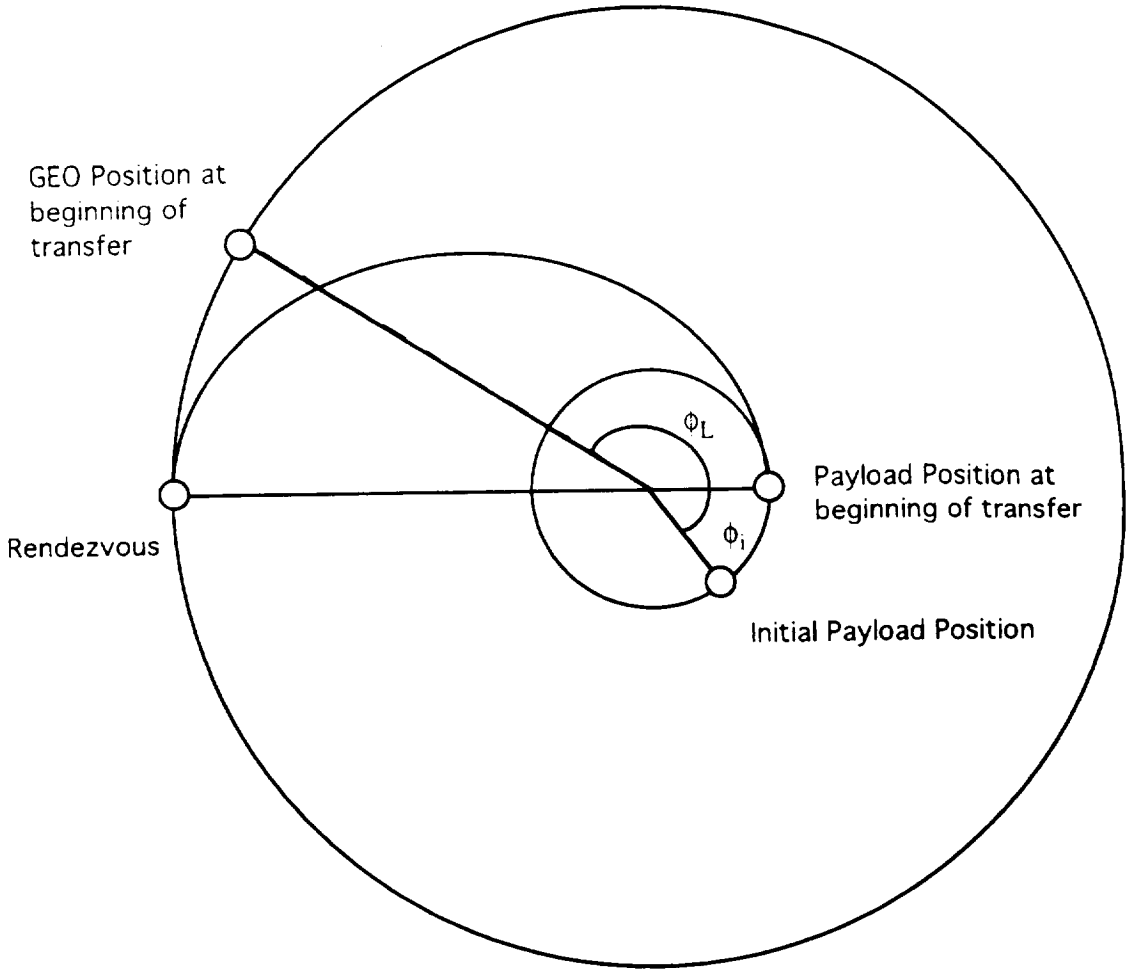

Figure 3.3 Geotransfer Phasing

ϕ_L is the angle by which the GEO destination point leads the orbiter when it makes the transfer to GTO, and ϕ_i is the angle between the orbital insertion point and the point where the transfer to GTO is made.

Now, ϕ_L must be the angle of the arc which the point in GEO travels while the payload is in GTO in order for the GTO to intersect GEO at the correct point. Thus, the following ratio holds true:

$$\frac{\phi_L}{2\pi} = \frac{\Delta t}{T_{GEO}} \qquad \text{(Eq 3.66)}$$

Substituting (Eqs 3.64-65) into (Eq 3.66) yields:

$$\phi_L = \pi\left(\frac{a_1 + a_2}{2a_2}\right)^{3/2} \qquad \text{(Eq 3.67)}$$

For a Hohmann transfer from 100 nm to GEO, Δt = 22,756 seconds, about 6.32 hr, and $\phi_L = 76.97°$.

Since ϕ_L is not necessarily 76.97° when the Gryphon achieves orbit, there is a wait period, Δt_{wait}, before the Hohmann transfer can be initiated. This wait time is determined by (Eq 3.68):

$$\Delta t_{wait} = \frac{\phi_i}{\omega_1 - \omega_2} \qquad \text{(Eq 3.68)}$$

where ω_2 is the orbital frequency of the destination point in GEO and ω_1 is the orbital frequency of the LEO parking orbit. These values can be determined from (Eq 3.69):

$$\omega = \frac{2\pi}{T} \qquad \text{(Eq 3.69)}$$

The maximum possible value of ϕ_i before ϕ_L reaches the necessary value is 2π. Thus, for the LEO to GEO transfer, the maximum waiting time is 5,946 s or 1.65 hr.

3.4.2. Multiple Payload Launches

In the case of a multiple payload deployment, the orbiter will perform the proper phasing maneuvers to insert the first satellite into the correct position. The orbiter will remain in GTO until it completes an orbit and once again intersects GEO. This will happen at a position 159.2° around the circular GEO from the first payload's position. The orbiter will continue in GTO in this manner until the second payload can be deployed near its proper position. The payload's thrusters will make the necessary adjustments to move it to the correct position in GEO. (See Chapter 5 for further information on multiple payload launches.)

3.4.3. Rendezvous with Space Station

The Gryphon will launch its payload directly to the Space Station Freedom's orbit. To ensure a swift rendezvous with the station, the launch must be timed correctly. Assume the orbit of the space station remains stationary while the Earth rotates beneath it. The inclination, i, of the station's orbit is 28.45°. The latitude, λ, of the launch site determines the heading of the launch, or the launch azimuth, A, and the number of launch opportunities per day. The launch azimuth is defined by (Eq 3.70):

$$\sin A = \frac{\cos i}{\cos \lambda} \qquad \text{(Eq 3.70)}$$

Assuming that the Gryphon is launched directly over Kennedy Space Center, which has a latitude λ_K of 28.45°, the Gryphon should be launched due east (A = 90°). The actual launch site will be east or southeast of Kennedy, within the 1,000 mile range of the Eclipse. If the latitude of the launch site is less than 28.45°, there will be two possible launch opportunities. Please refer to Figure 3.4.

As Space Station Freedom orbits, it will cross the launch site's latitude line. Sometimes it will cross headed north, away from the equator; sometimes it will be headed south, toward the equator. Each of these passings represents a launch opportunity. The launch azimuth A needed to reach Freedom's orbit as it makes its southward pass over the

launch site is given by (Eq 3.70), while the necessary launch azimuth as it crosses the launch site heading north is simply be the supplement of A, or 180° minus A.

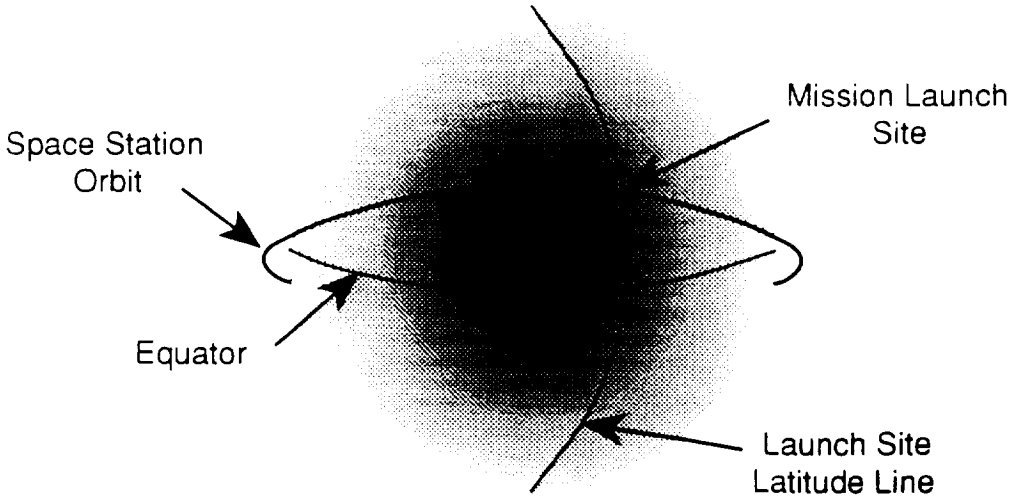

Figure 3.4 Launch to Rendezvous with Space Station Freedom

The Gryphon will be launched into an orbit that is identical to Space Station Freedom's in all respects except altitude. It will orbit at a slightly lower altitude than Freedom, allowing it a greater orbital frequency and having the effect of chasing Freedom. Once it catches up, it corrects its orbit and performs a rendezvous with the station. Since the station's altitude will vary from approximately 200 nm to 240 nm, the exact intermediate orbit will be mission dependent.

Once the payload has reached the vicinity of the space station, the final maneuvering will be dictated by the docking procedures mandated by NASA. These procedures are currently being reviewed and no final procedure has been announced.

3.5. SPIN RATES

A spin-stabilized payloads might require the Gryphon to impart spin to it upon deployment. To calculate a nominal spin rate, the maximum off-axis spin of a typical satellite under a given spin rate was estimated. The governing equation for this motion is:

$$\theta = \cos^{-1}\left[\frac{I_{mzz}\Psi + w_o \cot\theta}{\sqrt{I_{mxx} w_o^{\,2} + I_{mzz}\left(\Psi + w_o \cot\theta\right)^2}}\right] \qquad \text{(Eq 3.71)}$$

where I_{mxx} is the satellite's moment of inertia about the x-axis, I_{mzz} is the its moment of inertia about the z-axis, Ψ is the spin rate, and θ is the off-axis spin angle. Please refer to Figure 3.5.

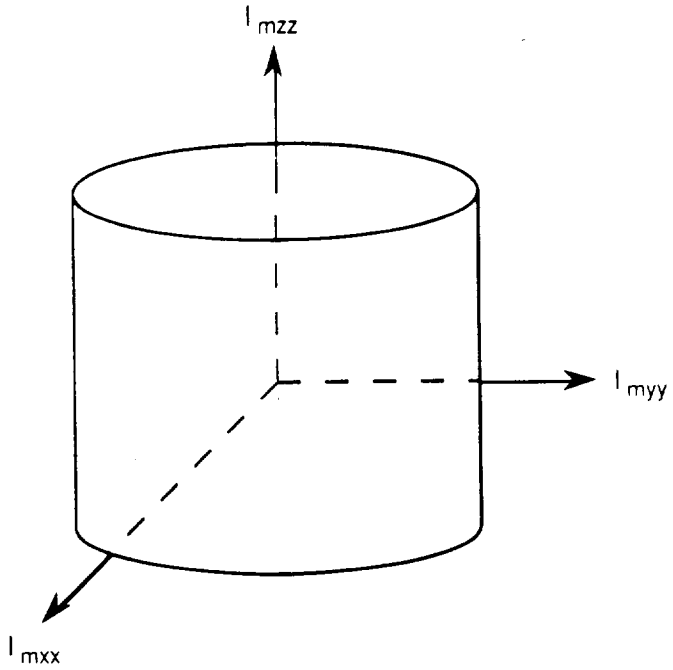

Figure 3.5 Typical Cylindrical Satellite

Given the off axis spin the satellite can tolerate and the initial spin rate, (Eq 3.71) can be solved numerically.

While this analysis is helpful, a much easier way to determine the spin rate was found. Using figures from the NASA Solid Spinning Upper Stage (SSUS) variant A and D data, a spin rate was interpolated. The data is presented in Table 3.8.

Table 3.8 SSUS spin rates

Variation	Spin Rate	Mass
A	Approx. 45 rpm	243 slug
D	Approx. 80 rpm	120 slug

According to the Payloads Group (see Chapter 5), the weight of a typical telecommunications satellite of the type to be carried by the Gryphon will be 2,000 lb, about 62 slugs. By linear interpolation, the spin rate is found to be 97 rpm. A factor of safety of 1.18 is incorporated to give a final spin rate of 105 rpm.

The Power/Thermal/Attitude Control Group is responsible for the Gryphon's spin and despin mechanisms. (see Chapter 8)

3.6 VEHICLE AERODYNAMICS

The Gryphon will be launched at a subsonic velocity of 500 mph, and quickly accelerate to supersonic velocity. Because of the differences in the calculation of aerodynamic properties

in different flow regimes, lift and drag computations were carried out separately for subsonic and supersonic flight.

3.6.1 Subsonic Aerodynamics

The subsonic aerodynamic analysis was divided into two parts. The Gryphon was analyzed along its body axis and in the vertical plane perpendicular to this axis. Each analysis assumed that the Gryphon's fuselage and two SRBs could be modeled separately, and the results added together. A series of equations from Reference 107 was used to calculate drag along the body axis, with a resulting C_d of 0.019861. Details of the analysis may be found in Appendix B.

To find the perpendicular component of the drag force, the Gryphon was modeled as three cylinders. First, Reynolds numbers were computed for a variety of velocities and altitudes that might be expected during the Gryphon's flight. To compute the Reynolds number the following equation was used:

$$Re = \frac{\rho V D}{\mu_v} \qquad \text{(Eq 3.72)}$$

where r is the density of the air, V is the freestream velocity, D is the diameter of the cylinder, and μ_v is the viscosity of the air. The results of this analysis are shown in detail in Appendix B. From these Reynolds numbers, the coefficient of drag was computed using a standard C_d vs. Re for the unit cylinder obtained from Reference 126.

Since the data is valid for unit cylinders in a free stream only, interference effects must be included. To account for this, 15 percent was added onto the drag coefficients of the SRBs.

As the velocity in the perpendicular direction increases, the cylinders reach drag crisis very quickly — about 55 ft/s on the SRBs and about 35 ft/s on the fuselage. Drag crisis occurs when a turbulent boundary layer completely surrounds the cylinder. This leads to a greatly reduced drag coefficient. However, since turbulent flow is unsteady it suggests that some device for roll control must be considered. The uncoupled drag force is calculated using the equation

$$D = \tfrac{1}{2}\rho S V^2 C_d L \qquad \text{(Eq 3.73)}$$

where S is the reference area and L is the length.

Release conditions for the Gryphon — a velocity of 733 ft/s at 40,000 feet — were assumed in creating the drag polar. Drag was computed for angles of attack from 0° to 20°, in 2° increments. Velocity components in the axial and normal directions were found by multiplying the velocity by the cosine and sine of the angle of attack, respectively. Then, the uncoupled drag forces on the SRBs and the fuselage were computed using the above formula. These were added to find the total uncoupled normal drag force, or D_{perp}. The drag, D_b, in the axial direction was computed in an analogous manner. The forces were decomposed to find total lift and drag forces:

$$D_{total} = D_b \cos\alpha + D_{perp} \sin\alpha \qquad \text{(Eq 3.74)}$$

$$D_{total} = D_{perp}\cos\alpha - D_b \sin\alpha \qquad \text{(Eq 3.75)}$$

where α denotes the angle of attack. Lift and drag coefficients were found as follows:

$$C_{\cdot} = \frac{D_{total}}{qS} \qquad \text{(Eq 3.76)}$$

where q is the dynamic pressure at 40,000 ft and 733.3 ft/s, and S is the reference area of the Gryphon. The results are summarized in Table 3.9:

Table 3.9 Computation of drag polar

α	V_b	V_{perp}	D_b	D_{perp} SRB	D_{perp} fuselage	Total D_{perp}	Total Drag	Total Lift	C_d	C_l
0	733.3	0	6297	0	0	0	6297	0	.0198	0
2	732.9	25.6	6290	111.1	371.0	482	6303	262.4	.0198	.0008
4	731.5	51.1	6267	210.9	1482	1693	6369	1252	.0200	.0039
6	729.3	76.6	6229	486.0	3328	3814	6593	3143	.0208	.0099
8	726.2	102.0	6175	861.5	5900	6761	7056	5837	.0223	.0184
10	722.2	127.3	6108	1341	9185	10526	7842	9306	.0247	.0294
12	717.3	152.4	6025	1923	13167	15090	9030	13509	.0285	.0426
14	711.5	177.3	5929	2603	17827	20431	10693	18391	.0338	.0580
16	704.9	202.0	5819	3379	23143	26523	12901	23893	.0407	.0753
18	697.4	226.5	5697	4247	29088	33336	15714	29946	.0495	.0944
20	689.1	250.7	5561	5203	35634	40837	19186	36475	.0605	.1150

Note: In Table 3.7, V is freestream velocity and D is drag. The subscript b indicates the property is measured along the body axis, while the subscript perp indicates the property is measured in the vertical plane perpendicular to the body axis. C_d is drag coefficient and C_l is lift coefficient. Velocities are expressed in ft/s and forces are expressed in pounds. The subsonic drag polar is shown in Figure 3.6.

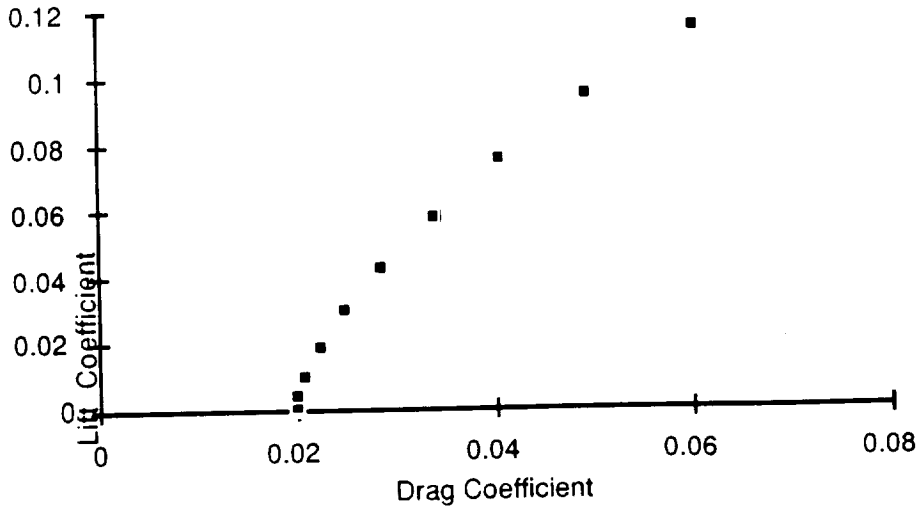

Figure 3.6 Subsonic Drag Polar

3.6.2 Supersonic Aerodynamics

The supersonic aerodynamics of Gryphon were calculated from missile aerodynamic theory. The most important factors in aerodynamics are the lift and drag of the vehicle, which can be calculated from the general equations:

$$L = \tfrac{1}{2}\rho V^2 S C_l \qquad \text{(Eq 3.77)}$$

$$D = \tfrac{1}{2}\rho V^2 S C_d \qquad \text{(Eq 3.78)}$$

Velocity can be changed into terms of Mach number, M, and the speed of sound, a.

$$V^2 = M^2 a^2 \qquad \text{(Eq 3.79)}$$

The lift coefficient, C_l, is simply a function of the angle of attack of the vehicle, α.

$$C_l = 2\alpha \qquad \text{(Eq 3.80)}$$

The reference area for lift is the base area of the vehicle, S_b. For the Gryphon, S_b= 269.02 ft^2.

Thus, the final equation for lift is:

$$L = \rho M^2 a^2 S_b \alpha \qquad \text{(Eq 3.81)}$$

Drag is more difficult to calculate. There are several types and sources of drag. Of primary concern to the Gryphon are the pressure foredrag of the rocket body, the drag due to lift, and the drag from the vertical tail. Other sources of drag are interference drag, skin friction drag, and base drag of the rocket. The total drag is the sum of the drags due to each item listed above. Directly, the total drag coefficient is the sum of the drag coefficients due to each type of drag.

$$C_d = c_{d_p} + c_{d_\alpha} + c_{d_t} + c_{d_i} + c_{d_{sf}} + c_{d_b} \qquad \text{(Eq 3.82)}$$

The drag coefficient due to pressure foredrag is taken from Figure 3.7. This graph shows the drag coefficients of cones of various thicknesses as functions of Mach number. This value will be called X in the drag equation. The pressure foredrag uses the base area of the rocket as its reference area. The Gryphon has a half-cone angle of 30°.

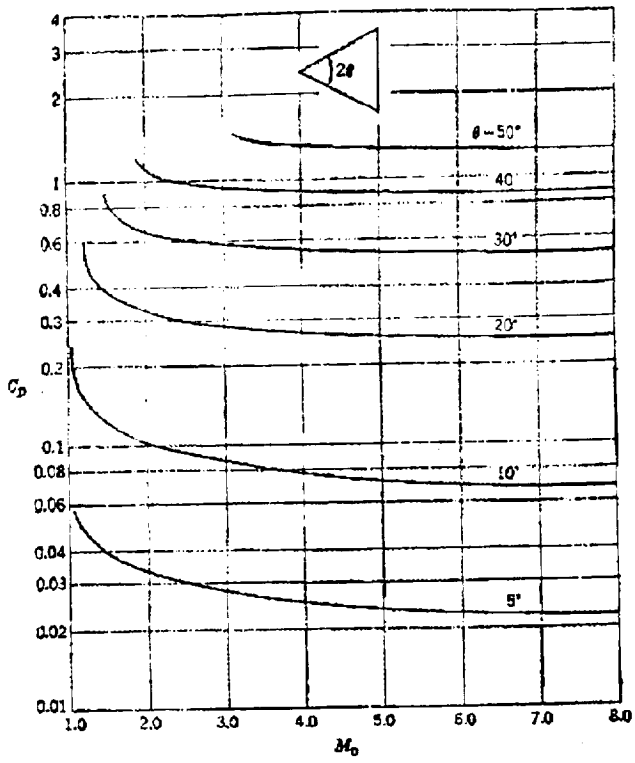

Figure 3.7 Drag Coefficients of Cones at Supersonic Speeds [Reference 94]

The drag coefficient due to lift is a function of angle of attack. The reference area for this type of drag is also the base area of the rocket.

$$c_{d_\alpha} = \alpha^2 \qquad \text{(Eq 3.83)}$$

The drag coefficient from the vertical tail is taken from supersonic wing theory and is a function of Mach number. The reference area of the tail, S_{Tail}, is the area of the tail along its chord. S_{Tail} for the Gryphon is 112.5 ft^2. The drag coefficient of the tail c_{dt}, is computed using the formula:

$$c_{dt} = \frac{4}{\sqrt{M^2 - 1}}\left(\frac{t_m}{c}\right)^2 \qquad \text{(Eq 3.84)}$$

Where t_m/c is the maximum thickness to chord ratio for the vertical tail. In the case of the Gryphon, this value is 0.10.

The interference drag, skin friction drag, and the base drag were accounted for by adding an error factor of twenty percent additional drag.

The final equation for drag is:

$$D = 0.6\rho M^2 a^2 \left\{ S_b\left(X + \alpha^2\right) + S_{Tail}\left[\frac{4}{\sqrt{M^2 - 1}} \left(\frac{t_m}{c} \right)^2 \right] \right\} \qquad \text{(Eq 3.85)}$$

where the value X is obtained from Figure 3.5.

See Appendix B for a listing of lift and drag values for Mach numbers from 1.5 to 8.0 at angles of attack from 2° to 18° for altitudes of 50,000 feet, 75,000 feet, and 100,000 feet. The supersonic drag polar is shown in Figure 3.8.

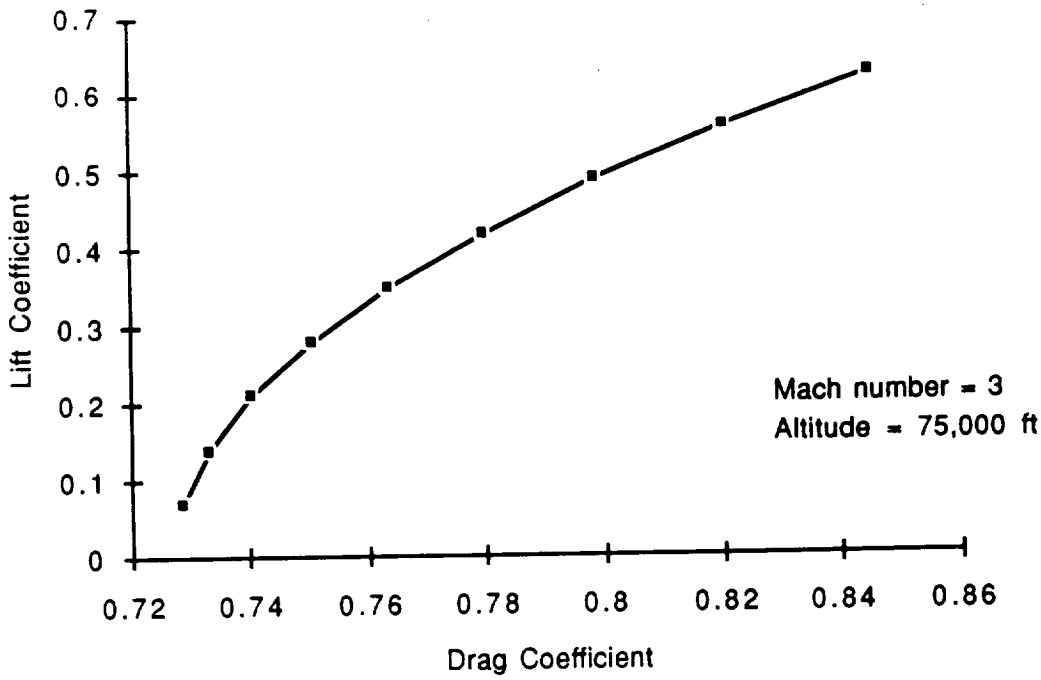

Figure 3.8 Supersonic Drag Polar

3.6.3 Center of Pressure

Another aerodynamic factor that was important to the design of the vehicle was the location of the center of pressure (CP). The CP is the point of action of the aerodynamic forces acting of the Gryphon—that is, the lift and drag can be taken as point forces acting at the CP.

For rockets, the center of pressure can be estimated by the location of the center of the projected area. Most rockets, Gryphon included, have the CP ahead of the center of gravity. With the CP ahead of the center of gravity, the vehicle is inherently unstable. The result of this instability lead to the consideration of various control mechanisms, including aerodynamic control surfaces. Table 3.10 shows the CP locations for each stage of the Gryphon. One can see that the CP is forward of the center of gravity for each stage.

Table 3.10 Center of Pressure Locations

	Center of Pressure	Center of Gravity
Stage 1, 2, 3, ANC	30.74	26.92
Stage 1, 2, 3	40.41	27.44
Stage 2, 3	59.37	40.12
Stage 3	73.47	65.34

Note: In Table 3.10, measurements are in feet from the base of the stage 1 nozzles.

3.6.4 Control Surfaces

Several of the design considerations included aerodynamic lifting and control surfaces to help control the Gryphon's attitude during the drop from the Eclipse and the initial pull up after first stage ignition. Three concepts were considered and analyzed for possible use: a delta wing lifting surface, winglet/canard pairs for pitch and roll control, and a vertical tail for yaw control.

The delta wing was designed to incorporate control surfaces that would aid in orientation control during the drop and subsequent pull up maneuver. It had the added advantage of providing lift, thereby reducing total fuel weight. However, the delta wing was found to be very heavy, compromising the possible savings on fuel. Moreover, it was very expensive, which hampered the Gryphon's ability to compete with other launch vehicles.

Since only control surfaces are necessary to keep the vehicle's attitude in check, winglets and canards were the next logical step. They would keep it properly oriented during the drop and pull up maneuvers. The winglets were to be mounted on the SRBs, while the canards were to be attached to the interstage hardware between stages two and three. Vertical tail fins were added to allow control of all three body axes.

The winglets were discarded for the following reasons:

- weight and cost were too great
- attachment to SRBs was very difficult
- The added area at the back end of the vehicle shifted the center of pressure (CP) far enough back to cause a severe pitch down motion during the drop

The canards were discarded for the following reasons:

- Roll analysis showed that the vehicle was stable enough in roll to not require roll control during the drop maneuver, despite the turbulent boundary layer around the SRBs.
- weight and cost too great

Shown in Fig. 3.9 are examples of the lifting and control surfaces considered and discarded.

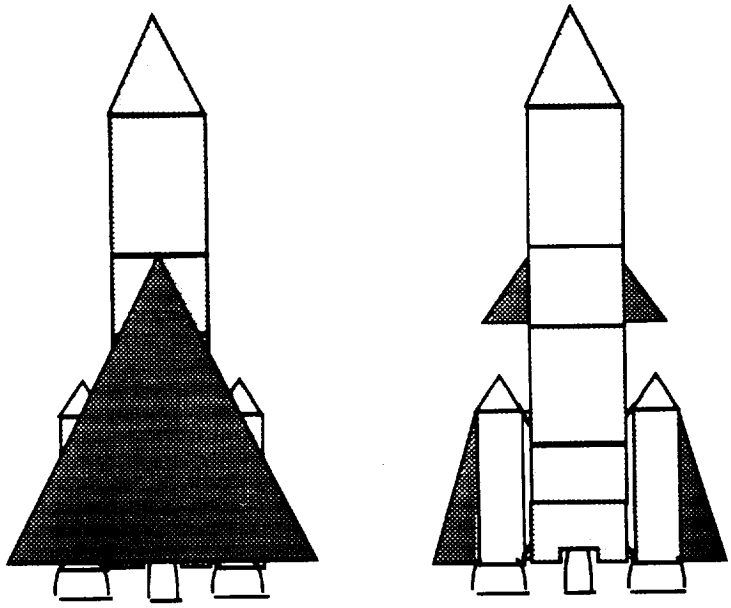

Figure 3.9 Control Surface Designs:
Delta Wing (left); Winglets and Canards (right)

The vertical tail was retained because the vehicle is unstable in yaw, requiring active yaw control during the drop maneuver. The tail, shown in Figure 3.10, was designed to counteract yaw moments created by an unsteady drop or cross winds experienced during the drop. The tail is locked in the no moment (straight ahead) direction once the rocket motors fire. The cross section for the vertical tail is that of a 10% thick diamond, and the thickest point is at the quarter-chord point. The tail is triangular in shape, having a 15 ft base chord length and a 15 ft height. This gives the leading edge a sweep back angle of 45°. The entire tail is deflectable, with the pivot point nine feet from the base of the first stage rocket nozzles.

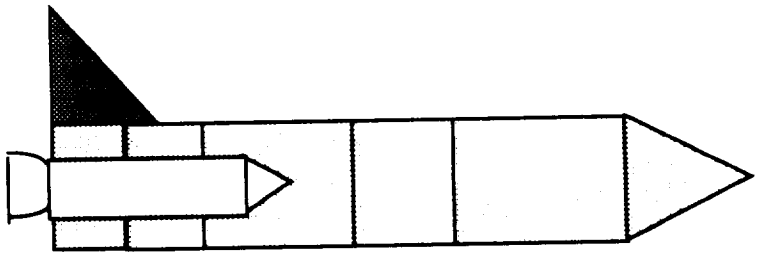

Figure 3.10 Control Surface Designs: Vertical Tail

The amount of force generated by the tail is given by the following equation:

$$F_{Tail} = \tfrac{1}{2}\rho S_{Tail} V^2 C_{l_{Tail}} \qquad \text{(Eq 3.86)}$$

The yaw moment created by the tail is:

$$M_{Tail} = F_{Tail} * (\text{Distance from tail to CG}) \qquad \text{(Eq 3.87)}$$

The angular acceleration in yaw is then found from:

$$M_{Tail} = I_{m_{zz}} \ddot{\beta} \qquad \text{(Eq 3.88)}$$

The yaw angle is then found by integrating twice

$$\beta = \tfrac{1}{2} \ddot{\beta} t^2 \qquad \text{(Eq 3.89)}$$

Note: (Eq 3.89) assumes initial conditions of $\beta_0 = 0$ and $\dot{\beta}_0 = 0$.

Table 3.11 shows the correctable yaw deviations. The values in Table 3.11 assume a drop velocity of 733 ft/s from 40,000 feet. The table uses a lift coefficient of 0.8 for lift (horizontal) from the vertical tail. The table also uses moment arms of 17.92 feet when the ANC is attached, and 18.44 feet once the ANC is detached.

Table 3.11 Correctable Yaw Angles

Time of Correction (sec)	Angle Correctable With ANC (deg)	Angle Correctable Without ANC (deg)
1	0.032	0.034
2	0.128	0.136
3	0.289	0.306
4	0.514	0.544
5	0.802	0.851
6	1.156	1.225
7	1.573	1.668
8	2.055	2.178
9	2.601	2.756
10	3.211	3.403

3.6.5 Aft Nozzle Cover Design

The aft nozzle cover (ANC) was designed to reduce the drag of Gryphon while it is being carried by the launch plane. See Appendix B for a four view diagram of the ANC. Since the ANC is dropped into the ocean following separation from the plane, the goals for this design were to make it as light as possible and as inexpensive as possible. Initial designs have the ANC being constructed out of reinforced molded fiber glass, this should reduce weight, while giving the ANC enough strength to support its own weight and any loads incurred during the plane flight, separation and drop.

3.7 MISSION TIMELINE

The Gryphon will be assembled in three phases that will each take 4 weeks to complete; leading to a total of 12 weeks of construction and assembly. The flight and post flight operations will take a total of 5 weeks; therefore, the overall length of a mission will be 17 weeks.

The first building stage involves receiving the motors, building the individual stages, and then doing pre-mate testing before moving on to the integration stage. The

second building stage is when the stages are integrated together and the mated vehicle is tested before the payload is added. During the third building stage, the payload is received and mated to the vehicle itself. Final systems tests are then performed and the fairing is mated to the vehicle.

After the vehicle is completed, there is a launch readiness review to ensure that the vehicle is ready, and the vehicle is then mated to the launch aircraft during the hours preceding launch. Fuel will be manufactured on site and added to the vehicle after it is mated to the aircraft. Final tests are then done on the mated vehicle. During this period the crew is being briefed and the vehicle is then ready for launch.

Immediately after the launch, the flight crew is debriefed. There is a post flight analysis leading to a post flight review. During this time, facility maintenance is also performed. The individual mission is then complete. See Appendix B for a pictorial view of the mission timeline.

3.8 FUTURE WORK

3.8.1 Trajectory Optimization

Currently, the Gryphon's ascent trajectory is not optimized. This is critical to maximizing the Gryphon's payloads. A computer model of the Gryphon was generated for use with the Simulation and Optimization of Rocket Trajectories (SORT) program from Lockheed Engineering and Sciences Corporation. However, the trajectory has not been successfully optimized.

Additionally, as the Gryphon's design specifications evolve, subsystem weights and aerodynamic data will change. Since this information is critical to modeling the ascent, a new trajectory must be calculated for each new design.

3.8.2 Orbital Maneuvers

When deploying multiple payloads to GEO, the orbiter might need to remain in GTO for multiple orbits before it reaches the appropriate GEO insertion position. A potential GEO insertion point is reached every time the orbiter reaches apogee on its GTO; this point is rotated 159.2° around the circular GEO from the previous insertion point. Given this lack of control over the insertion points subsequent to the first, a large number of GTO orbits may be required before reaching the proper position. This is not optimal, as the Gryphon has limited power supplies. To decrease the time interval between multiple GEO payload deployments, the remaining fuel in the third stage RL10A-4 can be used to rotate the geotransfer orbit.

If a radially directed force, F_r, is applied to the orbiter, the argument of perigee, ω, will change according to (Eq 3.90):

$$\frac{d\omega}{dt} = -\frac{\sqrt{1-e^2}}{e\sqrt{\mu/a}} F_r \cos\nu \qquad \text{(Eq 3.90)}$$

Note: $d\omega/dt$ is maximized at perigee, i.e. when $\nu = 0°$.

This essentially rotates the orbit about the center of the Earth, and can be controlled so as to move the apogee of GTO to the desired position of deployment for the second payload. The payload can then be deployed on the second orbit.

3.8.3 Aerodynamics

Currently, all aerodynamic data is based on calculations from theory. To make high-fidelity predictions of the Gryphon's aerodynamic behavior will require testing of a detailed scale model in a supersonic wind tunnel. This would give a truer picture of the aerodynamic forces and moments acting on the Gryphon.

The vertical tail also is not optimized. An optimally sized tail would increase yaw control and reduce drag and weight. Yaw-roll coupling effects from the tail have not been studied in detail, a step that would certainly be necessary to accurately control the Gryphon. Also, an interference analysis of the vertical tail and the airplane attach structure needs to be performed

The aft nozzle cover and payload shroud would also benefit from optimal sizing, which would reduce drag and weight. ANC separation techniques also must be studied so as not to damage the rocket nozzles or SRBs upon separation.

PROPULSION

Chapter Four

4.1 INTRODUCTION

The single purpose of any rocket propulsion system is to provide necessary thrust for the delivery of payload to a determined destination. In order to accomplish this task the system will consist of engines, propellant feed systems, and propellant tanks. This chapter will introduce the design of the Gryphon's propulsion system and the accompanying systems required to get the selected payload into orbit.

When designing the Gryphon's propulsion system three goals were recognized. The first goal highlights the safety of the vehicle. This space booster is attached to an aircraft (Eclipse) carrying crew members. Dangers of the different propellants had to be explored to minimize potential hazards to these humans and the airplane. The second goal of the propulsion system was that it would have the minimal amount of complicated connections with the aircraft. The third goal involves weight. The vehicle weight limit was designated to be 500,000 lb. This required a study into high performance engines that would give as much thrust as possible for minimal propellant. Consequently, the final design resulted in the Gryphon's three stage system composed of: (1) two Castor 120s and one LR91-AJ-11, (2) two LR91-AJ-11s, and (3) one RL10A-4. The following discussion describes the final configuration that was selected by the propulsion design team and the process that guided the team members to that decision.

4.2 ENGINES

The most basic structure of a propulsion system begins with its engines. Engine choice depends on several factors: the selection of fuel, the performance required from the system, the weight of the entire system, and cost. These four factors determined the final selection of engines to be the Morton Thiokol Castor 120, the Aerojet LR91-AJ-11, and the Pratt & Whitney RL10A-4.

4.2.1 Morton Thiokol Castor 120 Solid Fuel Rocket Engine

The purpose of the first stage engine is to produce enough thrust to overcome the large pull of gravity close to the Earth's surface. Because the vehicle is so heavy and contains the entire staging system, work horse solid engines are used instead of the more efficient

liquids. These solid engines are simpler in design than their liquid counterparts and are more easily handled as strap-on engines than the liquids.

The easiest decision made by the propulsion design team was the powerful engine to use for the first stage. Orbital Sciences had suggested the Thiokol Castor 120. This engine was developed as a cooperative effort between Orbital Sciences and Thiokol Corporation specifically with the Pegasus and Taurus programs in mind.

Performance

The Castor 120 was developed as a high reliability, expendable, low cost engine. The engine's main purpose was seen as first stage or strap-on type usage. The basic idea was to function in a ship-stack-shoot scenario. This scenario allows for fast assembly and modification of any space vehicle to fit to a particular payload. Industry's objective with this engine was to shoot for 99.9% reliability and to cut production costs by 50%. This is accomplished using new technology for case construction as well as a simplification in manufacturing.

The following data provides a performance overview of the Castor 120. All data was obtained through the cooperation of Orbital Sciences and Thiokol Corporation.

Table 4.1 Castor 120 Engine Parameters

Average Vacuum Thrust (lb)	403,759
Specific Vacuum Impulse (lbf-sec/lbm)	292
Expansion Ratio	17:1
Action Time (sec)	78
Total Engine Weight (lb)	117,687
Propellant Weight (lb)	108,159
Length (ft)	30
Width (ft)	10
Cost ($)	4,500,000

The first step in producing a Castor 120 is the mixing of the propellant. The propellant is a base of hydroxy-terminated poly-butadiene (HTPB) with a short mix cycle and has a Department of Defense classification of 1.3 (non detonable). Once the propellant has been mixed and poured into the mold, it is then allowed to cure. When this process is complete, the mandrel is removed and the inner layer of the grain is machined and conditioned for proper use. The Castor 120 is built with a carbon epoxy case structure. This case is manufactured through a continuous winding process which cuts manufacturing time by 65%. After the case is wound, the motor is fitted. The last step involves installation of the igniter and final inspection before shipment (See Figure 4.1 for Castor 120 components).

Thrust Vector Control

The Castor 120 motor may be fixed or vectorable. The vectorable version utilizes a cold gas blow down system for thrust vector control. This system employs helium to control the hydraulic actuators. The actuators allow the engine to rotate about a flex bearing $\pm 5^{\circ}$ from the home position in all 360° of its exit plane. Sensors located on the Gryphon analyze position and then send signals through the system computer to the actuators on

the Castor engines. This signal is then sent through the hydraulic system to maneuver the nozzle into the proper orientation.

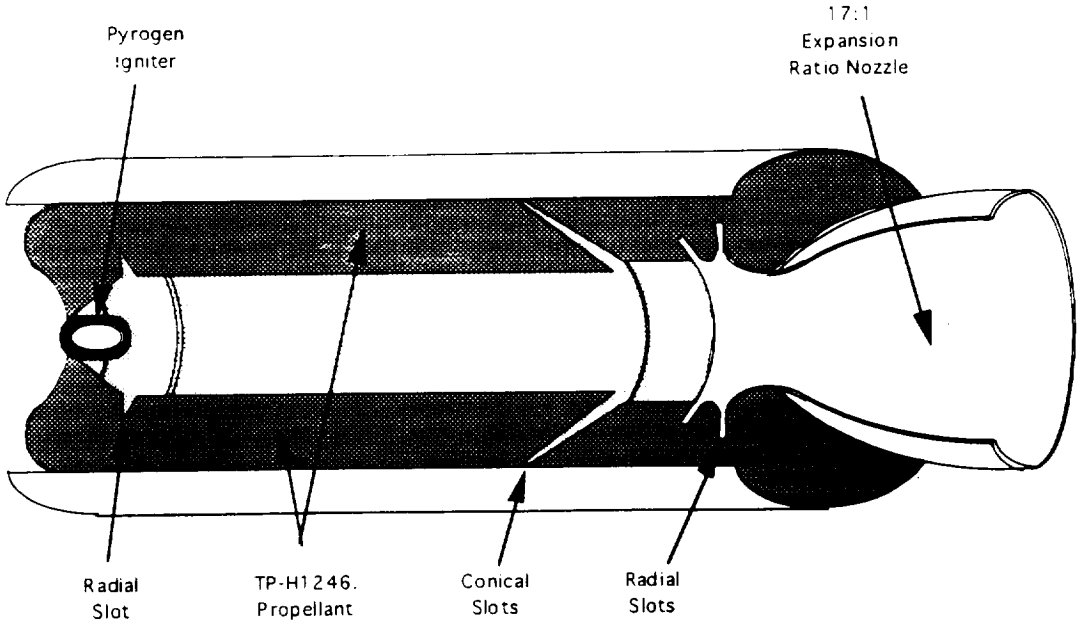

Figure 4.1 Castor 120 Propellant Grain and Engine Components

Ignition and Burn

The Castor 120 utilizes a pyrogen igniter to start its combustion. The igniter receives a 28 V impulse from the flight computer as the start up signal. Once ignition has occurred, combustion is unalterable and will continue burning until all fuel has been consumed. The grain of the Castor is manufactured in a progressive burning, cylindrical shape. There is a radial slot cut into the core at the igniter. Towards the nozzle end of the grain, conical slots are cut followed by radial slots located directly forward of the throat. (See Figure 4.1)

Conclusion

The Castor 120 is the solid, workhorse engine of the Gryphon's propulsion system. The objectives of its design coincide with the description of the space booster's ship-stack-shoot mission. An engine was needed that would be easy to manipulate, cost effective, and expendable. The simplified manufacturing process causes this engine to be affordable and readily available; therefore, we concluded that it was the perfect choice for our lead-off leg in the propulsion system.

4.2.2 Aerojet LR91-AJ-11 Liquid Fuel Rocket Engine

The Gryphon space booster uses a storable liquid fuel propulsion system in the first and second stages. This turbopump-fed rocket engine is designated as the Aerojet LR91-AJ-11 and develops about 105,000 lb of thrust in vacuum. The LR91 uses storable, hypergolic liquid rocket propellants. The fuel is Aerozine-50 which contains approximately 50% hydrazine and 50% unsymmetrical dimethylhydrazine (UDMH). The oxidizer used with these fuels is nitrogen tetroxide (N_2O_4). The engine itself

consists of various subsystems. These include the inlet pump suction lines, turbopump assembly, pump discharge lines, thrust chamber valves, gas generator system, fuel and oxidizer injector, thrust chamber, ablative skirt, roll control assembly, autogenous pressurization system, control and instrumentation harness, and engine frame (See Appendix C for diagrams).

Performance

The fuel and oxidizer are ducted from the storage tanks to the LR91 through the suction lines. The fuel is then directly brought into the turbopump assembly. This turbopump is driven by a 2000 horse-power turbine and pressurizes the propellants by more than 1000 psi. Because of the tremendous increase in pressure, the propellants are forced through the discharge lines and into the thrust chamber. At this point, valves are used to control the flow of propellants into the thrust chamber for the purpose of starting and shutting down the engine. The LR91 thrust chamber valves are not used for throttling since the engine does not have such a capability. Some of the propellant is ducted from the discharge lines to a gas generator. This generator is used to drive the turbine which maintains proper propellant flow rate (See Table 4.2). The combustion, which takes place in the thrust chamber as a result of mixing the propellants, produces a gas with pressure greater than 800 psi and temperature in the range of 5000 °F.

Table 4.2 LR91-AJ-11 Performance Parameters

Thrust Vacuum (lb)	105,000
Specific Impulse (sec)	316
Mixture Ratio	1.86
Expansion Ratio	49.2:1
Chamber Pressure (psia)	860
Service Life-Nominal (sec)	247
Oxidizer Flow Rate (lb/sec)	213.9
Fuel Flow Rate (lb/sec)	12.5
Weight (lb)	1298
Height (in)	110
Width (in)	64
Cost Per Engine ($)	1,200,000

Pressurization System

Maintaining the right level of propellant tank pressurization during engine operation is very important for the pumps to operate properly and for maintaining the structural integrity of the propellant tanks. In the LR91, the propellant tanks are pressurized on the ground, before engine start-up, using high pressure gaseous nitrogen. Just before lift-off, the nitrogen tanks are disconnected and the propellants tanks are sealed. In the case of the Gryphon, propellant tanks are pressurized on the ground right before the Eclipse takes off with the Gryphon under its belly, and sufficient pressure is maintained until the Gryphon is launched about three to five hours later. Initially this provides sufficient inlet pressure for the engine pumps to function. However, during operation, there is a pressure loss because propellants are constantly being removed from the tanks. To compensate for this loss, an autogenous (self-generating) system is used. This self-generating system uses cooled gases from the turbine inlet to pressurize the fuel tanks. The oxidizer tank is

pressurized by oxidizer which has been heated to a gaseous state by a heat exchanger in the turbine exhaust.

Electrical Systems

The main purpose of the instrumentation harness on the LR91 engine is to carry signals from various engine transducers. These transducers measure parameters such as propellant tank pressure, thrust chamber temperature, propellant flow rate etc. These signals are then converted using adapters and AC/DC converters and conducted through the instrumentation harness to the flight control computers. The flight computers then relay this engine performance data to ground receiving stations.

Thrust Vector Control

Pitch and yaw thrust vector control is achieved by pivoting the thrust chamber on a gimbal bearing mount. The gimbal assembly allows the thrust chamber to move 3.5° in both pitch and yaw directions. With snubbing and over travel, the thrust chamber is able to move a maximum of 4.9° from a neutral position. Gimbaling the two LR91 thrust chambers in the second stage can provide control in all three axes. However, in the first stage there is only one LR91 thrust chamber. In this case, a separate source of thrust for roll control is usually necessary since one thrust chamber can only provide thrust for pitch and yaw control. This thrust is then provided by directing the turbine exhaust through a nozzle. This nozzle can develop 860 lb of roll control thrust and can be swiveled $\pm 35°$ from a neutral position. In the case of the Gryphon, the first stage configuration is such that the LR91 operates simultaneously with the Castor 120 solid rocket boosters. These boosters have gimbaling capabilities; therefore, the LR91 turbine exhaust can be directed straight down for additional thrust and does not have to be used as a roll control thrust vector device.

Engine Operation

The LR91 engine does not require thrust control systems because it is hydraulically balanced. The oxidizer flow rate is preset at 213.9 lb/sec, while the fuel flow rate is preset at 120.5 lb/sec. The gas generator of the turbine is hydraulically set for a steady-state level thus establishing a set propellant flow rate and constant turbine speed over a wide range of downstream pressures. Although this leads to greater reliability and functional simplicity, there is one design tradeoff. The LR91 cannot be throttled to a desirable thrust level. The engine also does not require an ignition system since it uses hypergolic fuels i.e. the fuel and oxidizer combust spontaneously upon contact. The absence of an ignition system is beneficial since it makes the engine lightweight and less complex. The LR91 engine has demonstrated the ability to shutdown and restart again in ground tests; however, this capability is still in the developing stages and has not been used in practice. The shutdown command is automatically given when decreased acceleration is detected due to fuel exhaustion.

To begin engine operation, prevalves which are located in the tank-engine interface are opened. These valves are used to prevent propellants from entering the engine before they are required to do so. When these prevalves are opened, the engine is filled with oxidizer and fuel and electric signals are readied to receive startup signal. Releasing the prevalves also leads the engine to the bleed process. This process is necessary to insure that no air is left in the propellant lines. Once the bleed process has begun, about 1200 cc of propellant is flown over board per minute through a drain line until the process is stopped by starting the engine.

To start the engine, a 28 V DC signal is received from the flight computers and applied to a solid propellant cartridge mounted on the turbine inlet. This causes the turbine to accelerate and start fuel and oxidizer pumps. It takes about 0.9 seconds for the thrust chamber valves to completely open. As soon as the valves begin to open, oxidizer is pumped into the combustion chamber. The fuel is first directed into steel tubes used to cool the combustion chamber walls, and then the liquid is allowed into the fuel injector. As fuel and oxidizer are finally mixed in the thrust chamber, there is hypergolic combustion. A small amount of propellant is also forced into the gas generator. The gas generator begins to operate and supplies gas to run the turbine. This completes the starting procedure and the engine reaches its normal operating level within approximately one second of receiving the start signal.

4.2.3 Pratt & Whitney RL10A-4 Liquid Fuel Rocket Engine

The third and final stage of the Gryphon's propulsion system is used only for Geosynchronous Transfer Orbit (GTO) missions. This stage carries the payload from Low Earth Orbit (LEO) to the higher GTO For a third stage engine the choice had to have high performance characteristics as well as an exceptional reliability rating. Several engines were considered which utilized solid fuels, storable liquid fuels, and cryogenic fuels. Our final choice was the Pratt & Whitney RL10A-4.

Engine Choices

One category of motors that was considered were the Orbus motors from United Technologies. These have been used in upper stages as well as in maneuvering vehicles for satellites. Unfortunately, the Orbus motors had a higher thrust rating and a lower specific impulse than could be used for the final stage. This last reason caused them to be disregarded in the analysis. (See Table C.1)

A second engine that was considered was the Castor XX. This is a smaller engine than the Thiokol Castor 120. It produces about half the thrust and burns for a much longer time than the 120. However, the performance of this engine was still too low to be effective for the third stage. (See Table C.1)

The final third stage choice was the Pratt & Whitney RL10A-4. The earlier A-3 model was the original selected engine, but through numerous iterations we determined that only one A-4 could take the place of two A-3 engines. As a cost saving measure and reliability factor we decided to use one A-4. (See Table C.1)

Performance

The RL10A-4 is a regeneratively cooled engine that is fed by a turbopump system. It has a single combustion chamber, and the updated model has a 20 inch extension on the nozzle skirt which deploys prior to engine start. All of the A-4's valves are actuated with helium, and the helium supply is controlled by electronically actuated solenoids. This engine is flexible for use because it is vectorable and can withstand multiple starts. These last two points combined with its well known reliability made it the most attractive of all the engines under consideration. The only drawback is that it consumes cryogenic fuels. Both the Gryphon and Eclipse Design Teams wanted to avoid liquid fuels, especially cryogenics, as much as possible. However, the RL10 was seen as the best alternative. (See Section 4.2.4 for details)

The following is a list of performance parameters on the RL10A-4. All information was obtained through the courtesy of reference 133:

Table 4.3 RL10A-4 Basic Engine Parameters

Thrust (Lb)	20,800
Specific Impulse (sec)	449
Mixture Ratio	5.5:1
Expansion Ratio	84:1
Chamber Pressure (psia)	564
Nominal Run Time (sec)	380
Engine Weight (lb)	370
Length (ft)	8
Width (ft)	4
Cost ($)	1,200,000

The RL10A-4 requires delicate handling because of its propellants. Cleanliness is required, and purging of the fuel and handling systems is necessary prior to use. If any foreign matter is encountered by the propellants, an explosion could result. The purging is accomplished by running helium through all lines and chambers before the propellants encounter the engine system.

Operation and Tank Pressurization

Upon start up, the propellant tanks have been pressurized with helium. A 28 V signal is received from the system computer which allows the propellant supply valves to open. Small amounts of liquid are allowed into the spark chamber where the igniter activates for at least one second. This allows the combustion process to begin which starts hot gases flowing through the turbine to turn the shafts of the oxygen and hydrogen fuel pumps. Some of this hot turbine gas is bled off and used to pressurize the liquid hydrogen tank. As the liquid oxygen moves into the combustion chamber, some of the liquid is removed and allowed to change into a gas with the help of a heat exchanger. This gas is then rerouted back to the liquid oxygen tank and is used as the pressurizing gas, see Figure 4.3.

Thrust Vector Control

The thrust vectoring on the RL10A-4 is accomplished through a universal bearing system like the one discussed for the Castor 120. The gimbal assembly is composed of (1) a pedestal, (2) a conical engine mount, and (3) a spider block. This assembly enables the engine to be gimbaled $\pm 4^{\circ}$ from its neutral position in a square pattern (See Figure 4.2). This allows for control over pitch and yaw maneuvers of the vehicle.

Conclusion

The Pratt & Whitney RL10A-4 is a versatile engine with excellent performance characteristics. Its performance and reliability ratings are impressive, and the vectorability makes it even more attractive. By comparison, it overwhelmingly out-classed any engine that we considered and made it possible for the Gryphon to reach its payload goals.

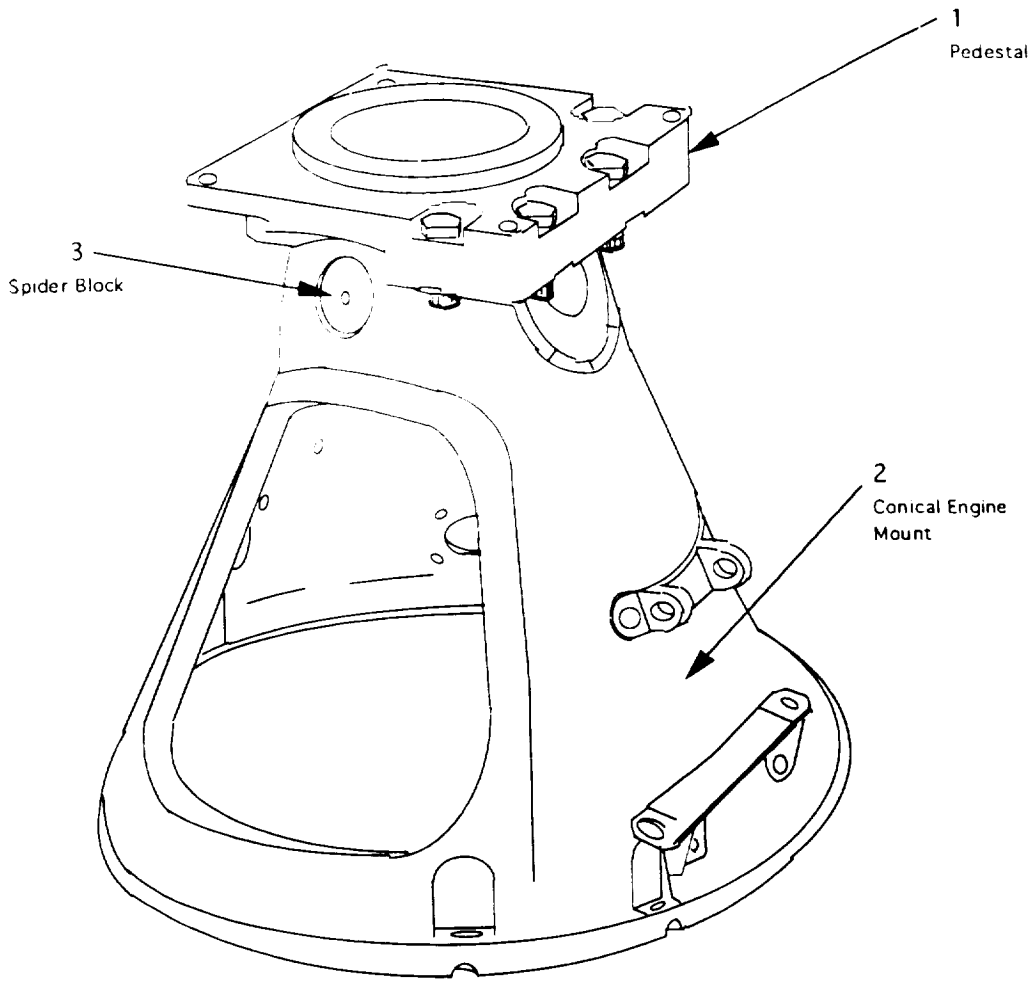

Figure 4.2 RL10A-4 Gimbal Mount

4.2.4 Conclusion

The Gryphon's propulsion system had several constraints that led to the final choice of engines. The first constraint was a safety concern by the Eclipse Design Team against using cryogenic propellants. Due to the hazardous nature of these chemicals, the contract between the two groups stated that usage of cryogenic propellants was to be kept to an absolute minimum. The second constraint was simplicity. This design project was given a completion time of four months. In that amount of time, a complete propulsion system had to be constructed with as much detail as possible. This made an entirely solid propellant system very attractive. A solid propellant system would make the design job much easier because each engine could be treated as a single unit. It would be possible to avoid designing fuel tanks and feed systems as well as baffles, diaphragms, insulation, and pressure systems. A final constraint was the concern of handling different kinds of propellants. Solid propellants are the easiest to handle because they are all prepackaged. Storable liquids are hazardous but can be safely used if proper precautions are observed. Cryogenic propellants can also be used safely, but their boil-off ability made them unattractive for a delay of four hours while the plane flies to the designated drop zone. All of these factors were considered when this propulsion system was being designed. It

was only through many iterations that the Castor 120, LR91-AJ-11, and RL10A-4 were chosen.

4.3 STAGING

The staging of a booster is a critical part of the propulsion system. It is an integration of every piece of hardware and every pound of matter that composes the vehicle. The three main variables of staging calculations are weight, velocity, and specific impulse. It is the combination of these numbers that permits or denies a given payload to reach the desired orbit. The following discussion is a presentation of the methods and calculations used to determine the staging configuration for the Gryphon.

4.3.1 Weight

The overall design goal of the Gryphon was to place 8,000 lb into GTO with a gross lift off weight of less than 500,000 lb. Three stages are used to achieve this goal, not including the launch aircraft. The first two stages reach Low Earth Orbit (LEO), and the final stage takes the payload to Geosynchronous Transfer Orbit (GTO).

Overall Weight

The Gryphon has a gross lift off weight of 465,059 lb. This is the weight of the Gryphon at the time of stage one ignition. Table 4.4 is a breakdown of the weight by stage. The following paragraphs describe the weights of each stage.

Table 4.4 Overall Weights

Payload	5,575 lb
Gross weight stage 3	12,748 lb
Gross weight stage 2	173,235 lb
Gross weight stage 1	273,501 lb
Gross lift off weight	465,059 lb

Stage 1
Stage one consists of an Aerojet LR91-AJ-11 and two Morton-Thiokol Castor 120 engines. The engines require 242,877 lb of propellant. The propellant is divided into 26,703 lb for the LR91 and 216,174 lb are for the Castor 120s. A total of 651 lb of liquid propellant for the LR91 remains unused.

The first stage weighs 30,624 lb dry (no fuel). The engines are 18,372 lb, 1,300 lb for the LR91 (nozzle and thrust chamber) and 17,072 lb for the two Castor 120s (casing and nozzle). Inert weight is 12,252 lb. Inert weight is structural materials, tanks, etc., engines are not included, and this inert weight remains with the stage through burnout. Included in this weight is 6,200 lb for the payload shroud. Although the payload shroud is not physically located on the first stage, its weight is included there because it is jettisoned shortly after first stage burnout. This fact is used by the performance spreadsheet described in Section 4.3.3. Other inert weights on the first stage are the tanks for the LR91, a vertical tail and the struts connecting the two Castor 120s to the center

body. Table 4.5 lists the overall weights for Stage 1, see Chapter 1 for a detailed breakdown of the components and weights of Stage 1.

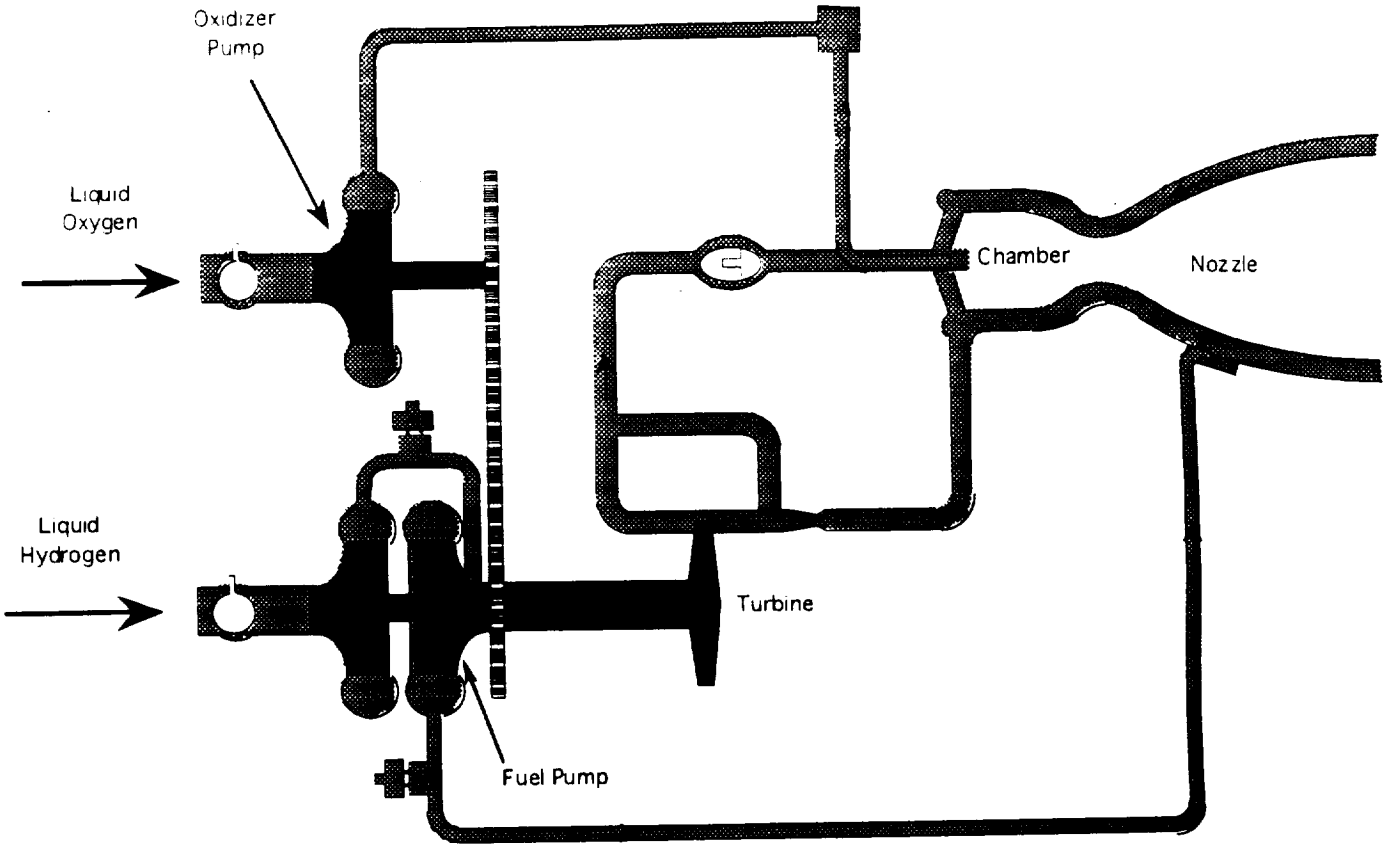

Figure 4.3 Propellant Flow Schematic for RL10A-4

Table 4.5 Stage 1 Weights

Dry Weight	30,624 lb
Propellant	242,877 lb
Gross Stage Weight	273,501 lb

Stage 2

Stage two is powered by two Aerojet LR91 engines. Each engine weighs 1,300 lb. The engines require 164,000 lb of propellant of which 4,000 lb is unused. This unused propellant is caused from losses of liquid trapped in fuel lines and adhering to tank walls. The dry weight of the stage is 9,235 lb. The fuel tanks weigh 2,500 lb. The gross weight of the stage is 173,235 lb. The Gryphon will be in a LEO upon stage two burnout. Table 4.6 lists the overall weights for the second stage, see Chapter 1 for a detailed breakdown of the components and weights of stage two.

Table 4.6 Stage 2 Weights

Dry Weight	9,235 lb
Propellant	164,000 lb
Gross Stage Weight	173,235 lb

Stage 3
Stage three is the upper stage that boosts the payload from LEO to GTO. The stage is powered by one Pratt & Whitney RL10A-4 engine. The engine weighs 370 lb and has 8,246 lb of propellant, of which 201 lb are unused. Similarly to Stage 1, this unused propellant is due to trapped liquid in lines and adhering to walls. The stage carries a payload of 5575 lb which is less than the 8000 lb goal. The reason for the reduction in payload will be discussed in the paragraph below. The dry weight is 4502 lb. Included in the third stage is the avionics, power and thermal control system. The stage has a gross weight of 12,748 lb. Table 4.7 lists the overall weights for the third stage, see Chapter 1 for a detailed breakdown of the components and weights of Stage 3.

Table 4.7 Stage 3 Weights

Payload	5,575 lb
Dry weight	4,502 lb
Propellant	8,246 lb
Gross Stage Weight	12,748 lb

4.3.2 Performance

Velocity Requirements

The velocity Gryphon is required to achieve is dictated by its mission. The basic mission consists of launch to LEO, followed by the third stage boosting the payload into GTO. In order for the Gryphon to be in LEO after second stage burnout it must reach the orbital velocity for this altitude. For LEO this velocity is 24,934 ft/s, corresponding to an altitude of 250 nautical miles. The velocity increment needed to enter GTO from LEO is an additional 7934 ft/s. This velocity is only provided by the third stage. For missions to LEO the third stage engine and propellant system is omitted and replaced by payload.

Ideal Velocity

The velocity that a rocket achieves in ideal conditions (no drag, no gravity) depends on the Specific Impulse of the engine (Isp) and the Mass Ratio (R)--(See Table 4.8) which is defined by equation (4.1). Since the Gryphon is a staged rocket the velocities of each stage are added together for the final velocity. Velocity increment ΔV is related to Isp and R by the following equation:

$$R = \frac{M_o}{M_f} \qquad \text{(Eq 4.1)}$$

$$\Delta V = I_{sp} \times g \times \mathrm{Ln}(R) \qquad \text{(Eq 4.2)}$$

where M_o and M_f are the initial and final masses of the stage and g is the acceleration of gravity equal to 32.174 ft/s^2. The Isp, in units of seconds, is a measure of engine performance and efficiency. Isp is total thrust divided by weight flow:

$$I_{sp} = \text{Thrust} \div \left[\frac{dm}{dt} \times g\right] \qquad \text{(Eq 4.3)}$$

Table 4.8 Engine Specifications

	Isp (sec)	Thrust (lb)	Weight Flow (lb/sec)
Castor 120	291.5	404,000	1,386
LR91	316	105,000	334
RL10A-4	449	20,800	44.5

Because specific engines have been chosen, Isp is fixed. Velocity is added or taken away as needed by varying the mass ratio. The speed is increased by adding propellant or removing payload or inert weight, and it is decreased by removing propellant or increasing payload or inert weight. However, adding or subtracting weight from one stage affects the performance of the earlier stages. To keep track of these changes a spreadsheet was programmed. This spreadsheet will be explained in more detail in Section 4.3.3. Table 4.9 lists the Isp, mass ratio and ideal ΔV for each stage.

Table 4.9 Stage Performance

	Isp (sec)	Mass Ratio	Ideal ΔV (ft/sec)
Stage 1	295	2.09	6,983
Stage 2	316	6.07	18,335
Stage 3	449	1.78	8,352

Velocity Losses

Ideally, the Gryphon's engines provide enough velocity for the LEO and GTO requirements. However, the Gryphon will experience velocity losses due to gravity, drag and atmospheric effects. Rising against a gravitational field, the Gryphon will lose kinetic energy as its gravitational potential energy increases. For a rocket directly opposing gravity (vertical flight) this energy conversion will cause a negative velocity increment:

$$\Delta V = -g \times T_b \qquad \text{(Eq 4.4)}$$

where T_b is the burn time. The acceleration from gravity is considered a constant during the burn time. Equation (4.4) gives the maximum velocity loss caused by gravity. If the rocket is not in vertical flight, the gravity loss is calculated using a specific angle from the vertical. This is determined by the trajectory, and a more detailed analysis of this loss may be seen in Chapter 3.

During Stage 1, the Gryphon must also overcome drag. Drag will reduce the velocity of the first stage at burn out, the second stage and third stages are assumed to operate in a vacuum. Precise calculation of the drag loss requires detailed knowledge of the variation of drag with time. This information was unavailable during this design phase, so a value was assumed. The amount of loss assumed during the design process was 750 ft/s. This figure was representative of the drag loss of ground launched rockets. Air launching means the Gryphon starts above 75% of the atmosphere which

considerably reduces the drag loss compared to other launch systems. An empirical method for determining the drag loss was found; however, its results were not plausible, see Section 4.3.3.

Atmospheric pressure also causes velocity to be reduced. More specifically it lowers thrust and consequently lowers Isp. The thrust of a rocket engine is given by the following equation:

$$T = \left[\dot{m} \times V_e\right] + \left[\left(P_e - P_\infty\right) \times A_e\right] \qquad \text{(Eq 4.5)}$$

where $\dot{m}$ is the mass flow rate, V_e is the exhaust velocity, A_e is the exit area, P_e is the exhaust pressure, and P_∞ is the ambient pressure. The Isp's specified earlier are measured in a vacuum, $P_\infty = 0$. At the launch altitude of 40,000 ft, $P_\infty \neq 0$. Calculation of velocity loss is difficult due to the variation of P_∞ with altitude and the variation of thrust produced by the solid rocket boosters. A method was found to estimate the loss from a ground launched rocket. The total loss for a ground launch was no more than 500 ft/s. Again the Gryphon has the advantage of launching at an altitude where the pressure is 25% that of sea level. This effect was combined into the assumed drag term discussed above.

Velocity Gains

Two effects of the launching technique improve the Gryphon's performance. The first is the rotation of the Earth. Launching the Gryphon eastward provides an additional 1,342 ft/s. The actual amount depends on the launch latitude and the azimuth angle of the trajectory. Launches to polar orbits would not have this benefit and would have a reduced payload as a result.

The Gryphon also benefits from the velocity of its launch vehicle, the Eclipse. The Eclipse and the Gryphon travel at a velocity of 733 ft/s prior to launch. The two effects combine for a velocity gain of 2,075 ft/s.

Burn Time & Service Life

Burn time (T_b) is controlled by two factors , the service life of the engine and the amount of propellant carried by each stage. The selection of Castor 120 solid rocket motors for the first stage fixed the burn time of the first stage at 78 seconds. This is the service life of the Castor 120. The amount of liquid propellant in the first stage is the amount required to fuel the LR91 for the same 78 seconds.

The burn time of the second stage is limited by service life as well. The LR91 has a nominal service life of 247 seconds. At a weight flow of 334 lb/s each and a service life of 247 seconds, two LR91s can burn 165,000 lb of propellant. This is the maximum amount of propellant that can be used by the second stage. The propellant of the second stage was fixed at 160,000 lb. This allows the engines to burnout and use thrust vector control which will extend burn time before service life expires.

The burn time of the RL10A-4 is controlled by the amount of propellant. The RL10 burns propellant at a rate of 44.5 lb/s. There are 8,045 lb of usable propellant on the third stage, resulting in a burn time of 181 seconds. Table 4.10 lists the service lives and burn times of the engines for each stage.

Table 4.10 Service Lives & Burn Times

Engine	Service Life (sec)	Burn Time (sec)
RL10A-4	380	181
LR91 (stage 2)	247	239
LR91 (stage 1)	247	78
Castor 120	78	78

Acceleration-Loads

Longitudinal acceleration loads, g-loads, of the Gryphon equals its thrust to weight ratio at all times. Physically, one pound force will accelerate one pound mass at 1g. Table 4.11 lists the extremes of the thrust to weight ratio, which occur at stage ignition and stage burnout. These are longitudinal g-loads only. Lateral loading requires the engines Power Spectral Density (PSD) which was not available.

The g-loading at Stage 2 burnout is 6.65 g. This value exceeds the recommended maximum value of 5.5. The high g-loading is due to the high mass ratio of stage two. The LR91 is not throttlable, thus it produces the full thrust of 210,000 lb even when the vehicle only weighs 31,558 lb. The structure of Stage 2 and 3 had to be designed to withstand these higher g-loads.

Table 4.11 Thrust to Weight Ratios

Stage	Ignition	Burnout
1	1.96 g	4.10 g
2	1.10 g	6.65 g
3	1.12 g	1.99 g

4.3.3 Methods

Performance Spreadsheet

The performance of the Gryphon is evaluated by solving equations (4.1), (4.2) and (4.5). At first this was done by hand. It was a slow process and had to be repeated for the entire vehicle if any changes were made. To save time and to keep a total of all weights, a spreadsheet was developed. The program can be found in Appendix C. Given the vehicle weight, mass of propellant, and Isp the program evaluates the mass ratio and velocity of the vehicle. This program allows the operator to change the vehicle weight distribution and quickly evaluate the results.

The program requires the following information for each stage:

- Weight of the engines
- Inert weight
- Weight of the propellant
- Isp of the engines
- Weight flow of the engines
- Flight angle (ß)
- Payload (third stage only)

The program calculates:

- Initial weights
- Final weights
- Weight of unused fuel
- Mass ratio
- Burn time
- Structural coefficients
- Gravity losses
- Ideal velocities
- Final velocity of the vehicle

The program was modified for certain constraints on the Gryphon. For example, the burn time of the first stage is fixed at 78 seconds and is not calculated. It remains 78 seconds regardless of any changes made. The program also adds 2.5% of the weight of all liquid fuels to account for unused fuel.

The program does, however, have three drawbacks. First, effects from thrust vector control cannot be calculated. The Ideal Rocket Equation, equation (4.2), assumes that all mass expelled contributes to the velocity. Thrust vector control expels propellant but does not contribute to the velocity of the rocket, i.e. it reduces Isp. The mass of the fuel is present at the beginning of each stage but is not there at the end. There is no way for the computer to calculate this reduction in Isp. Since the initial weight of the propellant must be counted, an extra 2.5% of the total weight of the propellant is assumed to remain onboard throughout the burn time.

The second drawback is caused by the payload shroud. The payload shroud is jettisoned shortly after second stage ignition. Similar to the fuel used by thrust vector control, its mass is present at the beginning of Stage 2 but not at the end. Once again its weight must be counted in the program. The program assumes the payload shroud is jettisoned along with Stage 1. For this reason its weight is included in Stage 1's inert weight.

The final drawback is the losses and gains from velocity. The program uses the values for losses and gains assumed by the Propulsion Group. The drag loss is assumed to be 261 ft/s. The program does not except any other aerodynamic data. The velocity of the launch aircraft is assumed to be 733 ft/s, the figure stated by the Eclipse Design Team. The Earth's rotation is assumed to contribute the full 1,342 ft/s. The program does not take into account the true launch trajectory.

There are definite drawbacks to this program, but it turned out to be a quick and easy way to check hand calculations and to compare values calculated by other groups. From the comparison with the Mission Analysis Group's trajectory calculation, it was determined that the payload goal of 7,900 lb of payload to GTO could be achieved.

Optimization

A handbook (reference 109) contained a method of estimating the performance of a ground launched rocket. When the method was attempted it failed to produce realistic results. According to the results, the Gryphon would lose 5,500 ft/s due to drag and 1,700 ft/s due to gravity in the first stage alone. The final velocity of the first stage would be -500 ft/s. Since this result made no physical sense it was disregarded. It is believed that the method failed because the book assumed a ground launched trajectory. Many of

the values used in computation came from graphs whose origin was unspecified. The information contained in them may not have been applicable to air launched vehicles.

SORT

SORT is a Lockheed computer program that the Mission Analysis Group has obtained. It is used to optimize trajectories for the Space Shuttle. SORT will provide independent verification of the performance of the Gryphon. The program uses more advanced methods to calculate the velocity losses on the rocket. However, the results must be carefully checked to ensure that the final weights given by the program are consistent with the designed weights. The latest results from SORT are inconclusive. The program has not been made workable and had to be abandoned.

4.3.4 Other Versions

Table 4.12 is a partial list of some configurations that were studied and rejected for the reason listed.

Table 4.12 Rejected Configurations

Configuration	Drawback
All solid Fuel	Not enough payload, Too Heavy
No cryogenic fuels	Not enough payload, Too Heavy
Cryogenic Second Stage	Safety concerns
Extra stage	Too expensive

The "All Solid Fuel" version was investigated because of the Eclipse Design Team's desire that no liquid fuels be carried. Various combinations of Castor 120s and Castor XXs were examined. No version was able to lift even 4000 lb to GTO except for one which weighed over 500,000 lb. The all solid configuration was rejected because of the large weight that would be required. Since then, liquid fuels have been considered a requirement.

Alternatives to the RL10A-4 were considered for the "No Cryogenic Fuel" version. The Orbus 7s and 21 upper stage boosters were investigated. The Orbus 7s is unable to boost 8,000 lb into GTO. The Orbus 21 is capable of boosting 8,000 lb. However, the Orbus raised the weight of the third stage to over 30,000 lb, which the lower stages were unable to lift into LEO.

A version was examined that used a cryogenic second stage. A Rocketdyne J-2 replaced the two LR91s on the second stage. The Gryphon's overall weight was lowered, and it was still capable of lifting 8,000 lb to GTO. This version was rejected because large amounts of cryogenic fuels were deemed too dangerous to be placed under the aircraft. Also, for large amounts of cryogenic fuels much larger fuel tanks are required. This greatly increases the total weight of the vehicle and decreases the structural efficiency.

The final alternative was to place an extra stage between stage two and stage three. The stage was powered by one LR91. This vehicle also lifted 8,000 lb to GTO and had a lower total weight. The extra stage also alleviated the high g-loading at second stage burnout. The version was rejected because of the added expense of the engine and the added length to the vehicle.

4.4 PROPELLANTS

The Gryphon's propulsion system is composed of three different engines that consume three different propellants. The first stage uses solid and storable liquids. The second stage is composed of only storable liquids. The third stage uses cryogenic liquids. Each of these propellants has very different performance and handling characteristics. The following discussion is a summary of data gathered on each of these chemicals. It includes performance data and safety precautions.

4.4.1 Castor 120 Solid Rocket Propellant

The Castor 120 is the only solid propellant engine in the Gryphon's propulsion system. It is an hydroxy-terminated poly-butadeine (HTPB) base with 88% solids. Very little data has been made available on the particular fuel combination that is employed in the Castor 120. The most information that has been gathered was produced in various books dealing with rockets and missiles. The following information is data taken from one of those books [reference 99] for one combination of HTPB/AP/AL (AP= ammonium perchlorate, AL= aluminum).

Table 4.13 Fuel Properties of the Castor 120

Is (sec)	260-265
Flame Temperature (°F)	5600-5800
Density (lb/in^3)	0.067
Metal Content (wt%)	4-17
Burning Rate (in/sec)	0.40
Pressure Exponent (n)	0.4
Hazard Classification	1.3

Combustion

The solid propellant of the Castor 120 is cast into a cylindrical grain. Once the pyrogen igniter is activated, burning cannot be stopped and will continue in a progressive process. As the cylinder burns from the inside out, more surface area of propellant is exposed; therefore, burning will accelerate. Spaced throughout the grain are radial and conical cuts. Each cut will have an effect on the burning process, but at this time it is not known exactly what that effect will be, see Figure 4.1.

The specifics on the solid propellant of the Castor 120 are not known. The design team has endeavored to find information about its actual chemical composition as well as its burning characteristics and storing properties. This information was not available for use; therefore, estimations had to be used for all calculations.

4.4.2 Aerojet LR91-AJ-11 Storable Liquid Propellants

The LR91 propulsion system used in the first and second stages of the Gryphon uses storable hypergolic liquid propellants to power the engines. The fuel used by the LR91 is Aerozine-50. It contains approximately 50 percent hydrazine and 50 percent unsymmetrical dimethylhydrazine (UDMH). The oxidizer is Nitrogen Tetroxide. These

propellants have two very significant properties. First, they are storable in ambient temperature and pressure conditions so they do not need refrigeration equipment. Second, these propellants combust on contact and therefore eliminate the need for an ignition system on board the vehicle. However, there are tradeoffs for having these two desirable properties. Because the propellants are storable, engine performance is vastly inferior to that of cryogenic propulsion systems. In addition, because the propellants are hypergolic, they present an extremely high potential for explosion, corrosion of surroundings, and toxic effects if spilled.

This section contains general descriptive information on the liquid propellants used to power the LR91s on the Gryphon space booster. It includes summaries of the physical and chemical properties of the propellants. Other information, such as material compatibility, is also provided because of its importance in storage and handling.

Aerozine-50

The two components of Aerozine-50, hydrazine and UDMH, are quite similar in chemical structure and in terms of physical properties. Hydrazine, by itself, is a better performing fuel than Aerozine-50, but its low thermal stability and tendency to violently decompose make it rather impractical. Mixing it with UDMH gives the fuel more stability. Aerozine-50 combines the improved stability characteristics of UDMH with the higher performing hydrazine to form a relatively stable fuel without much loss in performance.

Table 4.14 Physical Properties of Aerozine-50

Chemical Structure	50% 2H-2N-2H 50% $2CH_3$-2N-2H
Physical Description	Clear Colorless liquid
Molecular Weight	41.805
Specific Gravity at 77 °F	0.8987
Boiling Point (°F)	158
Freezing Point (°F)	22
Density at 77 °F (lb/gal)	7.5
Viscosity at 77 °F (lb/ft-sec)	.000543
Vapor Pressure at 77 °F (psia)	2.68
Critical Temperature (°F)	633
Critical Pressure (psia)	1731
Heat of Vaporization at 77 °F (Btu/lb)	346.3
Heat of Formation at 77 °F (Btu/lb)	522.9
Thermal Conductivity at 77 °F (Btu/ft-sec-°F)	0.0000458
Heat Capacity at 77 °F (Btu/lb-°F)	0.732

In appearance, Aerozine-50 is a clear and colorless liquid at ambient conditions. The volatility of the mixture is primarily due to the more volatile component, UDMH. That is why Aerozine smells more like UDMH than hydrazine i.e. fishy rather than ammonia-like. Aerozine can be mixed using any proportion of its components. To actually create a uniform mixture from hydrazine and UDMH, a sufficient amount of agitation, or forced mixing, is required. Aerozine itself does not decompose into its two components unless it is purposely distilled or until it is frozen.

Like its components, Aerozine is thermodynamically quite unstable. However, the decomposition rate on clean surfaces and in the absence of any catalysts is extremely low at ambient conditions. The mixture also presents a great fire and explosion hazard. Because the vapor above Aerozine is largely UDMH, the flammability hazards of Aerozine are also largely those of UDMH. At or above 18°F, the vapor pressure of Aerozine is sufficient to form a flammable vapor-air mixture. Therefore, under normal storage conditions care must be taken that the fuel is not placed in the vicinity of ignition sources. The flammability hazard becomes extremely high if temperatures exceed 500°F. In this range of temperatures, Aerozine vapor can easily auto-ignite in air. Any substance with which Aerozine reacts exothermally can cause such high temperatures. Examples are: common types of litter, oxidizers, acids, halogenated solvents, dirty or rusty surfaces etc.. Even an Aerozine and water mixture could be flammable if the solution contains more than 35% aerozine. One way of keeping Aerozine from becoming a fire hazard is to keep it blanketed with liquid nitrogen.

Various common materials react differently with Aerozine. Water, for example, gets readily absorbed in Aerozine and makes it even more. If significant amounts of water (more than 5%) are contained in Aerozine, damage can be done to the engine. Water, in any amount, does degrade the performance of the engine. Carbon Dioxide reacts rapidly with UDMH to form a water soluble product. These products of reaction can become solid particles if the temperature near the freezing point. In this respect carbon dioxide can be used as a fire extinguisher or to clean the UDMH vapor around Aerozine. Some industrial cleaners and solvents react with Aerozine similar to carbon dioxide. Solid particles or contaminants could be formed which may either block passages and joints, or corrode engine parts.

For storage and tankage purposes, metals are a usable group of materials. They are non-reactive and do not suffer corrosion by Aerozine-50 under most conditions. However, in the presence of contaminants such as water, air, or oxidizers, the corrosivity towards metals increases. Some metals, like magnesium, copper, zinc, and ferrous alloys are not recommended for use with Aerozine-50 because of incompatibilities such as possible contact with rust.

Generally, non-metals are incompatible with Aerozine-50 as far as storage vessels are concerned. In fact, contact with most non-metals can cause degradation or destruction of the materials. Materials like plastics, elastomers, lubricants, and coatings can be easily dissolved or decomposed in Aerozine-50. The fuel could extract materials from non-metal containers or be absorbed by them. This could change the physical and chemical properties of both. Some non-metals can be used with Aerozine for a short period of time, but very few can be used in service indefinitely as metals can. Teflon, for example, can be used with Aerozine-50 for 90-120 days depending on the conditions.

The two components of Aerozine-50 have differing toxic qualities. Hydrazine is very toxic. It can cause harmful effects if ingested, inhaled, or touched for a prolonged period. UDMH is also very toxic but less than hydrazine. However, UDMH can cause more toxic harm to a person since it is readily found in vapor form and is very volatile.

Nitrogen Tetroxide

The Oxidizer used for the LR91 in conjunction with the Aerozine-50 fuel is Nitrogen Tetroxide (N_2O_4). It is generally stable at ambient conditions and it is available in large quantities because of its widespread use for other industrial applications. Unlike Aerozine-50, Nitrogen Tetroxide is not a mixture, rather it is a compound. Propellant

-grade Nitrogen Tetroxide is at least 99.5% by weight N_2O_4 and no more than 0.17% water.

Anhydrous Nitrogen Tetroxide is a dense non-corrosive, non-flammable, hygroscopic (absorbs water) liquid. At room temperature, the color of the oxidizer is reddish-brown. As the temperature is lowered, the color approaches a pale brownish-yellow. As a propellant, N_2O_4 is hypergolic with many fuels including UDMH, hydrazine, aniline, and alcohol. On its own, the oxidizer is non-flammable and non-corrosive. However, it does support other combustion processes and when it is mixed with water it becomes substantially corrosive. As N_2O_4 reacts with water, its color changes to blue-green, indicating the formation of nitric or nitrous acids.

Nitrogen Tetroxide is considerably more stable than Aerozine-50. At normal temperatures an equilibrium exists between N_2O_4 and NO_2. As the temperature is raised, the amount of NO_2 increases proportionately. At still higher temperatures, around 350-400°F, the NO_2 dissociates into NO and O. Upon cooling, these reactions are reversible and the mixture returns to its previous condition.

Keep in mind that Nitrogen Tetroxide is a very strong oxidizer and although it is non-flammable itself, it can ignite automatically if it comes in contact with fuels. N_2O_4 will also in most cases promote ignition of other combustible materials. Fires involving N_2O_4 burn vigorously and produce toxic fumes. As with Aerozine, large amounts of water can be used to extinguish N_2O_4 fires and vessels used for storing N_2O_4 can also be cooled with water to prevent fires from spreading. Some organic compounds, such as solvents for degreasing metals, can also react with N_2O_4 and produce spontaneous explosions. Care should be taken in choosing solvents and degreasing agents which are compatible with N_2O_4. Potentially explosive mixtures can also form if N_2O_4 comes in contact with large amounts of hydrocarbon materials.

Table 4.15 Physical Properties of Nitrogen Tetroxide

Chemical Structure	2O-2N-2O
Physical Description	Red-Brown liquid
Molecular Weight	92.016
Specific Gravity at 77 °F	1.433
Boiling Point (°F)	70.1
Freezing Point (°F)	11.8
Density at 77 °F (lb/gal)	11.96
Viscosity at 77 °F (lb/ft-sec)	0.000267
Vapor Pressure at 77 °F	17.38
Critical Temperature (°F)	316.8
Critical Pressure (psia)	1440
Heat of Vaporization (Btu/lb)	178
Heat of Fusion at 77 °F (Btu/lb)	68.5
Thermal Conductivity at 77 °F (Btu/ft-sec-°F)	0.0000211
Heat Capacity at 77 °F (Btu/lb-°F)	0.378

Nitrogen Tetroxide with less than 0.17% water content is non-corrosive and can be used with almost all metal alloys for extended exposure. More non-metals are suitable for service with N_2O_4 than Aerozine. Materials such as Teflon and Kel-F 300 nplastics, perhalogenated lubricants, and certain silicone greases. These materials will however, be

physically deteriorated from prolonged exposure to N_2O_4. Other non-metals, like some inorganic materials (graphite, molybdenum, disulfide, and Pyrex glass) appear to be unaffected by N_2O_4.

Nitrogen Tetroxide is more toxic than Aerozine and proper precautions have to be taken while handling this chemical. If it comes in contact with the skin, it can produce a strong itching and burning sensation. If it is washed with water immediately, it leaves no scars. Prolonged contact can leave painful acid like scaring on the body. If N_2O_4 vapor is encountered, it can cause irritation to the lungs, throat, nose, and eyes. If it is splashed in the eye, it can cause permanent damage.

4.4.3 Pratt & Whitney RL10A-4 Cryogenic Liquid Propellants

Upon choosing Pratt & Whitney's RL10A-4 engine, which uses cryogenic propellants (liquid oxygen and liquid hydrogen), a large number of handling and storage concerns were raised. Although cryogenic propellants are very common liquid rocket propellants,

their extremely low temperatures and high reactivity posed a major problem. After further investigation, it was discovered that these propellants were no worse than storable fuels as long as strict handling and storage procedures were followed. In this section, properties of both liquid oxygen and liquid hydrogen will be discussed as well as certain safety precautions that must be followed.

Liquid Oxygen

The health hazards of liquid oxygen are due to its low temperature (boiling point of -297 °F, see Table 4.16). If liquid or cold gaseous oxygen comes in contact with skin, burns may result. These burns can range from only minor burns to complete embrittlement and permanent destruction of the tissue. No toxic effects are caused by oxygen; however, if cold gases are inhaled, some respiratory irritation may result.

Table 4.16 Physical Properties of Liquid Oxygen

Chemical Structure	O - O
Molecular Weight	31.9988
Specific Gravity at -297 °F	1.14
Boiling Point (°F)	-297.35
Freezing Point (°F)	-369.04
Density at -297 °F (lb/gal)	9.518
Viscosity at -297 °F (lb/ft-s)	0.000128
Critical Temperature (°F)	-181.08
Critical Pressure (psia)	736.90
Heat of Vaporization at -297 °F(Btu/lb)	91.738
Heat of Fusion at -287 °F(Btu/lb)	5.976
Thermal Conductivity at -297 °F (Btu/hr-ft-°F)	0.08643

Liquid oxygen will not burn, but supports combustion readily. Accidental spills are cause for concern if the liquid oxygen is mixed with any material that can burn, especially fuels. In addition to this hazard, oil or grease may explode spontaneously

when in contact with liquid oxygen. For this reason, all contact materials must be clean. When storing liquid oxygen, very complex insulation blankets must be used in order to minimize losses due to boiloff. Some materials that are compatible with liquid oxygen are; aluminum, stainless steel, nickel alloy, copper, Teflon, and Kel-F. For this particular application stainless steel was chosen as the tank material. This will be discussed in detail in section 4.5.

Liquid Hydrogen

The health hazards of liquid hydrogen are similar to that of liquid oxygen and are due to its low temperature (boiling point of -423 °F, see Table 4.17). As with liquid oxygen, burns may result from contact with liquid or cold gaseous hydrogen. The even lower temperature of liquid hydrogen makes this danger even more profound.

An unconfined mixture of air and gaseous hydrogen will burn but not detonate if a small ignition source occurs, such as a spark. If the mixture is confined and is ignited by a shock source, a detonation or an explosion can occur. When hydrogen burns in air, the flame is invisible. Hydrogen-air mixtures are readily ignited when the mixture has between 4 and 74 percent hydrogen by volume. Hydrogen-oxygen mixtures are flammable over a range of 4 to 94 percent hydrogen by volume. The most effective control of a hydrogen fire is to simply shut off the supply. Fires caused by hydrogen gas can be controlled effectively by the use of common extinguishers, such as; water, carbon dioxide, and steam. However, it must be noted that if the supply is not shut off and gaseous hydrogen continues to leak, a cloud of combustible gas will form and may explode if ignited. Because of these dangers the following sources of ignition must be controlled; open flames, electrical equipment, metallic sparks and static electricity.

Table 4.17 Physical Properties of Liquid Hydrogen

Chemical Structure	H - H
Molecular Weight	2.01594
Specific Gravity at -423 °F	0.071
Boiling Point (°F)	-422.99
Freezing Point (°F)	-434.425
Density at -423 °F (lb/gal)	7.112
Viscosity at -423 °F (lb/ft-s)	9.072e-6
Critical Temperature (°F)	-399.95
Critical Pressure (psia)	190.8
Heat of Vaporization at -423 °F (Btu/lb)	193
Heat of Fusion at -423 °F (Btu/lb)	25.0
Thermal Conductivity at -423 °F (Btu/hr-ft-°F)	0.0687

The low temperature of liquid hydrogen also makes the problem of choosing suitable tank and piping materials difficult, since most metals become very brittle at such low temperatures. Although the extremely low temperature of liquid hydrogen poses a handling problem, the most serious hazard is the danger of fire or explosion. The low specific gravity requires very large fuel tanks, which necessitates large vehicle volumes. Liquid hydrogen also requires complex insulation to minimize losses due to boiloff. Some materials that are compatible with liquid hydrogen are; stainless steel, nickel alloy,

C-2

aluminum alloy, and Kel-F. Again stainless steel was chosen as the tank material and will be discussed in detail in Section 4.5.

Handling and Cleaning

When handling both liquid oxygen and liquid hydrogen, trained supervision is essential. All personnel that will be around these propellants will be educated as to what materials are compatible, what type of protective equipment and clothing is needed, first-aid instruction, and the general nature of both propellants in their liquid and gaseous phases. All areas that contain these fuels will also be equipped with the appropriate fire extinguishers and personnel showers. In addition to personnel knowledge, strict cleaning procedures must be followed to avoid mixing the propellants with small foreign particles, which may be very dangerous together. Most importantly, parts must be degreased using perchloro-ethylene vapor or solvent for 30 minutes then rinsed well with alcohol and then with water. Stainless steel parts must be cleaned using a 4% detergent solution for 30 minutes and then bathed in a 40-50% nitric acid solution for at least 1 hour and rinsed clean with distilled water. Plastic parts should also be cleaned with a 4% detergent solution for 30 minutes and rinsed clean and dried.

If these guidelines are followed closely, as well as periodic inspection of the storage tanks, no problems are expected by using these propellants.

4.5 PROPELLANT TANKS AND INSULATION

4.5.1 Propellant Tanks

The propellant tanks were among the last things to be designed within the propulsion system. The design of the tanks was an evolution of several different schemes which were proposed. The fuel tanks were separated among the three stages and also into separate tanks for the oxidizer and fuel which must be kept separate until they are combined in the combustion chamber of the rocket engines.

The first and second stage tank designs are very similar in function. They both are pre-pressurized by nitrogen before engine start up and then employ engine bleed to maintain fuel tank pressurization during engine operation. These tanks are designed to carry storable fuels, and are not used as part of the Gryphon's overall structure to take the stresses created by the engines thrust and accelerations created during the ascent. In effect the thickness of the tanks was minimized by taking into account only the tank pressures required to provide adequate fuel to the engine's turbine fuel pump inlets.

The third stage tanks were designed much differently than the first two stages because they store cryogenic fuels and because they are to be used as the primary structure on the third stage. These fuel tanks will be pressurized by a separate helium tank incorporated in the third stage until engine ignition, then they will be pressurized by the third stage engine.

The volume, thickness, and weight of the propellant tanks is of primary importance to the design of the Gryphon. The volume of the tanks is directly proportional to the length of the vehicle which was to be minimized as much as possible. The thickness of the tanks is critical to the safety and operation of the propulsion feed

system. Finally, the weight of the tanks, which was minimized as much as possible, is a large portion of the weight which only hurts the rockets performance since it is neither propellant nor payload.

Preliminary calculations of fuel and oxidizer on Gryphon

The design of the fuel tanks originated from estimations of the required trajectory and from the staging procedures. A certain amount of fuel was allotted for each stage from this preliminary analysis. The amount of liquid fuel on each stage was then changed in order to maximize the performance of the Gryphon. Each stage was then designed to carry the following amounts of fuel, seen in Table 4.18.

Table 4.18 Stage Fuel Weights

Stage 1	23,924 lb
Stage 2	164,000 lb
Stage 3	9,057 lb

The propellant was then divided up into the amounts of fuel and oxidizer on each stage in accordance with the mixture ratios of each engine. The LR91 engines have a mixture ratio of oxidizer to fuel of 1.86:1 while the RL10 has a mixture ratio of 5.5:1. An extra 2.5 % fuel was also allotted for unusable fuel. The unusable fuel is fuel left over in the tanks after the engine has finished firing. From this information the amounts of fuel and oxidizer were computed , as shown in Table 4.19.

Table 4.19 Fuel and Oxidizer Weights Per Stage

Stage	Oxidizer (lb)	Fuel (lb)
1	15,948	8,574
2	112,057	60,246
3	7,547	1,510

Volumes of the tanks

Once the total amount of fuel and oxidizer upon each stage was known, the volume required for each tank was then calculated. The volume of the tanks also takes into account a 5% ullage, or empty space when the tanks are completely full. This ullage is included in order to deal with over pressure problems which may be encountered during the useful lifetime of the tank due to forces exerted on the fuel during ascent and pressure fluctuations within the tank.

The volumes of the tanks were calculated according to the equation:

$$V_p = \left(\frac{W_p}{\rho_p} \right) \times (1.05) \qquad \text{(Eq 4.6)}$$

Where subscript p stands for propellant. Calculating the volume required for the Stage 2 tanks used the following equations.

$$V_o = \left(\frac{112{,}057\,\text{lb}}{89.254\,\text{lb/ft}^3}\right) \times (1.05) = 1318\ \text{ft}^3$$

$$V_f = \left(\frac{60{,}246\,\text{lb}}{55.97\,\text{lb/ft}^3}\right) \times (1.05) = 1130\ \text{ft}^3$$

The volumes for the other tanks were calculated in the same manner yielding the volumes seen in Table 4.20.

Table 4.20 Volume of Propellant Tanks Per Stage

Stage	Volume of Oxidizer	Volume of Fuel
1	188 ft3	161 ft3
2	1318 ft3	1130 ft3
3	110 ft3	357 ft3

Tank pressures and Pressurization systems

The pressure at which the fluid inside the tanks must be pressurized to assure proper operation of the fuel pump is dictated by the following equation:

$$P_t = \text{NPSH} + (\text{feed line friction losses}) + (\text{vapor pres.}) - (\text{propellant head}) \qquad \text{(Eq 4.7)}$$

where NPSH = Net Positive Suction Head.

P_t was estimated to be 27 psi for all of the fuel tanks. This was an estimate based upon similar engine and propellant tank designs. An estimate of this function had to be made since some information in equation (4.7) was not available.

The ullage in the tanks is to be maintained at constant pressure of 27 psi both before and after launch until the useful life of the tanks and engines is over. To accomplish this on the first and second stage a pre-charged nitrogen fed pressurization system is used. To accomplish this on the third stage an on board helium pressurization system was employed.

The first and second stage pressurization will be accomplished initially by pressurizing the tanks shortly before the Gryphon is flown to its launching point. Once the engines are started, the fuel tank will then be pressurized by cooled turbine gas from the turbine manifold of the LR91-AJ-11, and the oxidizer tank will be pressurized by liquid nitrogen tetroxide taken from the oxidizer fuel pump and vaporized into nitrogen dioxide gas. This will in turn increase the tank pressure to a value high enough to break the burst diaphragms in the system and allow the fuel to flow from the tank to the engines and assume steady state operation. The pressure within the tanks will then be controlled by the use of monitors in the tank and variable controlled pressure valves in the pressurization system.

The third stage pressurization system will first be accomplished by a helium tank connected to both the cryogenic fuel and oxidizer tanks. The helium pressurization system is required due to the boil-off that occurs with cryogenic fuels. The helium tank

will be included with the third stage and will also provide some cooling to instruments within the avionics bay. Pressure will also be maintained in this tank through the use of pressure monitors and variable control valves in the helium lines. The volume required for the helium tank is 5.74 ft^3 and the pressure required to assure tank pressurization during the entire mission will be 1000 psi. The fuel tank will be pressurized by exhaust gas from the turbine fuel pump after the engine is operational, and the oxidizer tank will be pressurized by excess oxidizer from the turbine oxidizer pump.

Tank Material, Shape, and Thickness

The tanks to house the liquid propellant on all three stages are to be built out of 301 stainless steel with a density of 0.285 lb/ft^3 and a yield stress of 70,000 psi. Weight minimization and compatibility of the tank material with the storable and cryogenic propellants was the main factor in the decision to use 301 stainless steel.

Once the material, pressures, and volumes had been established the calculations of thickness and weight estimations could then take place. The thickness of the first and second stage tanks is based solely upon the pressure forces within the tank since the tank is not an integral part of the structure for these stages. Therefore the thickness can be found from the following equations:

$$t_c = \frac{k P_t d_t}{2\sigma} \qquad \text{(Eq 4.8)}$$

$$t_s = \frac{k P_t d_t}{2\sigma} \qquad \text{(Eq 4.9)}$$

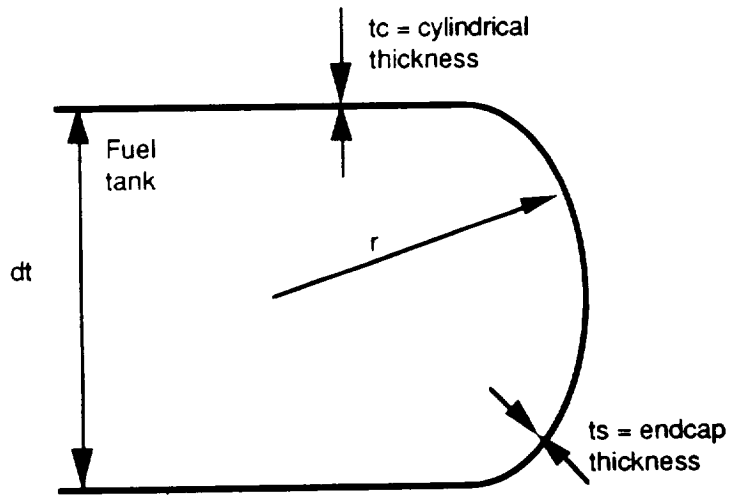

Figure 4.4: Tank Thickness

The radius of the endcap was chosen to be the same as the diameter of the fuel tank itself in an effort to make their construction homogenous and to reach a good compromise between the endcap height and its thickness.

The thickness of the second stage tank, using a factor of safety of 1.5, was then calculated using equation (4.8):

$$t_2 = t_1 = \frac{(1.5)(27\,\text{psi})(168\,\text{in})}{(2)(70{,}000\,\text{psi})} = 0.0486\,\text{in}$$

The thickness of the first stage was calculated in the same way.

The upper or third stage thickness depended upon the maximum force exerted upon it from above, since this stage is being used as an integral part of the structure on the third stage. This tank must also withstand pressurization forces, but these are less than those forces exerted on the tanks from above. These tanks can be estimated as thin walled pressure vessels, and the determination of the thickness of this stage proceeded as follows:

$$\sigma = k\left[\frac{Pr}{2t} + \frac{F}{2\pi rt}\right] \qquad \text{(Eq 4.10)}$$

Where F is the force of the payload at a maximum value of 6 times the force of gravity. Solving equation (4.10) for t with s < the yield stress of the material t = 0.02 in for the oxidizer tank on the third stage.

The thickness for the spherical fuel tank was calculated in the same manner and found to be equal to 0.022 in. A summary of the thicknesses and weights of the tanks is found in Table 4.21.

Table 4.21 Thickness and Weight of Propellant Tanks

Stage	Thickness (in)	Weight (lb)
1	0.0486	395
2	0.0486	2500
3 - Fuel	0.022	350
3 - Oxidizer	0.02	260

Overall Tank and Propulsion System Design

The tanks were designed using the preliminary calculations for the tank volume and thickness. The length of the tanks was minimized in an effort to minimize the length of the Gryphon while staying within a maximum diameter of 14 ft. Piping from the engines to the tanks was then laid out in as straight a line as possible to conserve weight and to provide good flow characteristics within the pipes. The piping will be constructed of stainless steel and will incorporate expansion fittings to accommodate for expansion and movement in the propulsion system. Outflow and filling ports were then integrated into the design, and weight estimates of each tank assembly was computed, see Figure 4.5.

The first stage tank was designed as a squashed spherical tank in order to make better use of the space provided. The fuel and propellant are separated by an internal spherical divider. The propulsion mechanism for the first stage is one LR91-AJ-11

rocket engine which was mounted three feet below the tank by an engine mount which also supports the tank weight and transfers the loads created by the engine to the Gryphon's outer structure, see Chapter 7 for details. The tank design along with the engine placement, piping and pressurization system is shown in Figure 4.6.

The second stage uses a cylindrical tank core with rounded endcaps. This shape provides the most efficient use of space for fuel. The fuel tank feed lines run through the inside of the oxidizer tank. This was done in order to make the most efficient use of space and to provide the two LR91s with the best flow conditions within the piping as possible, see Figure 4.7.

The third stage uses a spherical fuel tank and a partially cylindrical oxidizer tank in an effort to use space efficiently while at the same time providing a sturdy structure. The third stage also incorporates the helium tank used for tank pressurization before the firing of the RL10A-4. The third stage is also the sole structure between the payload and the LR91 engines of the second stage, see Figure 4.8.

4.5.2 Insulation

As mentioned earlier, the use of cryogenic propellants poses a problem with keeping the propellant tanks insulated enough to minimize losses due to boiloff. There are three types of heat flow that must be considered in choosing an insulation. These are conduction, convection, and radiation. Conduction is the type of heat flow caused by a higher temperature on the outside of the propellant tanks than on the inside, this will be discussed in detail later. Convection is a transfer of heat within the liquid itself, this type of heat flow is fairly advanced and was not analyzed for this report. Finally, radiation heat flow is caused by the sun, which emits radiant energy and is absorbed by the tank. In this section, we will present how these forms of heat transfer affected our choice of insulation.

In addition to the types of heat flow, many other criteria were used in selecting a suitable insulation for the cryogenic tanks. These criteria are weight, availability, cost, safety, ruggedness, reliability, and heat conductivity. A low heat conductivity is the most important feature for insulation.

Laminated

One type of insulation is the laminated-type which uses an aluminum foil and fiber-glass structure. The aluminum foil acts as a reflector, to reduce radiative heat, while the vacuum space between the layers prevents conductive heat transfer. One problem with this type of insulation is that the laminar insulation is not very rugged, and could therefore result in a loss of the vacuum layer because of cracks.

Honeycomb

Another type of insulation is the honeycomb-supported structure. With this type of insulation, the small honeycomb cells form individual vacuum spaces when cold. Because of the possibility of air penetrating the outer layer and then loosening the vacuum cells, they are often purged with helium because it will not freeze like air.

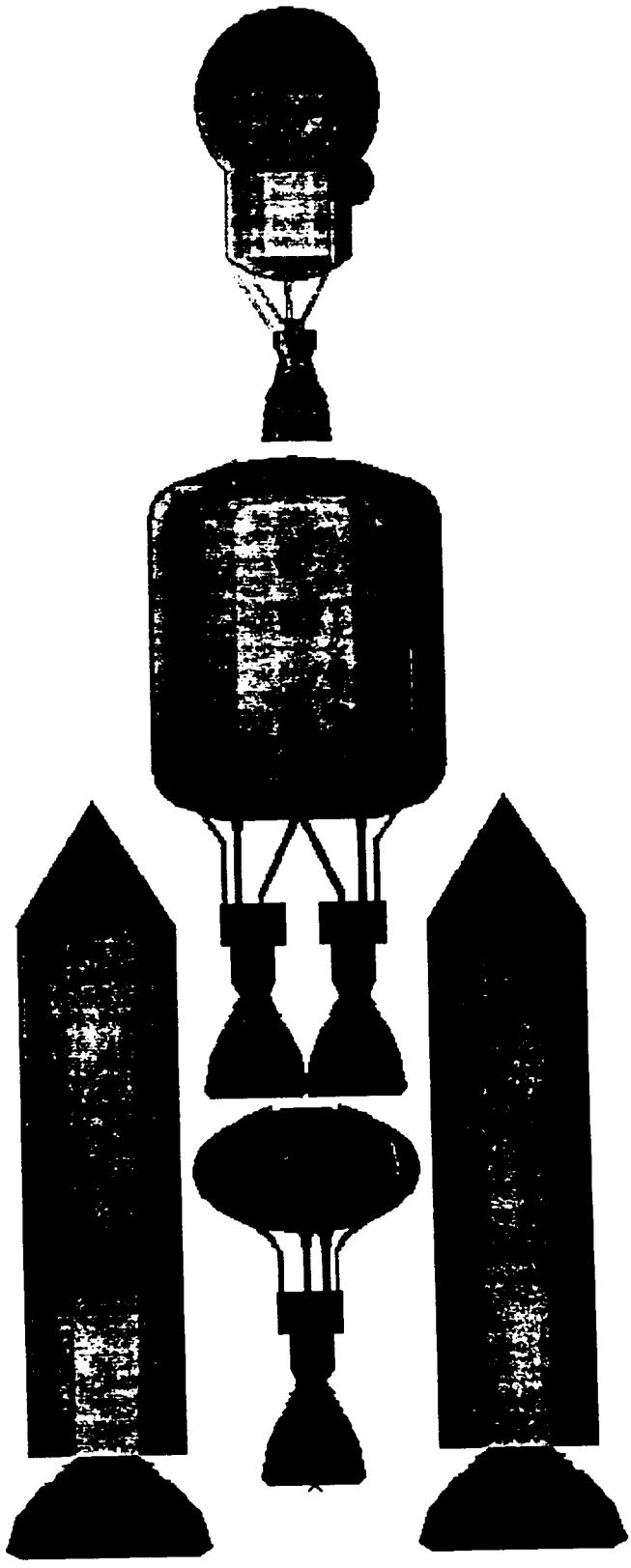

Figure 4.5 Overall Diagram of Propellant Tanks

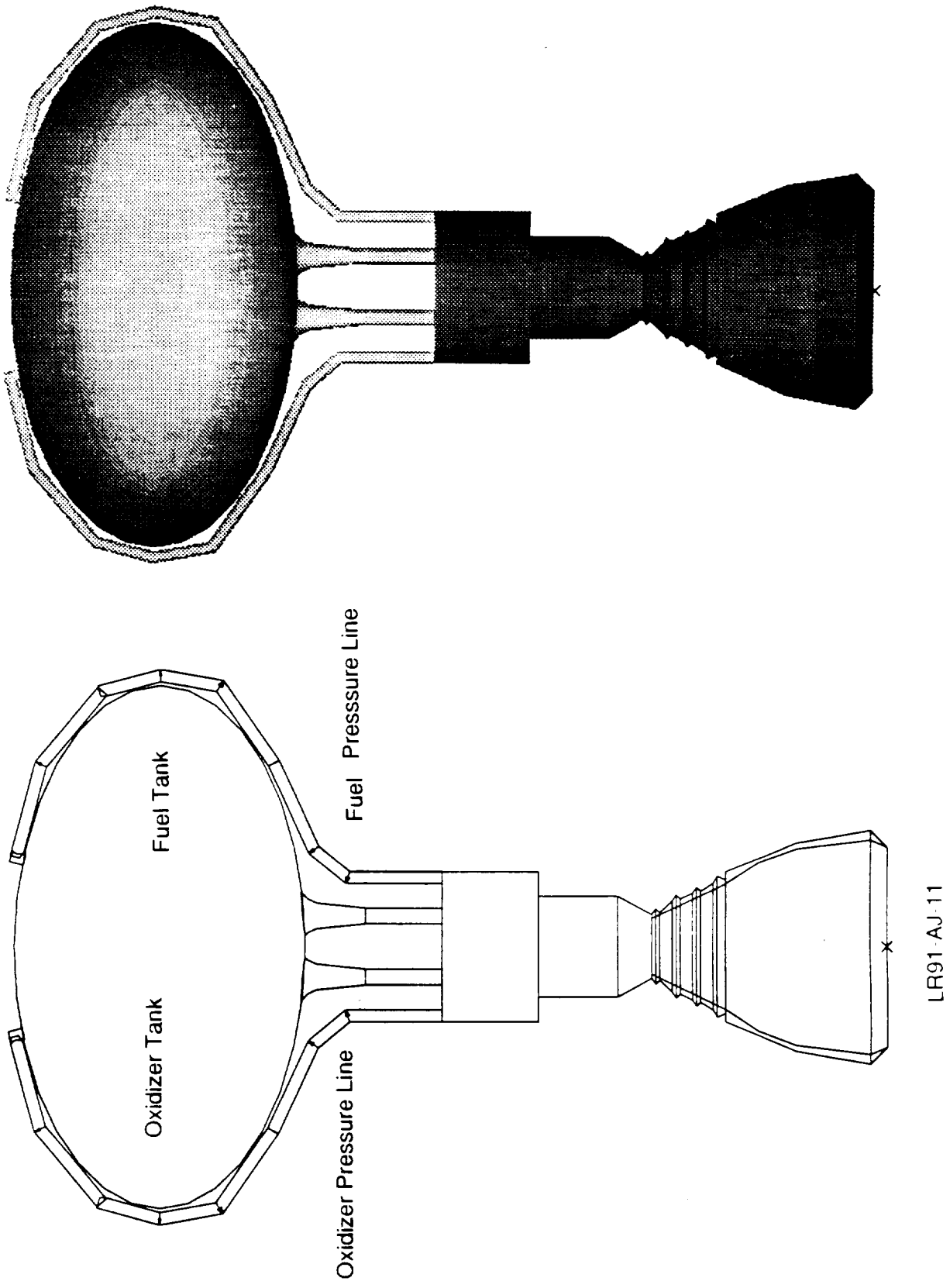

Figure 4.6 Stage One Propellant Tanks and Piping

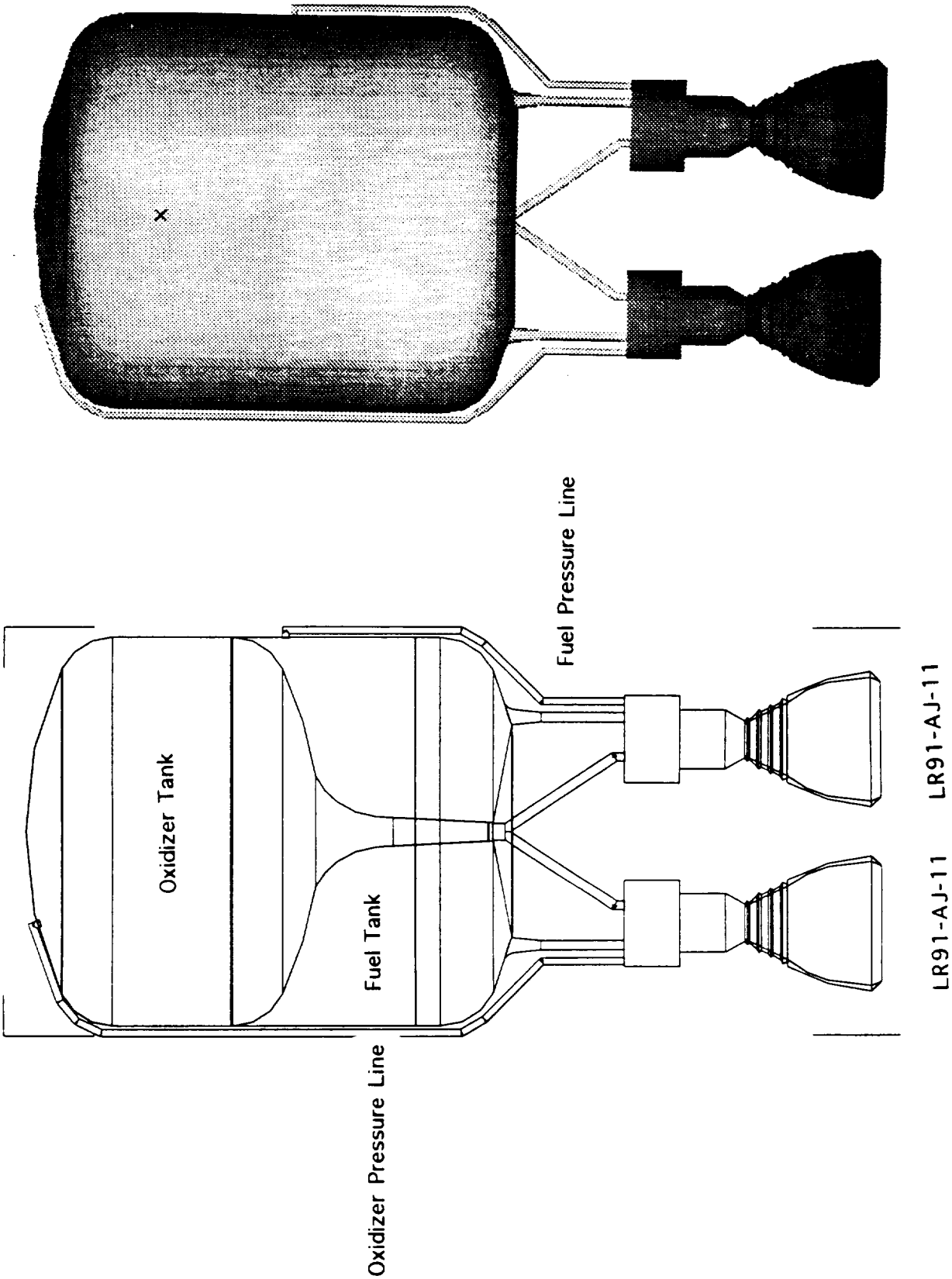

Figure 4.7 Stage Two Propellant Tanks and Piping

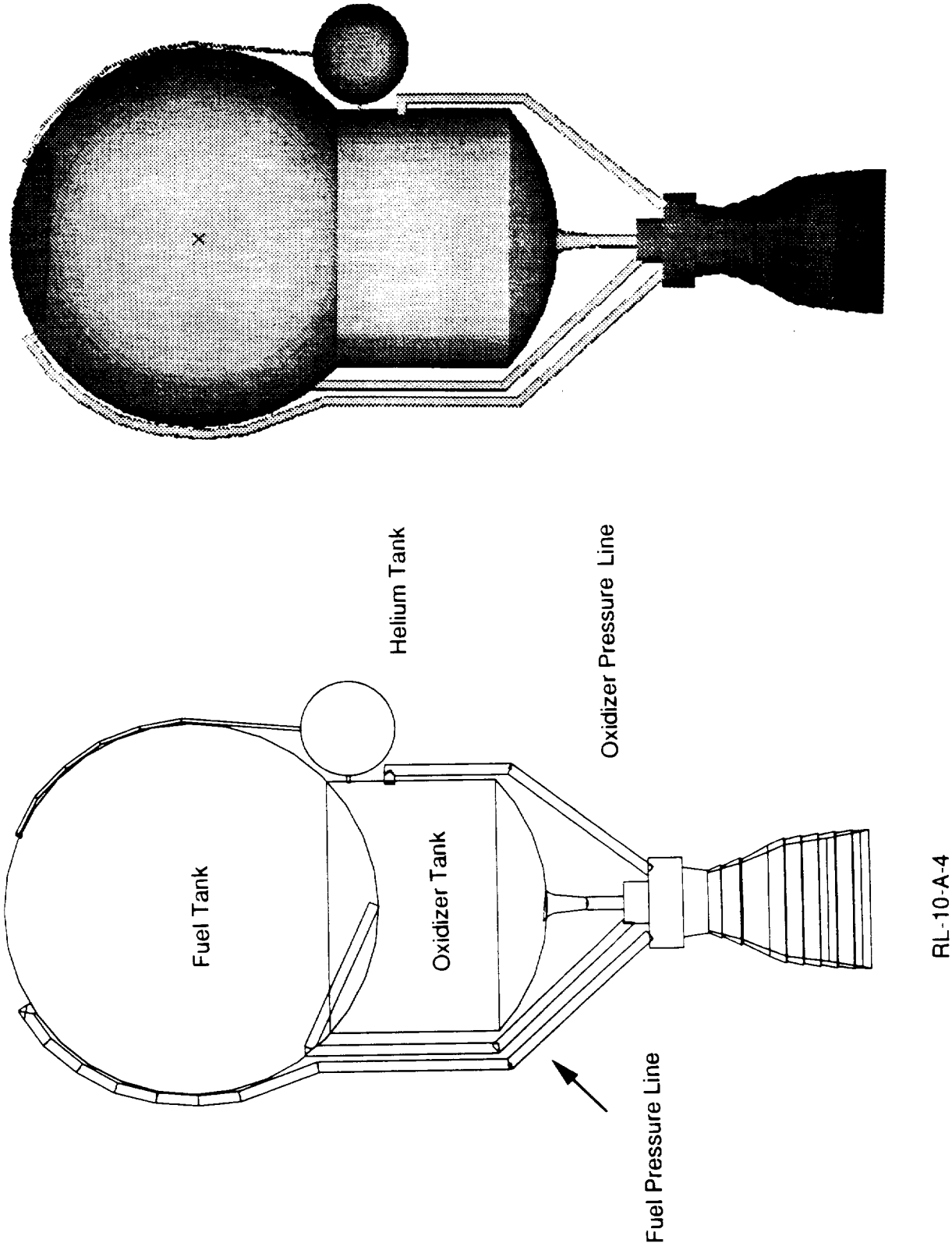

Figure 4.8 Stage Three Propellant Tanks and Piping

Chosen Design

The types of insulation that other launch vehicles use on their cryogenic tanks was investigated because of a lack of information available on current insulation. Therefore, the choice of insulation is based almost exclusively on Centaur information. Both the liquid hydrogen and liquid oxygen tanks will be using the same insulation.

Both tanks will have a sidewall insulation that consists of two 0.75 inch thick layers of insulation blankets covered by two radiation shields. Each blanket is made of two fiberglass reinforced Kapton face sheets and aluminized Kapton radiation shields evenly spaced by sheets of dimpled Kapton. The blankets are purged with helium to prevent the liquification of air or freezing water vapor. The outermost sheet is not aluminized to minimize the outer shield temperature to reduce boiloff.

An analysis of the boiloff rate caused by the conductive heat flow to the tank as given in equation 4.11.

$$q_h = k A \left(\frac{T_1 - T_0}{L} \right) \qquad \text{(Eq 4.11)}$$

Where q is the heat flux, k is the average thermal conductivity of the insulation (plus the tank itself), A is the area of the insulation, T_1 is the outside temperature, T_0 is the temperature inside of the tank, and L is the thickness of the insulation. The problem that was encountered is that no information on the thermal conductivity of this insulation is available. Had this information been available, a more accurate estimation of boil-off could have been obtained. In addition to this problem, there was no information on the purge system itself, namely what type of controlling device needs to be used or if the purge system needs power from the batteries in the avionics section of the Gryphon. It was also difficult to determine how much helium is needed in the insulation or how often it needs to be changed. These problems are left for further investigation.

The first and second stage LR91s were also thought to need insulation to avoid freezing at launch altitude. However, after speaking with Martin Marietta, the information that was given stated that the heat of friction caused by the air on the outside of the tanks may produce enough heat that insulation would not be needed. Further investigation will be needed to determine the requirements for the insulation.

4.6 FUTURE WORK

Lack of time has prevented a more in depth analysis of the Gryphon. Research and calculations have uncovered several topics which must be addressed in the future. This section is a projection of those ideas. The present analysis will not be continued, but some other engineering team may start where this study stopped.

4.6.1 Engines

More research could be done to find a propulsion system which is better than the current combination. In later parts of the process, when it was too late to change the Stage 2 engines, it was discovered that an engine with longer nominal life could have given better performance in some instances and could also have saved money. Also, it is conceivable that a storable liquid propellant engine exists which gives better performance in terms of Isp and thrust. More research could also be done into the usage of cryogenic rocket engines for better performance and the safety concerns associated with their usage could be further examined.

4.6.2 Staging and Dynamics

The staging and dynamics analysis of the Gryphon is the area most in need of work. At this time, the trajectory has been compared with data calculated by the propulsion design team, and final numbers tend to vary. The first objective should be to find an optimal trajectory. Once this has been completed a stage optimization analysis can be done. With these bits of information a better estimate of engine performance qualifications can be compiled, and the engines can then be chosen with more certainty.

4.6.3 Propellants

There is one very important concern left unaddressed due to lack of time. The problem of LR91 fuel separation could cause major design changes in the Gryphon if it cannot be solved. The fact that the LR91 will be cruising with the Eclipse at about 40,000 ft for extended periods of time could lead to freezing of the Aerozine-50 and thus separation of hydrazine and UDMH is possible. What needs to be done is an analysis of how the low temperatures at such high altitudes will effect the fuel, what type of insulation or other measures are required, and how much of the effect can be countered by the aerodynamic drag. This situation is unique to the Gryphon and a solution to this problem must be considered.

A second concern regarding fuel is a detailed analysis of the boil-off rates of the cryogenic fuels. The Gryphon has a delayed launch of three to five hours. The carrier plane takes off and ferries the booster to its launch site. During these hours certain portions of the cryogenic liquids change phase from liquid to gaseous form. This gas has to be vented overboard to prevent excessive pressure build up within the propellant tanks. If too much of this propellant is vented there will not be enough fuel and oxidizer to power the RL10A-4 to its final destination. This is a topic of much concern that has consumed much analysis time but has yielded few results. Future analysis of this problem is crucial to the overall success of Gryphon.

4.6.4 Propellant Tanks and Insulation

Future work in the area of the propellant tanks design will include many topics. First a detailed analysis of sloshing in all the propellant tanks needs to be performed. Using this data the interior of the tanks could then be designed with baffles in order to bring the sloshing frequencies within tolerable limits. Design of the fuel tank outlet piping to prevent cavitation in the propellant flow field should also be accomplished. In the present design of the fuel outlet pipes, they were only modeled after the correct curvature. Their curvature was never quantitatively calculated. The actual design of these outlets

would also require testing of the fluid properties in a controlled environment in order to provide proper fuel to the various engines on Gryphon. Minimization of the fuel tank wall thickness using exact pressures required by equation 4.8 should also be done since the tank pressure was only estimated. A final area of investigation would be process of manufacturing and construction of the tanks in an effort to minimize tank weight and construction costs.

A study of propellant tank insulation is a great necessity. This insulation will protect all fuels and oxidizers from freezing as well as unwanted heating. By eliminating the cold and hot extremes, the condition of the propellants will be kept relatively constant and will provide better performance as well as better stability and safety.

4.7 CONCLUSION

The original goals of the Gryphon called for an air launched space booster that would be able to carry 8000 lb of payload to LEO and 17,000 lb to GTO. The problem given to the Propulsion Group called for a staging system that would be able to convert to both types of payloads. Research into engines, staging, propellants, and tank design helped to achieve the design of the present system. This three stage system utilizing the Castor 120, the LR91-AJ-11, and the RL10A-4 is the most cost effective and optimal system that could be designed.

PAYLOADS

Chapter Five

5.1 INTRODUCTION

The overall design of the Gryphon was linked to decisions made about what its payload should be. Therefore, the first goal of the Payloads group was to find general information about satellites and other possible payloads. This information was useful in helping other groups to set their design parameters. After determining the payload goals for the Gryphon, work was completed to determine the market for satellites. The market was used to find the payload weights the Gryphon needed to be able to carry, and the required dimensions of the payload area. The next step was to determine the payload limitations of the Gryphon's design. The following sections describe the goals of the payload group, the payload market, the method of determining the dimensions and weights of the payload area, the limitations of the payload, some structural considerations, and the Space Station Freedom options.

5.2 PAYLOAD GOALS

The Gryphon air-launched space booster was designed with the goal of meeting several important payload delivery criterion. The payload related criterion are:

- The delivery of 7900 lb, including payload support structures, to Geosynchronous Transfer Orbits (GTO)
- The delivery of 17,000 lb, including payload support structures, to Low Earth Orbits (LEO)
- The maximization of usable payload envelope volume
- The capability for multiple-satellite deployments to both low earth and geosynchronous transfer orbits
- The compatibility of delivering Space Station Freedom related payload packages

These goals acted as the driving force behind the design of the Gryphon. The delivery weights of 7900 and 17,000 lb for geosynchronous and low earth missions, respectively, were decided upon after careful consideration of the likely market demand (see Section 5.3) and cost analysis (see Chapter 2). The geosynchronous delivery limit will allow the booster to carry a large majority of the currently existing commercial communication satellites to their transfer orbits, utilizing either single or multiple payload configurations. The low earth capability will allow for the delivery of a large variety of

scientific satellites, either in single or multiple configurations. The capability of a 17,000 lb, 15 ft diameter payload will also allow for the delivery of payload packages to the Space Station Freedom.

5.3 PAYLOAD MARKET

An important concern with the Gryphon was to determine its payload market. There were two main questions, each with several options:

- Which type of payload will the Gryphon be designed for?
    - Communications Satellite
    - Scientific Satellite
    - Defense Operations
    - Space Station Freedom Resupply
- Where will the satellite be placed?
    - Low Earth Orbit (LEO)
    - Geosynchronous Transfer Orbit (GTO)
    - Geosynchronous Earth Orbit (GEO)

After much consideration, the highest market was determined to be communications satellites in GEO by route of GTO.

5.3.1 Communication Satellites

The United States launched its first man made communication satellite, Project SCORE, in December 1958. The satellite lasted a mere twelve days at which time the batteries failed. Since this monumental launch, communication satellites have become the foremost instrument in long-distance international communications. In 1988, for example, INTELSAT linked 172 countries, territories, and dependencies around the globe using 1,738 full time earth-station to earth-station pathways.

A communication satellite is simply a spacecraft that receives electrical signals from a transmitter on the earth, amplifies the signals, changes the carrier frequency, and then re-transmits the amplified signals back to receivers on the earth. These satellites are placed in such an orbit around the earth as to seem stationary to the transmitters and receivers on the earth. To get an idea of the power of these satellites, one should note that one transmitter and one satellite can transmit a signal to receivers covering an area equal to one-third of the earth's surface. Satellite communications can relay both analog and digital signals. The transmitter on earth modulates a baseband input signal onto a carrier, amplifies the modulated carrier signal, and then radiates the signal up to the satellite. This path followed by the transmitted beam from the earth to the satellite is called an uplink. This signal is received by the satellite and without altering the information, the beam is amplified and the frequency is changed from a 6 GHz band to a 4 GHz band. The satellite next radiates the signal back to earth. This return path is called the downlink. The downlinked signal is received by antenna on the designated area of the earth, and is again amplified. This final step completes the path traveled by information to and from the communication satellite.

Since the mid-1970's, satellites have become an important aspect of domestic communications for the United States, USSR, Canada, Australia, Brazil, India, Indonesia, Mexico, and Japan. Other countries around the world have domestic systems in the planning stage. The world has realized the many uses of satellite communication, including broadcasting and fixed services.

The International Telecommunication Union (ITU) recognizes twelve categories of communication satellite services:

- Fixed satellite service
- Broadcasting satellite service
- Mobile satellite service
- Radio determination satellite service
- Space operation service
- Space research service
- Earth exploration satellite service
- Meteorological satellite service
- Inner-satellite service
- Amateur satellite service
- Radio astronomy service
- Standard frequency and time signal satellite service

The most prominent services in use today using communication satellites are fixed, broadcast, mobile, and radio-determination services. Also, since satellites are equipped with multiple transponders, and often have dual frequency capabilities, two or more of these services can be provided by the same satellite.

Traditionally, fixed satellite service has consisted of the telephone, telegram, and television distribution. These services were usually transmitted by cable, even across the ocean. However, televisions have wide-band requirements and special cables are needed if reverse-frequency transmissions are unavailable, but they can be sent through satellites.

In addition to the standard communication services, satellites can be used for business services such as providing mail, facsimile text, picture transmission, banking, and reservation data networks. Communication satellites can also provide businesses with extensive, high speed transmission of documents including text, graphs, pictures and newspaper print. Also, they can provide high speed data transmission among computers at rates in the megabit per second range. In addition to these services, satellites can supply businesses with video teleconferences, in which groups of people at different sites around the world can confer with each other through live television transmissions.

The broadcasting satellite service is now reaching maturity. As a result of low noise receivers, it is possible to distribute television by communication satellites. As of 1987, there are over 1.5 million C-band satellite dishes in the United States used for television reception. A broadcast satellite service can beam radio, TV, and cable signals from the originating stations directly to small, low cost, home mounted terminals, using high powered satellite transmitters.

Mobile satellite services allow communications between earth stations which are in motion, whether it is by land, sea, or air. These mobile satellite systems are used in shipping, aviation, railroading, medical emergencies, interstate trucking, and temporary sites. They can also be used for communication purposes in sparsely populated areas where the existing systems are unreliable or inadequate.

The United States and Canada are both heavily involved in mobile satellite technology. The United States is currently in a program called the Mobile Satellite Experiment (MSAT-X), which started in 1984, and is managed by NASA and the Jet Propulsion Laboratory. The purpose of this program is to initiate commercial mobile satellite services. MSAT-X concentrates on the development of new techniques for mobile communications in future generation high capacity systems.

In spite of the high costs involved with launching communication satellites, the flexibility and advantages allow satellites to make a valuable contribution to world wide communications. To some extent, the high costs are due to the backup satellites necessary to ensure continuous service. The high level of reliability of today's current technology gives satellites an operational lifetime of about fifteen years. When compared to microwave relays and undersea cables, and the fact that in some parts of the world there is no other way of communication, communication satellites are actually very cost effective.

As can be seen, there is more than enough applications for communication satellites in the world today to provide steady business for another launch vehicle. This is one of the main reasons we chose to design a cost-effective air launched space booster.

5.3.2 Geosynchronous Earth Orbit

A communication satellite in Geosynchronous Earth Orbit (GEO) is at an altitude of 22,282 miles above the earth's surface, and travels around the earth at 6879 miles per hour. This is the same as the speed of the earth's rotation giving the satellite a period of 24 hours. If a satellite is traveling in the equatorial plane, and is moving in the same direction as the earth's surface, it will appear to be stationary over one point on the earth. The satellite would then be called a geosynchronous satellite, and its orbit is called a Geosynchronous Earth Orbit.

Placing a communication satellite in GEO requires high precision maneuvers. The Gryphon will take the satellite to a GTO, an elliptical orbit with a perigee altitude at about 135 nautical miles, and an apogee altitude of about 19,322 nautical miles from the earth. The satellite is spin-stabilized in GTO to allow the earth stations to communicate with its telemetry system. This orbit is measured as accurately as possible so the satellite's orientation can be adjusted. This is necessary to ensure the satellite will be at the correct altitude for GEO. When the satellite is at the apogee, a motor on the satellite is fired to put it in a circular orbit around the earth. The satellite's velocity is then adjusted to the same velocity of the earth's rotation. Then, the attitude is changed so that its antenna points in the right direction. This is called a Geosynchronous Earth Orbit.

GEO has many advantages:

- The communication satellite remains almost stationary relative to the earth's antennas, so the cost of computer controlled tracking of the satellite is avoided. A fixed antenna is satisfactory.
- It is not necessary to switch from one satellite to another as one disappears over the horizon.
- There are no breaks in transmission. A geosynchronous satellite is permanently in view.
- Because of its distance, a geosynchronous satellite is in line of sight from 42.4% of the earth's surface (38% if angles of elevation below

5% are not used). A large number of earth stations may then intercommunicate.
- Three satellites give global coverage with the exception of the polar regions.
- There is almost no Doppler shift, which is the change in the apparent frequency of the radiation to and from the satellite caused by motion of the satellite to and from the earth station. Satellites in elliptical orbits have different Doppler shifts for different earth stations, and these increase the complexity of the receivers, especially when large numbers of earth stations intercommunicate.

Geosynchronous satellites also have some disadvantages:

- Latitudes greater than 81.25 degrees north and south (or 77 degrees if angles of elevation below 5 degrees are excluded) are not covered. There are mostly polar ice at these latitudes.
- Because of the distance to the satellite, the receiver signal power, which is inversely proportional to the square of the distance, is weak, and the signal propagation delay is 270 milliseconds.

Communication satellites in GEO can relay signals between two or more locations on the earth. The advantages of communication satellites greatly outweigh the advantages of other methods of communication such as microwave relays and fiber optic cables. Therefore, the decision to build a cost effective air launched space booster can be justified. The Gryphon is designed to carry a satellite to GTO, from which the satellite can maneuver itself to GEO.

5.3.3 Low Earth Orbit

A satellite in LEO travels in a circular orbit at 17,500 miles per hour and has a period of rotation of about 1.5 hours. This orbit is used mostly for scientific satellites and military purposes. The Space Station Freedom will also be located in LEO. Although the market is not very large for this orbit, the Gryphon will leave open the option of carrying scientific satellites and Space Station Freedom resupply modules to LEO.

5.4 DETERMINATION OF PAYLOAD BAY DIMENSIONS

The volume of the Gryphon payload envelope was maximized in order to ease satellite design and payload configuration constraints. The maximization of the payload envelope provides several attractive features for potential booster customers. First, a large payload volume allows customers to relieve launch cost burden by participating in multiple customer/satellite deployments. In this manner, a customer pays for only that portion of the payload volume which their package occupies. Second, a large payload bay eases the design constraints which commercial and scientific satellite producers must adhere to. One primary goal of satellite producers is to array their satellites with as many power generating panels as possible. This leads to a desire to maximize satellite surface area or solar array sizes. The limit to these sizes is the available payload volume of the launch system. By easing the volume constraints which the launch system imposes, satellite manufacturers are able to build satellites capable of generating more power. Third, a large

payload volume, in the case of the Gryphon air-launched space booster, allows for compatibility with proposed Space Station Freedom related payload packages. These packages have large diameters and lengths and are, therefore, able to be delivered by few launch systems.

The initial conception for the payload bay was a flat boat shaped volume. This configuration was considered because originally the height of the Gryphon was restricted by the Eclipse to 10 ft. With this configuration, satellites would be placed side by side for multiple launches. This did not seem the most efficient method, as it had never been done before. After discussion with the Eclipse Design Team, the height restriction was lifted and the payload bay (along with the rest of the Gryphon) became cylindrical in shape.

Satellites are usually cylindrical in shape when in the launch configuration. They cover a large range in size, but average 7-10 ft in diameter and 8-12 ft in length. The Space Station Freedom payloads are about 15 ft in diameter and 10-15 ft in length. The volume of the payload bay, approximately 19,675 cubic feet, is large enough to accommodate both of these payloads in various configurations (single, double, and possible triple stacked). The final design of the Gryphon payload envelope is shown in Figure 5.1.

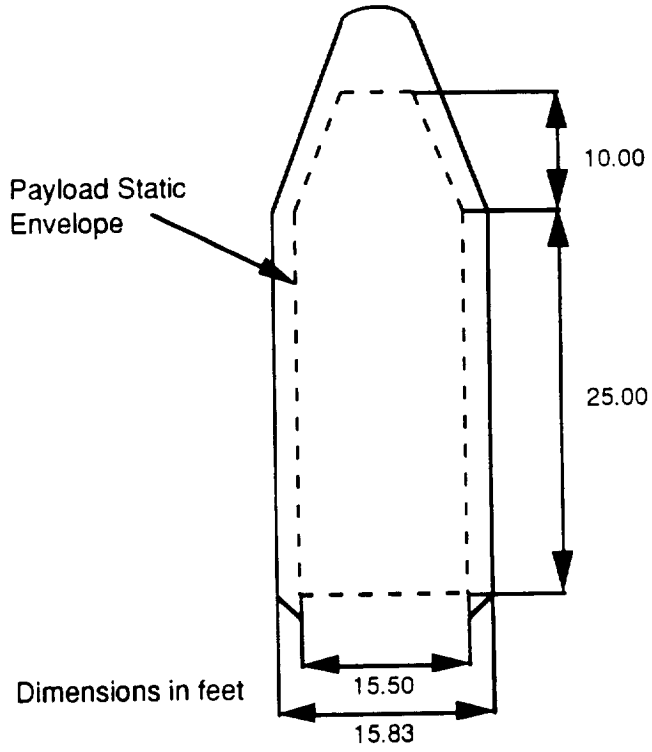

Figure 5.1 Gryphon Static Payload Envelope

The large static payload envelope (usable space in the payload area) has a diameter of 15.5 ft, which provides ample space for most existing communication satellites and many scientific satellites. This diameter is also comparable to that of the Space Shuttle launch system, which represents the currently proposed delivery system for space station payloads. The Gryphon is therefore capable of delivering most Space

Station Freedom Logistics Modules. The large envelope height of the booster provides adequate space for multiple-satellite stacking configurations. It also allows for the possibility of the delivery of satellites to orbit with a variety of large antennae arrays.

5.5 PAYLOAD LIMITATIONS

The purpose of this section is to describe all of the limitations that the payload will impose on the Gryphon design. Due to the nature of the possible payloads, restrictions are necessary to ensure that damage will not occur to the payload. Since the payload is the purpose for the entire project, these limitations must be strictly enforced. The following restrictions are in a general range, because the exact limitations are mission specific, as different satellites and other payloads require different standards. The following is a general envelope, which was obtained by examining several possible payload packages. This helps give an idea of what limitations the other parts of the space booster need to follow.

5.5.1 Cleanliness Requirements for Payload Envelope

The initial cleanliness for the payload fairing is achieved by baking the components in a vacuum at over 212°F. In order to avoid contamination of any of the satellite subsystems, the fairing is cleaned in a class 10,000 environment, which means that in a cubic foot of filtered air, there are no more than 10,000 particles larger than 0.5 microns. The fairing is then bagged using Llumaloy anti-static plastic film before being placed in storage. The satellites and payload shipping container are prepared in a similar manner. All payload preparation and assembly is done in these cleanliness conditions, and the interior of the payload is sealed and kept in this cleanliness envelope until it has left the earth's atmosphere.

5.5.2 Electrical and Thermal Requirements of Payload

For the typical communications satellite payload, the power and thermal needs are fairly small. The typical communications satellite is mostly self-contained, needing little from the launch vehicle. They are in an undeployed position, which means that they are in their most stable and their most dormant formation. Most of the electrical and thermal requirements occur after they are deployed. Once open and in orbit, the orientation of the satellite with respect to the sun and the earth causes many problems with regard to the thermal limitations. Also, because communication satellites are generally solar powered, they also face the problems of power supply once in orbit and open. Because we will be getting these satellites from vendors, these problems are not in the scope of our project, and therefore not included in this report. The following requirements and limitations are only for the undeployed satellites on the launch vehicle.

The satellites generally have battery packs of either NiCd or H_2 which are charged to 50% before the launch. This is usually done with an umbilical which is attached to the payload area, and the power is supplied from one of the ground stations. The status of the H_2 batteries is generally monitored by the use of strain gauges. The status of the batteries is reported as seen in the communications requirement Section 5.5.4. No power will be needed from either the Gryphon or from the Eclipse prior to deployment in orbit.

Inside the payload area, the thermal requirements are specific to the payload, but for many satellites, the temperature envelope is between 62°F and 82°F. On the ground, an air conditioner is generally used on the transportation vehicle and in the assembly clean room. Once mounted, the payload can stay in the environment of the other components, and usually no special thermal accessories for the payload are needed. If there is an abnormal flight path, or higher altitudes are reached before drop, simple heating coils may need to be installed.

5.5.3 Loading and Vibration Limits of Payload

The loading limits were determined from the original Pegasus to be 7.5 g's in the transverse direction, and 2.85 g's in the lateral direction. The final design of the Gryphon has g-loads below these limits. The resonance frequencies of most satellites are usually above 30 Hz longitudinally and 10 Hz laterally. The booster must be designed in such a way that the resonant frequencies do not couple with any of the satellite natural frequencies.

5.5.4 Communications Requirements of Payload

There are relatively few communication requirements for the payload area during flight. To assure that the satellite is operational during ascent, only the basic vital statistics need to be relayed to the launch vehicle. The communication requirements after deployment are critical to the use and applications of the satellite. However, since the requirements are part of post-launch considerations, they do not concern the scope of this report.

The communications requirements for the payload prior to deployment are basically to be sure that the payload is intact and functioning correctly or if any large problems occurred. The communications monitor simple vital signs such as the battery voltage level and the temperature. These are important statistics, which are very inexpensive and easy to monitor. No complicated devices are needed, just simple strain gauges for the batteries, and thermometers to ensure that the thermal requirements are met.

For an average satellite payload there are different communications requirements depending on the phase of the mission. On the ground, the attached umbilical will have the necessary information transmitted down it. When on the plane, the attachment wires will transmit this information. After it is dropped, there is a small R-F (radio-frequency) window which this information can be transmitted through.

5.6 STRUCTURAL CONSIDERATIONS

The Payloads group worked in conjunction with the Structures group to determine the needs for a shroud and a payload/booster interface. The shroud dimensions needed for given payloads (see Section 5.4) were given to the Structures group for their design. The payload interface requirements are discussed in the following sections.

5.6.1 Payload/Booster Interface

Communications satellites are designed to be attached to the booster through a payload interface ring that mounts to the bottom of the satellite near the apogee kick motor nozzle. This allows the load to be transferred to the satellite's structural central core. The layout of a typical satellite is shown in the following figure (Ref 40).

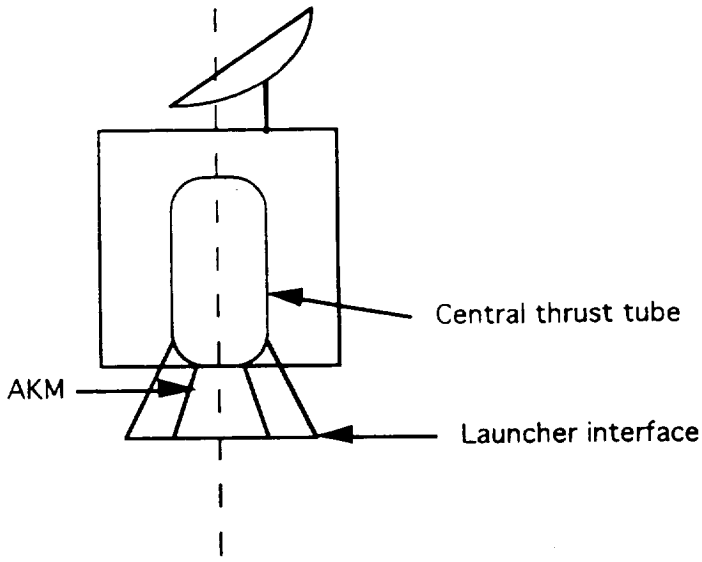

Figure 5.2 Typical Satellite Configuration

The size of the actual payload interface ring depends on the requirements of the satellite(s) being launched. Interface rings in general have compressed springs and explosive bolts to jettison the payload away from the booster when in space.

The Pegasus launch vehicle used two standard payload interface rings with diameters of 38 and 23 inches. Due to the large variance in the sizes of satellites to be carried by Gryphon, more than two standard sized rings will be required. As with the Pegasus, alternative ring sizes can be fabricated for satellites that do not lend themselves to mounting with the standard sized rings.

5.6.3 Double and Triple Satellite Mounting

With such a large payload volume and weight, most launches will carry two or more satellites. A special payload interface ring, or tandem adapter, needs to be designed for these situations. The basis for these designs were the SYLDA and SPELDA, seen in Figure 5.3. (Ref 35)

The purpose of the adapter is to allow the Gryphon itself to carry the acceleration forces of each satellite, rather than the bottom satellite carrying the loads of the top satellite. The satellites are released one at a time, with reorientation between orbital injections.

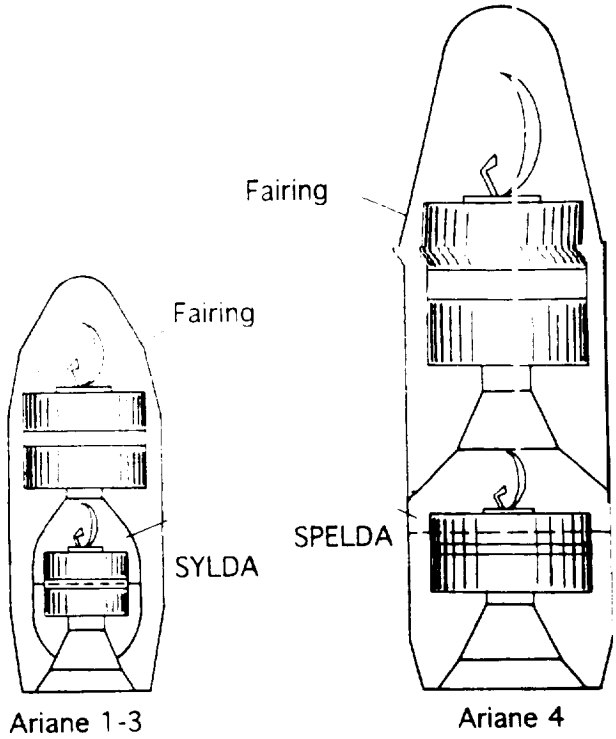

Figure 5.3 The SYLDA and SPELDA

5.7 SPACE STATION FREEDOM OPTIONS

The Space Station Freedom has been designed to be built and resupplied by the space shuttle. Although the shuttle may be the most efficient vehicle to boost the actual space station components into space, it is not the most efficient for some of the resupply payloads. Therefore, the Gryphon has been designed to be capable of boosting some of the space station resupply payloads more cost effectively.

5.7.1 Logistics Element Overview

All resupply of the space station has been compacted into four main elements each designed to be held in the space shuttle.

- Pressurized Logistics Module (PLM): This module stores resupply/storage racks, payload (user) racks, refrigerator /freezer racks, and has room for aisle stowage. These racks carry internal users, crew systems, and spares and maintenance resupplies. (See Appendix D)
- Mini-Pressurized Logistics Module (MPLM): This module is a smaller version of the PLM, carrying identical payloads. (See Appendix D)
- Unpressurized Logistics Carrier (ULC): This module is basically a flat stand which holds the cryo nitrogen carrier, the cryo oxygen carrier,

and the dry cargo carrier. It is used for cryogenic fluids, external users, spares and maintenance. (See Appendix D)
- Propellant Module (PM): This module carries the Hydrazine propellant. (See Appendix D)

5.7.2 Determining Which Elements the Gryphon Can Handle

The major consideration in determining which elements the Gryphon would be able to boost was size and weight. Therefore, listed below are all of the elements with their respective sizes and weights (with cargo). Diagrams of each module can be seen in Appendix D.

- PLM: This module is approximately cylindrical in shape, with a diameter of 14.58 ft. and a length of 23.08 ft. The PLM weighs 34,750 lb.
- MPLM: This module is also cylindrical in shape, with a diameter of 14.58 ft, and a length of 12.47 ft. Its weight is 18,050 lb.
- ULC: This module is simply a flat plate with holes in it. It can be any size, but it must be able to carry the Cryogenic Fluid Container (rectangular, 5.25 ft x 4.5ft x 10.33 ft) and the Dry Cargo Carrier (rectangular, 6.83 ft x 4.33ft x 12.5 ft). The ULC weighs 18,695 lb.
- PM: This module is also rectangular in shape, with dimensions 14.67 ft x 7.33 ft x 13.83 ft . The PM has a weight of 11,040 lb.

Although all of the above modules are about the right size to fit into the Gryphon, the PLM is much too heavy to be considered. The PM is well below the maximum weight of 17,000 lb to LEO. The MPLM and ULC are just a little above the maximum weight. However, 41.6% of the MPLM's weight and 18.4% of the ULC's weight is in the carrier alone; therefore, if these packaging weights could be reduced by as little as 10%, the Gryphon would be able to handle these modules. Consequently, the Gryphon has been designed to carry the MPLM, ULC, and PM.

5.7.3 Structural Considerations

The Gryphon will easily be able to support the self contained MPLM and PM by using a grapple fixture similar to that found in the space shuttle. The ULC will have to be designed specifically for the Gryphon, but will simply be a flat, circular plate with the same diameter as the Gryphon. The design of these attachments is an area for future work.

5.7.4 Docking With Space Station Freedom

The Gryphon will be able to boost any payload into the vicinity of Space Station Freedom (SSF), but it will not be able to maneuver directly to SSF. Any of the logistics modules will need to have an orbital maneuvering system attached to it similar to a satellite with thrusters. The module will then be able to move close enough to SSF so that a grapple arm can reach the module and pull it in.

5.8 CONCLUSION

In conclusion, formulation of the Gryphon payload capacities has involved extensive satellite-oriented research -- their market, their orbits, their sizes, and their limitations. The major market for a space booster is in communications satellites. These satellites need to be placed in a Geosynchronous Earth Orbit. When designing for this type of payload, there were a few limitations that had to be considered. The Gryphon will also be able to help resupply Space Station Freedom. The Gryphon designers have determined that there is a need to carry 7,900 lb to GTO and 17,000 lb to LEO with the specified payload volume, and the Gryphon will be able to satisfy this need.

MISSION CONTROL

Chapter Six

6.1 INTRODUCTION

Mission Control is an important and intricate part of any space system such as an air launched space booster. For the Gryphon, some specific goals were defined that had to be met. Mission Controls specific goals were to identify and gain an understanding of the required mission control systems and components, investigate upgraded components and alternate configurations, and to evaluate components and configurations

The main responsibilities of the mission control group were:

- Guidance, navigation, and control (GNC) of the booster and the payload
- Determining the location and structure of mission control
- Determining airborne support equipment on carrier aircraft
- Sizing of the Gryphon's on-board computer and the payload required to accommodate GNC operations, data storage and handling requirements
- Managing the tracking and data transmission between the ground station and the Gryphon, and between the Gryphon and the space station
- Outlining the flight termination system (FTS)
- Monitoring the health of the booster, payload, and carrier aircraft

The final components and configurations were based on evaluation of cost estimates, required capability, characteristics (weight, dimensions, power requirements, temperature and structural limits), reliability, compatibility with other components and systems, and present and predicted usefulness to Gryphon missions.

6.2 GUIDANCE, NAVIGATION, AND CONTROL

Guidance, Navigation, and Control (GNC) is the most important responsibility of Mission Control. Mission Control must be able to accurately keep track of the Gryphon's position, velocity, and acceleration in order to determine what attitude controls need to be implemented. The selection of components for GNC is based on accuracy, reliability, and cost. To insure that these criteria are met, selections have been limited to strictly "off the shelf" components.

The first aspect of GNC to be considered was the location of mission control, or the ground tracking station. In addition the following subjects will be discussed:

- The inertial guidance system, which is the primary tracking component on board the Gryphon.
- The Global Positioning System which is used in conjunction with the Inertial Guidance System
- A section on additional GNC support from the aircraft

6.2.1 Mission Control Ground Support

The ground support system will monitor the health of the Gryphon and its payload as well as track and determine its position. The attitude of the Gryphon will be determined by sensor information. The ground system will use Gryphon health monitoring telemetry and transmitted mission data to carry out the above functions. The mission control ground support will also determine when the flight termination sequence is necessary and when it will initiate it accordingly.

Because one of the goals of this project is to keep cost per flight at a minimum, it is necessary to compare the cost of using an existing system to the cost of building and maintaining a dedicated system. The main advantage to the use of an existing ground system is that it will be less expensive than building, maintaining, and making necessary upgrades to a new dedicated system. An existing system will also have a defined and predictable cost schedule with high predictable reliability and availability. The disadvantages to using an existing system include matching the mission and the system which may increase cost and reduce mission effectiveness. There are also contractual negotiations required for determining priority agreements such as mission importance relative to other network users, criticality of events, and the amount of control the user has over ground assets.

Since the Gryphon is similar in concept to Orbital Sciences Corporation's Pegasus and will be performing similar missions to the Pegasus there is no justification for building a new existing system. If the Gryphon uses the same ground support systems as the Pegasus, the missions will have already been matched to the system, because of this mission similarity. Mission similarity will also have the advantage of reducing contractual negotiations required for the Gryphon. In keeping with the goal of minimizing costs, the continued use of the existing ground support systems is recommended.

Each Gryphon mission is supported with a tracking, telemetry, and command (TTC) ground based facility. Tracking is accomplished with a network of ground based

radar sites, supplemented with a global positioning satellite system (GPS). The ground facility is the locus of all downlink telemetry from the vehicle. This includes navigational data as determined by the on board navigation system, and all data from health and subsystem monitoring. All carrier aircraft operations will be monitored by the facility, and it will provide a direct radio link with the Launch Panel Operator (LPO) aboard the aircraft. The ground facility also determines the range safety specifications for each particular mission, and is responsible for activation of the flight termination system in accordance with any violation of range safety specifications.

The Gryphon project will employ all TTC services from the Eastern and Western Space and Missile Centers. All captive carry takeoffs from Kennedy Space Center will be supported by the eastern range, and all those from Vandenberg AFB will be supported by the western range. A high end cost estimate for TTC services from these locations is $75,000 per launch.

6.2.2 Inertial Guidance, Navigation and Control

Hardware description

The system's central hardware consists of a strapdown inertial measurement unit (IMU) supplemented with a navigation processor card (NPC), and the flight computer's autopilot processor.

The IMU consists of integrating gyroscopes, linear accelerometers, and sensor electronics. A single gyro produces one component of the total angular inertial reference, which is known in body defined coordinates (along one of the axis). Each accelerometer provides one component of the linear inertial constant, where each component corresponds to one body defined coordinate axis.

The IMU is supplemented with the NPC which receives a position and velocity reference from a GPS receiver in the avionics bay. The NPC performs all navigational and control calculations, and transmits navigation data and flight control data to the flight computer's autopilot processor. The NPC uses the GPS supplied position and velocity reference to improve the accuracy of these calculations. The GPS reference is compared to existing computed values, and their comparison is monitored to control error propagation in computational iterations.

The flight computer's autopilot processor operates stage separation and the flight control mechanisms. It integrates navigational data and flight control data with the pre-programmed mission data, steering the Gryphon along the desired trajectory. The mission data is programmed specifically for each mission. The autopilot also transmits the computed navigation data to the ground station via downlink telemetry. This data is used for post-mission analysis of the systems operation. The hardware control block diagram in Figure 6.1 is a general schematic of the hardware functions, which vary with specific systems.

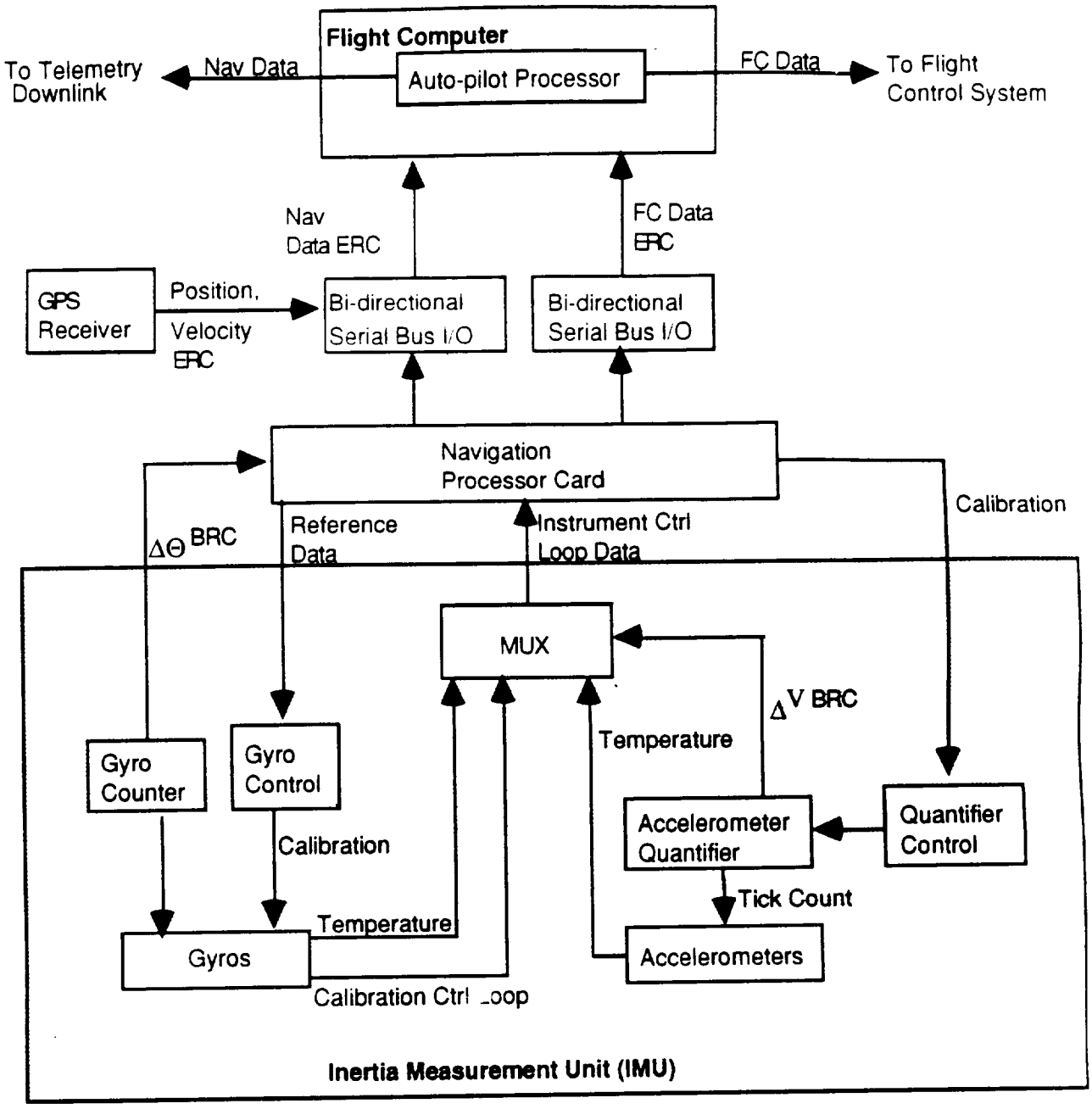

Legend:

Nav Data = Navigation data includes flight control data and position
FC Data = Flight Control data includes linear and angular rates, linear acceleration, attitude
ERC = Earth Reference Co-ordinate
BRC = Body Reference Co-ordinate
MUX = multiplexor
$\Delta\Theta$ = Attitude angular change
ΔV = change in velocity vector

Figure 6.1 GNC Hardware Functional Block Diagram

Software description

The system software functions at three levels:

- Inertial instrument control and sensing (ICS)
- Navigation and control calculations
- Flight control.

ICS software is integrated into the IMU electronics. It performs high speed sampling of the inertial instruments. This raw data is converted to velocity and attitude angle change and transmitted to the NPC. This software also maintains the performance of the inertial instruments. The gyros are calibrated with a closed loop control to compensate for angular drift and momentum loss due to environmental disturbances and mechanical friction respectively. The accelerometer quantifier is also operated with this software in a closed loop control.

The NPC holds the navigation and control software. The NPC inputs a position and velocity reference from the GPS receiver. Using the data from the NPC, velocity and attitude angle change are converted into instantaneous position, velocity, attitude, attitude rate, and linear acceleration. Numerical methods are employed in quaternion integration, direction cosine matrix transformation, and 313 Euler angle transformation from body defined coordinates to the inertial frame.

Flight control software (FCS) is preprogrammed with mission data load software (MDL), which specifies the mission for the autopilot FCS to follow. The navigational data and flight control data, both calculated in a closed loop iteration process, are used by FCS to operate the flight control mechanisms on the exterior of the vehicle.

Hardware selection

Using "off the shelf" hardware minimizes cost and maximizes confidence. The Litton LR-81 system is the choice for the GNC subsystem by OSC. It is currently under contract for use and is thus readily available and cost effective, while providing the functions desired on the Gryphon system. Information used in the consideration of spacecraft integration is given in Table 6.1. The autopilot processor is an element of the flight computer, included in Section 6.3.

6.2.3 Global Positioning System

The Global Positioning System (GPS) works in conjunction with the Inertial Measurement System to obtain accurate measurements for position, velocity, and acceleration. The GPS functions in this tracking system to update the IMU on frequent intervals on the vehicle's current position and velocity reference. As was mentioned previously, the GPS reference is compared to existing computed values, and their comparison is monitored to control error propagation in computational iterations.

Table 6.1 Litton LR-81 Inertial Measurement System Characteristics:

Cost	$100,000
Size of Sensor assembly	6.3 x 2.5 x 3.0 in.
Electronics assembly	7.0 x 7.5 x 3.2 in.
Navigation processor assembly	7.0 x 7.5 x 3.2 in.
Weight (Lb.)	12.8 lbs
Power requirements	28 Vdc, 43W ave., 200W peak
Cooling	air conduction
Output data rate	100 Hz
I/O	RS-422 bi-directional serial bus
	(Synchronous Data Link Control)

A GPS receiver makes measurements of the distance between its antenna and a number of GPS satellites. By combining those measurements with the knowledge of the satellites position stored in an ephemeris, the receiver is able to determine its own position. The GPS receiver takes the ephemeris parameters and computes the coordinates of the satellite in an earth-centered, earth-fixed (ECEF) coordinate system. A new set of orbital parameters is computed for each one-hour period using overlapping spans of four hours. A GPS satellite broadcasts the appropriate set of parameters during a particular one-hour interval.

The details of this computation have been carefully spelled out by the designers of the Global Positioning System and can be found in a number of reference publications. The particular ECEF system used by GPS is the World Geodetic System 1984 (WGS 84) of the Defense Mapping Agency (DFA). For all intents and purposes, the reference frame of WGS 84 and the North American Datum of 1983 (NAD 83) are identical.

The broadcast ephemeris is computed with sufficient accuracy to guarantee the design goal of horizontally positioning a GPS receiver with an accuracy of 16 meters. This is the accuracy of the Precise Positioning Service (PPS), the service afforded to authorized (primarily military) users. When GPS is fully operational, the accuracy of the broadcast ephemerides are intentionally degraded as one of the mechanisms for implementing the policy of selective availability (SA) for the Standard Positioning Service (SPS) available to civilian users.

Using both cost effectiveness and reliability as primary criteria for selection, the Trimble Quadrex is the GPS Receiver chosen for use on Gryphon. Trimble also provided the six-channel GPS Receiver that was used on Pegasus, but the Quadrex is an improved version because it includes a multiple antenna. The multiple antenna provides better visibility and attitude determination. The quadrex's characteristics are detailed in Table 6.2.

Table 6.2 Trimble Quadrex GPS Receiver Characteristics:

Cost	$ 14,000
Size	7" x 7" x 2"
Weight	3 lbs
Power Requirements	3.5 W
Operating Temperature	-40° F to +158° F
Max. Velocity	25,000 ft/sec
Accuracy	75 ft (with SA: 300 ft)
I/O	RS-422 bidirectional serial bus
	(Synchronous Data Link Control)

6.2.4 Aircraft Support

For a variety of reasons the Gryphon will need support from one or more additional crew members on board the carrier aircraft. The aircraft must be able to monitor the Gryphon's systems before launch and keep track of the Gryphon immediately after launch for safety purposes. In addition, the Gryphon IMU needs to be updated before launch since the GPS is not activated until after the launch. This is most conveniently done from the carrier aircraft.

It was decided that one additional crew member, a Launch Panel Operator (LPO), would be sufficient to provide these external needs. His/her responsibilities will include:

- Monitor Gryphon and payload status
- Provide external power (aircraft power) to Gryphon
- Switch between external and internal power (prior to launch)
- Update Gryphon IMU prior to release
- Download mission data to the flight computer and verify mission data load
- Prepare and enable vehicle for drop
- Capture, record, and display data from the vehicle and payload

The LPO will be seated at a special console that consists of:

- Ruggedized PC
- Display devices
- Mass data storage device
- Precision IMU

The most important unit in the special console is the ruggedized computer, a North Atlantic KMS. All of the telemetry between the aircraft and Gryphon are handled through the PC, along with the data storage, switch of power sources, and the processing of IMU information. There will be three monitors for visual display. The first two will be fore and aft camera views from Gryphon, as part of the health monitoring system. The third will be a variable display, depending on what the LPO is currently checking. It could display IMU, power, storage, or health-monitoring data. The mass data storage device is the largest component in the LPO console. For a more detailed version of the LPO's console, see section 6.4.1

The precision IMU is a ring-laser gyro, the Litton LN-93. The ring-laser is much more accurate than the rate gyro on board Gryphon, and updates the latter every second. Only after Gryphon has been launched will it switch to GPS for updating.

Launch Control Organization and Decision Process

The launch control organization will consist of three basic functional areas. They will be the Management Group, the Operations/Engineering Group, and the Airborne Operations Group.

The Management Group will include:

- Payload Mission Director
- Gryphon Mission Director
- Range Mission Director
- Flight Operations Director
- Launch Services Director

The Operations/Engineering Group will include:

- Test Conductor
- Vehicle Engineer
- Payload Engineer
- Range Control Officers

The Airborne Operations Group will include:

- Flight Controller
- Carrier Aircraft Crew

A mission specific launch process should have coordinated GO/NO GO situations during actual launch operations. The process should be structured so that all critical events and GO/NO GO situations are coordinated through the appropriate mission director. The flow for launch decisions will mirror the launch control organization, where anomalies are worked by the appropriate groups and decision-making is passed to the Management Group.

6.3 ON-BOARD COMPUTER SYSTEM

Once launched from the carrier aircraft, the Gryphon operates as an autonomous system that is able find it's way to GTO along a pre-programmed flight trajectory. Except for the event of flight termination, the Gryphon receives little or no flight command from the ground. The ability to execute the mission independently relies on the on-board computer system.

The on-board computer system interfaces with the sub-systems and determines the course of action that the sub-systems should take. In short, it functions as the brains behind the Gryphon and plays a critical role in the success of the mission. In defining the computer system for the Gryphon, the following steps are taken, most of which are discussed in the subsequent sub-sections :

- Identify mission objectives and mission characteristics.
- Establish a baseline for system characteristics based on mission requirements and typical design values.
- Use baseline to source for specific computer systems in the market.
- Establish method of integration and control between computer system and sub-systems.

6.3.1 Calculation of System Characteristics

The main characteristics of a computer system are the throughput and the memory size. The throughput defines the speed at which instructions are executed by the system and is measured in KIPS (Kilo Instruction Per Second) and MIPS (Mega Instruction Per Second). The memory size defines the capacity for storing information and is measure in KW (Kilo Words) and MW (Mega Words). For further detail see Table 6.3.

The memory size is divided into two categories: Code and Data sizes. Code size defines the memory size that is used to store the instruction sets. Data size defines the memory size that is used to store the input and output variables. For example, the operating instructions in a hand-held calculator will be defined as code while the numbers that are displayed will be data. Together, the throughput and the memory size are the essential driving parameters behind the design of a computer system. Table 6.4 records a simple method used to obtain the throughput and memory size of a computer system that suits the mission requirements of the Gryphon. The method and its associated typical data are from James R. Wartz and Wiley J. Larson. Certain assumptions are used in the calculations which are based on industry-wide standards which provide a valid framework and are seen below:

1) 1750A class Instruction Set Architecture
2) Ideal class S , minimal class B classification [1]
3) 50% redundant processing capacity at launch
4) 50% redundant processing capacity for development [2]
5) A Word is 16-bits long

6.3.2 Other estimated system parameters and considerations

Pegasus I used a flight computer system that was developed by AI Tech. (Israel) while the existing Pegasus uses one that was developed by O.R. computers (Germany). Table 6.3 information applies to the Pegasus computer system and was used as relevant baselines in the Gryphon's system.

---

(1) 'Class S' labels the computer system as space-ready. 'Class B' is label for space-ready systems that has not gone through extensive tests as class S. 'Class B' systems are consequently less expensive but less reliable.

(2) 50 % redundancy is used to accommodate unexpected increases in computing requirements that are typical in the development cycle of a computer system.

Table 6.3 Characteristics of Gryphon Computer

Processor	32 bit, 68000 Motorola based
Architecture	Versa Module Europe Bus
Telemetry processor	16 bit
Weight	10 lb.
Dimensions	4" x 8" x 8"
Power requirement	22-36 Volts D.C.
Temperature tolerance	-40 °C to +85 °C (optimum 25 °C)
Reliability	0.95 at end of 10-year period
Estimated cost	$2 Million (includes software development)
Radiation protection	hardening to 1 Mrad
Vib. amplification	close to factor of 1

Table 6.4 Throughput and Memory Calculations

On Board Applications	Code (K W)	Data (K W)	Throughput (KIPS)	Execution Freq. (Hz)
1) command processing	1.0	4.0	7.0	10.0
2) Telemetry	1.0	2.5	3.0	10.0
3) Attitude sensor processing	2.0	15.0	2.0	0.01
4) Attitude determination and control				
a) Kinematics integration	2.0	0.2	15.0	10.0
b) Error determination	1.0	0.1	12.0	10.0
c) Thrust control	0.6	0.4	1.2	2.0
d) Complex Ephemeris	3.5	2.5	4.0	0.5
e) Orbit propagation	13.0	4.0	20.0	1.0
5) Complex autonomy	15.0	10.0	20.0	10.0
6) Fault monitors	4.0	1.0	15.0	5.0
Fault correction	2.0	10.0	5.0	5.0
7) Power management	1.2	0.5	5.0	1.0
Thermal control	0.8	1.5	3.0	0.1

Operating software	Code (K W)	Data (K W)	Throughput (KIPS)
8) Executive	3.5	2.0	21.0
9) I/O handlers	2.0	0.7	40.0
10) Built-in tests & diagnostics	0.7	0.4	0.5
11) Math utilities	1.2	0.2	0.0
12) Run-time kernel	8.0	4.0	0.0
Sub-total	62.5	59.0	173.7
Redundancy	15.4	59.0	173.7
Grand total	125.0	118.0	347.4

In order to appreciate the magnitude of the figures computed, Table 6.5 compares the Gryphon's computer system characteristics with existing commercial workstations and other space-based computer systems:

Table 6.5 Comparison with Existing Systems

System	Applications	Throughput	Memory
Gryphon	Gryphon	347.4 KIPS	243 K W
TDY 750	Milstar	450 KIPS	512 K W
ATAC 16ms	Galileo	500 KIPS	64 K W
GPC	Shuttle	200 KIPS	32 K W
Sun-Sparc IPX	commercial	15.8 MIPS	32 M W
Sun-Sparc 1+	commercial	15.8 MIPS	2 M W
Dec 3100	commercial	14.0 MIPS	1 M W
Dec 5000	commercial	24.0 MIPS	1 M W

Besides meeting the computing requirements of the mission, some other considerations involved in the choice of a flight computer are cost, compatibility with existing support equipment, and reliability. A breakdown of each is as follows:

Cost involves the price of the hardware as well as the cost of the software development. The cost of software development is usually more substantial than the hardware cost since the software is developed specifically to meet different mission requirements.

The flight computer communicates with the carrier plane LPO computer during transit to launch altitude and also with the ground support computer during flight preparation. It is important that all three systems are compatible with each other for effective communication.

The reliability of the flight computer is increased by having redundancy, radiation protection and data error detection and tolerance. Redundancy comes in the forms of hardware and information redundancies. Hardware redundancy is the addition of extra hardware (memory units, CPU, etc.) for detecting or tolerating errors. Software redundancy is the addition of extra software needed to detect and tolerate errors. Many techniques are involved in each form of redundancy.

Cosmic rays at GTO are strong enough to cause temporary or permanent data errors. To prevent this, radiation shielding is necessary. Typical protection level is set at 1 Mrad._In view of the considerations mentioned above, the on-board computer system developed by O.R. computers is favored because of its proven reliability and accuracy when used on the Pegasus.

6.3.3 Flight termination system

The flight termination system (FTS) is activated in the event of a mission termination and premature stage separation. It is the only semi-autonomous system in the Gryphon and operates independently from the flight computer system. Essentially, the FTS detonates shape charges placed in strategic locations at each stage. The explosions deactivate the propulsion system without fragmenting the motors which is accomplished by rupturing

the motor case which relieves the motor case pressure. The disabled Gryphon then falls towards the ocean.

The FTS is mechanically disabled until after the release from the carrier aircraft and is armed prior to first stage ignition. This approach ensures that the FTS cannot endanger the carrier aircraft prior to the release. After the release, the FTS is electrically enabled for range safety before first stage ignition.

The FTS can be initiated either by automatic or by ground control command. Automatic flight termination is initiated in the event of premature stage separation. Separation sensors relay signals to the microprocessor of the FTS, which then initiates the detonation sequence. Ground command flight termination is initiated when range safety is violated. For example, if the Gryphon flies off-course from the pre-planned flight trajectory. The detonation sequence is initiated when the FTS receives the relevant signal on its receiver. A decured decoder on the FTS receiver ensures that only the right ground command signal will by accepted by the FTS. This is to done to ensure that the system is not activated by unwanted signals.

The control block diagram for the FTS is shown in Figure 6.2.

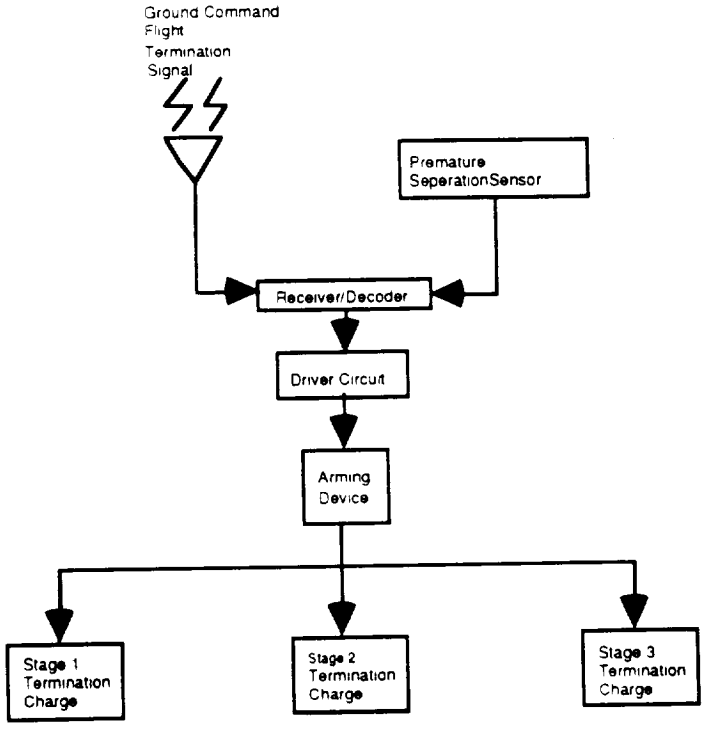

Figure 6.2 Flight Termination System Block Diagram

6.3.4 Sub-systems Integration and Control

The flight computer interfaces and controls the propulsion, interstage separation, attitude sensing and control, guidance and navigation, and communication sub-systems. During its flight to launch altitude, the flight computer communicates with the carrier plane's LPO computer via an umbilical RS-422 cable. The Gryphon's IMU system is updated by the LPO's IMU and GPS systems.

During launch, sensors located near the separation mechanism detects the Gryphon's separation from the carrier aircraft (Stage 0) and relays the information to the flight computer system through a multiplexer[3] via RS-422 cables. Taking this cue, the computer initiates the ignition of the first stage rocket motors after a time interval for the carrier plane to reach safety distance from the Gryphon. The motors are started, setting the Gryphon on its independent trajectory to GTO.

Signals from the GPS and the IMU systems are compared with the pre-programmed flight trajectory. Through a closed-loop control scheme, the flight computer adjusts the attitude of the Gryphon by hydraulically gimballing the rocket motors. Attitude control is also made possible by six hydrazine thrusters located on stage 3. These thrusters are controlled by the flight computer via a pyro driver.

The flight computer initiates the separation between stages. Sensors mounted on the propulsion system provides signals to the computer system. The computer system continually monitors the signals until a preset threshold is reached, after which interstage separation is initiated via interstage pyro drivers. Telemetry data from the computer system is fed to the S-band telemetry transmitter for transmission to ground control. Figure 6.3 shows the integration of the flight computer with the sub-systems mentioned previously.

6.4 COMMUNICATIONS SYSTEM OVERVIEW

The goal of the communication system is to provide the best signal transmission in terms of power, accuracy, reliability and security for the least amount of mass, size, and expense. The Gryphon's communications system will provide the link between the spacecraft and ground control after launch from the carrier aircraft. The communication system's primary functions will be to transmit telemetry and tracking data to the ground control station and to transmit termination commands, if necessary, from the ground to the Gryphon. The responsibility of effectively broadcasting and receiving these signals makes this system crucial to any successful Gryphon launch.

Telemetry consists of functions such as voltages, temperatures, and accelerations, which require monitoring to determine whether all subsystems are operating correctly. The sampling of each telemetry sensor in sequence creates telemetry data. Tracking data consists of position, velocity, attitude, and acceleration information received from the GPS and the IMU. If necessary and for security purposes, the termination command will be sent via an encoded signal from the ground to be received and decoded by specific FTS hardware on the Gryphon.

---

(3) A multiplexer is a device which selectively channels one of many input signals to one output. The output of the multiplexer is connected to the input port of the computer system.

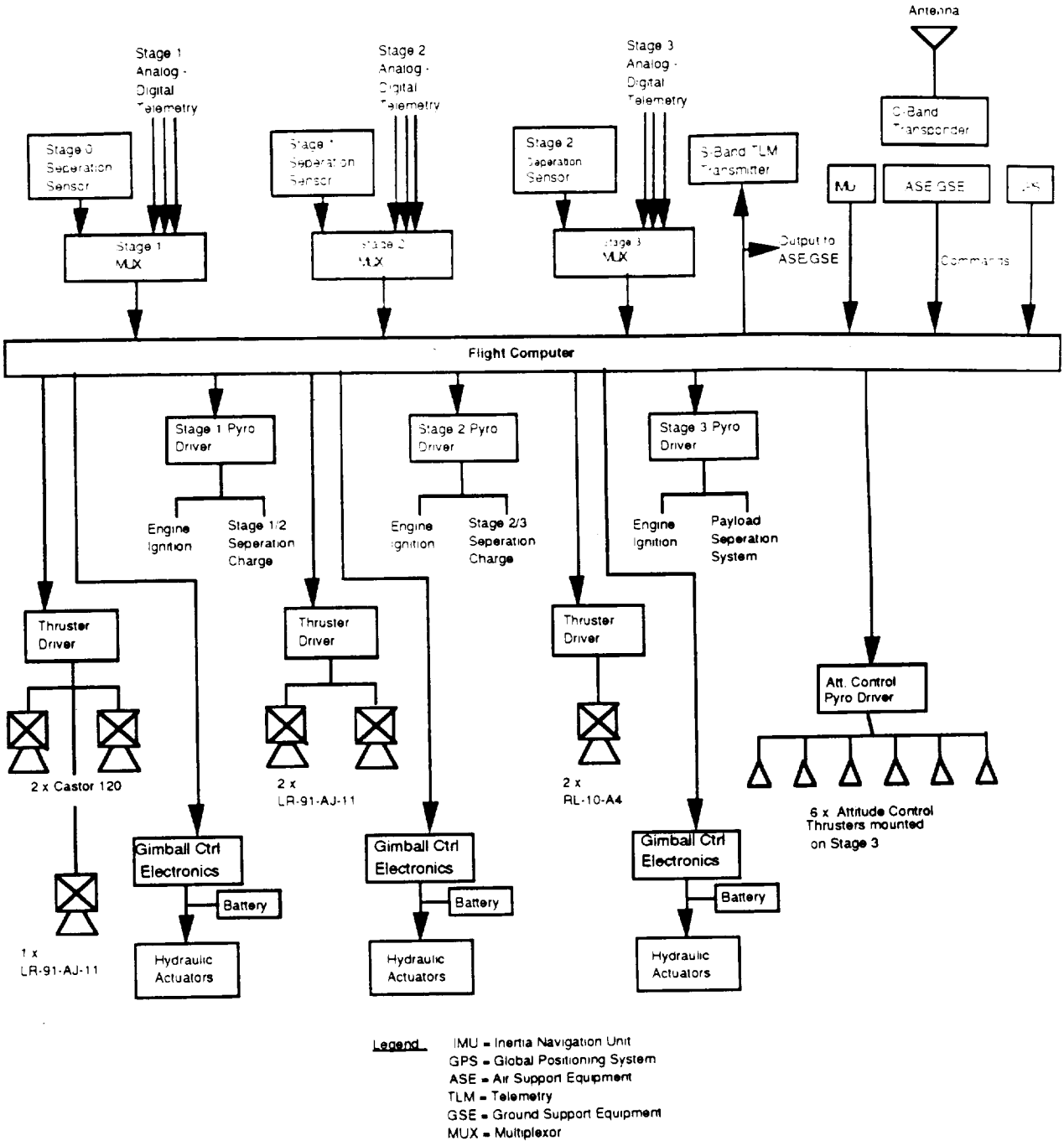

Figure 6.3 Overall Sub-System Block Diagram

The communications system components will include the system antennae, transmitter, multiplexers, receivers, decoders, and radar transponder (see Figures 6.2 and 6.3). The antennae and transmitter, together, allow the system to transmit composite signals to the ground station. The multiplexers modulate the downlink carrier wave with mission telemetry by varying the amplitude, frequency, or phase of the carrier wave for the transmission of data. The multiplexer combines all telemetry data into a single bit stream. This compacted signal allows for a greater data transmission rate. The receivers and decoders will work together to acquire, demodulate and decode the flight termination command if necessary. The radar transponder will receive, amplify, and re-transmit radar signals for the purpose of enhancing the vehicle's radar return for better determination of the vehicle's position.

6.4.1 Data Storage

The LPO console requires a mass data storage device for the storage of mission data before download to the flight computer and recording of data from the vehicle and payload. Typical devices for storing data are shown in Table 6.6.

Table 6.6 Typical Data Storage Devices

Data Storage Device	Capacity
Tape recorders	75×10^9 bits
Solid-state recorders	128×10^6 bits
Bubble memory	128×10^6 bits

Optical data storage is developing into a more efficient way of storing large amounts of data in a small amount of space. Because of the mass data storage requirement for the Gryphon, it is recommended that optical storage be implemented when it becomes available.

6.4.2 Telemetry, Mission Data, and Radar Frequency Selection

The choice of communication band frequency defines the signal between the spacecraft and the ground station. The radio frequency (RF) spectrum has been divided into several categories based on frequency. Agreements on these bands originated with the International Telecommunications Union (ITU) and the World Administrative Radio Conference (WARC). Some of the frequency bands are shown in Table 6.7. These frequencies determine the wavelength of the signal in accordance with:

$$c = \lambda f \qquad \text{(Eq 6.1)}$$

where:

c = speed of light
λ = wavelength of signal
f = frequency of signal

Designers have little control in determining at which frequency their spacecraft's information will transmitted. While the designer can choose the desired frequency, the actual allocation of frequency bands for commercial users is regulated in the United States by the Federal Communications Commission (FCC).

Table 6.7 Limitations on Frequency Bands Established by International Telecommunications Union (ITU)

Frequency Band	Uplink Frequency Range (GHz)	Downlink Frequency Range (GHz)	Service
UHF	0.2 - 0.45	0.2 - 0.45	Military
L	1.635 - 1.66	1.535 - 1.56	Maritime/Navig
S	2.65 - 2.69	2.5 - 2.54	Broadcast
C	5.9 - 6.4	3.7 - 4.2	Domestic Commsat
X	7.9 - 8.4	7.25 - 7.75	Military Commsat
Ku	14.0 - 14.5	12.5 - 12.75	Domestic Commsat
Ka	27.5 - 30.1	17.7 - 19.7	Domestic Commsat
SHF/EHF	43.5 - 45.5	19.7 - 20.7	Military Commsat
V	60	60	Satellite Crosslinks

Because space is limited on each band, it is becoming more difficult to acquire permission to broadcast at certain frequencies such as the C, S, and Ku bands. Indeed, for a new communication service, the approval process may take 3 to 5 years. With other users of close frequency signals, in close proximity interference also becomes a problem. Since the Pegasus is already cleared to use the S-band for telemetry transmission, there is no need to choose a different band for the Gryphon since it will perform similar missions.

The Gryphon will also carry a radar transponder which is a receiver-transmitter combination that typically amplifies the signals it relays. The purpose of the radar transponder is to enhance the Gryphon's radar return for better position accuracy. Since one of the expected missions of the Gryphon will be to re supply the Space Station Freedom, the Gryphon's radar system should operate at the band at which the space station operates. This will allow the space station to make use of the signals on a position transmitted by the Gryphon. As an alternative, the Ka band is suggested since it offers greater availability and design flexibility.

6.5 CONCLUSION

After significant investigation and research was performed, a better understanding of mission control systems and components was reached. While researching the design for the system, it was necessary to keep costs down, which can be accomplished by using existing technology. As a result of this investigation, a cost effective and sophisticated system has been designed by the Mission Control Group. However, since this is the first phase of design, further research must be performed to insure that the most cost effective and advanced design is used on the Gryphon.

STRUCTURES

Chapter Seven

7.1 STRUCTURES GROUP RESPONSIBILITIES

The structures group is responsible for the structural integrity of the Gryphon. In addition to the weight constraints imposed by aerospace design, the Gryphon project is very concerned with minimizing cost. Structural designs will reflect this by using proven technology, inexpensive materials, and simplistic, easy to manufacture parts.

The structural design of the Gryphon begins with the main booster structure. This includes the exterior hull of the vehicle which houses the engines and all fuel tanks. Yield due to static g-loads and aerodynamic loads is the first priority. Determination of natural modes and frequencies and global buckling loads will also be explored.

The payload shroud and fairings comprise another area of interest. The shroud and fairings protect the payload from aerodynamic heating and pressure, and reduce the overall drag on the vehicle. Their composite construction is susceptible to failure from ply yield and localized buckling, both of which are analyzed.

Inside the payload bay, the payload interface ring physically connects the payload with the lower stages. Not only must the ring withstand the acceleration loads imposed by the vehicle, but it must be resistant to engine vibrations. Extensive static and dynamic analysis was performed to insure the stability of the payload under these load conditions.

In the upcoming chapters, each of the above components will be analyzed in turn. Loads will be determined in each case, and appropriate structural analysis will be performed. Finally, the weights and dimensions of each part will be listed.

7.2 MAIN BOOSTER STRUCTURE

The Main Booster Structure is comprised of three major groups of components:

- Stages 1 through 3 hull including skin, longitudinal stringers and lateral buckling rings.
- Two Castor 120's attached to the main hull through struts.
- Strut and plane attach rings, some of which replace buckling rings.

The role of the Main Booster Structure is to provide attachment points for the engines, tanks and control equipment while at the same time withstanding longitudinal and lateral aerodynamic and thrust loads. The driving design objective was to minimize the weight and cost of the structure. This implied using traditional aerospace materials such as aluminum alloys as well as requiring the manufacturing and assembly to remain simple. In general, proven concepts were preferred over more advanced ideas.

While designing each group of components, an initial guess for dimensions and configurations was derived from an approximate analysis. This guess was then used in an iterative process utilizing Finite Element Modeling software to arrive at the final values. Most of the time, the final FE. model did not drastically deviate from the initial guess, but provided more detailed results and a deeper understanding of the interaction between the individual components.

For all components, two distinct structural problems were investigated:

- Static analysis, considering maximum stresses, deflections as well as global and local buckling behavior.
- Dynamic analysis, specifically the normal modes and their respective natural frequencies.

These two problems are closely coupled, because the minimum weight requirement on the structure resulted in very low natural frequencies.

Several assumptions were made regarding the FE. modeling of the Main Booster Structure:

- The hull and the Castors, including all the sub components were modeled as a beam. For this reason all local design (i.e. stringers and rings) had to be done analytically.
- Thrust loads and aerodynamic forces and moments were resolved into longitudinal and lateral loads and moments. The worst case loading was assumed to occur when Stage 1 would acquire a 2.5g longitudinal and 2.5g lateral acceleration at burn-out.
- The second load case of interest occurs when the Gryphon is carried by the plane. A 2.5g lateral load was applied for this case.

7.2.1 Main Hull - Static Analysis

The exterior hull as mentioned previously houses the engine and all fuel tanks. A breakdown of the main hull is as follows:

- Outer Skin
- Longitudinal stringers
- Lateral buckling rings

The main role of the skin is to reduce drag on the vehicle and protect sensitive interior components such as the avionics equipment. The stringers take most of the axial and bending loads incurred from accelerations and aerodynamic forces such as lift and drag. Since the stringers are basically long, slender beams, local buckling is prevented by placing lateral buckling rings at appropriate stations along the hull. The rings together with the skin will also take any shear loads present. All components of the main hull are manufactured from 6061 Aluminum alloy. The two global design requirements for the hull were:

- Maximum von Mises stress is not to exceed the yield stress divided by a 1.25 safety factor.
- The critical global buckling load of the hull is to exceed twice the maximum axial load.

Outer Skin Design

The outer skin of the hull is bolted to the stringers and the buckling rings. It has a thickness of 1/64 inches for all stages. The skin is assumed to carry bending loads only and will buckle locally. The thickness represents a lower estimate, below which local failure might be expected. Besides buckling, no further analysis was completed on the skin.

For the analysis of the skin, the thickness of the outer skin was chosen as 1/64 inches. Since the skin is expected to carry some bending loads, local buckling was examined. Treating the skin locally as a plate, we can utilize the plate-buckling equation:

$$\sigma_{cr} = -K \frac{p^2 E}{12(1-\nu^2)} \left(\frac{h}{b}\right)^2 \qquad \text{(Eq 7.1)}$$

Where σ_{cr} represents the critical buckling stress, h is the plate thickness and b the local plate width. Sample values for Stage 2 were used in the plate buckling equation because this stage has the most severe loading conditions. h is the distance between buckling rings and b is the distance between stringers:

$$h = 0.015625 \text{ in}$$
$$b = 23.6 \text{ in (approx.)}$$

Also, K is a constant dependent on the local height over width ratio as well as the boundary conditions and is estimated to be around 4 from the literature [Eisley]. Using material properties for aluminum, the resulting critical stress turns out to be:

$$\sigma_{cr} = -47.5 \text{ psi}$$

We can safely conclude that the skin will not carry any significant axial compressive or bending loads. It will only resist shear. Its torsional modulus equals:

$$J_{skin} = \frac{\pi}{2}(r_{out}-r_{in})^4 \qquad \text{(Eq 7.2)}$$
$$= 71500 \text{ in}^4$$

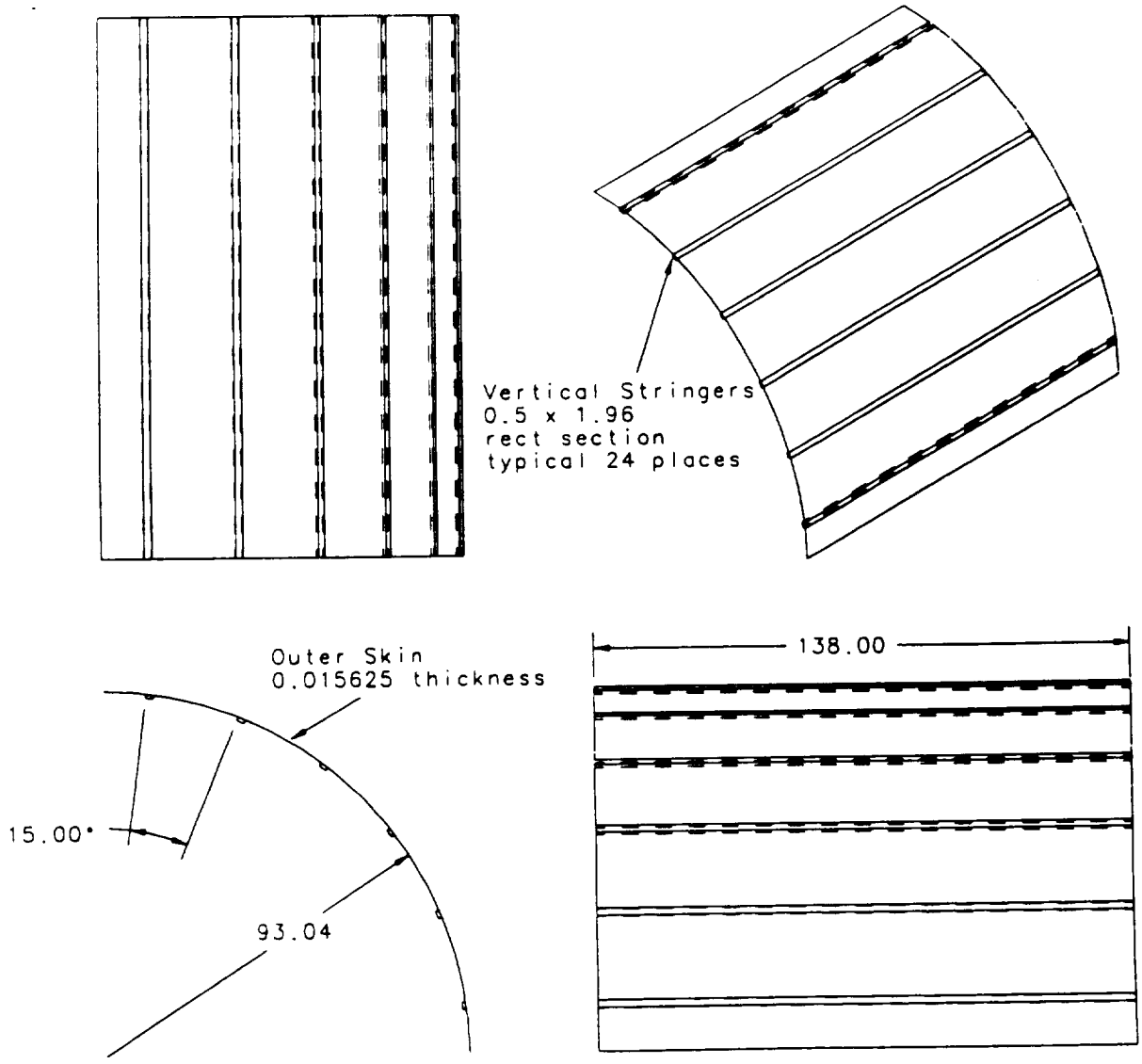

Figure 7.1 Typical Skin Stringer Arrangement

Longitudinal Stringer Design

The major load carrying components of the hull are the longitudinal stringers, 24 of which evenly space out a 15 foot diameter circle, as shown in Figure 7.1. They are designed to withstand axial and bending loads with a safety factor of 1.25. Their cross

section is rectangular, with the long side facing away from the center of the circle. Since the loads vary between stages, so do the cross sectional areas.

With the skin not taking much axial compressive or bending loads, the longitudinal stringers had to be designed to function as the major load carrying components. In order to find the maximum loads, the following assumptions had to be made:

- The worst g-loads occur while Stage 1 is burning. At maximum thrust gimbal angle, they correspond to: 2.5g longitudinal and 2.5g lateral.
- The total drag force equals 165,000 lb. and the total lift force equals 115,000 lb. These are upper limits of lift and drag, given the launching altitude of the Gryphon and maximum speed during ascent.

A finite element model for the Gryphon was created, using beam elements for all components such as the stages, Castors, struts and payload shroud. The masses of the individual components were modeled as lumped masses at the mid-point of each beam element (see Figure 7.2, Table 7.1). The components modeled are as follows.:

- Stage 1: LR-91, propellant stage, Castor 120 (2)
- Interstage between Stages 1 and 2
- Stage 2: propellant stage
- Stage 3: RL-10, propellant stage, power/avionics stage

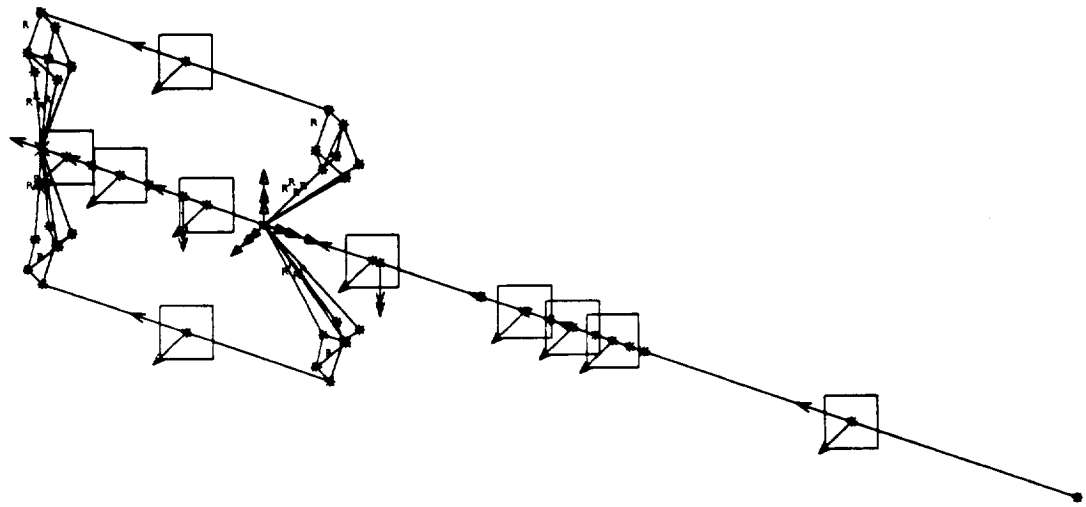

Figure 7.2 Static Finite Element Model of the Gryphon

The lengths and approximate masses of these components are listed below:

Table 7.1 Lengths and Masses of components for Finite Element model

Component #	Component Name	Total Length [ft]	Total Mass [lb.]
1	LR-91 Stage 1	9.25	3070
2	LR-91 S1 Propellant	3.25	27200
3	Interstage	7.00	6300
4	Stage 2 Propellant	23.50	176200
5	RL-10	6.00	790
6	Stage 3 Propellant	6.80	9000
7	Power/Avionics	6.80	1600
8	Payload Shroud	43.40	11000
9	Castor 120 (2)	37.00 (each)	236000 (total)

- Note that these were the masses and lengths used in the final modeling run. Updated data became available after the deadline, but was beyond the scope of this report.

Because the Gryphon is unrestrained during flight, the model was clamped at the center of mass, free to pivot around it. In order to make the model statically equivalent, the following moments were added (all moments about the y-axis) to account for the moment of inertia of the stages. (See Table 7.2) More detailed values are given in Appendix F.2.

Table 7.2 Moments acting on the Gryphon

x location [ft]	Magnitude [lb. ft]
16.6	$-2.50\ 10^6$
31.0	$-3.23\ 10^7$

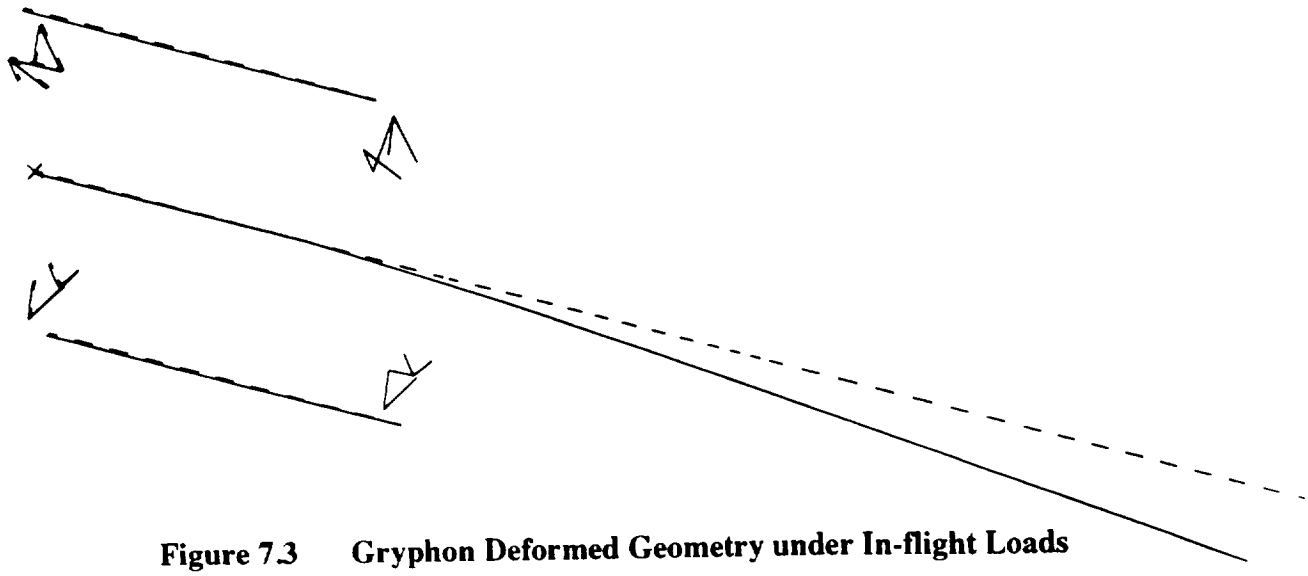

Figure 7.3 Gryphon Deformed Geometry under In-flight Loads

After the model was run, the maximum element forces and deflections were found. Figure 7.3 shows the maximum deflection of the Gryphon under in-flight loads to be 22". Stresses could not be found for any components except the struts, because the KEY-IN option in I-DEAS was used to define the beam cross sections. Considering axial forces and bending moments, the stress in the vertical stringers can be approximated as:

$$\sigma_x = \frac{P}{A} + \frac{Mc}{I_{ayy}} \qquad \text{(Eq 7.3)}$$

With P being the axial compressive load, A the total cross section area, M the bending moment about the y-axis, and c the radius of the main booster. Since the stringers are comparatively small, their total moment of inertia can be a approximated as:

$$I_{ayy} = \frac{Ad^2}{2} \qquad \text{(Eq 7.4)}$$

Given a maximum P and M, the maximum stress is now only a function of area. Using the following values from I-DEAS output given in Appendix F.1 for the Stage 2 cross section:

$$P = 235{,}000 \text{ lb.}$$
$$M = 1.01\ 10^8 \text{ lb. in}$$
$$c = 90 \text{ in}$$
$$\sigma_x = \sigma_{yield}/1.25 = 48 \text{ ksi}$$

We can find

$$A = 49 \text{ in}^2$$

This area would be needed for Stage 2. Less severe load conditions which exist in Stages 1 and 3 require a stringer cross sectional area of only 28 in^2. The area of the skin is now added to yield the total cross sectional area of each hull section, which is shown below in Table 7.3.

Table 7.3 Total Cross Sectional Areas by Stage

Component	Total Area [in^2]	Weight (lb.)
Stage 1	36.8	550
Interstage	57.8	485
Stage 2	57.8	1630
Stage 3	36.8	865

Lateral Buckling Ring Design

Lateral rings are spaced such that the stringers will not buckle. The spacing varies by stage since each stage is subjected to different loads. Their cross section is T-shaped (see Figure 7.4), such that the skin may easily be bolted to them. Since the rings only carry shear loads, their cross sectional area is small, 1/2 square inches, for all rings. Some of these rings coincide with the larger plane attach, strut attach and interstage rings.

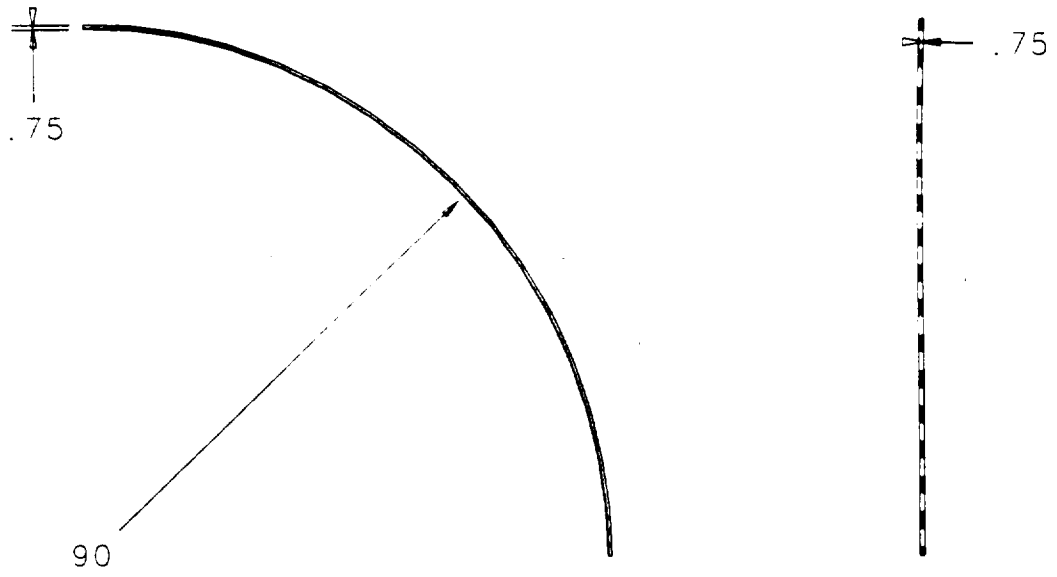

Figure 7.4 Lateral Buckling Rings

The next step was to find the longitudinal distance between the buckling rings. For this the stringers were treated as long, slender beams. The buckling equation for beams, simply supported on both ends is shown in Eq 7.5.

$$P_{cr} = \left(\frac{\pi}{a} \right)^2 E I \qquad \text{(Eq 7.5)}$$

P is the critical load and a is the length (the longitudinal distance to be determined). The moment of inertia of one stringer in Stage 2 is approximately 0.04 in^2. This value results from using 24 vertical stringers with rectangular cross sections and a 1 : 7.5 aspect ratio. Assuming a worst case P from above for Stage 2, it is found:

$$a = 8 \text{ in}$$

Again, the official spacing assumed a much smaller than P, such that for stage 2:

$$a = 23.5 \text{ in}$$

The summary for all components is shown in Table 7.4. The cross sectional area of the rings is 0.5 square inches for all stages. The rings are expected to react to shear loads only.

Table 7.4 Vertical Spacing of Buckling Rings

Component	Spacing [in]
Stage 1	35.0
Interstage	23.5
Stage 2	23.5
Stage 3	35.0

7.2.2 Main Hull - Global Buckling Analysis

To check for global instability under drag and acceleration loads, a buckling analysis was performed. In this case the total moment of inertia of the main booster section was used. I-DEAS reported a buckling load factor of 34 on the first mode (see Figure 7.5).

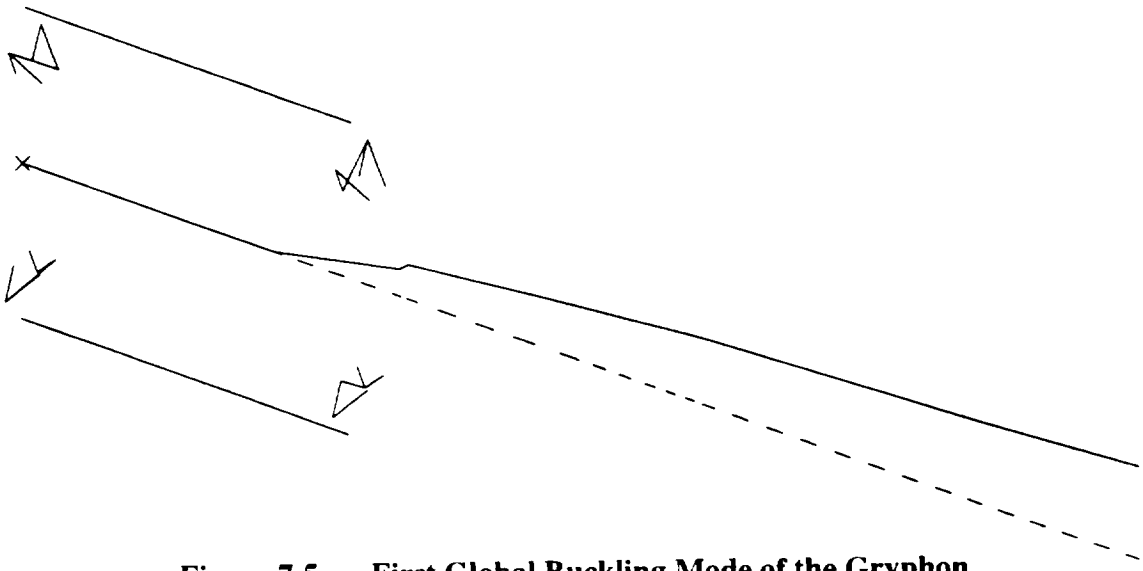

Figure 7.5 First Global Buckling Mode of the Gryphon

Therefore, it was concluded that the Gryphon is not in danger of collapsing due to global elastic instability. The area moments of inertia used for this analysis are given in Table 7.5.

Table 7.5 Area Moments of Inertia by Stage

Component	I [in^4]
Stage 1	132000
Interstage	215500
Stage 2	215500
Stage 3	132000

Modes 2 and 3 have buckling load factors of 42. Their buckled mode shapes are given in Appendix F.3

7.2.3 Main Booster Modal Analysis

For the dynamic analysis the Gryphon was assumed to be free-free (in flight). This was realized by using a Degree of Freedom set in I-DEAS. Translations were set active, rotations inactive. The first six elastic-body modes and their frequencies are:

Table 7.6 Normal Modes and Frequencies of the Gryphon

Mode #	Frequency [Hz]
7	4.25
8	4.76
9	9.09
10	9.87
11	9.96
12	14.25

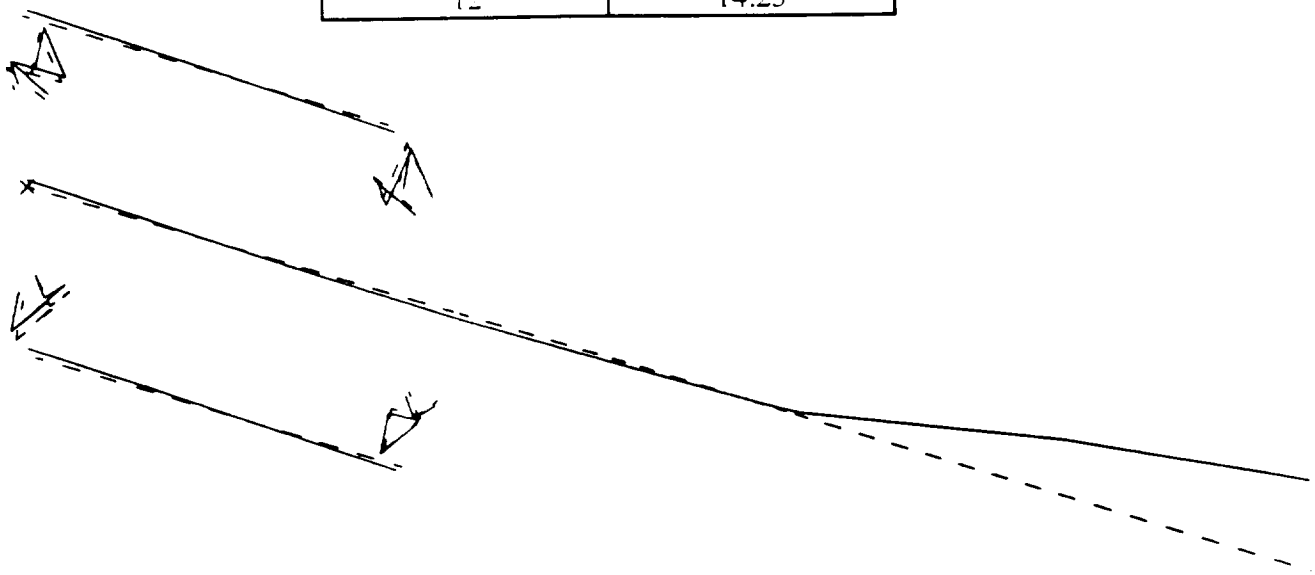

Figure 7.6 Free Vibration Mode 7 for Gryphon

The first six modes are rigid body modes. Mode 7 is the lowest frequency mode and is shown in Figure 7.6 The other modes are included in Appendix F.4. From the free vibration frequencies, it is necessary to conclude that some damping mechanism should be included for the payload, since most satellites will not survive these low frequency vibrations.

From the mode shapes we can also observe that the interface between the payload shroud and Stage 3 is a critical point, since the shroud pivots strongly about this point. As mentioned previously, some stiffening mechanism should be considered for this critical point.

7.2.4 Struts and Strut Attach Rings

The Thiokol solid boosters are connected to the main hull by way of attach struts. These struts impart a shear force to rings located inside the main hull. The shear force acting on

each strut attach ring is estimated from the thrust of the Castor 120 motors. The worst case scenario would be if the Castor 120's fire and the Liquid Rocket Booster fails to do so.

Since there are 4 strut attach rings, each ring takes about 150,000 lb. of shear force. Assuming the yield strength of the aluminum alloy in shear is to be approximately one-half the yield strength in axial loading, the required area of the strut attach rings are found to be equal to 5 square inches (see Figure 7.7)

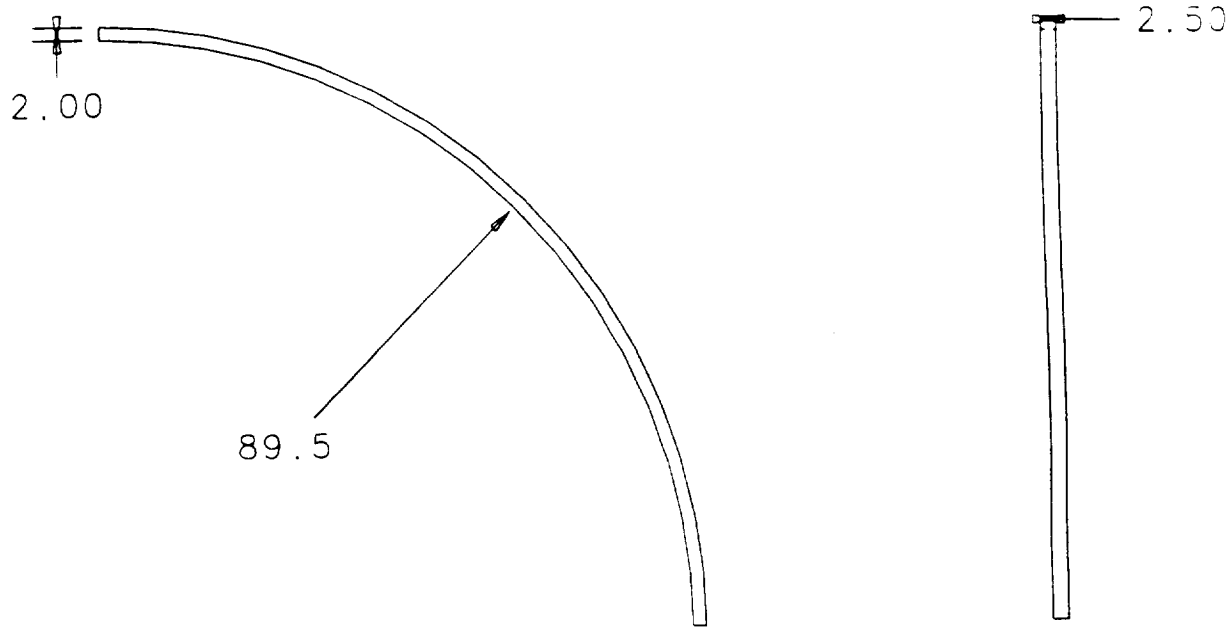

Figure 7.7 Strut Attach Rings.

The struts are made from an aluminum alloy and have cross sectional areas of 15.7 and 10.5 square inches. The larger struts have an outside diameter of 6 inches and an inside diameter of 4 inches. For the smaller struts, the outside diameter is 5 inches and the inside diameter is 3.8 inches. The struts are arranged as shown in Figure 7.8. The two most forward struts at each attach station are large and the other attach struts are smaller. The maximum stresses in the struts were found to be about 50 ksi by I-DEAS. This is within the specified safety factor of 1.25.

Several separation and jettison mechanisms for the struts were identified. The pyro-thrusters which appear to be the best option will perform both jettison and separation functions and are located on the Castor 120 side of the struts. This option reduces debris and increases reliability.

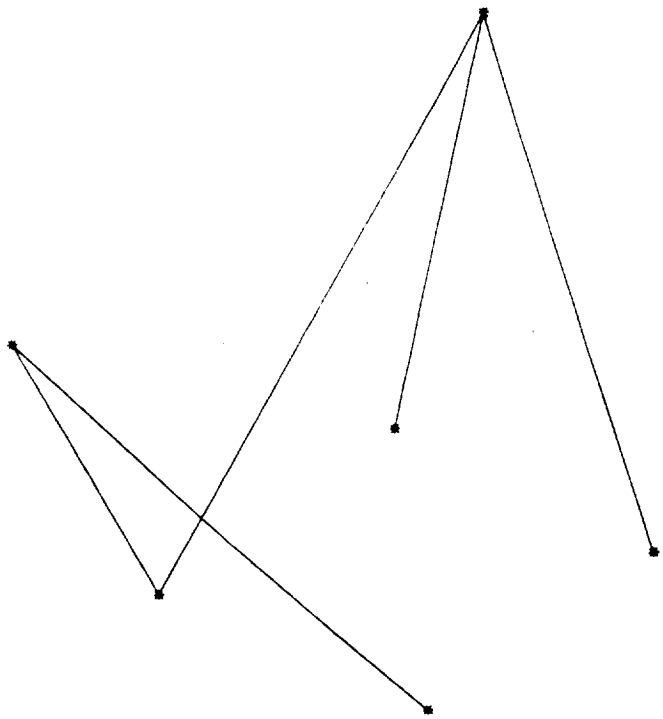

Figure 7.8 Strut Configuration

7.2.5 Plane Attach Rings

The plane attach rings carry the weight of the Gryphon under a maximum lateral g-load of 2.5g. Again, there are 4 plane attach rings, but depending on the flight conditions, one ring may take the majority of the load. Assuming an aluminum alloy construction and a 1.25 factor of safety, the resulting upper limit of the total cross section area equals:

$$A = \frac{W_{rocket}}{2s_{ys}} = 24 \text{ in}^2 \qquad \text{(Eq 7.6)}$$

A conceptual design is shown in Figure 7.9.

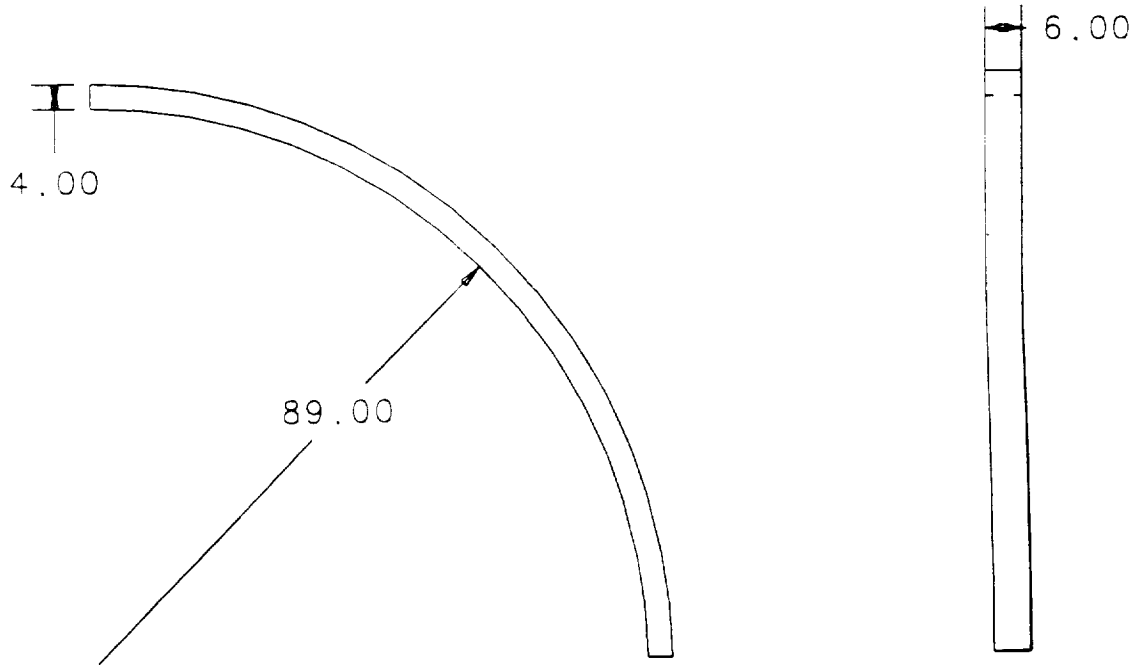

Figure 7.9 Plane Attach Ring

7.2.6 Conclusion

It is concluded that the design of the main booster structure is a formidable problem, and it is extremely difficult to minimize the weight, while at the same time withstand large g-forces and low-frequency vibrations. Nevertheless the physical concepts involved were investigated thoroughly. The main goal was to quantify the stringer/skin/ring structure and solve for the cross sectional area given the axial compressive and bending loads.

Regarding the struts and the attach rings, many iterations were performed. Other materials than aluminum were considered. Titanium was an excellent option since it could provide a significant reduction in weight. For example, one plane attach ring made from aluminum alloy would weigh 360 lb.. Made from titanium, the same ring would only weigh 110 lb.. However, titanium is very expensive and much harder to shape than aluminum. For a final design of the Gryphon, titanium should be seriously considered for highly stressed, massive components.

7.3 DESIGN OF PAYLOAD SHROUD AND SOLID BOOSTER FAIRINGS

To ensure the protection of the payload and reduce overall drag on the booster, a payload shroud and two solid booster fairings, one for each Castor 120 engine, were designed. During atmospheric flight, the payload shroud separates the payload from the environment by absorbing heat, and reduces the overall drag on the Gryphon. Due to its extreme size, it was important to compare various structures to reduce the shroud's weight. Also, to reduce drag, conical fairings were introduced on the tops of the solid booster engines. Since minimal weight is one of the major concerns of the Gryphon project, different options for structural weight reduction were also examined for the solid booster fairings. Therefore, this section of the report examines the design procedure for the payload shroud and solid booster fairings, the assumptions that were made in design, the options that were considered, and what design worked and why.

7.3.1 Structural Design of the Payload Shroud and Its Attach Ring

The following section describes the final payload shroud design, dimensions, material, and weight. The payload shroud is made of a 0.948" thick carbon-epoxy/aluminum honeycomb sandwich composite. In the sandwich composite, a 0.75" thick 5056 aluminum honeycomb is sandwiched between 18 plies, on each side, of 0.0055" thick IM7-8551-7 carbon-epoxy (Table 7.7 & 7.8, Figure 7.10). The aluminum honeycomb is made by Hexcel Corporation and is listed as 0.75-5056-3.0, with 0.75 for the thickness, 5056 for the type of aluminum, and 3.0 for the density in pounds per cubic feet. The thickness chosen was needed to resist buckling, and the density was increased from the density that was used on the Pegasus honeycomb. This increase was do to the large size of the Gryphon shroud. The IM7-8551-7 carbon-epoxy material is manufactured by Hercules Corporation and is in the pre-preg form, which means it contains the epoxy to bond the plies together. IM7-8551-7 was chosen because of its strength, the large amount of data on the material, and its extensive use in aerospace applications.

Table 7.7 Material Properties of 0.75-5056-3.0 Aluminum Honeycomb

Property	Value
Modulus of Elasticity in x-direction	9.2×10^4 psi
Modulus of Elasticity in y-direction	9.2×10^4 psi
Modulus of Elasticity in z-direction	9.2×10^4 psi
Poisson's Ratio in xy-plane	0.3
Poisson's Ratio in yz-plane	0.3
Poisson's Ratio in xz-plane	0.3
Density	3.0 lb/ft^3
Mass Density	4.493×10^{-6} lbm/in^3
Shear Modulus in xy-plane	4.3×10^4 psi
Shear Modulus in yz-plane	4.3×10^5 psi
Shear Modulus in xz-plane	4.3×10^5 psi
Coefficient of Thermal Expansion	13.5×10^{-6}/°F
Thermal Expansion Reference Temperature	529.67°R (room temperature)

Allowable Stress in Tension in x-dir.	300 psi
Allowable Stress in Compression in x-dir.	300 psi
Allowable Stress in Tension in y-dir.	300 psi
Allowable Stress in Compression in y-dir.	300 psi
Allowable In-Plane Shear Stress	200 psi

Table 7.8 Material Properties of IM7-8551-7 Carbon-Epoxy Ply Material

Property	Value
Modulus of Elasticity in x-direction	21.5 X 10^6 psi
Modulus of Elasticity in y-direction	1.21 X 10^6 psi
Modulus of Elasticity in z-direction	1.21 X 10^6 psi
Poisson's Ratio in xy-plane	0.29
Poisson's Ratio in yz-plane	0.0163
Poisson's Ratio in xz-plane	0.0163
Density	0.058 lb/in^3
Mass Density	0.00015 lbm/in^3
Shear Modulus in xy-plane	8.5 X 10^5 psi
Shear Modulus in yz-plane	8.5 X 10^6 psi
Shear Modulus in xz-plane	8.5 X 10^6 psi
Coefficient of Thermal Expansion	7.396 X 10^{-6}/°F
Thermal Expansion Reference Temperature	529.67°R (room temperature)
Allowable Stress in Tension in x-dir.	40000 psi
Allowable Stress in Compression in x-dir.	23500 psi
Allowable Stress in Tension in y-dir.	11000 psi
Allowable Stress in Compression in y-dir.	11000 psi
Allowable In-Plane Shear Stress	17000 psi

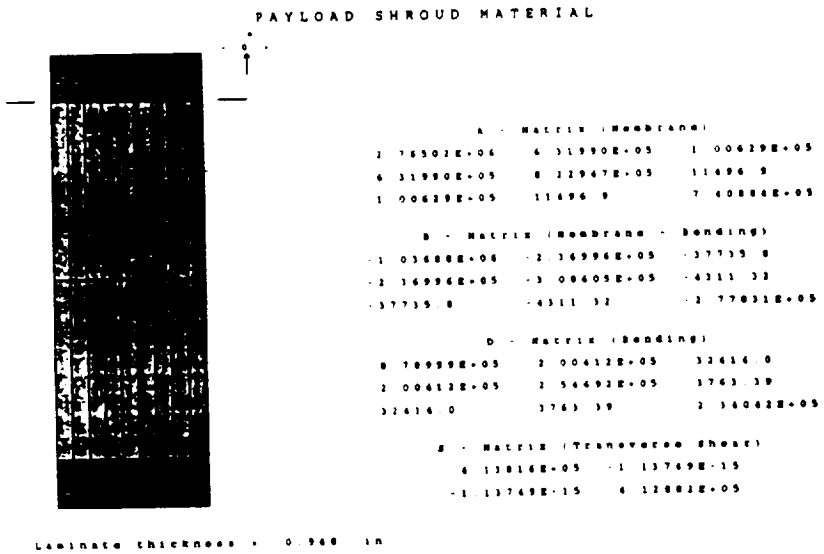

Figure 7.10 Payload Shroud Sandwich Composite Cross Section

The 18 plies on each side and honeycomb are arranged in the following order:

Table 7.9 Table of Shroud Sandwich Composite Arrangement

Ply Number	Ply Name	Thickness (inches)	Angle of Orientation
1	IM7-8551-7	0.0055	45°
2	IM7-8551-7	0.0055	-45°
3	IM7-8551-7	0.0055	15°
4	IM7-8551-7	0.0055	-15°
5	IM7-8551-7	0.0055	15°
6	IM7-8551-7	0.0055	-15°
7	IM7-8551-7	0.0055	45°
8	IM7-8551-7	0.0055	-45°
9	IM7-8551-7	0.0055	15°
10	IM7-8551-7	0.0055	15°
11	IM7-8551-7	0.0055	-45°
12	IM7-8551-7	0.0055	45°
13	IM7-8551-7	0.0055	-15°
14	IM7-8551-7	0.0055	15°
15	IM7-8551-7	0.0055	-15°
16	IM7-8551-7	0.0055	15°
17	IM7-8551-7	0.0055	-45°
18	IM7-8551-7	0.0055	45°
19	0.75-5056-3.0	0.75	0°
20	IM7-8551-7	0.0055	45°
21	IM7-8551-7	0.0055	-45°
22	IM7-8551-7	0.0055	15°
23	IM7-8551-7	0.0055	-15°
24	IM7-8551-7	0.0055	15°
25	IM7-8551-7	0.0055	-15°
26	IM7-8551-7	0.0055	45°
27	IM7-8551-7	0.0055	-45°
28	IM7-8551-7	0.0055	15°
29	IM7-8551-7	0.0055	15°
30	IM7-8551-7	0.0055	-45°
31	IM7-8551-7	0.0055	45°
32	IM7-8551-7	0.0055	-15°
33	IM7-8551-7	0.0055	15°
34	IM7-8551-7	0.0055	-15°
35	IM7-8551-7	0.0055	15°
36	IM7-8551-7	0.0055	-45°
37	IM7-8551-7	0.0055	45°
	Total Thickness =	0.948"	

The carbon-epoxy ply facing the outside is coated with a material used to reduce thermal loads. The shroud is composed of a 190" inside diameter, 25" high cylindrical section, and an ogive top with a 190" inside diameter base that is 14' high (Figure 7.11).

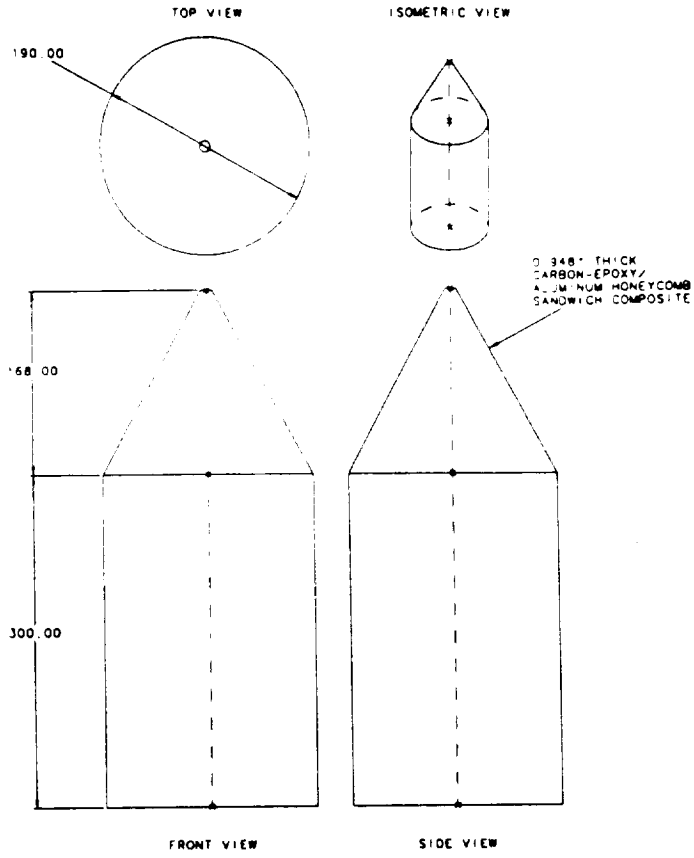

Figure 7.11 Three-View Drawing of the Payload Shroud

The bottom 2" of the shroud is made only of carbon-epoxy plies with no honeycomb. This is done to allow for connection to the shroud attach ring, and to connect the shroud to the third stage. Holes through the plies are located around these bottom 2" of the shroud to allow for bolting to the attach ring. The shroud is built into two halves with explosives along the connection line, so the two halves can separate easily during jettison. The top of the payload shroud contains a small nose cap, embedded with explosives. When the explosives in the cap and along the midline of the

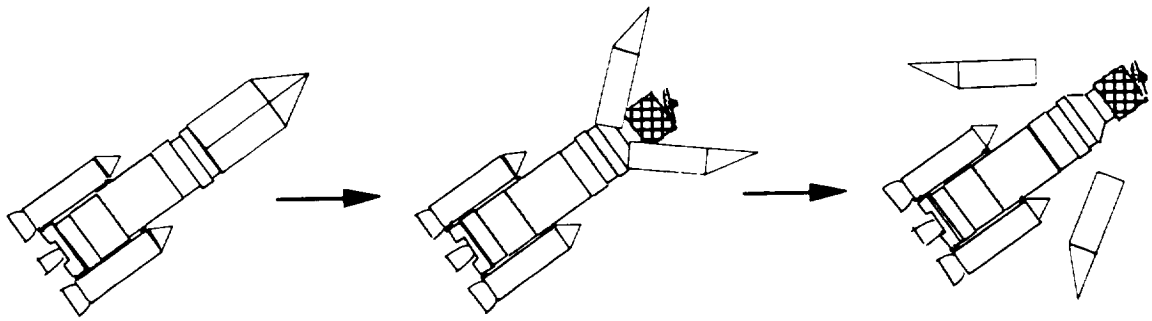

Figure 7.12 Separation System of the Payload Shroud

shroud detonate, the shroud falls back along its two halves, rocking about hinges connecting the two halves to the attach ring and breaking (Figure 7.12).

Connecting the payload shroud to the third stage is the attach ring (Figure 7.13). It is made of 7075-O tempered aluminum, and its material properties are listed in Table 7.10. The payload shroud attach ring is also used as an adapter to drop the overall inner diameter from 190" in the shroud to 180" in the third stage.

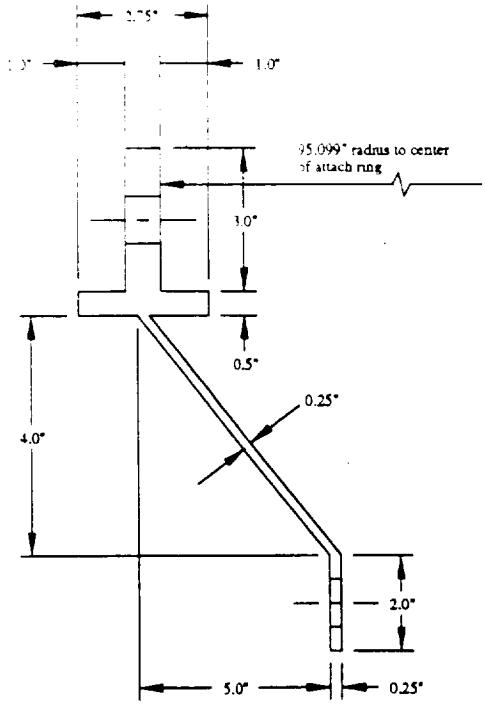

Figure 7.13 Payload Shroud Attach Ring Cross Section

Table 7.10 Material Properties of 7075-O Tempered Aluminum

Property	Value
Modulus of Elasticity in Tension	10.3×10^6 psi
Modulus of Elasticity in Shear	3.9×10^6 psi
Modulus of Elasticity in Compression	10.5×10^6 psi
Poisson's Ratio	0.33
Density	0.101 lb/in^3
Mass Density	2.614×10^{-4} lbm/in^3
Coefficient of Thermal Expansion	13.5×10^{-6}/°F
Yield Strength	15×10^3 psi
Tensile Strength	38×10^3 psi
Shear Strength	22×10^3 psi

By using a sandwich composite design, the material weight of the payload shroud is reduced to 2,300 lb.. This includes 1,970 lb. of carbon-epoxy material and 330 lb. of aluminum honeycomb. However, because of the addition of access doors, thermal and acoustic insulation, separation systems, and other strengtheners, the total weight of the shroud is about one and one-third times as much as the structure alone. This is about 6,200 lb. according to past data [Shen and Pope]. The shroud attach ring weighs approximately 300 lb..

7.3.2 Structural Design of the Solid Booster Fairings and Their Attach Rings

For this section, the final solid booster fairing design, dimensions, material and weight are noted. The fairings are constructed from the same materials used in the payload shroud, but with a different ply orientation and core thickness. The overall thickness of the fairings is 0.485 inches with the sandwich composite made of a 0.375" aluminum honeycomb core, and 10 plies of 0.0055" thick carbon-epoxy material on each side. Figure 7.14 shows the cross section of the fairing composite, and its relevant matrix properties calculated using laminate modeling in I-DEAS.

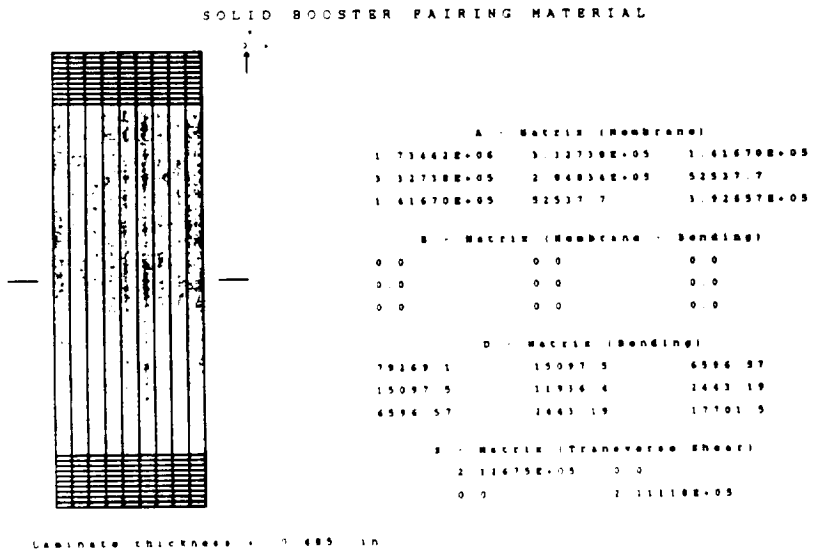

Figure 7.14 Solid Booster Fairing Sandwich Composite Cross Section

The 10 carbon-epoxy plies on each side and the aluminum honeycomb are arranged in the order shown in Table 7.11:

Table 7.11 Table of Fairing Sandwich Composite Arrangement

Ply Number	Ply Name	Thickness (inches)	Angle of Orientation
1	IM7-8551-7	0.0055	30°
2	IM7-8551-7	0.0055	-30°
3	IM7-8551-7	0.0055	15°
4	IM7-8551-7	0.0055	-15°
5	IM7-8551-7	0.0055	30°

6	IM7-8551-7	0.0055	30°
7	IM7-8551-7	0.0055	-15°
8	IM7-8551-7	0.0055	15°
9	IM7-8551-7	0.0055	-30°
10	IM7-8551-7	0.0055	30°
11	0.375-5056-3.0	0.375	0°
12	IM7-8551-7	0.0055	30°
13	IM7-8551-7	0.0055	-30°
14	IM7-8551-7	0.0055	15°
15	IM7-8551-7	0.0055	-15°
16	IM7-8551-7	0.0055	30°
17	IM7-8551-7	0.0055	30°
18	IM7-8551-7	0.0055	-15°
19	IM7-8551-7	0.0055	15°
20	IM7-8551-7	0.0055	-30°
21	IM7-8551-7	0.0055	30°
	Total Thickness =	0.485"	

The carbon-epoxy ply on the outer surface, as on the shroud, is also coated with a material to reduce the thermal loads. Exposed to heat, the carbon-epoxy can only withstand temperatures up to 300-350°F.

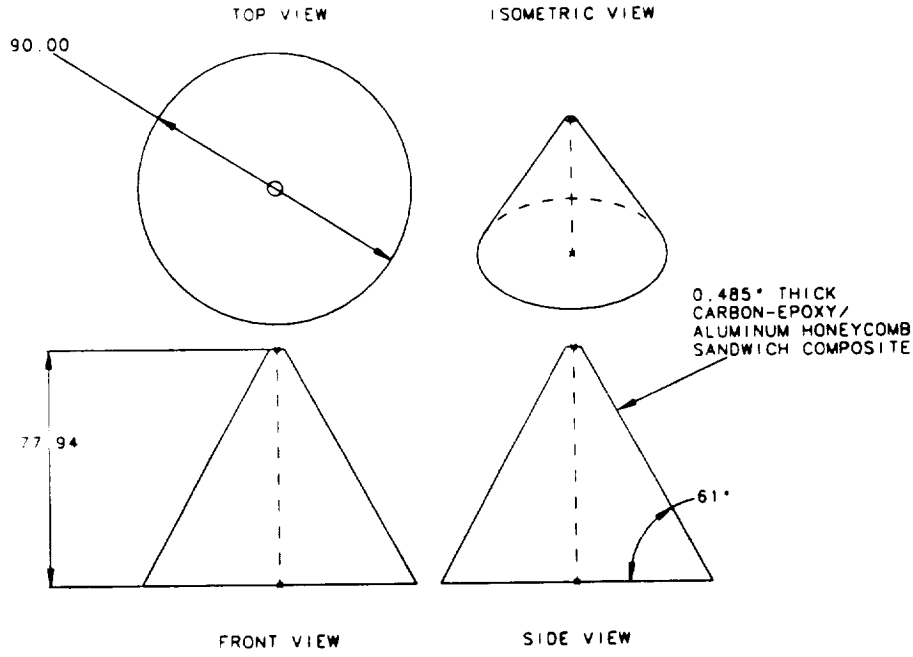

Figure 7.15 Three-View Drawing of the Solid Booster Fairing

The solid booster fairings attach to the Castor 120 engines, and have an have an outside diameter of 7.5 feet to match the diameter of these engines. The sides of the cone are at 60° angles, making the cone equilateral, and the peak height of the fairing 6.495 feet (Figure 7.15). The bottom two inches of the fairing are curved so the sandwich composite becomes vertical, and can be attached to the attach ring. In these two inches,

there is no aluminum honeycomb. The attach ring reaches into the fairing, and attaches to the outer plies of the carbon-epoxy material at hole locations around the fairing. Since the fairings are so small and lightweight, they experience much less compressive forces than the shroud. Therefore, the attach ring only attaches to the outer plies. The attach ring is made of 7075-O tempered aluminum, and allows for the fairing to be secured to the ring on the Castor 120 engines.

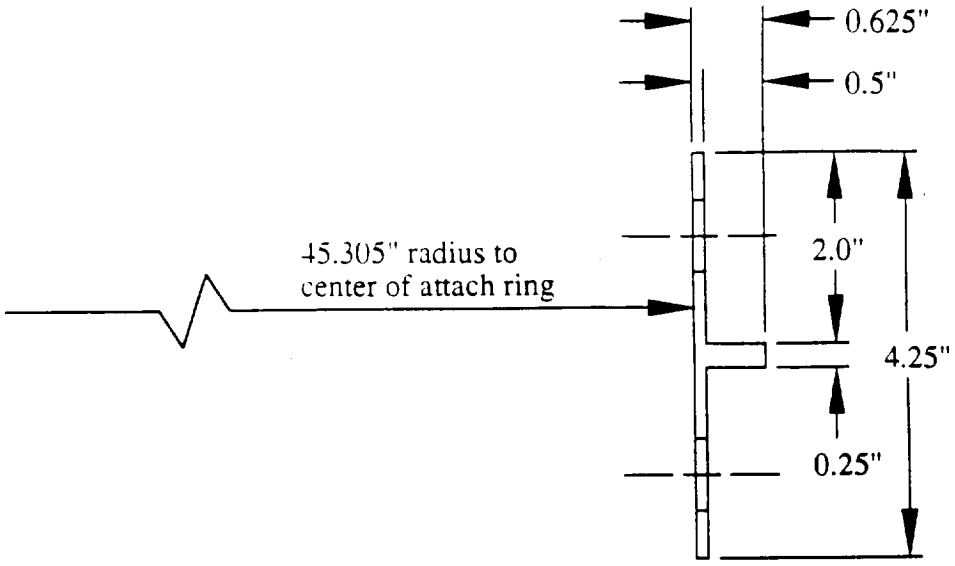

Figure 7.16 Solid Booster Fairing Attach Ring Cross Section

Each solid booster fairing weighs approximately 52.5 lb., for a total of 105 lb.. Of this, 95 lb. is for the carbon-epoxy material, and 10 lb. for the aluminum honeycomb. The attach rings for the fairings weigh 25 lb. each, for a total of 50 lb..

7.3.3 Laminate Modeling

The payload shroud was designed using:

- I-DEAS
- FORTRAN program to find modulus of elasticity in a composite plate and the stiffness of a laminate tube
- FORTRAN program written to calculate buckling in a composite laminate plate

To be able to use I-DEAS for static analysis, it was necessary to model the sandwich composite as a laminate. Therefore, proof was needed to say a sandwich payload shroud was nearly equivalent to a laminate payload shroud.

The shroud material was based on the sandwich composite used on the Orbital Science Corporation's Pegasus launch vehicle. A sandwich composite was used on the Gryphon for three basic reasons: it is extremely lightweight in comparison to solid aluminum and comparable in strength, automated manufacturing techniques make high volumes of composite shrouds inexpensive to produce, and sandwich composite

structures are becoming more popular and have a bright future as a material in aerospace applications.

To find the stiffness of the laminate and sandwich tubes, it was first necessary to derive the equations for equivalent stiffness from theory. For comparison, the isotropic equation is included here:

Isotropic Tube: $$(EI)_{eq} = E\,\frac{\pi}{64}\left(d_o^4 - d_i^4\right) \qquad \text{(Eq 7.7)}$$

Laminate Tube: $$(EI)_{eq} = \pi \int_{r_i}^{r_o} [Q]\, r^3\, dr \qquad \text{(Eq 7.8)}$$

Sandwich Tube:

$$(EI)_{eq} = \frac{\pi}{4}\sum_{i=1}^{k} Q_{11}^{(i)}\left(r_o^{(i)4} - r_i^{(i)4}\right) + \frac{\pi}{4}\sum_{i=1}^{1} Q_{11}^{(1)}\left(r_o^{(1)4} - r_i^{(1)4}\right) \qquad \text{(Eq 7.9)}$$

where E = modulus of elasticity, I = I_a = area moment of inertia, d_o and d_i = outside and inside diameters, r_o and r_i = outside and inside radii, Q = stress matrix or stress matrix components.

After further derivation of the laminate tube equation, it is found that the equivalent modulus of elasticity of a laminate is approximately equal to the following, where :

$$E_{eq} = \frac{A_{11} - \dfrac{A_{12}}{A_{22}}}{h} \qquad \text{(Eq 7.10)}$$

The A's are values from the composite material A-matrix (which the FORTRAN program solves for), and h is the overall height of the laminate, from the inner ply surface to the outer ply surface.

By using the basic definition for the area moment of inertia of a circle with thickness,

$$I_a = \frac{\pi}{64}\left(d_o^4 - d_i^4\right) \qquad \text{(Eq 7.11)}$$

and multiplying to the result of Eq 7.10, the equivalent stiffness of the laminate is found. For the laminate tests, it was assumed the laminate contained the entire thickness of the sandwich composite, including the aluminum honeycomb core.

For comparison, Eq 7.9 was explicitly solved using a FORTRAN program to calculate the various matrices. In the sandwich theory, it was assumed the sandwich consisted only of the carbon-epoxy plies, because the aluminum honeycomb basically adds no stiffness to the overall structure.

Example materials were then tried in the programs. For tests between the two theories, there was approximately a 1% difference. From this calculated proof, it was then logical to assume that the shroud could be modeled in I-DEAS, building the materials as laminates. (NOTE: A listing of the FORTRAN program used is contained in Appendix F.5.)

7.3.4 Static Loads for the Payload Shroud

The loading conditions applied to the I-DEAS shroud model were the worst combination of loading that would be experienced during atmospheric flight. It was assumed that if the shroud was designed for the point where the Gryphon is in supersonic flight, and beginning its turn to go into the vertical position, the shroud would be able to withstand any other point during flight. For all static load calculations, a factor of safety of 1.25 was used.

Since the shroud is used exclusively in the earliest parts of the mission, only conditions during the first stage firing, and the Gryphon in its ascent turn are considered. From this assumption, it was discovered that the worst flight conditions occurred at an angle of attack of 18° and at a speed of Mach 2. These conditions correspond to a total drag of 165,000 lb., and total lift of 115,000 lb., on the Gryphon. However, only a percentage of lift and drag acts on the shroud. Since the lift and drag calculations are modeled on the base area of the entire booster, the percentage acting on the shroud is about two-thirds of the total. The components are calculated by multiplying the lift and drag by two-thirds, and then finding the x- (bending) and y- (compression) components for an angle of attack of 18°. Also, since the component of lift along the length of the Gryphon acts on the frontal area only, the lift needs to be multiplied by its frontal area ratio which is approximately 0.5.

Calculations

Y-Component of Drag:

$$= D_y\left(\frac{A_{S1}}{A_B}\right) * SF = (D\cos 18°)\left(\frac{\frac{\pi}{4}d_S^2}{2\left(\frac{\pi}{4}d_F^2\right)+\frac{\pi}{4}d_S^2}\right)(SF) \qquad \text{(Eq 7.12)}$$

$$= (165000)(\cos 18°)(0.66)(1.25) = 129{,}463 \text{ lbs.}$$

X-Component of Drag:

$$= D_x\left(\frac{A_{S1}}{A_B}\right) * SF = (D\sin 18°)\left(\frac{\frac{\pi}{4}d_S^2}{2\left(\frac{\pi}{4}d_F^2\right)+\frac{\pi}{4}d_S^2}\right)(SF) \qquad \text{(Eq 7.13)}$$

$$= (165000)(\sin 18°)(0.66)(1.25) = 42{,}065 \text{ lbs.}$$

Y-Component of Lift:

$$= L_y\left(\frac{A_{S1}}{A_B}\right) * SF = (L\sin 18°)\left(\frac{\frac{\pi}{4}d_S^2}{2\left(\frac{\pi}{4}d_F^2\right)+\frac{\pi}{4}d_S^2}\right)(SF) \qquad \text{(Eq 7.14)}$$

$$= (115000)(\sin 18°)(0.66)(1.25) = 29{,}316 \text{ lbs.}$$

X-Component of Lift:

$$= L_x\left(\frac{A_{S1}}{A_B}\right)\left(\frac{A_{S2}}{A_{LB}}\right)*SF = (L\cos 18°)\left(\frac{\frac{\pi}{4}d_S^2}{2\left(\frac{\pi}{4}d_F^2\right)+\frac{\pi}{4}d_S^2}\right)\frac{b_S h_S}{b_{LB}h_{LB}}(SF) \qquad \text{(Eq 7.15)}$$

$$= (115000)(\cos 18°)(0.66)(0.5)(1.25) = 45{,}115 \text{ lbs.}$$

Acceleration Load in X-Direction

$$F_x = W(SF)(\#\text{ of } g's) = (mg)(SF)(\#\text{ of } g's)$$
$$= (6000)(1.25)(2.5) = 18{,}750 \text{ lbs} \qquad \text{(Eq 7.16)}$$

Acceleration Load in Y-Direction

$$F_y = W(SF)(\#\text{ of } g's) = (mg)(SF)(\#\text{ of } g's)$$
$$= (6000)(1.25)(5.0) = 37{,}500 \text{ lbs} \qquad \text{(Eq 7.17)}$$

where, as shown in Figure 7.17:

A_{S1} = the base area of the shroud
A_{S2} = the longitudinal area of the shroud
b_S = the diameter of the shroud
h_S = the height of the shroud
d_S = diameter of the shroud
d_F = diameter of the fairings
A_B = the base area of the entire booster
A_{LB} = the longitudinal area of the liquid booster area
b_{LB} = avg. diameter of the entire booster
h_{LB} = height of the entire booster
SF = factor of safety
W = weight

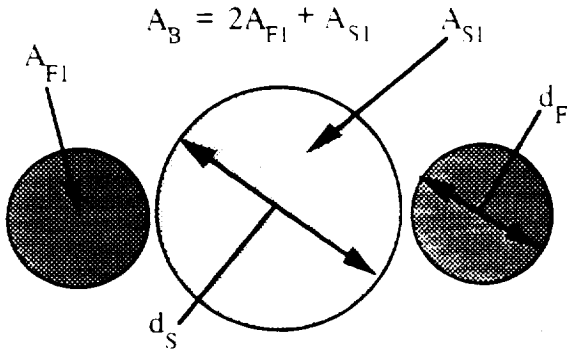

Front (Base) View of Gryphon

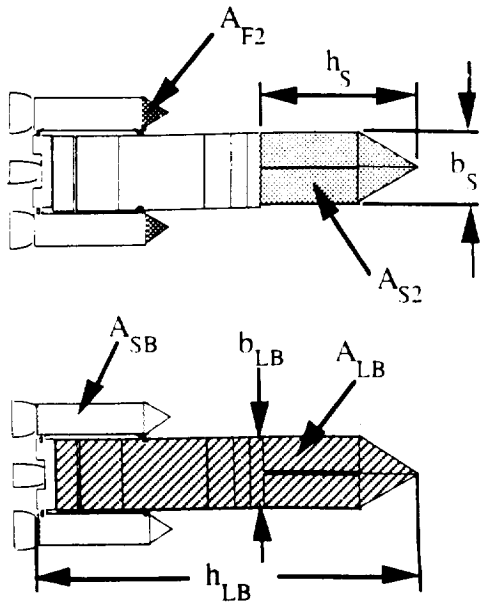

Longitudinal View of Gryphon

Figure 7.17 Sketch of Components from Load Calculations

Since the Gryphon is accelerated through a lateral turn, the shroud experiences lateral as well as longitudinal acceleration. Along the booster, there is an acceleration load equal to 5.0 g's for the structure only during stage one. Adding on the additional acceleration due to the entire weight of 6200 lb. brings the total acceleration up to 15 g's, or 5790 lbf. This acceleration works in the same direction as the compressive load acting on the shroud.

The lateral acceleration during stage one is equal to 2.5 g's. Adding on the additional acceleration load for the entire weight of 6200 lb. sets the actual acceleration load that the shroud sees to 7.5 g's, or 2895 lbf. The lateral acceleration opposes the lift force, and therefore acts opposite to that force in the I-DEAS model.

Finally, all of the calculated loads are multiplied by 1.25 to account for the factor of safety. The following table lists all static loads applied to the finite element model made in I-DEAS, including factors of safety.

Table 7.12 Static Loads Applied to the Payload Shroud in I-DEAS

Type of Load	Y-Component (Compression)	X-Component (Bending)
Drag	129,463 lb..	42,065 lb..
Lift	29,316 lb..	45,115 lb..
Acceleration	37,500 lb..	18,750 lb..
Σ Forces	196,279 lb..	105,930 lb..

7.3.5 Shroud Buckling Analysis

Since the shroud is a large, thin structure, local buckling was a major concern in its design. It was decided that the buckling analysis should be completed first, thereby outlining a baseline design. Further iterations were then performed to design the shroud to withstand ply failure.

Using the aerodynamic and acceleration loads on the structure, the local stress state of the shroud was characterized. This was compared to critical stress values obtained from cylindrical buckling theory. A factor of safety of 2.3 was used in comparing the two stresses to account for uncertainty in loading, the catastrophic nature of buckling failure, and the sensitivity of shell structures to local imperfections.

The shroud is composed of two sections, one cylindrical and the other conical. Each had to be analyzed independently. A $[45/-45/15/-15]_S$ (symmetric) IM7-8551-7 skin lay-up with a 3/4" aluminum honeycomb core was necessary to prevent buckling in the cylindrical section. Using the same materials, a $[30/-30]_S$ skin and a 3/4" honeycomb prevented buckling in the conical section.

Load Definition

Using the lift, drag, and acceleration forces in Table 7.12, the local state of stress in the shroud due to bending and compressive forces was defined. Thermal loads were neglected since the structure is free to expand vertically. By combining the bending and compressive loads, an expression for stress can be derived as shown in Eq 7.18.

$$\sigma_{buckling} = \frac{P}{A} + \frac{Mr}{I_A} \qquad \text{(Eq 7.18)}$$

P is the compressive force, A is the cross sectional area of the shroud, M is the bending moment, r is the radius of the shroud, and I_A is the area moment of inertia of the cross section.

A critical stress was calculated using cylindrical buckling theory [Vinson and Sierakowski]. This theory uses the constitutive description of the laminate to compute its critical buckling stress. The buckling stress is dependent upon the number of half waves, so a FORTRAN program was used to iterate a solution. It is presented in Appendix F.6.

Cylindrical Section Analysis

The cylindrical section receives the full load condition of the shroud. Aerodynamic lift and drag apply both compressive and bending loads. The loads were assumed to act equally over the entire shroud, so the moment arm of the bending portion was assumed to be half the total height. Using the values for these forces in Section 7.3.2, and Eq 7.18, the stress on the cylinder was calculated.

$$\sigma_{cylinder} = \frac{157{,}000 \text{ lbs}}{500 \text{ in}^2} + \frac{(84{,}800 \text{ lbs})(234 \text{ in})(95 \text{ in})}{2{,}280{,}000 \text{ in}^4} = 1{,}097 \text{ psi}$$

A sandwich structure with $[45/-45/15/-15]_S$ (symmetric) skins and a 3/4" aluminum honeycomb has a critical stress of 2,881 psi. Therefore, the cylinder must have a minimum of 8 ply skins with a 3/4" honeycomb. Further analysis to check for the ply over stressing and honeycomb failure finalizes the design. This result was used as an initial guess to check for ply failure. If additional layers had to be added, they would only increase the critical buckling load. Therefore, no further buckling analysis was needed.

Conical Section Analysis

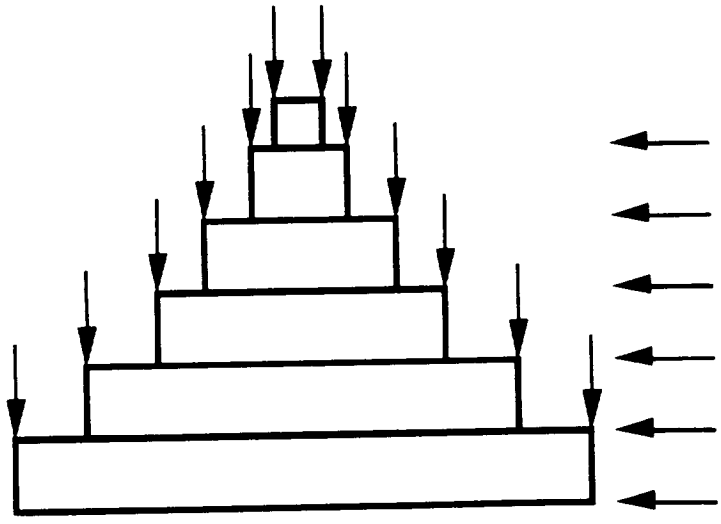

Figure 7.18 Load Distribution of a Cone Under Buckling Loads

Cones have a natural resistance to buckling due to their geometry. Loads applied in a compressive direction do not directly act as buckling loads because the sides of a cone are angled. To model this, the cone was represented as a stacked series of cylinders (see Figure 7.18).

By modeling the cone in this manner, the bottom cylinder is subjected to all of the compressive and bending loads with a moment arm equal to half the cone height. It has a diameter which is an average of the bottom cone diameter, and the cone diameter at the height of the bottom cylinder. However, since the bottom cylinder is shorter than the full cone, it has a higher critical buckling load. By using the shortened length, cylindrical buckling theory yields a value for this stress. For the purpose of analyzing the conical section of the shroud, a stack of six cylinders of equal height was used. Using Eq 7.18, the applied stress was computed.

$$\sigma_{cone} = \frac{210{,}400 \text{ lbs}}{500 \text{ in}^2} + \frac{(35{,}800 \text{ lbs})(84 \text{ in})(83 \text{ in})}{1{,}420{,}000 \text{ in}^4} = 686 \text{ psi}$$

A critical stress of 1,578 psi was required to maintain a 2.3 factor of safety. Using buckling theory for $[30/-30]_S$ skins, and a 3/4 " honeycomb the critical load was found to be 1,675 psi. Four ply skins were sufficient to prevent buckling, and became the initial geometry used in ply failure analysis. The addition of more plies to prevent failure only increases the buckling load, so no further buckling analysis was needed.

7.3.6 I-DEAS Modeling of Payload Shroud

By using SDRC- IDEAS, the model was designed, the laminate material was created and applied to the model, and the loads of Table 7.11 were applied. Since the shroud material can withstand temperatures up to 300-350°F, a temperature load of 300°F was also applied to the shroud. As a restraint, the base of the shroud was clamped. Since the shroud is rigidly connected to the rest of the Gryphon, it moves as the rest of the booster moves. Therefore, it is safe to assume that the way the shroud deflects due to aerodynamic forces is the same as clamping the shroud to the ground, and applying the forces seen during flight.

After running the model, parameters such as displacements, in-plane stresses, transverse shear stresses, and ply failure index were examined. The major constraint in the design was to assure that none of the carbon-epoxy plies, or the honeycomb core, would fail. The honeycomb carries all transverse shear loads and increases the area moment of inertia of the cross section without significantly increasing the weight. On the other hand, the carbon-epoxy is designed to take nearly all the axial load along its two sets of plies. As was discovered in the model, the determining factor in the material design was failure due to axial loading of the honeycomb core. There were not enough carbon-epoxy plies, so some of the axial load was being transmitted to the honeycomb, which fails easily in the axial direction.

By adding extra carbon-epoxy plies, the axial load on the honeycomb core was reduced, and as an additional bonus, the critical buckling load is increased. Figure 7.7 and Table 7.9 show the final material description used for the I-DEAS model. The composite includes mostly ±15° plies (nearly longitudinal) because bending and compressive loads act in this direction.

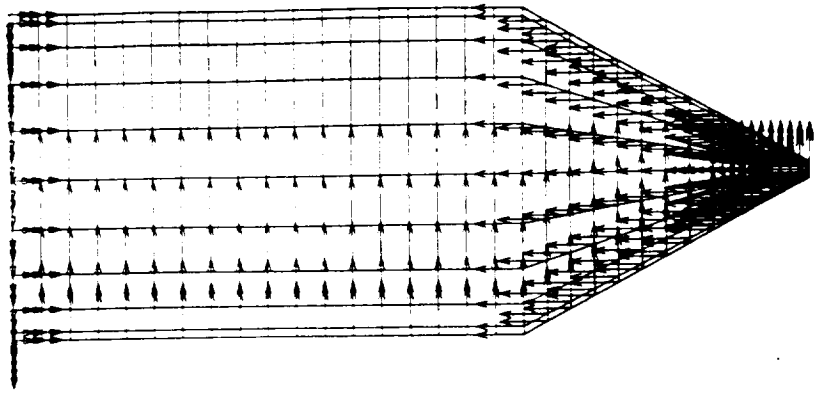

Figure 7.19 I-DEAS Model of the Payload Shroud with Applied Loads

Figure 7.19 shows the payload shroud with its applied loads and restraints, and Figure 7.20 shows the displacement of the shroud due to those applied loads.

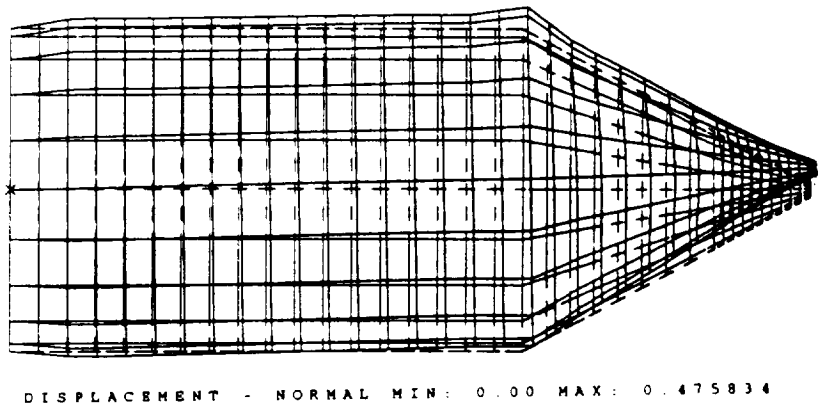

Figure 7.20 Total Displacement of the Payload Shroud

The maximum deflection of the shroud due to static loading occurs at the tip. For conditions listed in Table 7.12, the tip deflection is 0.476 inches in either direction. Inside the payload shroud is the payload and the payload interface, which supports the payload. One major concern is that the payload interface and the shroud do not deflect, and as a result, crash into each other creating significant damage. As is discussed in Section 7.4 of this report, the maximum deflection of the payload interface/payload combination is 0.836 inches in either direction. Since there is 7 inches between the payload and the shroud, the closest that they could be to each other is 5.688 inches. Therefore, due to static loading, the payload shroud and payload/payload interface will not collide.

To determine failure characteristics of the payload shroud, the Hoffman failure theory was applied to the loaded model in I-DEAS. The Hoffman failure theory is listed in Eq 7.19 where X_T, Y_C, Y_T, Y_C are the yield stresses in the x and y tension and

compressive directions, S is the yield strength in shear, and s is the stress in the ply in a particular direction. A value greater than unity occurs if the composite layer has yielded.

$$\frac{\sigma_{11}^2}{X_T X_C} + \frac{\sigma_{22}^2}{Y_T Y_C} - \frac{\sigma_{12}\sigma_{22}}{X_T X_C} + \frac{X_C - X_T}{X_C X_T}\sigma_{11} + \frac{Y_C - Y_T}{Y_T Y_C}\sigma_{22} + \frac{\sigma_{12}^2}{S^2} \quad \text{(Eq 7.19)}$$

By applying this theory, a ply failure index for each ply is obtained. The ply failure index is a measure of how close a ply in a laminate is to failure, based on material properties and loading conditions. If the ply failure index is less than one, the material will not fail, if it is equal to one, the material is at the failure boundary, and if it is greater than one, the material will fail. Figure 7.21 and 7.22 show a contour plot of the ply failure index for the honeycomb core (ply number 19), and for one of the carbon-epoxy plies (ply number 27) respectively. As seen in the plots, the honeycomb failure index is higher than the carbon-epoxy ply failure index. The compressive load is handled by the carbon-epoxy with relative ease, but a small amount of load transmitted to the honeycomb can cause failure of the overall material structure.

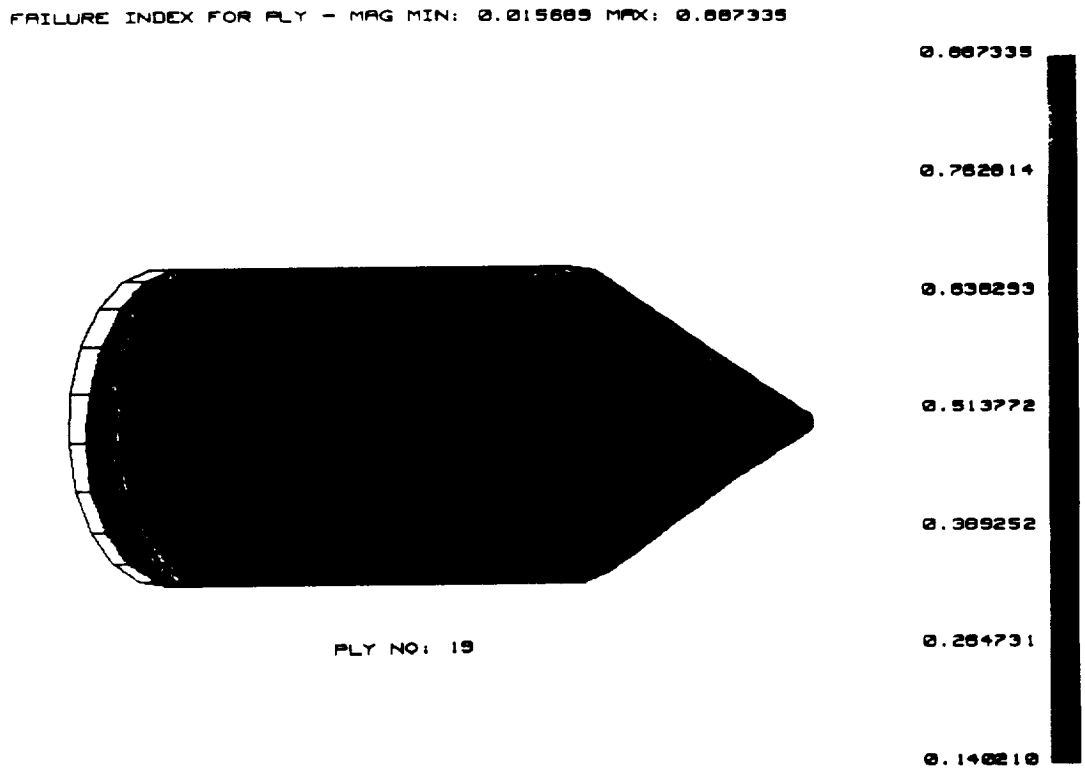

Figure 7.21 Ply Failure Index Plot for the Shroud Honeycomb Core

The spots on Figure 7.21 with the highest ply failure index are of particular interest. Therefore, plots were made of the in-plane stress and transverse shear stress throughout the thickness of the material for the elements with high ply failure index. An

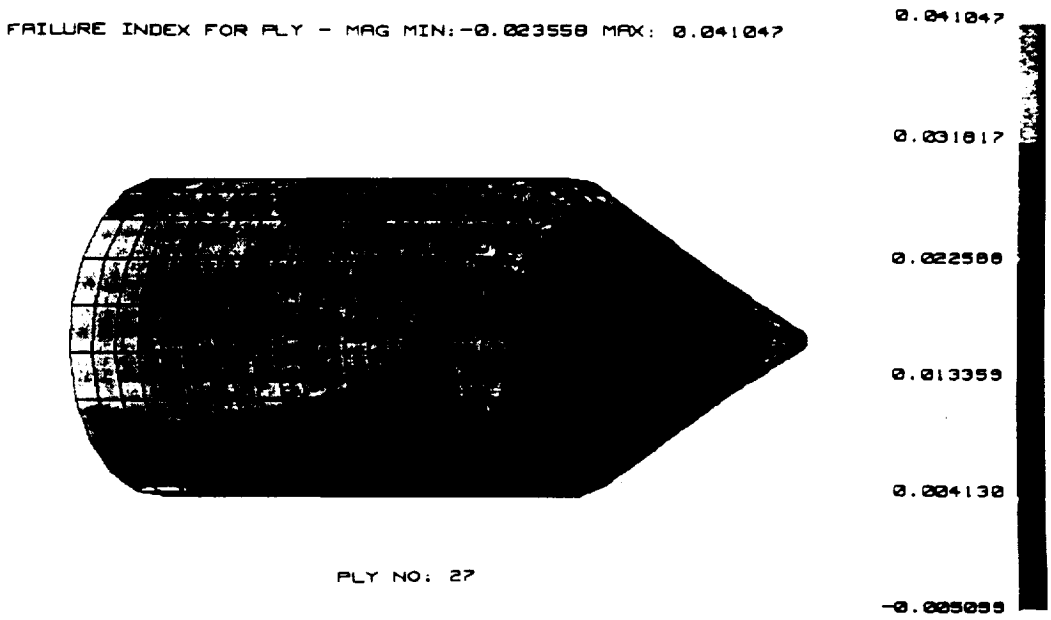

Figure 7.22 Ply Failure Index Plot for a Shroud Carbon-Epoxy Ply

example of the plots of elements with highly stressed honeycomb are shown in Figure 7.23 and 7.24.

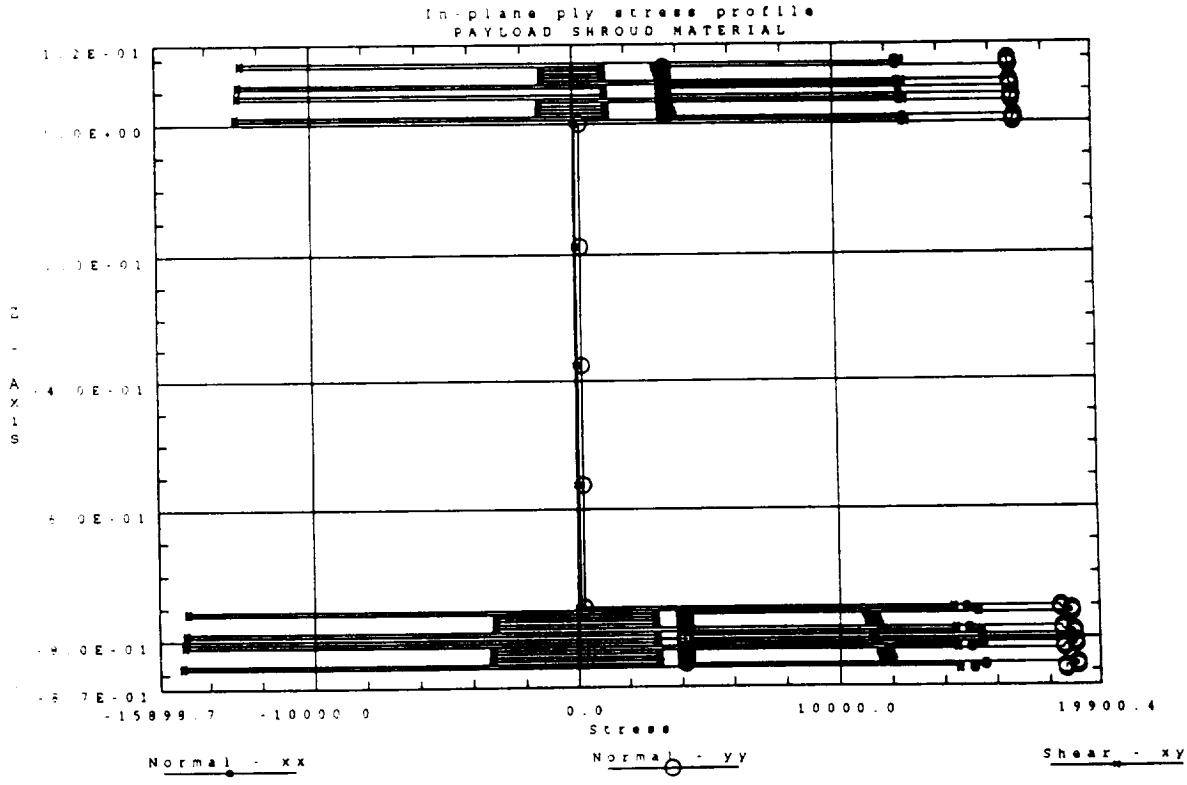

Figure 7.23 In-Plane Stress for a Shroud Model Element with Highly -Stressed Honeycomb Core

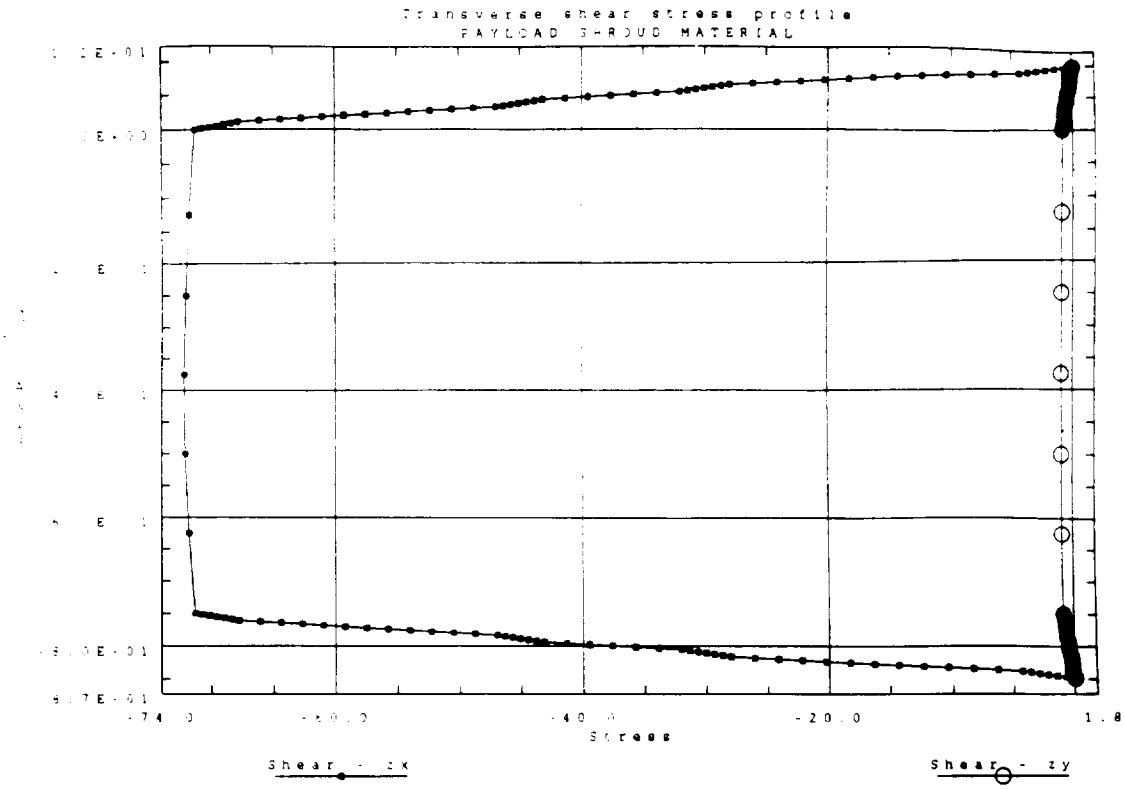

Figure 7.24 Transverse Shear Stress for a Shroud Model Element with Highly-Stressed Honeycomb Core

As shown in Figure 7.23, the in-plane stress does not exceed the strengths of the material properties for any of the laminate plies, and Figure 7.24 in conjunction with 7.22 proves that the honeycomb carries transverse shear stress but not axial forces. The payload shroud will not fail due to in-flight loads.

Results

From Eq 7.11, the approximate area moment of inertia of the shroud is calculated assuming no honeycomb core adding to the moment of inertia:

$$I_{a_{shroud}} = \frac{\pi}{64}\left(d_o^4 - d_i^4\right)_{outer\ plies} + \frac{\pi}{64}\left(d_o^4 - d_i^4\right)_{inner\ plies}$$
$$= \frac{\pi}{64}\left(191.896^4 - 191.698^4\right) + \frac{\pi}{64}\left(190.198^4 - 190^4\right) = 5.413 \text{ X } 10^5 \text{ in}^4 \qquad \text{(Eq 7.20)}$$

Using the A-matrix values obtained in the FORTRAN program for calculating laminate properties, an equivalent modulus of elasticity for the shroud material is found from Eq 7.11.

$$E_{eq} = \frac{A_{11} - \frac{A_{12}}{A_{22}}}{h} = \frac{2.765 \text{ X } 10^6 - \frac{6.32 \text{ X } 10^5}{8.229 \text{ X } 10^6}}{0.948} = 2.917 \text{ X } 10^6 \text{ psi} \qquad \text{(Eq 7.21)}$$

By multiplying the two numbers above, the equivalent EI, or stiffness of the shroud, is found to be 1.579 X 10^{12} psi.

The maximum stress, on average, in any of the carbon plies is 22,000 psi which is below material property values. The maximum von Mises stress in the honeycomb core is 241.97 psi, slightly below the allowable value. Even including the 1.25 factor of safety, all the requirements are met.

Knowing the overall dimensions, and the dimensions of the materials, the weight of the cylindrical section and the ogive section are calculated. The cylindrical section is as follows:

$$\begin{aligned} W_{cyl} &= \rho_{carbon} V_{carbon} + \rho_{Al} V_{Al} \\ &= \rho_{carbon}\left[\pi\left(r_o^2 - r_i^2\right)_{outer\ plies} + \pi\left(r_o^2 - r_i^2\right)_{inner\ plies}\right] * h + \rho_{Al}\left[\pi\left(r_o^2 - r_i^2\right)h\right] \\ &= (0.058)\left[\pi\left(95.948^2 - 95.849^2\right) + \pi\left(95.099^2 - 95^2\right)\right] * (25*12) \\ &\quad + (1.736 \text{ X } 10^{-3})\left[\pi\left(95.849^2 - 95.099^2\right)\right](25*12) \\ &= 2066.7 + 234.31 = 2301.01 \text{ lbs.} \end{aligned} \qquad \text{(Eq 7.22)}$$

The weight of the ogive section can be calculated similarly:

$$\begin{aligned} W_{ogl} &= \rho_{carbon} V_{carbon} + \rho_{Al} V_{Al} \\ &= \rho_{carbon}\left[\frac{\pi}{3}\left(r_o^2 - r_i^2\right)_{outer\ plies} + \frac{\pi}{3}\left(r_o^2 - r_i^2\right)_{inner\ plies}\right] * h + \rho_{Al}\left[\frac{\pi}{3}\left(r_o^2 - r_i^2\right)h\right] \\ &= (0.058)\left[\frac{\pi}{3}\left(95.948^2 - 95.849^2\right) + \frac{\pi}{3}\left(95.099^2 - 95^2\right)\right] * (14*12) \\ &\quad + (1.736 \text{ X } 10^{-3})\left[\frac{\pi}{3}\left(95.849^2 - 95.099^2\right)\right](14*12) \\ &= 385.79 + 43.74 = 429.53 \text{ lbs.} \end{aligned} \qquad \text{(Eq 7.23)}$$

There will be additional material at the base of the shroud where aluminum will be added around the entire circumference for the edge close-out. This is done to end the honeycomb, and allow for a place to connect to the attach ring. A diagram of the edge close out for a cross section of material is shown in Figure 7.25. After optimizing material design by changing the ply orientations and the number of plies, the total weight of the material for the shroud should be approximately 2,300 lb..

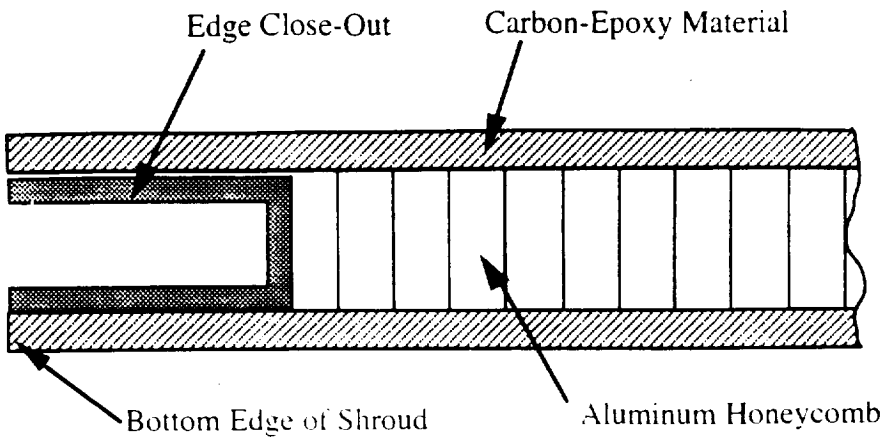

Figure 7.25 Edge Close-Out at the Base of the Shroud

Conclusion

The payload shroud is designed to protect the payload from the environment, and because of its enormous size, weight is a major factor. To reduce weight, a carbon-epoxy/aluminum honeycomb sandwich composite was chosen as the material. This keeps the high bending and torsional stiffness of the shroud high, and keeps the overall weight low. The total structure weight of the shroud is 6,200 lb., yielding a lower weight than a comparable structure of solid aluminum, which would weigh approximately twice as much. The stress observed in the honeycomb core is still quite high, and during redesign of the payload shroud, reduction of the stresses in the honeycomb will be the top priority. Also, an optimization of ply orientation angles and number of plies needs to be performed. Other concerns that will need to be addressed are how to manufacture such a large shroud as well as the specifics of how the shroud is fixed to the attach ring. Investigations must be made as to how the explosive mechanism and the explosives will interact to jettison the shroud during flight. Finally, research must be done on how the hinge at the base of the shroud will work, and how the mandrel, used to wind the carbon-epoxy material, will be designed.

7.3.7 Static Loads for the Fairings

Since it was proven that modeling the sandwich composite as a laminate was acceptable, and the sandwich composite material was extremely light, the same type of material was chosen to design the solid booster fairings. The fairings are much smaller than the shroud size, and are to be used for only aerodynamic purposes. Therefore, the goal in designing the fairings was to make them as light as possible, and just strong enough to take the applied loads. Also, because of the reduction in size, the loads experienced by the fairings are much smaller than seen on the shroud.

As with the shroud, the worst loading conditions were chosen to be at the same point during atmospheric flight. With a total drag of 165,000 lb.. and a total lift of 115,000 lb.., the same procedure was followed for calculations, except the pertinent area is now the fairing instead of the shroud.

Y-Component of Drag:

$$= D_y\left(\frac{A_{F1}}{A_B}\right)*(SF) = (165000\cos 18°)(0.18)(1.25) = 35{,}308 \text{ lbs.} \qquad \text{(Eq 7.24)}$$

X-Component of Drag:

$$= D_x\left(\frac{A_{F1}}{A_B}\right)*(SF) = (165000\sin 18°)(0.18)(1.25) = 11{,}472 \text{ lbs.} \qquad \text{(Eq 7.25)}$$

Y-Component of Lift:

$$= L_y\left(\frac{A_{F1}}{A_B}\right)\left(\frac{A_{F2}}{A_{SB}}\right)*(SF) = (115000\sin 18°)(0.18)(1.25) = 7{,}996 \text{ lbs.} \qquad \text{(Eq 7.26)}$$

X-Component of Lift:

$$= L_x\left(\frac{A_{F1}}{A_B}\right)*(SF) = (115000\cos 18°)(0.18)(0.217)(1.25) = 5{,}333 \text{ lbs.} \qquad \text{(Eq 7.27)}$$

Acceleration Load in X-Direction:

$$F_x = W(SF)(\#\text{ of g's}) = (mg)(SF)(\#\text{ of g's}) = (400)(1.25)(2.5) = 1{,}250 \text{ lbs} \qquad \text{(Eq 7.28)}$$

Acceleration Load in Y-Direction:

$$F_y = W(SF)(\#\text{ of g's}) = (mg)(SF)(\#\text{ of g's}) = (400)(1.25)(5.0) = 2{,}500 \text{ lbs} \qquad \text{(Eq 7.29)}$$

where, as shown in Figure 7.17:

A_{F1} = the base area of one fairing
A_{F2} = the longitudinal area of one fairing
A_B = the base area of the entire booster
A_{SB} = the longitudinal area of the solid booster
SF = factor of safety
W = weight

Table 7.13 summarizes the above loads. These static forces are what was applied to the solid booster fairing model created in I-DEAS.

Table 7.13 Static Loads Applied to the Solid Booster Fairing in I-DEAS

Type of Load	Y-Component (Compression)	X-Component (Bending)
Drag	35,308 lb..	11,472 lb.
Lift	7,996 lb..	5,333 lb.
Acceleration	2,500 lb..	1,250 lb.
Σ Forces	45,804 lb..	18,055 lb.

7.3.8 Fairing Buckling Analysis

The fairings are similar in design to the conical portion of the shroud. Although buckling was not the critical factor in the design of the shroud, it provided a good baseline design for stress analysis. The same technique was applied to the fairings. Buckling analysis resulted in a $[30/-30]_S$ (symmetric) IM7-8551-7 skin with a 3/8" aluminum honeycomb core. The critical stress of this lay-up was 1,970 psi. Stresses due to aerodynamic and acceleration loads amounted to only 1,127 psi.

7.3.9 I-DEAS Modeling of Solid Booster Fairings

For the fairings, the model was designed, and a new laminate was created and applied to the model. The loads of Table 7.13 were applied to one solid booster fairing as well as a temperature load of 300°F. This temperature was also applied to the payload shroud. The base of the fairing model was clamped since it will be clamped to the attach ring. The attach ring connects the fairing to the ring provided with the Castor 120 solid rocket engines.

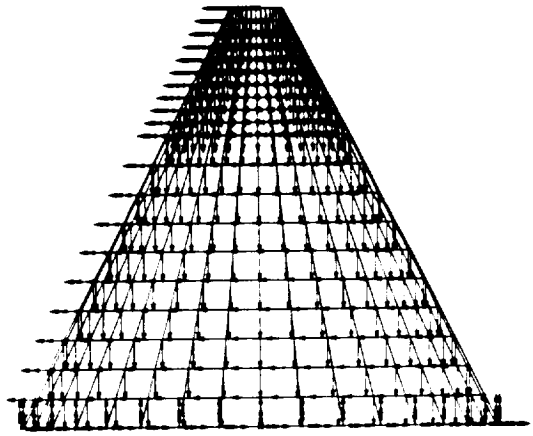

Figure 7.26 I-DEAS Model of the Solid Booster Fairing with Applied Loads

Since the loads on the fairings are not as high as on the shroud, not as much material was needed to design against buckling and failure. This reduction in the number of plies also reduces the total weight of the fairings. Displacement, in-plane stresses, transverse shear stresses, and ply failure index were calculated by running the model, and resulting material changes were made based on the test results. Figure 7.14 and Table 7.10 show the final sandwich composite arrangement for the fairing. Figure 7.26 shows the solid booster fairing model used in analysis, with applied loads and restraints, and Figure 7.27 shows the net displacement due to the applied loads.

The maximum deflection of the fairing due to static loading is 0.107 inches at the tip, which is quite reasonable for a 7.5 foot diameter cone exposed to nearly 50,000 lb. of force.

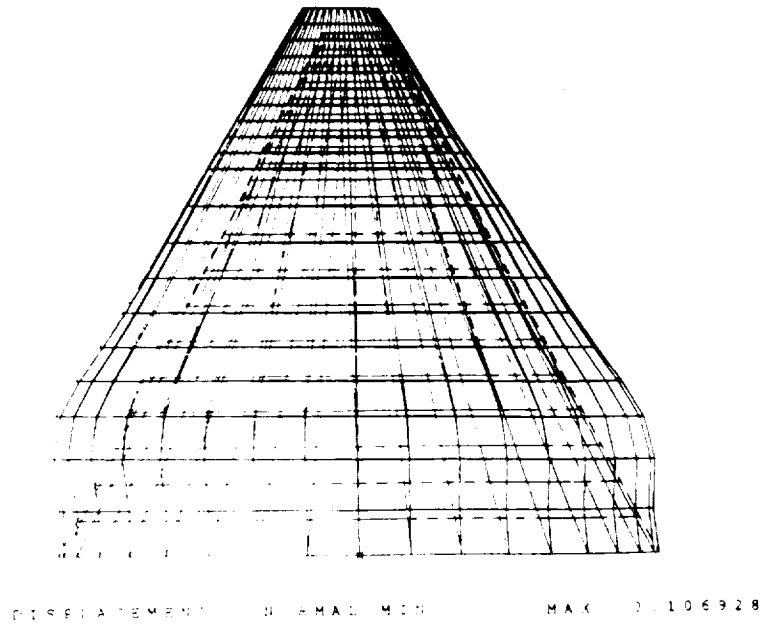

Figure 7.27 Total Displacement of the Solid Booster Fairing

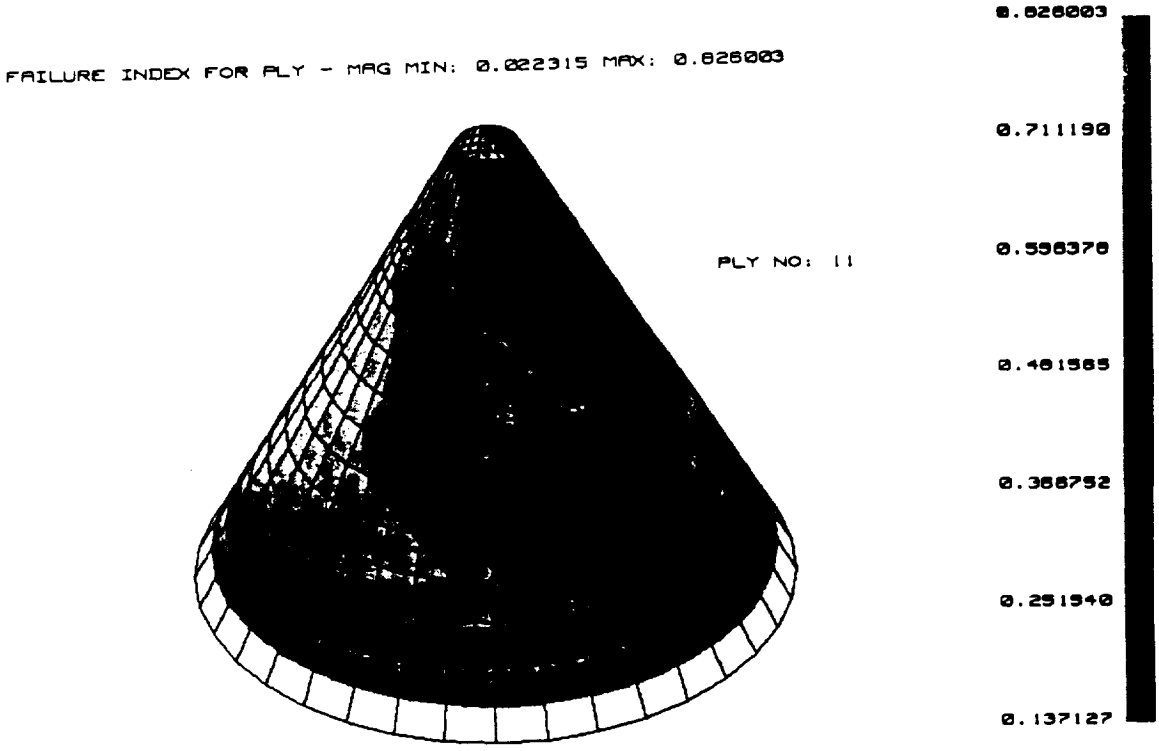

Figure 7.28 Ply Failure Index Plot for the Fairing Honeycomb Core

As done for the payload shroud, Figures 7.28 and 7.29 show contour plots of the ply failure index based on the Hoffman failure theory (Eq 7.19). Figure 7.28 is for the honeycomb core (ply number 11), and Figure 7.29 is for one of the carbon-epoxy plies (ply number 4). The failure index reaches a maximum of 0.826 for the honeycomb, and the carbon-epoxy material is fairly consistent around 0.05. As in the shroud, the honeycomb core is the weak link in the material. However, if enough surrounding plies are made to carry the load, the sandwich composite works well.

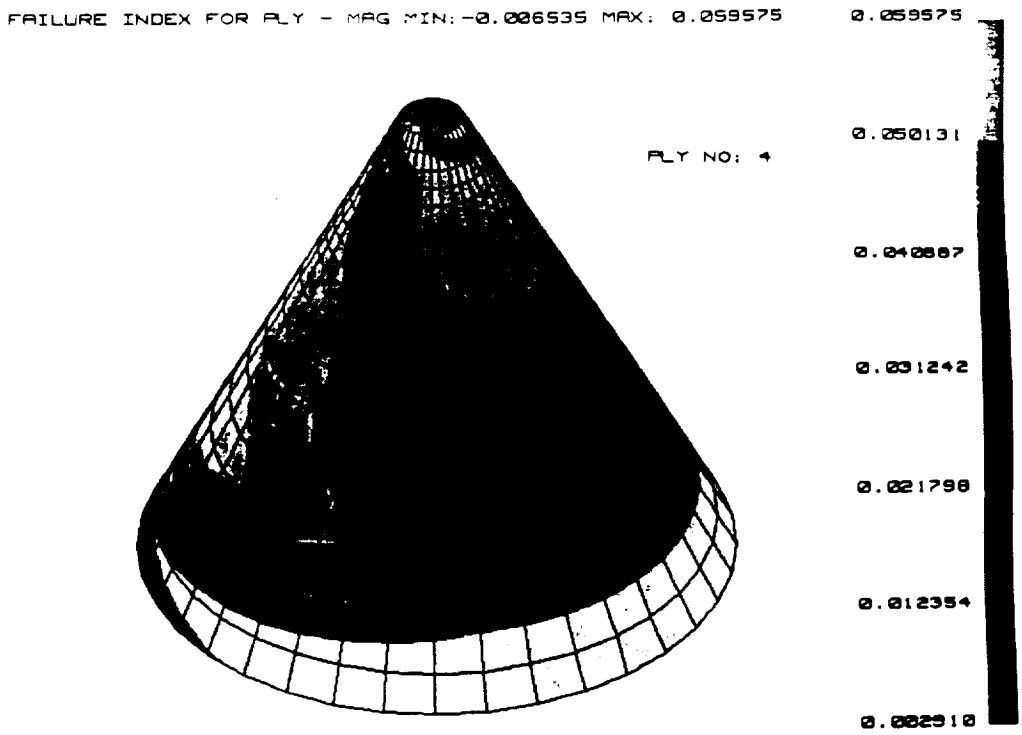

Figure 7.29 Ply Failure Index Plot for a Fairing Carbon-Epoxy Ply

Highly stressed elements in the honeycomb were also checked to prove that the material was not experiencing stresses greater than it can withstand. Figures 7.30 and 7.31 are plots of the stress throughout one element, showing that the stress does not exceed material properties. Once again, the transverse shear stress plot, Figure 7.31, shows that any failure of the honeycomb would be due to axial loads and not transverse loads. Any failure of the honeycomb core could be eliminated by adding more carbon-epoxy plies to take the axial load.

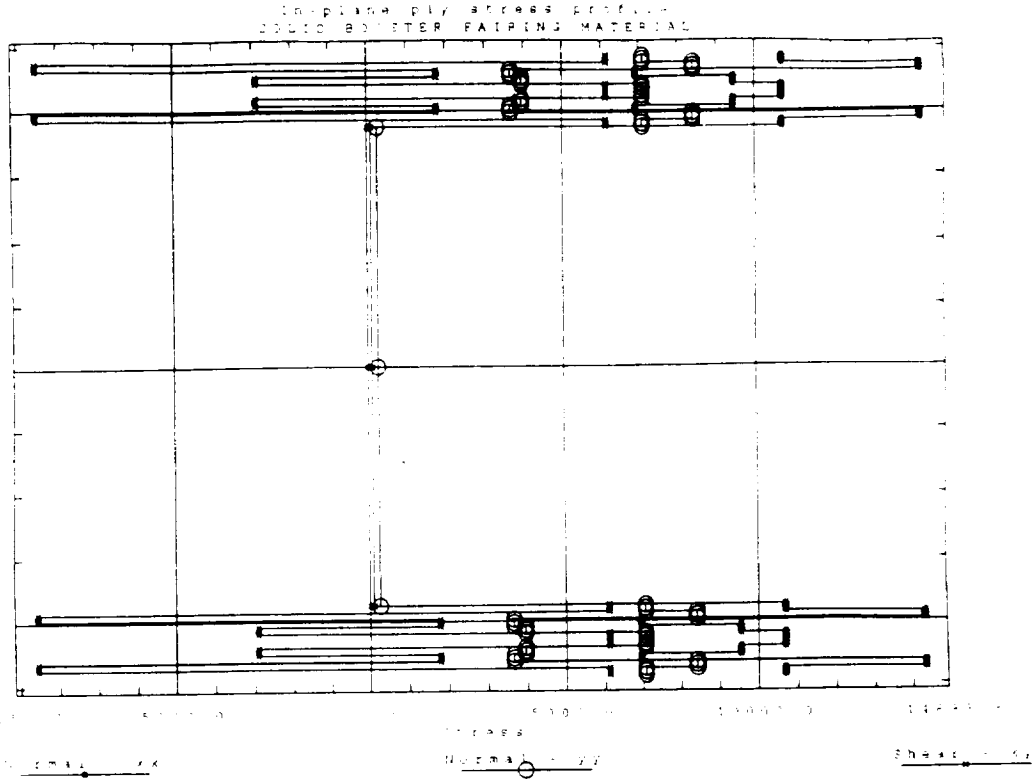

Figure 7.30 In-Plane Stress for a Fairing Model Element with Highly-Stressed Honeycomb Core

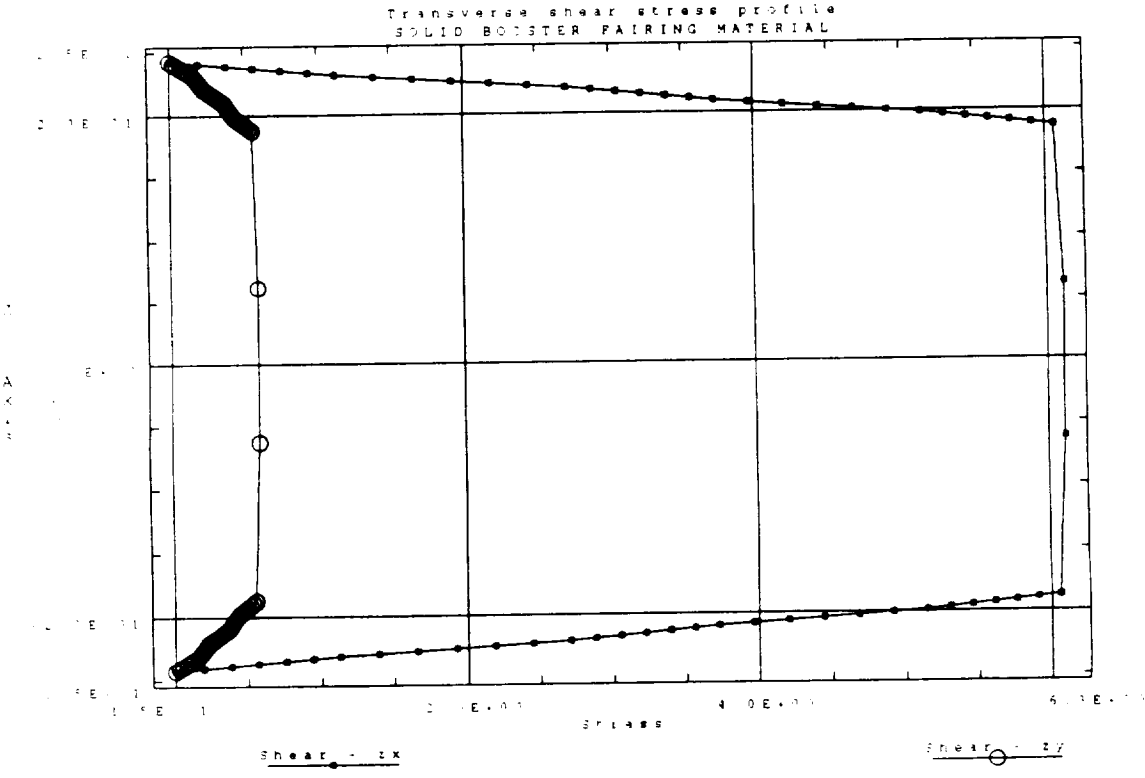

Figure 7.31 Transverse Shear Stress for a Fairing Model Element with Highly-Stressed Honeycomb Core

Results

The maximum stress in any of the carbon-epoxy plies of the fairing is 22,000 psi, below the allowable stress in compression or tension, and the maximum von Mises stress in the honeycomb core is 226.75 psi, also below the allowable value. All the requirements are met, including the 1.25 factor of safety.

As with the payload shroud, the weight for each of the solid booster fairings is calculated, using the data in Tables 7.7 and 7.8. The weight of one fairing is as follows:

$$W_{fairing} = \rho_{carbon} V_{carbon} + \rho_{Al} V_{Al}$$

$$= \rho_{carbon}\left[\frac{\pi}{3}\left(r_o^2 - r_i^2\right)_{outer\ plies} + \frac{\pi}{3}\left(r_i^2 - r_i^2\right)_{inner\ plies}\right] * h + \rho_{Al}\left[\frac{\pi}{3}\left(r_o^2 - r_i^2\right)h\right]$$

$$= (0.058)\left[\frac{\pi}{3}\left(45^2 - 44.945^2\right) + \frac{\pi}{3}\left(44.57^2 - 44.515^2\right)\right] * (6.495*12) \qquad \text{(Eq 7.30)}$$

$$+ (1.736 \text{ X } 10^{-3})\left[\frac{\pi}{3}\left(44.945^2 - 44.57^2\right)(6.495*12)\right]$$

$$= 46.61 + 4.76 = 51.4 \text{ lbs.}$$

As with the payload shroud, there will also be an edge close-out, as shown in Figure 7.23, around the entire circumference of the fairings. Therefore, the total weight for one fairing will be about 53 lb., and for the two together, about 105 lb..

Conclusion

Two identical solid booster fairings will be built for the Gryphon, each to be mounted on the top of one of the Castor 120 solid rocket engines. The fairings, used for aerodynamic purposes, are comprised of a carbon-epoxy/aluminum honeycomb sandwich composite, which significantly reduces weight. Each fairing, a 7.5 foot diameter by 6.495 foot high cone, weighs approximately 53 lb.. As of now, the fairings are slightly over designed. Therefore, to optimize the design, buckling and static yielding cases must be considered. The design may also work with slightly less material, thereby,, reducing the overall weight. As with the shroud, the manufacturing of the fairings and the specifics of how they are fixed to the attach rings needs to be investigated.

7.3.10 Static Analysis of Attach Rings for Payload Shroud & Solid Booster Fairings

For the payload shroud and the solid booster fairings, attach rings needed to be designed to work as an adapter. In each case, a sandwich composite structure needs to be connected to the attach ring, which attaches to the main structure of the Gryphon.

The payload shroud attach ring connects the payload shroud to the third stage external structure. It also is used to match the size of the shroud to the size of the rest of the Gryphon. The diameter of the shroud is required to be 190", or 15.83 feet. However, the rest of the booster is 15 feet in diameter. The attach ring reduces the diameter size to 15 feet. Also, the attach ring needs to be strong due to the large loads imparted to the ring.

The attach ring for the fairing is much more basic than that for the shroud. The loads on the fairing are much less than that of the shroud, and therefore the attach ring for the fairing does not need to be as strong. Also, the fairing attach ring acts as a connection between the solid booster fairing and the ring accompanying the top of the Castor 120 solid rocket engine.

Payload Shroud Attach Ring

It is assumed that static loading conditions are the governing forces acting on the attach rings. Therefore, if the attach rings are designed for static loading, they will be strong enough for use. To design the attach ring for the payload shroud, a basic design was used. The ring, as shown in Figure 7.13, is made of 7075-O tempered aluminum, with its material properties listed in Table 7.10. The same material is also used in the design of the fairing attach rings.

The cross section view in Figure 7.13 shows how the shroud is supported by two flanges that jut out from the center-body of the ring. A portion of the ring sticks into the shroud, where the edge close-out is located. This portion is the same size as the space between the carbon-epoxy plies. It is three-quarters of an inch, so that it will fit snugly. After dropping below the flanges, the ring cross section jogs inward, dropping the overall diameter of the ring down to the required 15 feet. To physically connect, holes are located along the circumference of the base of the shroud, the portion of the ring that sticks into the shroud, and along the bottom vertical part of the attach ring. Bolts will then connect the entire system together.

The attach ring was then modeled in I-DEAS, and loaded on the flanges with the full drag force experienced in the compressive direction. The analysis provided the information necessary to approve the design. Shown in Figures 7.32 and 7.33 are the two important drawings proving the strength of the structure. Figure 7.32 shows that the maximum tip deflection is 0.000412", and Figure 7.33 shows that the von Mises stress in the ring cross-section does not exceed 165.71 psi. Therefore, at this point, it is obvious that the payload shroud attach ring is over designed. The next step would be to reduce the weight, and maximize the design until optimal values which maximize the material properties are achieved.

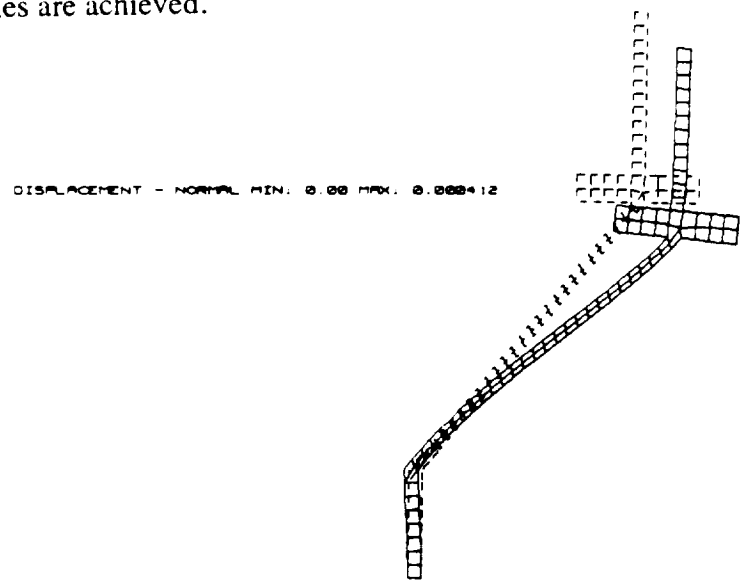

Figure 7.32 Total Displacement of the Payload Shroud Attach Ring Cross Section

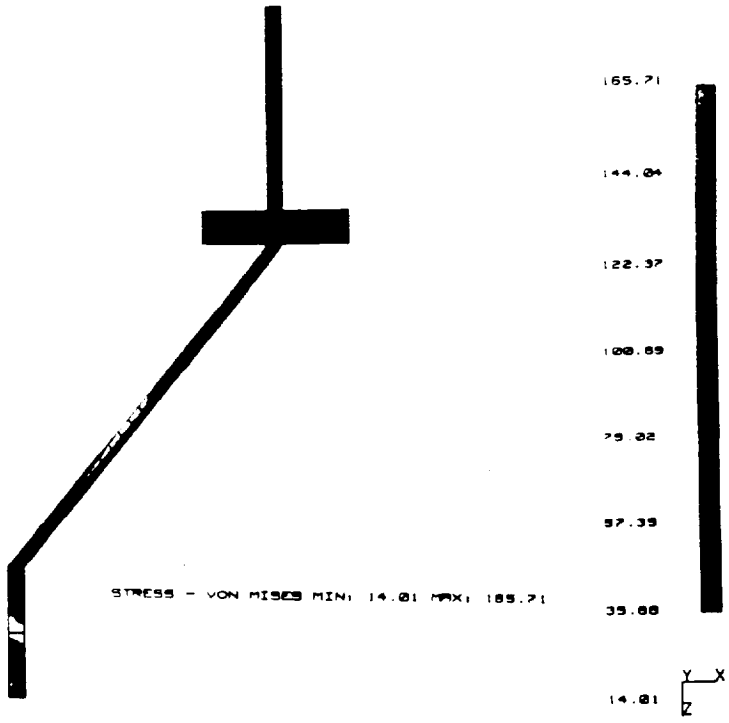

Figure 7.33 von Mises Stress Distribution for Shroud Attach Ring Cross Section

The weight of the attach ring material can be calculated using the following equations:

$$W_{\text{attach ring}} = \rho_{7075-Al} V_{7075-Al} = \rho_{7075-Al} A_{x-sect.} (\pi D_{avg.})$$

$$= (0.101)\begin{bmatrix}(2"*0.25")+(6.403"*0.25")\\+(0.5"*2.75")+(0.75"*3")\end{bmatrix}(\pi*185") \qquad \text{(Eq 7.31)}$$

$$= 336 \text{ lbs}$$

The attach ring weighs approximately 300 pounds, as stated in Section 7.3.1. Using basic analysis, the stress in the attach ring can also be estimated using Eq 7.32:

$$\sigma = \frac{P}{A} \pm \frac{My}{I} \qquad \text{(Eq 7.32)}$$

s is the stress in the attach ring, P is the applied load, and A is the area on which the applied load acts. M is the moment on the area A, y is the distance from the neutral axis that the stress is being found, and I is the area moment of inertia of the area A. For the payload shroud attach ring, the dominant load is the compressive force. Therefore, the bending moment will be not included. The load is being applied to the flanges, so the area on which the applied load acts is the top area of the flanges. This area is approximately 1194 square inches. The load applied to the flanges is the 129,463 lb compressive force on the shroud due to drag. Dividing the load by the applied area yields a stress equal to 108.45 psi in the flanges. Looking at the von Mises contour plot in Figure 7.33, this number is quite comparable to the stress found in the flanges. In the

figure, the von Mises stress in the flanges is approximately 100.69 psi. The value obtained from Eq 7.32 is a basic approximation yielding an answer too conservative by 7.7%.

Solid Booster Fairing Attach Ring

The load on the solid booster fairing, 35,308 lb. of compressive force, is quite small in comparison to the 129,463 pound load on the shroud attach ring. Also, the shape of the ring, as shown in Figure 7.16, is completely vertical, unlike the offset in the shroud attach ring. Therefore, it was assumed that doing calculations using Eq 7.32 would be reliable to a high enough level that the ring would not need to be modeled on I-DEAS. The fairing attach ring is basically the shape of a T with the vertical part taking the compressive load. Using Eq 7.32 to find the stress in the flange and assuming the imparted moment is small enough that it can be assumed to be zero:

$$\sigma = \frac{P}{A} \pm \frac{My}{I} = \frac{35308\ \text{lbs.}}{\pi D_{avg}\, t} = \frac{35308\ \text{lbs.}}{\pi(7.5 \text{@} 12)(0.5")} = 249.75\ \text{psi}$$

The stress in the flange is 249.75 psi, and the yield strength of the 7075-O aluminum is 15,000 psi. Therefore, the attach rings for the fairings are also over designed. Reducing the size would reduce the weight and would make more efficient use of the material. The weight of this ring can be calculated in the same way that it was calculated for the shroud attach ring. Completing these calculations:

$$\begin{aligned} W_{\text{attach ring}} &= \rho_{7075-Al} V_{7075-Al} = \rho_{7075-Al} A_{x-sect.} \left(\pi D_{avg.}\right) \\ &= (0.101)[(4.25" * 0.125") + (0.5" * 0.25")](\pi * 7.5 \text{@} 12) \qquad \text{(Eq 7.33)} \\ &= 18.74\ \text{lbs.} \end{aligned}$$

Therefore, two attach rings will weigh approximately 35 lb..

Conclusion

Three attach rings will be made in total for the payload shroud and fairings, one for the shroud and one for each of the fairings. The rings will be made of 7075-O tempered aluminum, and can support maximum compressive loads with a 1.25 factor of safety. The shroud attach ring is used as an adapter to drop the overall outside diameter from 190" to 180", and to connect the payload shroud to the third stage. The fairing rings are simply used as a connection from the solid booster fairings to the attach ring located on the Castor 120 solid rocket engines. At this point, all of the rings are over designed, and in the future, would need to be changed to minimize weight and effectively use material. Also, problems such as how the rings will be manufactured, where the exact attachment points are located, and how many and what type of bolts will be needed, will have to be answered in future work.

7.4 PAYLOAD INTERFACE

7.4.1 Introduction

The Payload Interface (PI) supports and protects the payload during ascent. It is roughly 16 feet high and has a diameter which varies between 10 and 14 feet. It can support two satellites with a maximum weight of 5000 lb each.

7.4.2 Presentation

Several considerations were taken into account in the design of the PI:

- The design had to be light weight.
- The PI had to withstand axial and lateral acceleration loads.
- The PI had to withstand dynamic loads from random vibration and thrust fluctuations.
- The design had to be cost effective.

The PI consists of an aluminum skin that is 1/64" thick. The skin is reinforced with beam supports. Along the outside, eight I beams run the length of the PI. These are Aluminum beams with a 1" I-beam cross section. Around the top of the PI, a ring is positioned to interface with an upper satellite. This ring was modeled as a 3" I beam section, made of aluminum. A second ring, 14' above the base of the PI, supports the structure against buckling and is a 1" I beam made of titanium. Finally, a third supporting ring is positioned 10' above the base of the structure. Again this ring mainly prohibits buckling, and is composed of titanium. The lower satellite is supported by a truss structure originating from the base of the PI, and running inside the skin. The entire structure weighs 636 lb. The payload interface is shown in Figure 7.34.

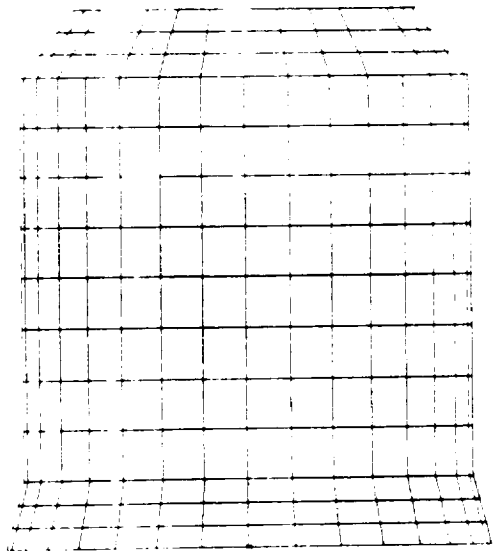

Figure 7.34 Payload Interface

7.4.3 Loading

The PI loads originate from the two satellites. The vehicle is subjected to a 5.5g axial load and a 3g lateral load. The axial load results solely from the static thrust of the rocket engines, since dynamic loading of the PI proved to be negligible in this direction. The lateral load has two causes. The first part of the lateral load results from a pull up maneuver during ascent. This maneuver incurs a load of 2.5g. An additional 0.5g results from dynamic loading during the flight. Each load includes a factor of safety of 1.25.

Static Loading

Static loading information was obtained from the mission analysis group. Using the trajectory, the static loads on the PI were determined to be 5.5g axially and 2.5g laterally. Again, these loads arise from the thrust acceleration of the rocket engines and a 2.5 g pull up maneuver.

Dynamic Loading

Dynamic loads result from engine vibration. These loads proved to be the most difficult to determine. Vibration loads resulted in a negligible axial component and a 0.5g lateral component.

7.4.4 Modeling

Modeling began with intuitive reasoning and hand calculations. The original model of the Payload Interface consisted of a solid tapered cylinder, modeled after the Pegasus' configuration. This proved to be a very weak configuration in terms of buckling strength and weight.

The next modeling step involved reinforcing the cylinder with titanium stiffeners. The titanium beams offer a greater buckling strength than the aluminum skin. The use of stiffeners saved a great deal of weight as compared to a comparable solid shell. Use of an I beam shape offers a high moment of inertia, and therefore, a higher buckling strength.

The dimensions of the PI were determined from the payload size. The structure was designed to hold two 12' long satellites with a 12' diameter and a combined weight of 7900 lb.. A Finite Element model was created on I-DEAS for static and dynamic analysis.

7.4.5 Results

The design of the PI was started by hand. Intuitive work and hand calculations were used for rough estimates. The early results showed that a solid aluminum skin would be too heavy if it were to withstand the loads generated during ascent. The first improvement upon this design was the use of stringer supports which allow the skin to be much thinner, hence lower in weight. Eight beams were placed around the outer edge of the PI to stiffen the cross section where high moments of inertia and a low cross sectional area are desired The beam sections would carry most of the load and protect the structure against buckling. The optimal beam shape was determined to be I shaped due to its high moment of inertia and low cross sectional area, therefore providing lower weight.

At this point the model consisted of a twelve foot diameter cylinder that was ten feet high. An increase in complexity resulted from determining the size of the lower stages, and the outer shroud. Initial estimates put the third stage diameter at 15'. The payloads group decided to aim for a two satellite configuration with a maximum payload of 7900 lb, including a 10% allocation for structural weight. The maximum size the two satellites can be is 12' tall and 12' in diameter with a 5000 lb maximum weight. Although two 5000 lb satellites would exceed the vehicle's payload capacity, this design allows the versatility to place the heavier satellite in either spot. This also allows for heavier payloads in the future if the booster configuration allows the Gryphon to take higher payloads to orbit.

From this point on all modeling was performed using I-DEAS to allow for fast analysis of potential design changes. Using this model it was apparent that the skin could be made very thin, and still support the static load. The major concern with the thin skin was buckling, since early models showed that the supporting beams would buckle well before the skin material would exceed the material limit. To rectify this problem horizontal stiffener rings were placed on the PI. The final configuration had deformations and stresses within acceptable limits. Maximum von Mises stresses were found to be 30 ksi, below the material limit for wrought aluminum (35 ksi). The maximum deflections was on the order of 0.8". Stress contours for the PI are shown in Figure 7.35.

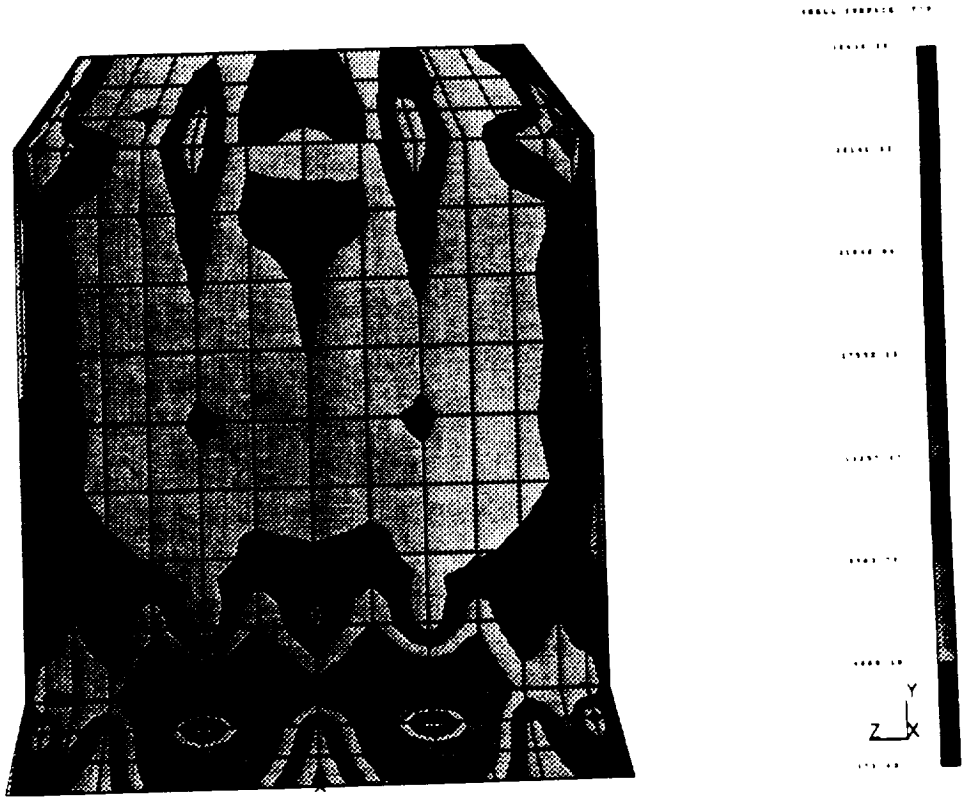

Figure 7.35 Stress Contours of Payload Interface

Although the material limits were not exceeded, other issues needed to be considered. The PI would support the weight, but how much would it move the satellite? Upon analyzing the deformed geometry, it was apparent that the deflections incurred during flight would not cause the satellite to interfere with the outer shroud. The deformed geometry of the PI is shown in Figure 7.36.

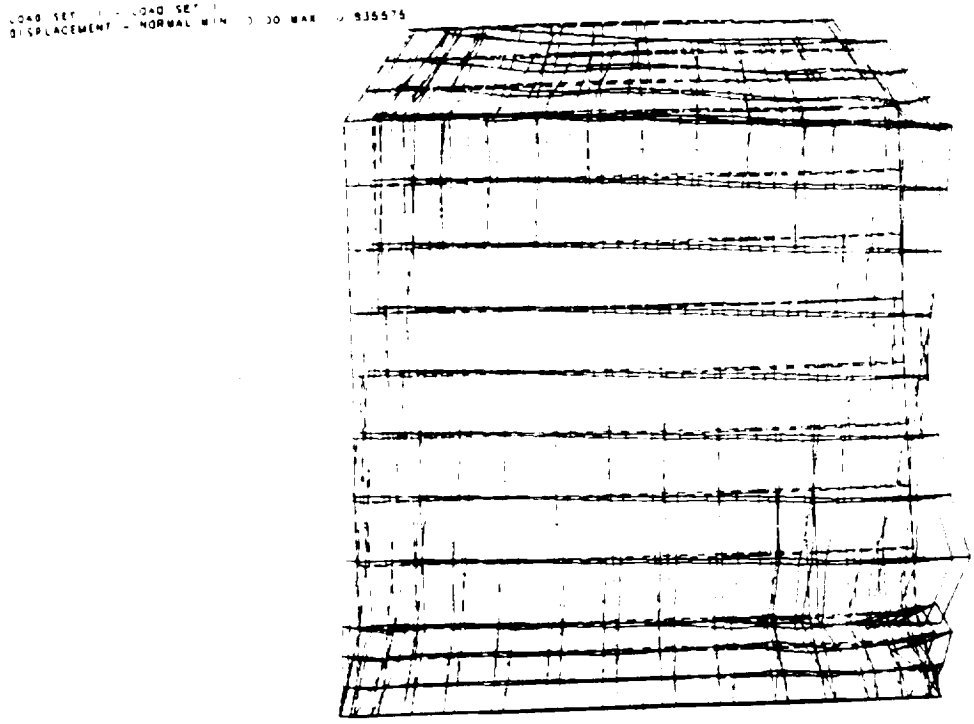

Figure 7.36 Deformed Geometry of PI

Although the upper ring moved very little, the fact that a 12' high satellite rested on top of it had to be considered. The largest deflection was found to be 0.8". The worst case assumed that two points opposite one another on the ring each deflected 0.8" in the vertical (y) direction, which created a total displacement of 1.6". Since the diameter of the ring is 13 feet, this meant a twist angle of 0.76°. If the entire satellite rotated through this angle the movement of the uppermost part of the second satellite would be 1.9" which is well within the shroud inner diameter of 15' 10". This is shown in Figure 7.37.

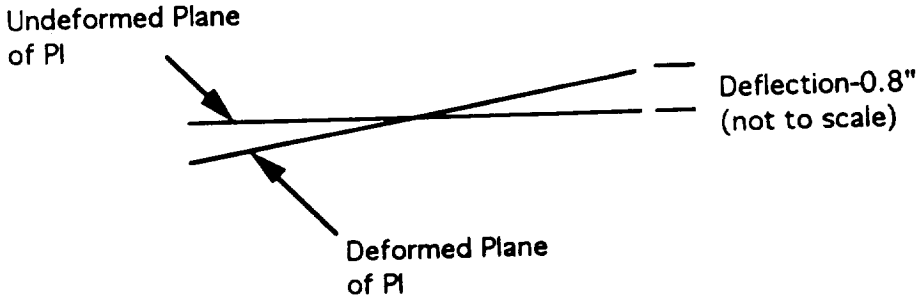

Figure 7.37 Deflected Plane of Payload Interface

Similarly, the lower satellite support could experience motion. In this case the sizes were designed about the worst case which occurs when the shell of the PI experiences its maximum deflection in one direction, and the satellite deflects in the opposite deflection.

Static Considerations

The static deformation and stress were fairly easy to find. Early results indicated that the material would withstand he static load but problems resulted from buckling of the entire structure. More specifically, buckling occurred at either the top ring or in material near the second ring. In order to increase the buckling strength of the PI, horizontal rings were added to lower the effective column length of the PI. Initial results showed that a ring placed 14' above the base of the PI increased the buckling strength. The use of this ring solved the immediate problem of buckling at the top of the PI, but instead created the problem of buckling approximately 14' from the base. Another horizontal stiffener was added to remedy the problem. This stiffener again moved the critical stress region lower on the PI. Finally a third ring was added which solved the buckling problem, and gave a Buckling Load Factor (BLF) of 1.34. The BLF in I-DEAS is the ratio of the buckling load to the current load. A BLF greater than one indicates that the structure will not buckle under the applied load conditions.

Dynamic Considerations

Dynamic loads proved to be the most difficult to derive. These loads result from random engine vibration. Investigation of this load case began with an investigation of the normal mode shapes of the entire Gryphon. In I-DEAS the first 12 flexible body modes were found. Vibration loads were determined starting from these modes. Beginning with the

$$\mathbf{M}x'' + \mathbf{C}x' + \mathbf{K}x = \mathbf{F}(t) \qquad \text{(Eq 7.34)}$$

equations of motion for the entire booster, the coordinate system was modified into a modal coordinate system. If proportional damping is assumed, i.e.

$$\mathbf{C} = \alpha\mathbf{M} + \beta\mathbf{K} \qquad \text{(Eq 7.35)}$$

the system can be represented by:

$$\mathbf{M}x'' + (\alpha\mathbf{M} + \beta\mathbf{K})\,x' + \mathbf{K}x = \mathbf{F} \qquad \text{(Eq 7.36)}$$

Using a coordinate transform to modal coordinates,

$$x = \phi\,\eta \qquad \text{(Eq 7.37)}$$

the system may be written as:

$$\phi^t \mathbf{M} \phi\ \eta'' + (\alpha\,\phi^t \mathbf{M}\,\phi + \beta\phi^t \mathbf{K}\,\phi)\,\eta' + \phi^t \mathbf{K}\,\phi\ \eta = \phi^t \mathbf{F} \qquad \text{(Eq 7.38)}$$

Since

$$\phi^t \mathbf{M}\,\phi = I \qquad \text{(Eq 7.39)}$$

a system of equations in η can be written due to the eigenvectors, ϕ, being mass normalized:

$$\Phi^t K \Phi = \begin{bmatrix} \omega_i^2 & \\ & \omega_n^2 \end{bmatrix} \qquad \text{(Eq 7.40)}$$

which is really the system of independent equations:

$$\eta_i + 2\rho_i\omega_i \eta_i + \omega_i^2 = 0 \qquad \text{(Eq 7.41)}$$

where ω_i is the undamped natural frequency and ρ is the modal damping coefficient of the ith mode. Knowing the input and output of the system (i.e. the modal shape), a transfer function can be written in the following form:

$$H(s) = \sum_{i=1}^{n} \frac{\gamma\beta}{s^2 + 2\rho_i\omega_i s + \omega_i^2} \qquad \text{(Eq 7.42)}$$

The damping ratio of the structure was assumed to be 2%. This is a valid assumption since it is composed mostly of rigid members which provide little damping. Some damping could arise from fuel sloshing, but would be minimal.

Another important area of concern was the system input and output. Since the system consists of multiple inputs with a singular output, one finds:

$$a(s) = \begin{bmatrix} H_1(s) & H_2(s) & H_3(s) \end{bmatrix} \begin{bmatrix} U_1(s) \\ U_2(s) \\ U_3(s) \end{bmatrix} \qquad \text{(Eq 7.43)}$$

In this case the input is a Power Spectral Density (PSD) of a rocket engine. The input PSD was multiplied by the derived transfer function to get an 'equivalent' PSD at the base of the payload interface. Due to difficulties in finding an accurate PSD for a Castor 120 or the LR-91 the PSD of the original Pegasus was used. Since U_1, U_2, and U_3 are identical the above expression may be written as:

$$a(s) = [H_1(s) + H_2(s) + H_3(s)]\ U(s) \qquad \text{(Eq 7.44)}$$

where a(s) represents the output in terms of acceleration. A simple substitution changes the expression for a into frequency terms:

$$a(jw) = [H_1(jw) + H_2(jw) + H_3(jw)]\ U(jw) \qquad \text{(Eq 7.45)}$$

where a(jw) represents the 'equivalent' transfer function. Mode shapes were created for the first two axial modes, and the first three lateral modes. Using mode shapes a transfer function can be derived. The transfer function was assembled and plotted using MATLAB. From this expression, an equivalent acceleration was found by taking the integral of a in the frequency domain. The expression for the equivalent acceleration can be written as shown in Eq 7.46.

$$A_{eq}^2 = \int_{\omega_1}^{\omega_2} a(j\omega)d\omega \qquad \text{Eq 7.46)}$$

where ω_1 and ω_2 are the frequency limits. To be complete one should integrate a over the entire frequency spectrum. The Pegasus PSD used for analysis is shown in Figure 7.38.

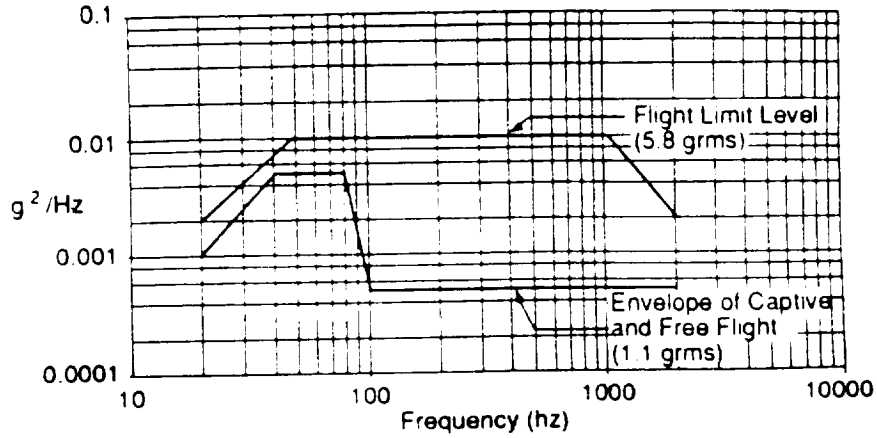

Fig 7.38 Pegasus Power Spectral Density

Dynamic Analysis of Gryphon

The results of the dynamic analysis show that axial vibrations contribute little to the overall loading, and can be neglected. The transfer function was assembled using MATLAB and by utilizing the components of the transfer function as the mode shapes. The structural model of the Gryphon is shown in Figure 7.39.

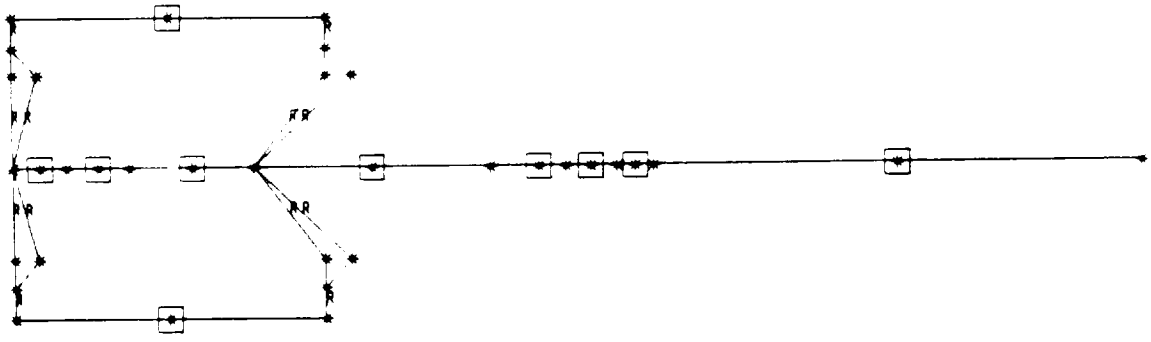

Fig 7.39 Beam Model of Gryphon

The inputs for the model are applied at the rocket motors. The LR-91 is represented at node 1, while the bottom of the castor motors are represented by nodes 18 and 47. The output is at the base of the PI and is represented by node 8.

Axial mode analysis

The results show that the important frequency response at the base of the PI occurs in a low frequency range (<10 Hz), and that the PSD value over this region is so low that the acceleration value over this range is negligible. Furthermore, when the PSD value increases to a higher level, the transfer function gain rolls off so fast that again any acceleration becomes negligible. Using the input and output from the beam model of the Gryphon, the transfer function takes the form:

$$H(s) = \frac{-44.48s^2 - 2.76s - 107.46}{s^4 + 0.1207s^3 + 4.5617s^2 + 0.2745s + 5.1704}$$

zeros: -0.031 +/- 1.553 i

poles: -0.031 +/- 1.559 i
-0.029 +/- 1.458 i

A bode plot of the axial transfer function is shown in Figure 7.40.

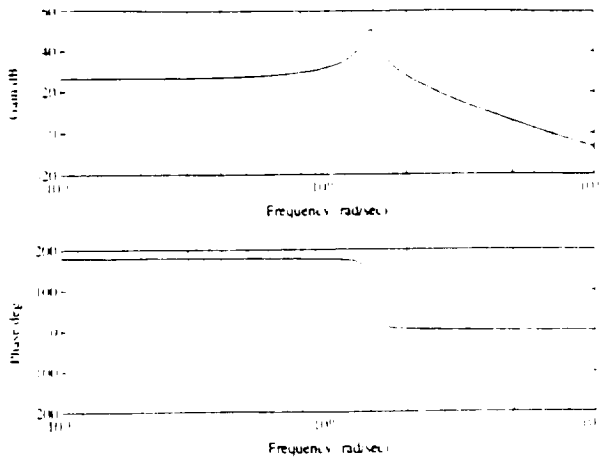

Fig 7.40 Bode Plot of Axial Frequency Response

From the plot, peaks near 1.45 are expected, along with a phase shift of -360 The reason for this behavior is that two poles and one zero lie in close proximity to one another. The two second order poles combine to give a -360° phase response and the second order zero causes a +180°phase shift. The net effect of these poles and zeros is a -180° phase shift. To determine the equivalent acceleration, the PSD was assumed to have a constant value of 0.0001 g^2/ Hz for frequencies below 10 Hz. To determine the value of the acceleration it was necessary to convert the frequency response into

magnitude. To accomplish this, each value was converted from gain to magnitude by the relation in Eq 7.47.

$$\text{magnitude} = 10^{\left(\frac{\text{gain}}{20}\right)} \qquad \text{(Eq 7.47)}$$

H(jω) needed to be multiplied by the PSD and integrated over a frequency range which was accomplished by a numerical integration method. For the axial modes the value of H(jw) was assumed to be negligible at frequencies above 10 Hz. From the Bode Plot in Figure 7.40, it is seen that the frequency response rolls off at 40 dB/ decade. After making this assumption, it was necessary to integrate a(s) over the frequency range from 0 - 10 Hz.

If I represents the value of the definite integral of A_{eq}^2 from 0 - 10 Hz, it can be approximated by Equation 7.48.

$$I = \sum_{i=1}^{\infty} M(w)\Delta w \qquad \text{(Eq 7.48)}$$

M(ω) represents the magnitude of the frequency response at a frequency ω, and Δω represents the interval over which M(ω) is considered constant. For the axial modes the value of A_{eq} was found to be 0.002g, which was considered negligible.

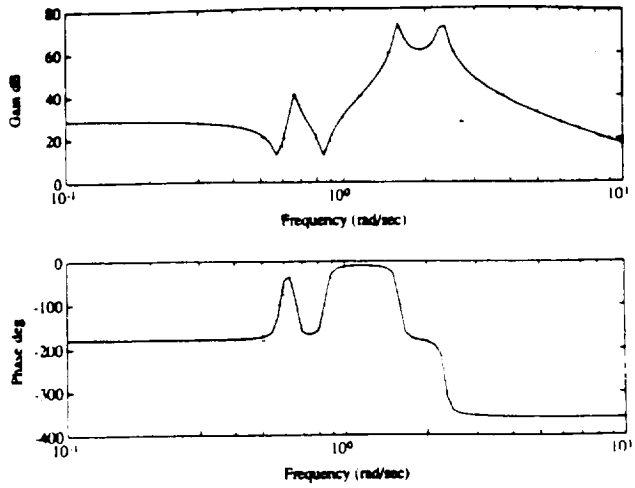

Fig 7.41 Bode Plot of Lateral Frequency Response

Analysis of lateral behavior yielded an equivalent acceleration of 0.5g. The analysis proceeded in a manner similar to the axial case. For the lateral analysis, the first

three lateral mode shapes (Modes 7,8, and 11) were obtained. Use of the mode shapes led to the following transfer function:

$$H(s) = \frac{-692.4s^4 - 48.7s^3 - 728s^2 - 23.91s - 165.42}{s^5 + 0.182s^4 + 8.3s^3 + 16.93s^2 + 0.6s + 5.9}$$

zeros: -0.031 +/- 1.559 i
-0.014 +/- 1.457 i

poles: -0.046 +/- 2.306 i
-0.032 +/- 1.591 i
-0.013 +/- 0.662 i

The lateral frequency response is slightly different than the axial response (see Figure 7.41). Due to the two high peaks the system has positive gains over part of the frequency range 10-100 Hz. To determine the acceleration value of A_{eq} it was not possible to consider H(jw)=0 at frequencies above 10 Hz. For this case, the assumption that H(jw)=0 was used when ω was above 100. Again a numerical method of integration was used to determine A_{eq}. However the value of the PSD in this case was estimated by the relation in Eq 7.47.

$$U(j\omega) = \begin{Bmatrix} 0.0001 & \omega < 10 \text{ Hz} \\ 0.001 & 10 < \omega < 20 \text{ Hz} \\ 0.01 & \omega > 20 \text{ Hz} \end{Bmatrix} \qquad \text{(Eq 7.47)}$$

Gain was transformed to magnitude and integrated over the frequency range 0 to 100 Hz. The result was a value of 0.521g for A_{eq}. For FEA, a load of 0.5g was added to the 2.5g pull up maneuver load, giving a combined load of 3g in the lateral direction.

Beam Selection

As stated earlier, beam sections were used to stiffen the outer shell of the PI. The beams were made of aluminum and titanium. Aluminum possesses acceptable strength, and in addition, is light weight. Titanium is approximately 50% heavier, but has a higher modulus of elasticity, and, more importantly, an extremely high yield stress.

The cross section shape of the stiffener beams was very important. Since the beams had to increase the buckling performance, it was important for the beam cross sections to have a high moment of inertia. Also, the cross section had to posses a low cross sectional area to minimize weight. For these two reasons, an I beam section was chosen which offers a high moment of inertia along with a low cross sectional area. Furthermore, an I-beam is a conventional shape, and can be easily manufactured. For the applications on the payload interface, the beams selected were I-beams roughly 3" by 3", and 1" by 1". A drawing of these cross sections is shown in Figure 7.42.

The 3" cross section beams were made of aluminum and were used to model the attach ring of the satellites. They represent the support of the lower satellite interface as well as support the structure against buckling

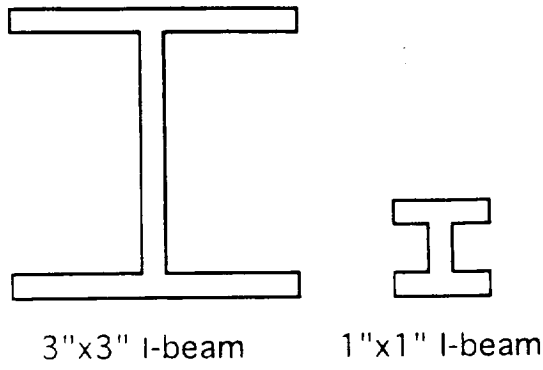

Fig 7.42 Beam Cross Sections Used for the Payload Interface

7.4.6 Conclusion

From the analysis it was found that the Payload Interface could support two 5000 lb satellites throughout the ascent of the Gryphon. The overall weight of the structure fell within the 790 lb weight limit imposed by the Payload group. However, there were several areas not analyzed, which are important for future work on the Gryphon. First of all, shocks to the payload generated by a separation mechanism have yet to be studied. Second, a thorough investigation of the dynamic behavior of the structure is in order. Ideally, it should be subjected to physical testing. Due to the scope of this project, construction of prototypes, and access to the required testing equipment was not possible.

7.5 ENGINE MOUNTS

Each liquid stage requires an engine mount to transmit thrust from the engine to the exterior hull. The Stage 1 engine mount attaches a single LR-91 engine to the exterior hull. The Stage 2 engine mount attaches two side by side LR-91 engines to the hull and the Stage 3 attach system is slightly more complex. It consists of an engine mount which connects a single RL-10 directly to a spherical fuel tank, and a support structure to join Stage 3 with the Stage 2 exterior hull.

7.5.1 Stage 1 Engine Mount

The LR-91 engine includes a 15" diameter attach ring used to join the engine to the structure. The base of the Stage 1 engine mount connects to this ring, and a tubular truss structure transmits the thrust load to the exterior hull via four attach points (see Figure 7.43). The mount is constructed of A333 steel, due to its high yield strength (75 ksi), high stiffness, and availability in pipe form. Having a total weight of 349 lb., the mount is capable of transmitting 105,000 lb. of thrust from an LR-91 engine to the exterior hull. It has a height of 48" and fits inside the 180" hull diameter.

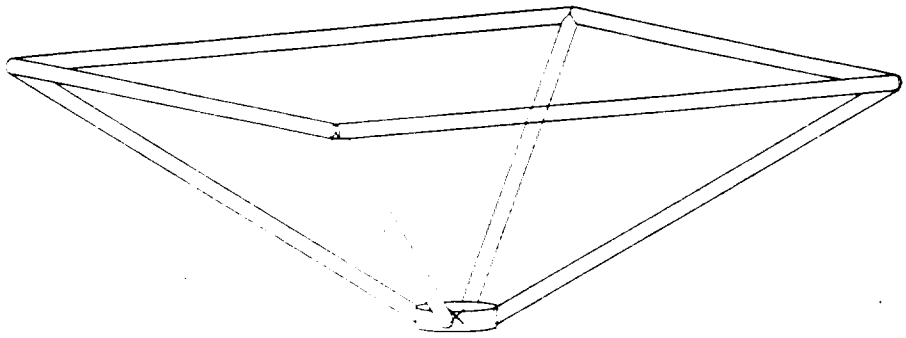

Figure 7.43 Stage 1 Engine Mount

Modeling

The LR-91 engine provides 105,000 lb. of thrust. Using a 1.25 factor of safety, the total load applied to the model was 131,250 lb.. A standard finite element beam model (see Figure 7.44) was used to analyze the structure. The thrust load was applied by attaching rigid elements to the four main members in order to distribute the load the same way the attach ring on the LR-91 motor does. Vertical stiffeners were added to represent the stringers on the hull, in order to, insure that the hull cross section did not become deformed from the resulting forces at the engine mount attach points. Table 7.14 gives dimensions and weights for each member. It references Figure 7.44 for the element labels.

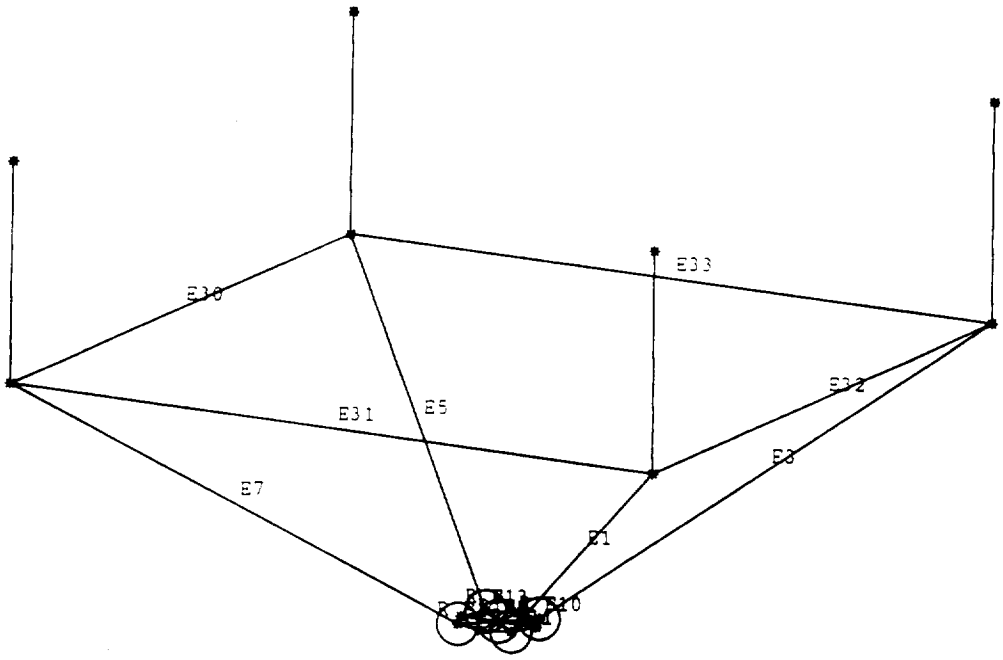

Figure 7.44 Stage 1 Engine Mount Finite Element Model

Table 7.14 Dimensions and Weights for Stage 1 Engine Mount

Element	Length (in)	Outer Dia (in)	Inner Dia (in)	Weight (lb.)
E1	95.5	3.0	2.625	45.7
E3	95.5	3.0	2.625	45.7
E5	95.5	3.0	2.625	45.7
E7	95.5	3.0	2.625	45.7
E30	127.3	3.0	2.750	41.6
E31	127.3	3.0	2.750	41.6
E32	127.3	3.0	2.750	41.6
E33	127.3	3.0	2.750	41.6

Results

A maximum deflection of .504" occurred at the point of application of the load. The maximum von Mises stress was 48 ksi which is well below the 75 ksi yield strength. However, since the maximum deflection was already over a half inch, no further optimization was performed. Lessening the cross sectional area would have lowered the factor of safety on the material, but would have contributed to engine instability in the form of higher deflection. Because of the extensive length of the lower members and the high axial loads, it was necessary to calculate critical column buckling loads. The deformed geometry is shown in Figure 7.45.

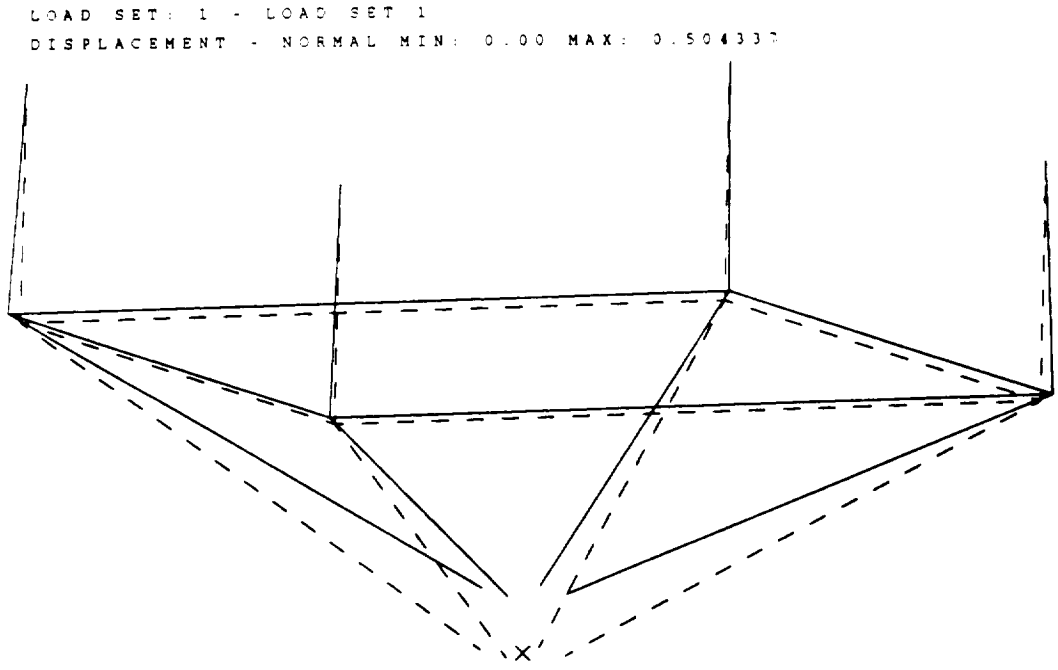

Figure 7.45 Stage 1 Engine Mount Deformed Geometry Plot

Assuming clamped conditions at the welded joints, equation 7.49 is a valid approximation:

$$P_{cr} = \frac{4\pi^2 EI_x}{L^2} \tag{7.49}$$

When computed, the critical buckling load of the 95" member was 208,000 lb.. Since 64,660 lb. is the maximum applied compressive load, buckling was not a factor in designing the engine mounts.

Conclusion

The Stage 1 Engine Mount has been designed to support a 105,000 lb thrust with a 1.25 factor of safety. Failure due to yield and to buckling was considered in the design of the structure. The final mount weighs 349 lb and its tubular A333 steel truss structure was designed to be easily manufactured at a low cost.

7.5.2 Stage 2 Engine Mount

The Stage 2 Engine Mount holds two LR-91 engines side by side and connects them to the external hull. The mount attaches to the engines at its base, similarly to the Stage 1 mount, and to the hull at six connection points on the top. The Stage 2 mount is shown in Figure 7.46.

The mount is constructed of A333 steel, due to its high yield strength (75 ksi), high stiffness, and availability in pipe form. With a total weight of 646 lb., the mount is capable of transmitting 210,000 lb. of thrust to the exterior hull. It has a height of 40" and fits inside the 180" hull diameter.

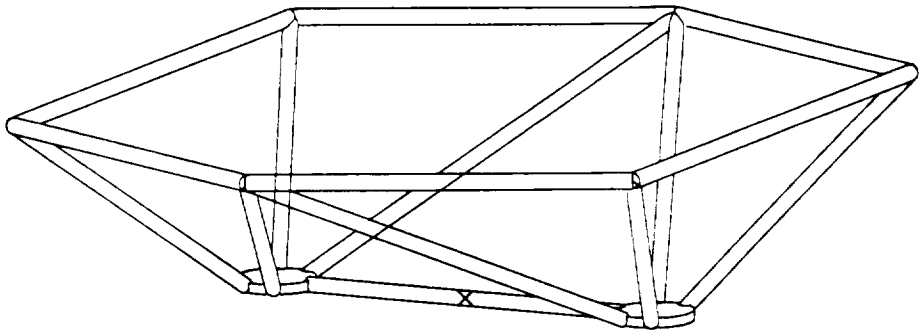

Figure 7.46 Stage 2 Engine Mount

Modeling

A finite element beam model was used to analyze the loads on the mount (see Figure 7.47). Thrust loads of 130,000 lb including a 1.25 factor of safety were applied with rigid elements at the location of each engine. This effectively models the distribution of load caused by the attach ring on the LR-91 engine.

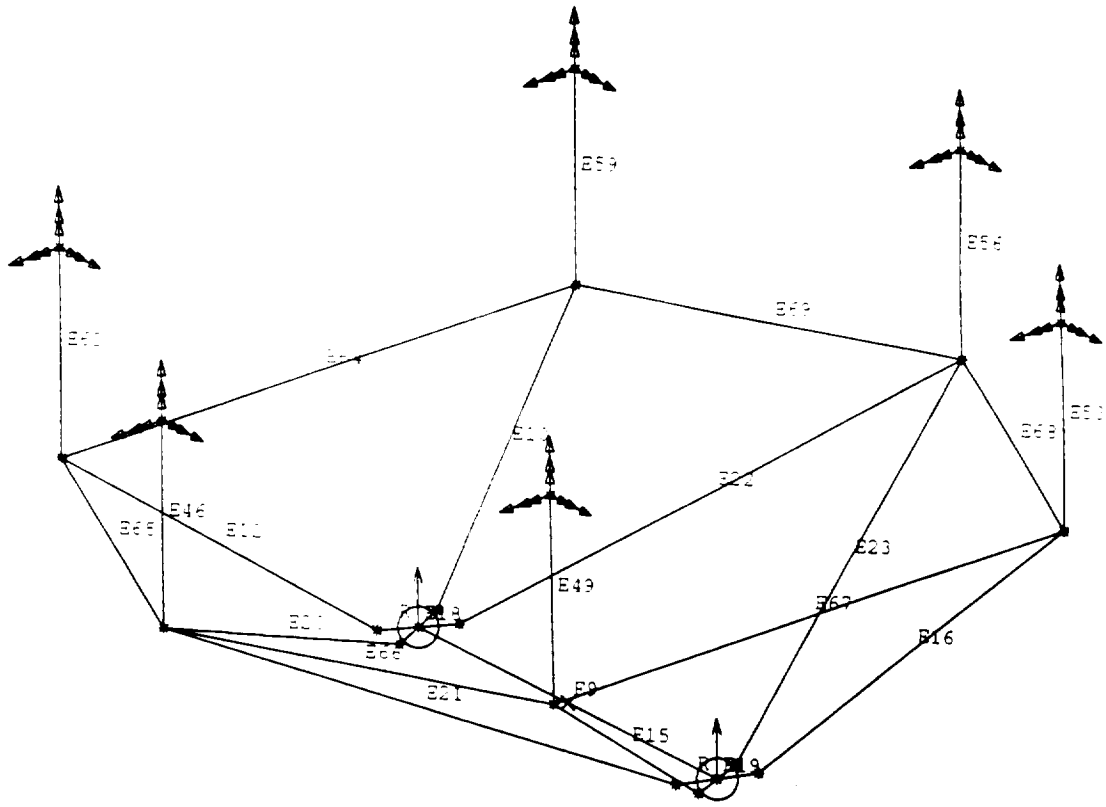

Figure 7.47 **Stage 2 Engine Mount Finite Element Model**

Longitudinal stiffeners clamped at one end were added to represent the stringers on the hull. The stiffeners were included to check the cross section of the hull for deformation at the engine mount attach points. Table 7.15 details the dimensions and weights of each member. The element numbers listed are referenced from figure 7.47.

Table 7.15 **Dimensions and Weights for Stage 2 Engine Mount**

Element	Length (in)	Outer Dia (in)	Inner Dia (in)	Weight (lb)
E9	69.0	3.25	3.000	24.3
E10	69.2	3.50	2.900	60.3
E12	69.2	3.50	2.900	60.3
E15	69.2	3.50	2.900	60.3
E16	69.2	3.50	2.900	60.3
E20	100.2	3.00	2.625	50.0
E21	100.2	3.00	2.625	50.0
E22	100.2	3.00	2.625	50.0
E23	100.2	3.00	2.625	50.0
E64	115.6	3.25	3.000	40.8
E67	115.6	3.25	3.000	40.8
E65	77.0	3.25	3.000	27.1
E66	77.0	3.25	3.000	27.1
E68	77.0	3.25	3.000	27.1
E69	77.0	3.25	3.000	27.1

Results

A maximum deflection of .589" occurred at the point of application of the engine loads. The maximum von Mises stress was 68.7 ksi which is below the yield strength of 75 ksi. As with the Stage 1 mount, many members are subjected to high compressive loads. However, none of the members failed due to buckling. The maximum compressive force on a particular member was 79,000 lb.. Its critical buckling load is 187,700 lb. which is significantly higher.

Conclusion

The Stage 2 Engine Mount has been designed to carry a 210,000 lb thrust with a 1.25 factor of safety. Failure due to yield and buckling was considered in the design of the structure. The final mount weighs 646 lb. and its tubular A333 steel truss structure was designed to be easily manufactured at a low cost.

7.5.3 Stage 3 Support Structure

The Stage 3 support structure has two primary functions. First, it supports stage 3 in the early stages of the mission and second, it connects the RL-10 engine to the stage 3 spherical fuel tanks. Figure 7.48 shows the support structure and engine mount together.

During stage 1 and stage 2 burn, the structure acts as a support, carrying the

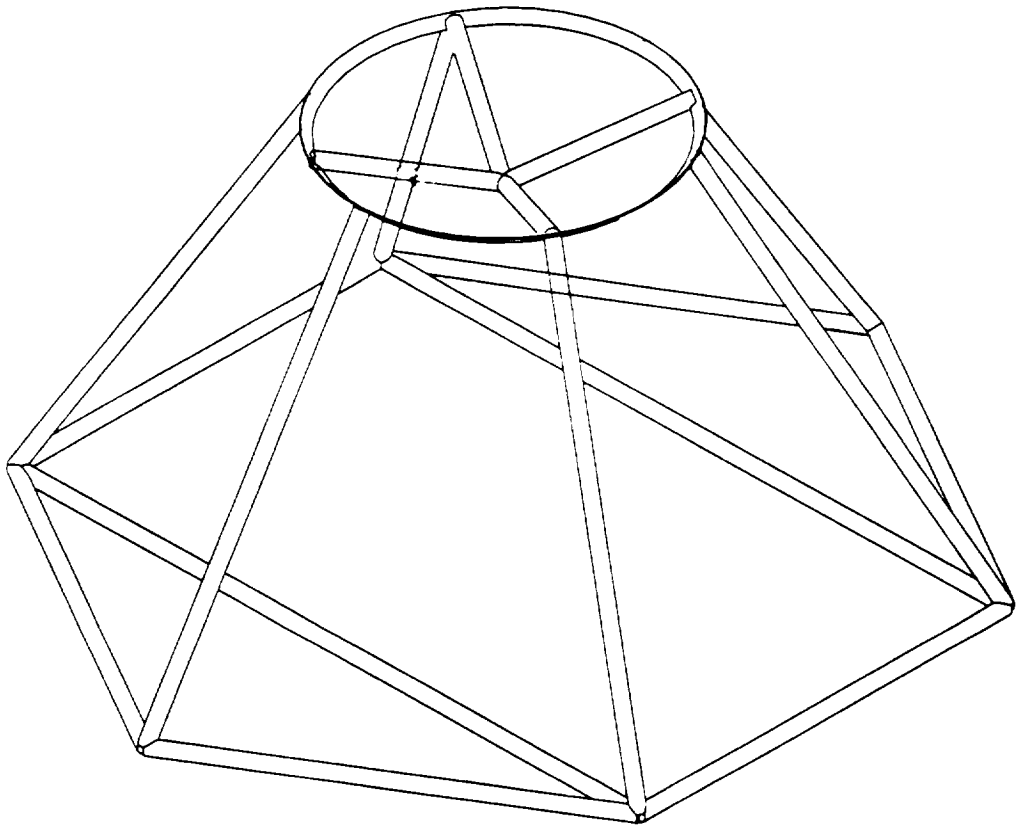

Figure 7.48 Stage 3 Support Structure and Engine Attach

17,400 lb stage 3 under acceleration loads of up to 5 g's. After stages 1 and 2 burn out, the engine attach transmits 20,000 lb. of thrust from the RL-10 engine to the load carrying fuel tanks. The support structure is a tubular aluminum truss with a total weight of 234 lb.. Aluminum provides a high strength to weight ratio and an acceptable stiffness for
this application. The Stage 3 structure has a height of 90" in order to accommodate the RL-10 nozzle inside it, and its sides slope from a diameter of 180" where it connects with stage 2, to a 72" diameter at the fuel tank interface ring.

Loads - Support Structure

During flight, the support structure must withstand a 17,400 lb load at 5 g's. This weight includes 8,900 lb. in fuel tanks and fuel, 8,000 lb. of payload, and 500 lb. of avionics and mission support equipment. The total load on the structure is 108,750 lb. when a 1.25 factor of safety is employed.

Modeling - Support Structure

A beam model of the support structure is shown in Figure 7.49. As in previous models, these vertical members represent the longitudinal stringers of stage 2. The compressive load due to the mass of stage 3 components is applied as a point load distributed evenly with rigid elements at the top of the model. The dimensions and weights of each beam element is tabulated in Table 7.16 with reference to the element labels in Figure 7.49.

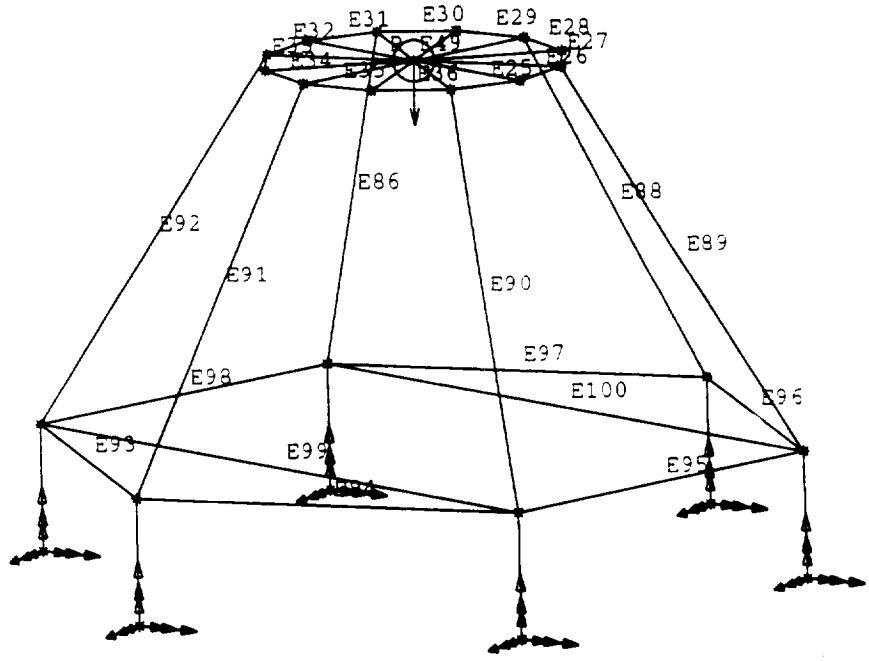

Figure 7.49 Stage 3 Support Structure Finite Element Model

Table 7.16 Dimensions and Weights for Stage 3 Support Structure

Element	Length (in)	Outer Dia (in)	Inner Dia (in)	Weight (lb.)
E25-E36	226.2	height = 3	thickness = .25	16.9
E86	100.4	3.25	3.0	12.2
E88	100.4	3.25	3.0	12.2
E89	100.4	3.25	3.0	12.2
E90	100.4	3.25	3.0	12.2
E91	100.4	3.25	3.0	12.2
E92	100.4	3.25	3.0	12.2
E93	93.0	3.25	3.0	11.3
E94	93.0	3.25	3.0	11.3
E96	93.0	3.25	3.0	11.3
E97	93.0	3.25	3.0	11.3
E95	93.0	3.25	3.0	11.3
E98	93.0	3.25	3.0	11.3
E99	161.0	3.25	3.0	19.6
E100	161.0	3.25	3.0	19.6

Results - Support Structure

The deflection of the support structure is shown in Figure 7.50. The maximum deflection occurred at the top ring and had a value of .373". The maximum value of von Mises stress was 24 ksi, well below the yield strength of most aluminum alloys. Further optimization was prevented by the desire for stability of the structure and the desire to minimize displacements. The buckling loads of the support structure were analyzed, but did not play a role in its design.

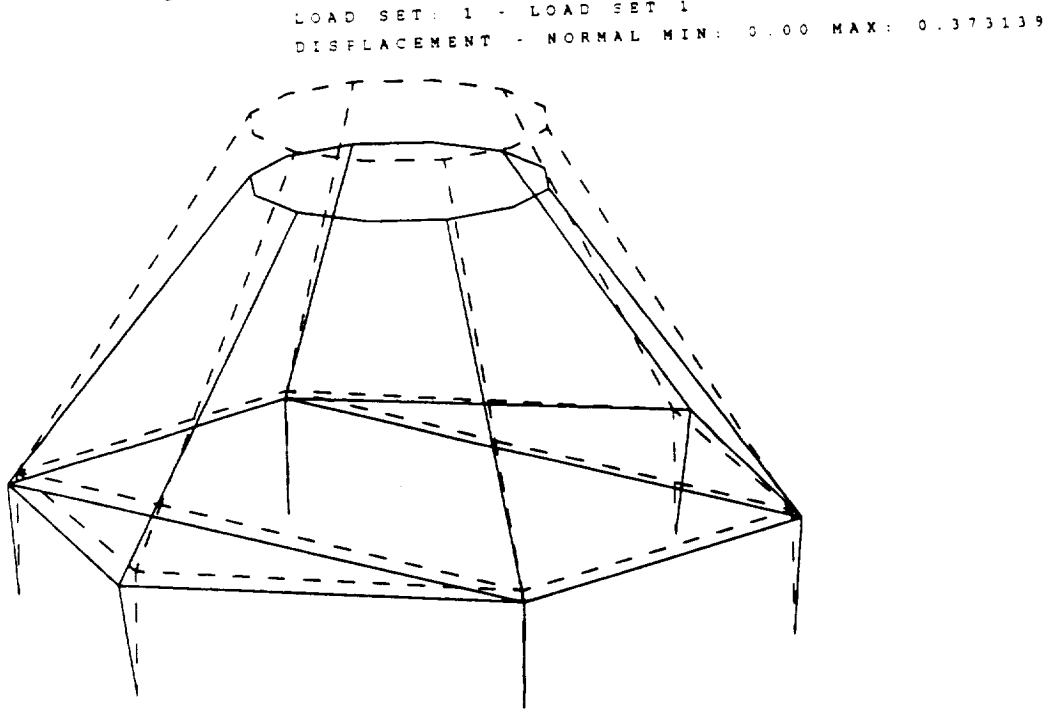

Figure 7.50 Stage 3 Support Structure Deformed Geometry Plot

Loads - Engine Attach

Since the engine attach is supported directly by the support structure, it does not carry any acceleration loads. However, once stage 3 ignites, the engine attach transmits 20,000 lb. of thrust from the RL-10 engine to a fuel tank. With a factor of safety of 1.25, this translates into a 25,000 lb load for the attach structure.

Modeling - Engine Attach

The engine attach was analyzed with the basic beam model shown in Figure 7.51.

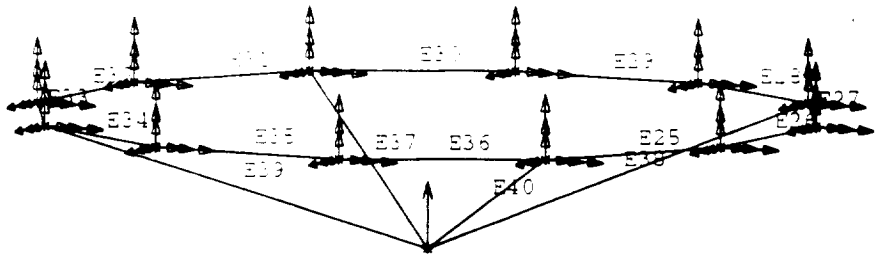

Figure 7.51 Stage 3 Engine Attach Finite Element Model

Because the engine attach structure is rigidly connected to the fuel tank, it was assumed that clamped conditions exist at this connection. In actuality, the RL-10 has a 3" diameter attach ring which connects at this point. Each member is 37.9" long, has an outer diameter of 3.25", and an inner diameter of 2.875". The load was applied at the vertex of the four main supports.

Results

The maximum deflection of the structure was .311". The maximum von Mises stress was 38,110 psi, which is well within the yield strength of aluminum alloys. Buckling did not occur in any member.

Conclusions

The Stage 3 Support Structure and Engine Attach must withstand two separate load cases. During stage 1 and 2 burn, the support structure must withstand 108,000 lb. of load caused by accelerating the stage 3 fuel tanks and payload at 5.0 g's with a 1.25 factor of safety. When stage 3 ignites, the load transfers to the engine attach, which must withstand 25,000 lb. of thrust including a 1.25 factor of safety. The use of aluminum alloy results in a combined weight of only 234 lb. for the support structure and engine attach.

7.6 INTERSTAGE RINGS

Interstage rings are located at the top and bottom of each interstage. They are used to maintain the structural integrity of the stages and interstages by withstanding the

enormous loads imparted by the engines. These loads are on the order of 10^7. The rings must be considerably thicker than the interstages themselves because there are concentrated loads applied at these points.

The ring was designed to withstand all forces imparted to it using a factor of safety of 1.25. The following is a listing of its various dimensions:

- outer diameter of the ring is 15.50 feet
- inner diameter is 15.44 feet.
- height is 0.25 feet

To calculate the weight of the rings, the following equation was used.

$$W = \rho V \qquad \text{(Eq 7.50)}$$

where W is the weight in lb_m, ρ is the density of the material (aluminum) given in lb_m/in^3 and V is the volume of the ring given in in^3. See Table 7.2.9 for values of weight, density and volume used.

To analyze these rings the following theoretical equations were used. In doing the analysis it was assumed that to find the number of bolts to withstand the shear, the bolt material and diameter were needed. A standard bolt diameter of 1/2" was used and it was assumed these would be steel. For a steel bolt τ approx. 80,000 psi. To calculate the loading on these bolts the point of maximum force due to the trajectory was used.

$$\tau = \frac{4P}{b\pi d^2} \qquad \text{(Eq 7.51)}$$

where τ is the shear force of the material, P is the total force acting on bolts, b is the total number of bolts needed, d is the diameter of the bolt and πd^2 is the area of bolt upon which the force acts. The minimum number of bolts needed for structural stability was calculated to be 96 from Equation 7.51, but for aerodynamic considerations 120 bolts will be used.

To prevent the bolts from shearing through the Aluminum ring, a shear analysis had to be done. The shear force (τ) equals 39,000 psi. The theoretical equation for this is given in Eq 7.52.

$$\tau_{max} = \frac{3P}{2x_{min}tb} \qquad \text{(Eq 7.52)}$$

where x is the ring height across which the shear acts and t is the thickness of the ring. This equation was used to determine the minimum ring height needed for the ring with a factor of safety of 1.25, so it would not shear when loaded. It is therefore evident, that to find the minimum ring height, the maximum shear must be used.

$$x_{min} = \frac{3P}{2t\tau_{max}b} \qquad \text{(Eq 7.53)}$$

The total force acting through the bolts is given by:

$$P = F + T \qquad \text{(Eq 7.54)}$$

F is the force due to bending and T is the force due to engine thrust. This value of P was then multiplied by the factor of safety of 1.25. The force due to bending is given by:

$$F = \frac{My}{I} A \qquad \text{(Eq 7.55)}$$

To find the maximum bending force that the rings will have to support, M_{max} was taken from the moment diagram which is shown in Appendix F.2 and Figure F.3. The variable y is maximum at the outside radius of the Gryphon interstage. In this case I is the area moment of inertia for the interstages and the stages which came from the finite element analysis. Table 7.17 shows the values attained using given data and equations 7.50 to 7.55. In the final calculation of the weight the volume of aluminum rings and steel bolts were combined to come up with the total weight.

Table 7.17 Stage and Interstage Ring Values for Gryphon.

Total:	$F = 400000\ lb_f$
including 1.25 F.S.	$T = 900000\ lb_f$
	$P = 1499583\ lb_f$
	$x_{min} = 1.28$ in
	$V = 656.05\ in^3$
	$\rho_{Alum} = 0.1\ lb_m/in^3$
	$\rho_{Steel} = 0.3\ lb_m/in^3$
	$W = 83.28\ lb_m$

The thickness of the rings was chosen to be 3/8" thick because it is less expensive and easier to manufactured than thicker material.

According to the analysis done, all of these rings willbe able to withstand any loads that could be imparted to them throughout the course of the mission. These forces include lateral, longitudinal and body forces.

7.7 CONCLUSION/FUTURE WORK

Each component discussed in the preceding chapters has been analyzed well beyond the Phase I stage. Secondary structural components still need to be explored such as tank attach structures, the Aft Nozzle Cover, hardware mounts for the avionics area, and access panels in the shroud and interstages. Many of the finite element models used in the above sections require refinement with updated loads and acceleration values based on later trajectory data. All components were designed with the goal of having the lowest cost for the maximum performance. For the most part, this included the use of ordinary materials even when higher performance could have been gained from advanced materials technology. If weight becomes a problem on the vehicle, the use of

titanium may be considered for highly stressed bulky components such as the strut and plane attach rings. However, these preliminary results should be sufficient to decide upon the feasibility of the Gryphon structurally. Design is an iterative process, and by no means are any of the above components ready for flight testing. However, each component has had enough analysis and design to give a basic idea for how the Gryphon would fit together if the project proves to be practical.

POWER/THERMAL ATTITUDE CONTROL

Chapter Eight

8.1 INTRODUCTION

This chapter begins with a discussion of the attitude control systems used to guide the Gryphon through the duration of its flight trajectory. The electrical power system is detailed in Section 8.3. The elements that provide thermal protection to the Gryphon are explained in Section 8.4. The chapter concludes with a discussion of the venting system that is used to regulate the cleanliness and pressurization of the payload bay.

8.2 THE ATTITUDE CONTROL SYSTEM

The Gryphon, similar to all spacecraft, will experience some form of disturbance torques. During the mission, disturbance torques will appear due to separation forces, aerodynamic forces, gravity gradient during coast periods, or misalignment because the thrust vector of the main engines does not pass directly through the center of mass. Trajectory, velocity, and pointing corrections must be made by using some type of reaction control system to counteract these disturbances. Additionally, Gryphon needs to deploy its payload with some angular velocity. To fulfill the requirements of attitude control and payload deployment, the Reaction Control System (RCS) will use thrust vectoring from the main rocket engines and an additional series of small thrusters (See Figure 8.1 on the next page).

8.2.1 Design Considerations & Selections

When choosing an RCS, several concerns were addressed. System selection was based on application requirements, minimizing cost, weight, and fuel, and demonstrating accuracy, reliability, and quick response time. After researching several reaction control techniques, thrust vectoring and Hydrazine thrusters were selected.

Of all the systems investigated, cold gas thrusters were the heaviest and provided insufficient thrust. The increase in performance characteristics of other systems such as cryogenics or bipropellant systems was negated by added complexity and increased cost. Hydrazine thrusters showed excellent reliability, good operation characteristics, and offer

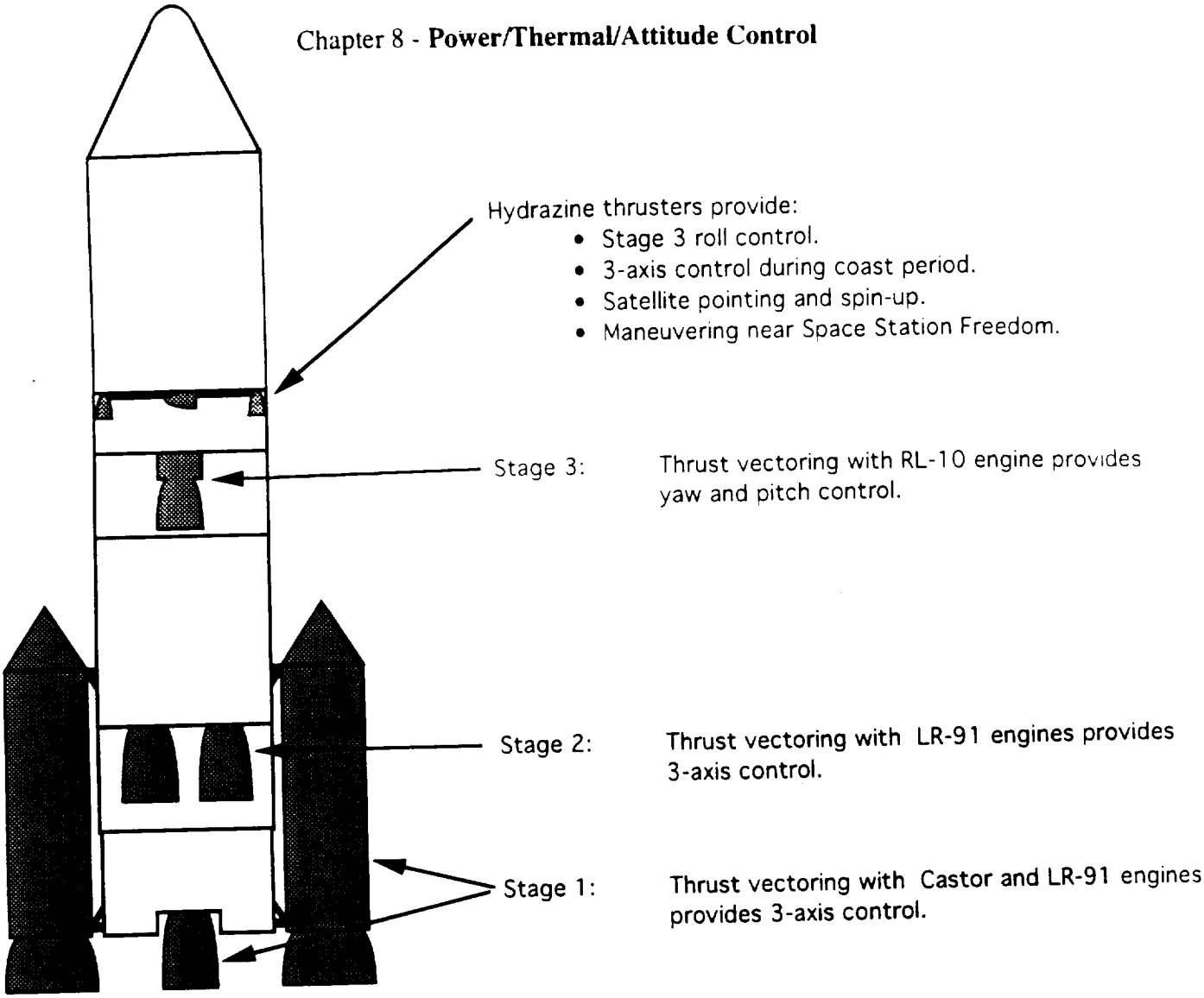

Figure 8.1: The Gryphon's Attitude Control System

simplicity for a low cost and moderately low weight. Table 8.1 summarizes some basic characteristics of Hydrazine.

Table 8.1 Hydrazine Characteristics

Formula	Molecular Weight	Specific Gravity	Boiling Point	Heat of Formation	Mixing Ratio
N_2H_4	32.05	1.008	235.9°F	21600 Btu/lb-mole	0.75

8.2.2 Attitude Control During Free Fall

Because of the danger of an explosion when the first stage main engines are ignited, the booster must be at least a half mile (2640 ft) from the airplane before ignition can occur (see Section 2.4). The plane carries out a simultaneous bank and climb maneuver directly after the release of the booster. Thus, to ensure the half-mile separation distance, the Gryphon must drop through a vertical distance of 1188 ft for the Low Earth Orbit (LEO) configuration (1258 ft for the Geosynchronous Transfer Orbit (GTO) configuration). The Mission Analysis group determined that a vertical tail will provide the required control in the yaw direction (see Chapter 3). This section details the systems that will be used to control the booster pitch and roll attitudes.

During the free fall period, which lasts approximately 8.5 seconds, the booster pitches up 20 degrees to allow the main engines to propel the booster into the correct trajectory after ignition. A detailed aerodynamic analysis showed that this pitch-up maneuver can be satisfactorily accomplished by using the aerodynamic forces that naturally result from the free fall. The maneuver calls for the separation of the Aft Nozzle Cover (ANC) from the booster as soon as enough clearance exists between the booster and the plane. For LEO and GTO configurations, this occurs approximately 2.25 seconds after release at an absolute distance of 261 ft from the plane. The separation of the ANC shifts the booster's center of pressure forward nearly 10 ft, greatly increasing the aerodynamic pitch-up moments that result from the booster's downward velocity.

A detailed analysis of the aerodynamic forces and the resulting motion of the booster showed that after 8.5 seconds and the vertical drop distances mentioned in the above paragraph, the booster is pitched at the correct 20 degree inclination from horizontal. The vertical drop distances mentioned above are greater than those required for the minimum half-mile separation distance. This additional drop distance was required in order to complete the pitch-up maneuver. As a point of future study, the addition of small canards or a wing to the booster could increase the pitch-up moments and reduce the vertical drop distance to the optimum value of 1056 ft. This increased altitude at first stage ignition would have to be compared to the cost and weight penalty that would be incurred through the addition of these control surfaces.

In order to analyze the pitch-up maneuver, the differential equations that govern the booster's motion during the free fall were derived. These equations were dependent on the aerodynamic forces on the booster, which in turn were dependent on the booster's velocity. To solve these differential equations, the free fall drop time was divided into small time intervals during which the forces and moments on the booster were assumed to be constant. These forces and moments were then translated into corresponding linear and angular accelerations using Newton's Second Law. By integrating the accelerations over the small time interval, the change in the booster's position and orientation over the interval could be determined. Thus, the position and orientation of the booster at the beginning of the next time interval was known, and the process was repeated to find new forces, accelerations, and orientations. In addition, the moments generated by thrust vectoring of the first stage main engines were incorporated to determine if they were capable of regaining control of the booster's attitude and pitch rate after ignition. The above method was implemented using a Microsoft Excel Spreadsheet. It was extended through the duration of the free fall so that the position and attitude of the booster was found for every 0.25 second interval. See Appendix G for a complete discussion of this method.

The optimal pitch angles and sequence of events that were found for the free fall using the above method are shown for the two booster configurations in Figure 8.2

below. As was mentioned above, the ANC separates from the Gryphon 2.25 seconds after release from the plane. The immediate increase in the booster's pitch angle that results from this separation is evident. The first stage main engines ignite at 8.5 seconds, when the booster reaches the required 20 degree pitch angle. The analysis showed that the engines were capable of regaining control of the booster's attitude and pitch rate, and that full recovery (zero angular velocity) occurred at 14.25 seconds. The plot shows that the final recovery angle for the LEO configuration (84 degrees from horizontal) is higher than that for the GTO configuration (62 degrees from horizontal). Because the center of mass for the LEO booster is closer to the base of the rocket, the moment arm of the aerodynamic forces is greater for this configuration. The resulting increase in the aerodynamic pitch-up moments on the booster cause the increase in the final recovery angle.

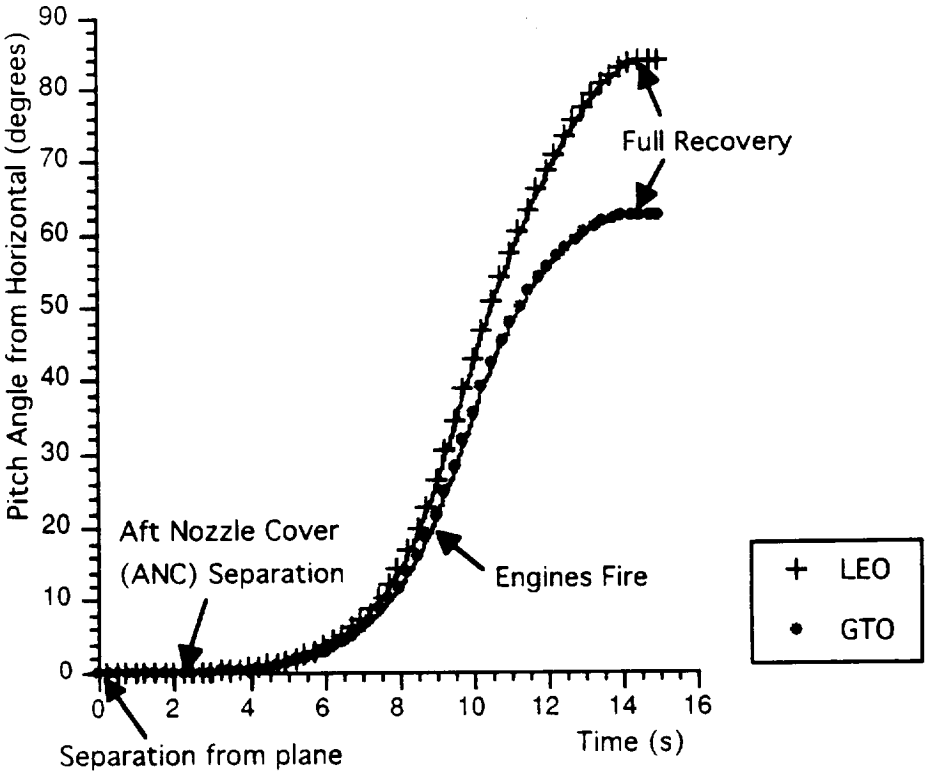

Figure 8.2 Pitch Angle vs. Time During Freefall

Preliminary analysis also showed that the Hydrazine thrusters have sufficient thrust (100 lb) to provide control in the roll direction for the third stage. Natural aerodynamic conditions aid in creating stability in the roll direction (see Figure 8.3 below). As the booster falls through the atmosphere, deviations in roll from the nominal attitude create an aerodynamic condition in which correcting moments are applied to the booster. These moments, when added to those generated by the Hydrazine thrusters, will provide the required angular accelerations to bring the booster back to the nominal attitude.

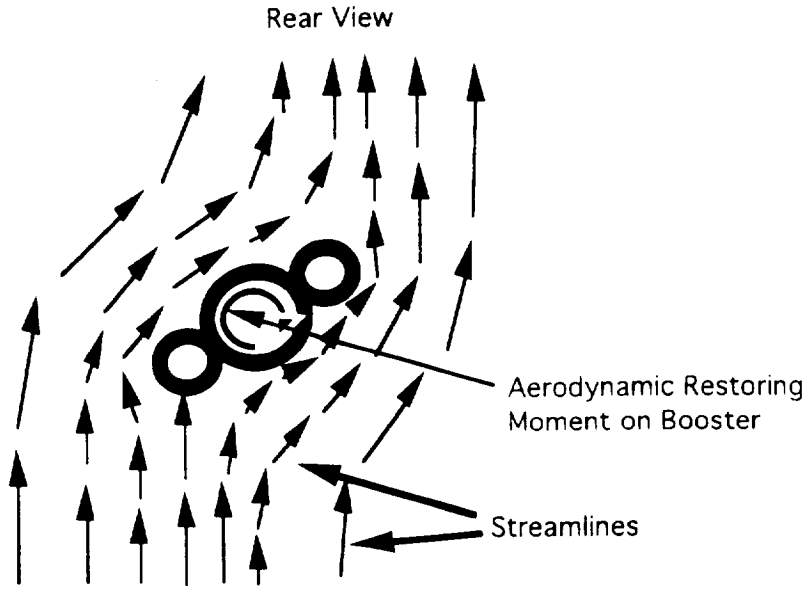

Figure 8.3: Aerodynamic Roll Moment Induced on Deflected Booster During Free Fall

8.2.3 Attitude Control During Stages

The engines selected for each of the three stages possess thrust vectoring capability. Thrust Vector Control (TVC) provides attitude control and trajectory correction around the pitch and yaw axes. Also, it can provide roll control if more than one engine is used. By using the nozzle gimballing capability of the engines, the system complexity is minimized, while only increasing fuel consumption by 3%. Stage 1 and Stage 2 both use multiple engines whose nozzles gimbal up to 4 degrees. Stage 3 uses only one engine; therefore, roll control must be provided by the hydrazine thrusters located above the avionics bay. The guidance system will provide information about attitude, and will indicate whether or not TVC is needed. The main rocket nozzles will then respond by gimballing for a specific amount of time. They will be actuated hydraulically since other systems such as electromechanical actuation does not provide enough power.

8.2.4 Hydrazine Thrusters

The Reaction Control from the Hydrazine thrusters serve four main functions. These include:

- Spin/Despin for payload deployment, or maneuvering at Space Station Freedom
- Attitude corrections during all coast periods
- Roll control on stage 3
- Reorientation before entering GTO

The MR-104 Hydrazine thrusters, manufactured by the Rocket Research Company, will be located immediately above the avionics section, and attach to the payload interface ring. The tanks for the fuel and oxidizer will be located in the avionics

bay. Two thrusters will be placed on each of the three axes: yaw, pitch and roll. Typically, the two thrusters should be placed an equal distance around the center of gravity (CG). This is done to limit the imparted load to only pure rotational momentum. Also, the thrusters should be placed as far away from the CG as possible to increase the torque, thereby minimizing the required thrust.

The tanks will be made from stainless steel 347. The oxidizer and fuel weight will equal 450 lb. This will compensate for payload deployment, coast attitude control, roll control, and any unforeseen emergencies. We approximated the time of use based on a twenty-four hour mission. The Appendix G contains the calculations and formulas used to obtain these numbers.

Currently, the Gryphon's configuration is not realistically capable of using the thrusters as a redundant system for thrust vectoring of the three stages. This is due to the limited amount of Hydrazine fuel available to accomplish this task. Future redesign would allow for enough fuel to take advantage of this possiblity for control.

8.2.5 MR-104 Characteristics

The Rocket Research Company produces the Hydrazine (N_2H_4) thrusters which were chosen for the Gryphon. They use gaseous nitrogen as the oxidizer, and decompose using a Shell 405 catalytic bed. It does not require ablative materials, since the nozzles are cooled radiatively. Table 8.2 summarizes some of the characteristics of the MR -104.

Table 8.2 MR-104 Characteristics

Dry Mass	Length	Diameter	Thrust	Nozzle length	cooling	Specific Impulse	Total impulse
0.1274 slugs	18.11 in	5.984 in	100 lb	7.008 in	radiative	228-239 s	156 X 10^3 lb-s

Listed below is typical operation sequence of a Hydrazine thruster:

- a dead zone is set, which means that the thrusters are not required until a specific angle is passed
- after interpreting information received from the guidance system, the attitude control system indicates the need for the thrusters
- a 30W single seat electric-solenoid valve opens, and Hydrazine flows for a specific amount of time
- the thrust output of the thruster varies as a function of the tank pressure; therefore, the tank pressure changes depending on the thrust requirement
- the pressure forces the propellant into an injector, and then enters the chamber and comes in contact with the Shell 405 catalyst beds
- the catalyst beds act to decompose the Hydrazine into NH_3, H_2 and N_2
- the decomposition products then exit the catalyst beds, and chamber through an exhaust nozzle which produces thrust

8.3 POWER SYSTEM

The on-board power systems are broken into two major sub-systems--the principal system and the ignition system. The principal power sub-system supplies power to the on-board systems (such as the computer and communications equipment), while the ignition power sub-system supplies power to the engines for startup. The principal power sub-system will be made up of long lasting (low rate) lithium thionyl chloride ($Li/SOCl_2$) primary cells, while the ignition sub-system will consist of short lived (high rate) silver zinc batteries.

8.3.1 Principal Power Sub-System

The principal power sub-system will consist of lithium thionyl chloride batteries. This type of primary battery (non-rechargeable) is available off-the-shelf and is packaged in individual cells, each of which operates at a specific voltage and contains a fraction of the required power. To find a suitable sub-system, it was necessary to examine the power requirements of all the Gryphon's on-board systems (see Section 8.3.2). It was determined from this information that $Li/SOCl_2$ cells with an energy density of 642 W-h/kg and an open circuit voltage of 3.63 volts would be the most sufficient principal power sub-system to use. They optimize the power system performance, while minimizing the cost and weight of the overall system. This sub-system will consist of four modules, each containing 8 cells, and providing operational power to the Gryphon for 24 hours.

Table 8.3 Power Requirements of On-Board Systems

Components	Power (W)
Flight Computer	250
GPS Receiver	3.5
Telemetry Transmitter (x2)	98
Radar Transponder	31
Communications	323
Thrusters	200
Inertial Receivers	200
Misc.	250
TOTAL	1356

Note: Misc. includes pumps, values, and other small devices which will require electrical power.

8.3.2 Sizing of Principal Power Sub-System

To determine the size of the battery system, an in-depth study of the power requirements of the Gryphon was performed. First, for each on-board sub-system, the maximum power requirements were examined. As shown in Table 8.3, a total of 1356 Watts (W), excluding the ignition power, was required during full operation of the Gryphon. To ensure that the Gryphon could operate under any electrically "stressful" situation, the total power requirement was then increased by 71.5% to 2325 W. This large increase in

the power only marginally increases the cost of the overall system, while ensuring safe operation of the Gryphon at all times. Also, this power increase will give the Gryphon extra time to deliver its payload to the required orbit in the event that problems occur.

The next factor that was considered was the mission time. For resupply of Space Station Freedom, the Gryphon would only need to be operational for 1-2 hours. However, for placement of satellites into Geosynchronous Earth Orbit (GEO), the Gryphon would need to be operational for 17 hours (for two satellites). This presented a problem, because it was unclear if there should be two separate battery configurations, one for each type of mission, or one configuration, which would supply enough power for both types of missions. The final decision was based on several factors:

- When resupplying the space station, extra power would need to be supplied to the payload. This power requirement would be highly dependent on the contents of the resupply payload, and therefore would vary from mission to mission.
- If the Gryphon either missed the space station, or the proper place in GEO, it must cycle around for another attempt. Both of these cases would require the Gryphon to remain in orbit for additional time. During this time, only minimal power would be needed.
- A margin of safety of at least 4 hours is needed to ensure that any delays during orbit do not jeopardize the mission.
- Since there is a relatively low overall power requirement, the effects on monetary cost of supplying more power are minimal, when compared to the major monetary costs of the Gryphon.
- Having two separate battery configurations will add complications to the assembly process and increase the possibility of errors.

Based on the above facts, planning for a 24-hour mission would ensure the success of each type of Gryphon mission. For the 1-2 hour re-supply mission, the extra power that the batteries have stored can be used for the payload power requirements. For the 17-hour satellite missions, necessary power will be supplied while maintaining a satisfactory margin of safety. Also, there will be enough power to keep the Gryphon functional if the orbital target is missed. The battery system will need to supply a nominal 2325 W for 24 hours, a total of 55,800 Watt-hours (W-h) of energy. Another factor involved in sizing the system is its operating voltage, which will be a standard 28 volts DC for the Gryphon. At each sub-system which requires power, there will a power converter. A power converter is used to step-up or step-down the voltage to meet the component's requirements.

In order to meet all of these requirements, a lithium thionyl chloride battery system configuration was chosen. The configuration consists of 32 $Li/SOCl_2$ cells, each containing 1798 W-h of energy and each operating at 3.63 volts. The 32 cells will be broken up into four 8 cell modules (see Figure 8.4 on the next page) which are connected in parallel for an operating voltage of 29.04 volts. This voltage will be dropped to 28 volts before the battery system is connected to the various components.

This system will supply 57,524 W-h of energy over a 24-hour period, an increase of 1724 W over our requirement, at an operating voltage of 29.04 volts.

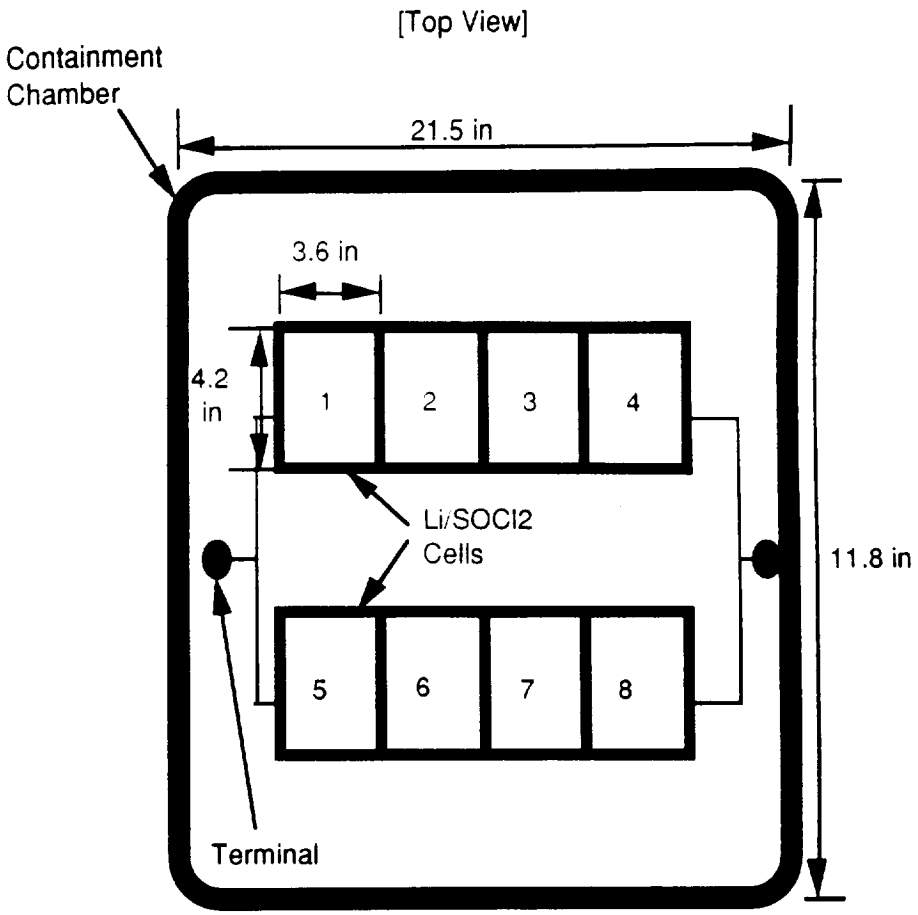

Figure 8.4 Layout of Battery Containment Modules

8.3.3 Cost and Weight of Principal Power Sub-System

A space-qualified system such as the one described above will cost approximately $3000. This information was gathered by contacting lithium battery manufactures such as Eagle-Picher and Honeywell Inc. The weight of the system, which was based on the battery and the accompanying equipment, is 250 lb.

8.3.4 Concerns of Principal Power Sub-System

For preservation, the lithium thionyl chloride batteries must be stored between 14° and 50°F. If this is done, they will still contain approximately 97% of their original power after five years. During operation, the batteries must be maintained between -148° and 68°F. This is accomplished by the on-board thermal control sub-system, which is responsible for the temperature control in the avionics bay.

An additional concern is the operation of lithium batteries. First, when lithium batteries are over-discharged or experience voltage reversal, they may release vapors, which leads to large pressure buildups inside the individual battery cells. If this vapor is not properly vented, an explosion can result. In order to prevent this, special pressure

release values are installed on the cells, and diodes placed in the circuit. The diodes help prevent over-discharge and voltage reversal, while the release values ensure that if venting does occur an explosion will not occur. Since the primary battery system is located in the avionics bay, it is very important to assure that the lithium vapor from venting not be released directly into the bay. To facilitate this, each module, containing the 8 individual cells, will be self-contained in its own pressure chamber to prevent leakage of the vapors (See Figure 8.5).

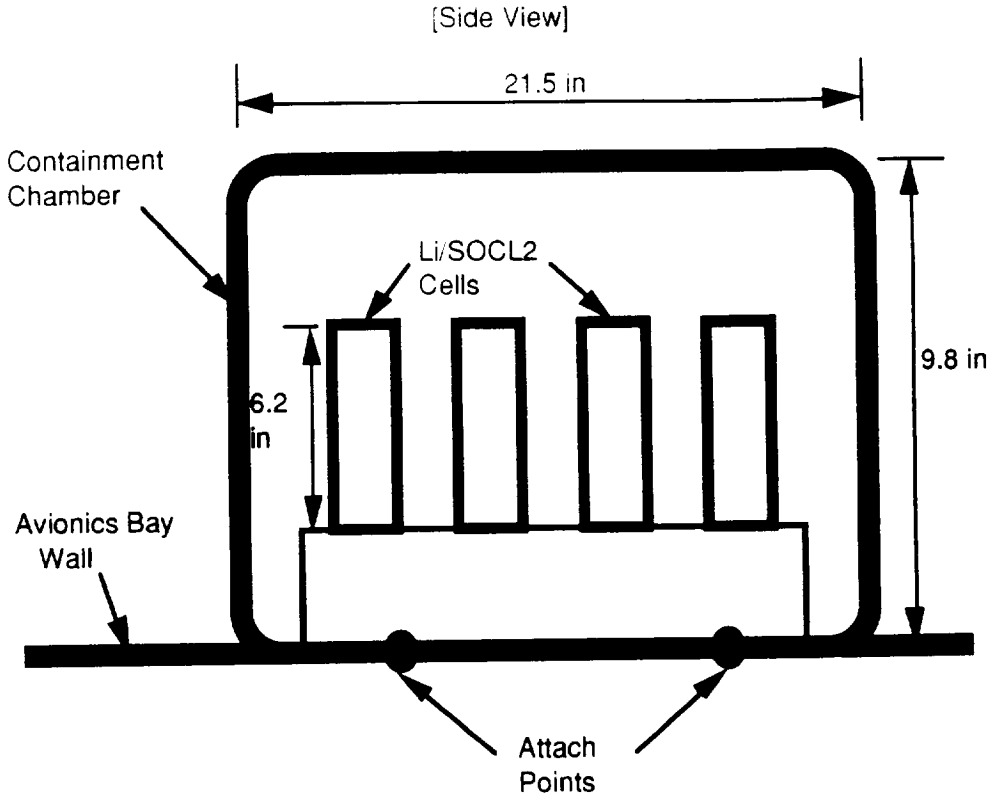

Figure 8.5 Layout of Containment Chamber

Another concern is the activation or startup of lithium batteries. After long storage periods (4-5 years), a layer of lithium chloride builds up on the surface of the lithium anode. This layer of buildup delays the cells from immediately reaching their operational voltage when a load is first applied to them. To prevent this from becoming a problem, the lithium anode will be coated, and an electrolyte additive will be used. This will allow full power-up within 10-15 minutes after initial activation of the system. Because of the 10-15 minutes needed to reach full power-up, it is of great importance that the power system on-board the Gryphon be activated at least 20 minutes before separation of the vehicle from the carrier aircraft.

It should be noted again that the cells will be contained in four separate modules. Therefore, if one module is destroyed by some type of collision, or if the cells in it vent, the other three modules will escape destruction. The other three modules will be capable

of supplying enough power to keep the Gryphon functional, and allow the payload to be deployed.

8.3.5 Ignition Power Sub-System

The rocket engines and the two solid rocket motors require 5 amps at 28 V DC applied for up to one second to achieve ignition. It is quite possible that this power surge of 140W could damage the principal power sub-system, and even cause the lithium cells to vent. Therefore, this short duration, high power requirement is met by a separate power system for the engines.

8.3.6 Sizing of Ignition Power Sub-System

The system will consist of three modules of silver zinc primary cells. Each module will be completely independent, and responsible for the ignition of all the rockets in each stage of the propulsion system. In order to meet the specifications of 5 amps at 28 V DC for one second, each module will need to contain 20 high rate silver zinc cells. Each of these cells contains 1.5 W-h of energy and operates at 1.4 volts. The result is that each module will supply 30 W-h of energy at 28 V DC, more than is needed to activate each stage.

8.3.7 Cost and Weight of Ignition Power Sub-System

This system will be extremely lightweight, and moderate in cost. The battery modules and support equipment (i.e. mountings) will weigh under 150 lb. The cost for space qualified batteries will be at most $1000.

8.3.8 Concerns of Ignition Power Sub-System

A major concern with the silver zinc batteries is their discharge characteristics. After being connected to a load, their discharge voltages can vary from 1.3 to 1.55 volts. However, this does not present a problem for the ignition system, because the rockets will activate provided a voltage between 22 and 31 V DC is applied. Therefore, even with fluctuations, the output voltage will still activate the engines.

8.3.9 External Power Connections to Gryphon

From the time that the Gryphon leaves the hangar, to the time it is dropped from the carrier aircraft, it must be supplied with power. Instead of having the on-board power system supply this power, there will be external power connections. For this, the Gryphon will be equipped with two external power ports, one for receiving power from a ground based source, and one for receiving power from an umbilical connection to the carrier aircraft. The Gryphon will need two separate ports so that it will be possible to change power sources without having to shut one off, thus interrupting the power supply to the on-board systems, while attaching the second. Power converters will be used to either step-up or step-down the incoming power to match the 28 volts that the on-board system will be maintaining.

8.3.10 Cabling, Wiring and Insulation

From an investigation of the power loss in the cabling (see Appendix G.3), it was determined that the losses would not be a factor. They are small enough, 0.5 W at most, that they can be ignored.

The wiring will be 2 gage, and will be made of standard annealed solid copper. This will provide a very low resistance conducting path for all of our electrical circuits. Since most of the wiring will be confined to the avionics bay, only 100 lb of wire will be required. All of the cabling that is on-board will be coated with space qualified insulation. This will adequately shield it from any radiation that it might encounter during the mission.

8.3.11 Power System Layout

The principal power sub-system will be located around the outside of the avionics bay, with the four 8-cell modules mounted on the inner payload support ring (see Figure in Chapter 2: Spacecraft Integration). The ignition power sub-system modules will be located on the main truss of the Gryphon, in a location central to the stage that it is igniting.

8.3.12 Future Work

From the final analysis of the Gryphon, it is evident that the inert weight in the third stage of the booster needs to be reduced. When the power sub-system was being designed, an effort was made to minimize weight, while still ensuring a rather large margin of safety. It was decided that a small weight penalty would be worth assuring that the batteries would work, and the Gryphon would be able to launch or correctly position its payload. Now that the final analysis results are available, it is clear that a more in-depth study needs to be done to determine how much the margin of safety can be reduced without endangering the Gryphon's mission. As future work, it is recommended that this be considered in order to cut as much weight as possible from the power systems, while keeping the Gryphon safe and functional.

8.4 THERMAL CONTROL SYSTEM

It is the goal of the thermal control system to keep all components within their specified temperature envelopes, while minimizing cost and weight, and maintaining reliability. The thermal control system for the Gryphon is concerned with two major areas. These areas are the external structure, and the avionics bay (See Figure 8.6). The external structure will use ablative coatings to provide thermal protection against aerodynamic heating during the ascent of the booster. The avionics bay will use a multi-component system, which includes a helium purge, a heat sink radiator, enamel coatings, and multilayer insulation. This system will maintain the temperatures of all the electronic equipment located in the avionics bay.

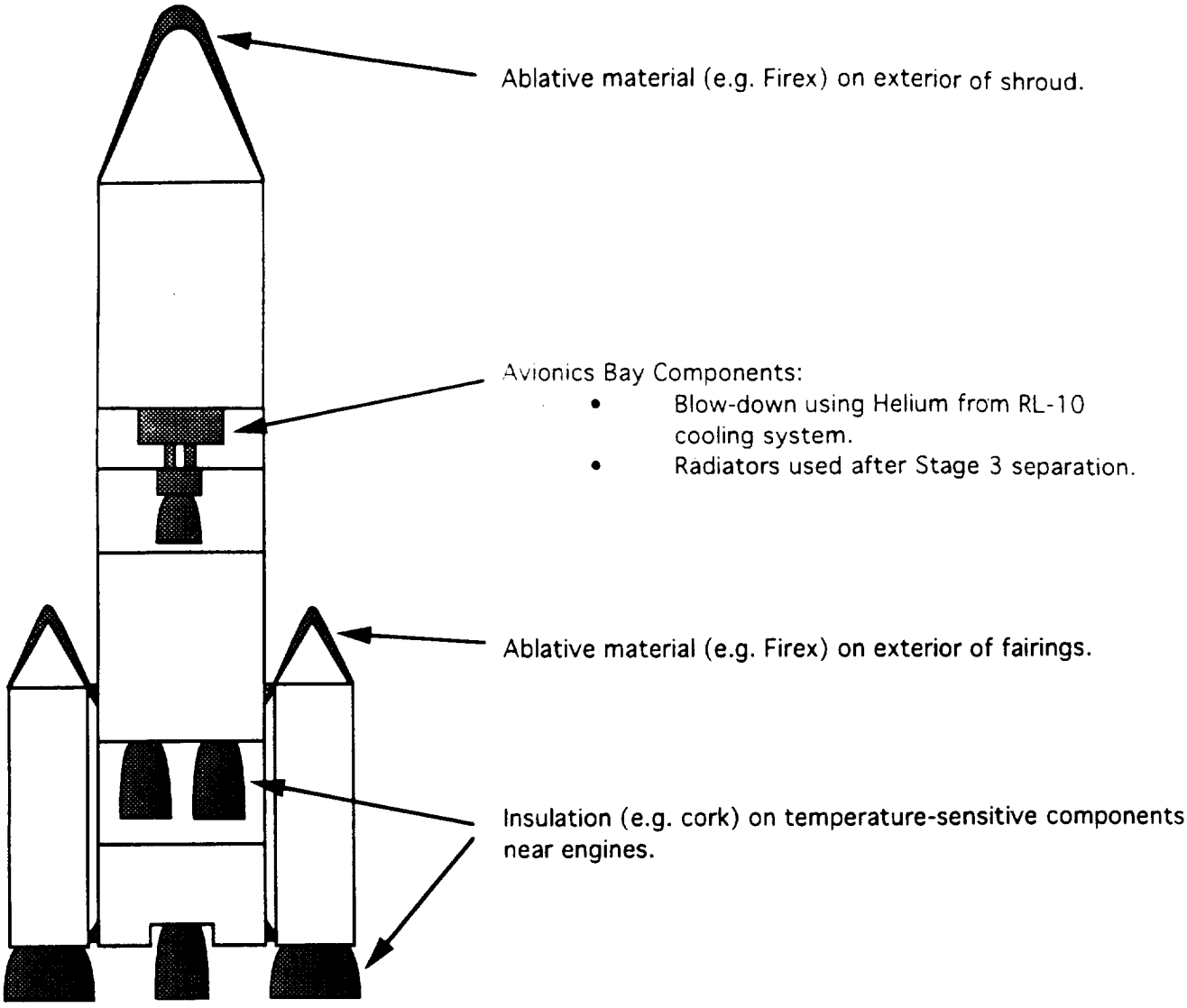

Figure 8.6: The Gryphon's Thermal Control System

8.4.1 Thermal Control of the External Structure

Because of hypersonic speeds during ascent, aerodynamic heating becomes an important factor in the design of the Gryphon. At speeds of Mach 8.0, temperatures of 4900°F are present on the booster. The composite material used for the external structure has a usable realm of up to 350°F. Therefore, ablative coatings will be applied to surfaces where high heat rates occur, to provide thermal protection. The ablative coatings that will be used for the Gryphon are Firex and Thermal-Lag. The major surfaces exposed to high heat rates have been identified as:

- the nose cone of the payload shroud
- the nose cones of the solid rocket boosters
- the leading edge of the vertical tail surfaces

A maximum thickness of 2.5 inches of ablative coating will be applied to the stagnation surfaces of each of the mentioned surfaces. The coating will then taper as the heat rates decrease along the body of the Gryphon.

Firex and Thermal-Lag are ablative coatings used on many space boosters. The coatings were chosen because they are relatively inexpensive, and they can be applied easily. Other types of ablative protection include silicate chin panels similar to those used by the Space Shuttle. Chin panels were not chosen because they must be integrated into the external structure of the booster. This integration would ultimately add cost and weight to the project.

8.4.2 Ablative Material Sizing

The thickness of the ablative material was based on the steady state heat conduction equation. The following assumptions were made in the sizing of the ablative material:

- The thermal conductivity of the ablative material used would equal the thermal conductivity of graphite
- The stagnation heat flow of the Gryphon would not change from the stagnation heat flow of Orbital Science Corporation's (OSC) Pegasus
- The nose cone of the Gryphon would be modeled as a sphere 16 feet in diameter
- The heat flow would take place for a period of 180 seconds
- The heat flow would be concentrated on 1/8 of the area of the sphere

The steady state heat transfer equation is :

$$q_H = \frac{0.5\pi\, r_0 r_1 (T_0 - T_1)(\Delta t)}{(r_0 - r_1)} \qquad \text{(Eq 8.1)}$$

Where:

q_H	=	58.6×10^3 Btu
k	=	1.16×10^{-5} Btu/s/(in-°R)
T_0	=	5400°R
T_1	=	809°R
r_1	=	96 in
Δt	=	180 sec

This leads to an outer radius of 98.5 inches, and implies an ablative coating thickness of 2.5 inches.

8.4.3 Thermal Control of the Avionics Bay

Spacecraft electronics typically have temperature limits from 0 to 80°F. The lithium thionyl chloride batteries must operate at temperatures below 100°F. Consequently, a thermal control system must be provided in the avionics bay. Thermal control of the avionics bay consists of a multi-fold system. The system includes: purging with helium, heat sink radiators, enamel coatings, and multilayer insulation. The system will be used

to maintain all electronic equipment located in the avionics bay within their specified temperature envelope.

Helium will be bled from the propulsion system, and purged through the avionics bay. The purge will take place until the payload shroud is deployed. The helium purge provides forced convective cooling of the flight computer, the batteries, and certain transmitters. The helium purge will also be available for use after the payload shroud is deployed, if the heat sink radiator fails. The decision to use helium for convective cooling was based on the needs of the propulsion system. The propulsion system's third stage rockets use helium to control the boil-off rates of the cryogenic fuels. A helium purge is considered a feasible option since it is an inert gas with similar heating characteristics as nitrogen (a commonly used purging gas). This option eliminates the need for two separate systems, and will help minimize the cost and weight of the Gryphon.

After the payload shroud is deployed, a heat sink radiator will provide cooling for the flight computer. The radiator has a surface area of 144 in^2, and is made of aluminum. Its outer surface will be coated with white enamel to improve radiative heat transfer effects. The radiator will increase the effective surface area for which the computer can dissipate heat, and has a fairly high emissivity so the heat will be dissipated into space. A heat sink radiator was chosen for two reasons. Since only a small amount of heat needs to be dissipated, the use of a large radiator system would be unwise. Also, a heat sink radiator is a passive system. Cooling with pumped, looped systems requires moving parts, and are much more complex. These types of systems add weight and cost to the project. The heat sink radiator was the best choice to provide cooling of the flight computer after the payload shroud is deployed.

Coatings will also be applied to critical components in the avionics bay. These coatings include white enamel and black paint, to increase or decrease the net radiative effectiveness. These coatings are simple devices that can be used to control the temperature passively, and will add little weight or cost to the project.

Finally, multilayer insulation will be used to protect important electrical boxes and the electrical wiring against any radiative heat transfer. The insulation will consist of alternate layers of aluminized Mylar and a coarse netting. Multilayer insulation was chosen because it is the primary kind of insulation used on most spacecraft.

8.4.4 Sizing of Heat Sink Radiators

The sizing of the radiators needed in the avionics bay is based on an area/temperature tradeoff. The steady state heat radiation equation was used to find the area needed to dissipate enough heat so the electrical equipment would have a desired surface temperature of 77°F. The following assumptions were made in the sizing of any radiator needed in the avionics bay:

- The heat generated by all electrical equipment would equal 50-80% of the power required to operate the equipment.
- All equipment can be coated with white enamel to increase the net radiative effectiveness.

The steady state heat radiation equation is then:

$$q_H = A\sigma_B\varepsilon\left(T_s^4 - T_o^4\right) \qquad \text{(Eq 8.2)}$$

Where:

q_H	=	The heat dissipated in Btus
A	=	The surface area in in^2
σ_b	=	The Stefan-Boltzmann Constant
ε	=	The emissivity of the object
T_s	=	The surface temperature in °R
T_o	=	The ambient temperature in °R

Table 8.4 shows that the flight computer is the only piece of equipment that produces a significant amount of heat for its area. Therefore, a radiator must be attached to the flight computer. A simple heat sink radiator will be used for cooling. The table also shows that some type of insulation is needed for the electrical wiring to protect against any radiative heat transfer.

Table 8.4 Heating of Electronic Equipment

Equipment	q_H (Btu/s)	T_S (°F)	Area (in^2)
Electrical Wiring	0.398	20	0.0521
Flight Computer	631	77	144
GPS Receivers	11.0	77	0.356
Telemetry Transmitters	155	77	19.0
Radar Transponders	98.0	77	13.0

8.5 VENTING SYSTEM

The venting system is composed of eight independently operating units. Design considerations included possible pressure differences, and cleanliness problems due to air exchange in the payload bay during the course of the mission. It was important for the design be as inexpensive, small, and lightweight as possible, while maintaining a degree of adaptability for the varying payloads. The final system design meets all these requirements, while requiring no power to function.

8.5.1 Pressure

To prevent unnecessary fluctuations in pressure, it is important the exchange of air be as controlled as possible. The Gryphon will experience pressure differences in the payload bay during the mission due to an air-tight design. This pressure must be relieved to prevent any damage to the payload, or the spacecraft itself. The two possible cases resulting in a pressure difference are: the internal pressure is greater than the external pressure resulting in the outflow of air from the vehicle, or the external pressure is greater than the internal pressure resulting in the inflow of air into the vehicle.

8.5.2 Cleanliness

To minimize possible contamination from the inflow air, the air must be filtered. When the pressure difference is such that there is an inflow of air, there is the possibility of payload contamination from dust or debris. This contamination must be reduced as much as possible to prevent damage to the payload during the mission.

8.5.3 Pressure Equalization and Filtration Unit

Figure 8.7 shows a conceptual drawing of a Pressure Equalization and Filtration Unit to be used on the Gryphon:

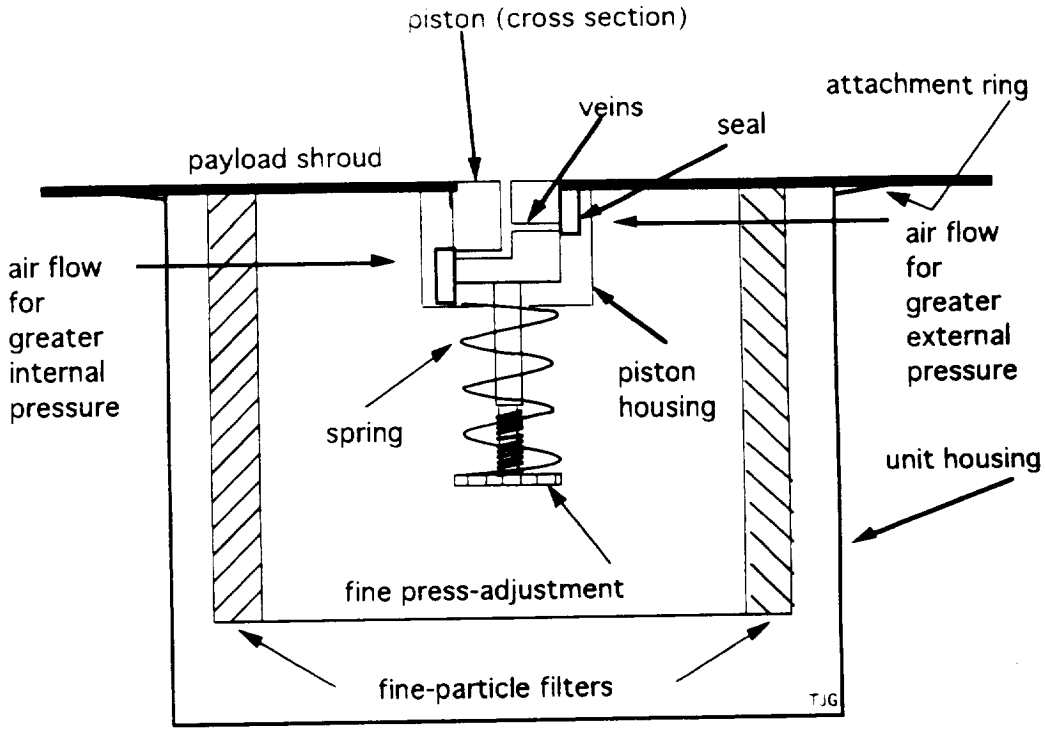

Figure 8.7 Conceptual Drawing of a Pressure Equalization and Filtration Unit

The piston has two functions: it acts as a switch to direct the air flow, and as a large-particle filter. While acting as a switch, the piston has three positions: *up* (left vein open, right vein closed), *down* (right vein open, left vein closed), or *neutral* (left and right veins closed). When the force due to pressure acting on the piston is greater internally, the piston moves upward. This allows the air to vent through the left vein and pass out, while the passage through the right vein remains blocked. Once the internal and external pressure difference reaches the critical point determined by the spring constant, the valve will move to the neutral position where no veins are open. If the external pressure exceeds the internal pressure, the piston moves to the down position. The air is allowed to enter and vent through the right vein, where it passes through the fine-particle filters and into the payload bay. Again, when the internal and external pressure difference reaches the critical point, the piston will move to the neutral position.

To control contamination, the piston acts as a filter by deflecting larger particles, such as pebbles from a runway, from entering. The fine-particle filter encloses the piston mechanism, and filters smaller incoming airborne elements, such as pollen or dust.

The dictating elements in the unit can be changed to suit individual payload requirements. For different payloads, the spring can be changed, and the spring tension adjusted, to provide a larger or smaller pressure difference. The fine-particle filter can be of different specifications depending on payload requirements.

8.5.4 Pressure Equalization and Filtration System

The venting system will consist of eight Pressure Equalization and Filtration units. Each unit operates independently to ensure that the total system will not fail in the event that one or more units fail. The units will be attached by an adherent, such as an epoxy, to the interior wall of the payload shroud. The eight units will be equally spaced around the payload shroud. The sizes, weights, and costs for the venting system are given in Table 8.5.

Table 8.5: Size, Weight, and Cost for the Venting System

	Unit	System (8 units)
Size (ft^3)	0.16	1.33
Weight (lb)	1.50	12.0
Cost ($)	100	800

AIRCRAFT INTEGRATION

Chapter Nine

9.1 INTRODUCTION

The Eclipse was specially designed by the Eclipse Design Team to act as the 'zero' stage of the Gryphon. In the same manner that booster stages must be interconnected in order for the system to function, the Gryphon must be physically and functionally attached to the Eclipse to capitalize on the air launched system. This is where Aircraft Integration performed several different duties during this design phase. The duties which affected the Aircraft Integration Group were as follows:

- Gryphon Assembly Building (GAB)
- Transportation and attachment of Completed Booster
- Physical attachment from Eclipse to Gryphon/Drop mechanism
- Fueling and Safety Concerns
- Power connections to the Eclipse in the Pre-Drop phase
- Placement of support systems on Eclipse

Aircraft Integration's concerns begin the moment any of the base components leave their manufacturing center and become the property of the launch company. Each component is received and constructed into a complete launch booster, and then mated with the payload. As the launch window approaches, the Gryphon is rolled out to the Eclipse, connected, and fueled. The Eclipse either uses its prime facility as its base of operations (for geosynchronous orbits), or flies to the secondary launch facility (for Polar orbits) by a series of 'hops'. When the launch criteria have been met, a technician on the Eclipse handles the release/launch phase.

9.2 GRYPHON ASSEMBLY BUILDING

The main requirements for the design of the GAB were determined to be the following.

- Provide facilities and equipment needed to assemble the Gryphon vehicle from its various sub-components
- Provide facilities and equipment needed to integrate payloads with the Gryphon

- Perform the above tasks at the rate of one completed Gryphon rolled out every two weeks

9.2.1 Assembly Schedule and Task Determination

The first step in the design process was to determine what work would need to be done at the GAB, and how long that work would take. With this information the building could then be sized correctly to support the required launch rate of one completed Gryphon every two weeks.

This step was done by basing the Gryphon's assembly schedule on the Pegasus's assembly schedule. Due to the much larger size and complexity of the Griffin's liquid fueled stages, as compared with the Pegasus, considerably longer times were assumed necessary for certain assembly steps. The following table compares the two assembly schedules.

Table 9.1 Pegasus/Gryphon Timeline Comparison

Step	Pegasus	Gryphon
Stage Build-up and Pre-Integration Testing	3 weeks	4 weeks
Stage Integration and Integrated Vehicle Testing	1 1/2 weeks	4 weeks
Payload Integration	1 week	2 weeks
Final Systems Tests	1 1/2 weeks	2 weeks
Total	7 weeks	12 weeks

The following sections describe the various tasks performed in the steps listed in Table 9.1.

Stage Build-up and Pre-Integration Testing

Stage build-up and pre-integration testing involves any work which must be done to the various stages, interstages, fairings etc. prior to their being assembled together into the Gryphon. All components of the vehicle will be delivered to the GAB in as close to final configuration as possible. This will minimize the amount of work which must be done during stage build-up. The components will also be delivered to the GAB at a time just prior to their being needed for assembly. This will eliminate the need for on-site storage facilities.

Stage Integration and Integrated Vehicle Testing

Stage integration and integrated vehicle testing involves the actual assembly of the various stages and interstages to form the Gryphon vehicle. Due to the large size and increased complexity of the Gryphon, four weeks were allowed for this step as opposed to one and one half weeks for the Pegasus.

Payload Integration

Payload integration involves connecting the payload with the payload interface. Typically, the Gryphon will launch two satellites whereas the Pegasus can only carry one. Consequently, two weeks were allowed for this step instead of one week for the Pegasus.

Final Systems Tests

Final Systems tests involve any last checks done to insure that the Gryphon is assembled correctly and will function properly when launched. Due to the increased size and complexity of the Gryphon two weeks were allowed for this step as opposed to one and a half weeks for the Pegasus.

9.2.2 Gryphon Assembly Building (GAB) Layout

The basic scheme for assembly of the Gryphon was based upon the method used for assembling the Pegasus. The Gryphon is assembled horizontally because it is attached to the Eclipse in a horizontal position. Rather than assemble the Gryphon on a fixed cradle and then lifting the entire booster onto a transportation trailer to carry it out to the Eclipse for attachment, it was decided to assemble the Gryphon directly on its trailer. This eliminates the need for a large crane capable of lifting the entire 500,000 lb weight of the vehicle and allows it to be moved easily from one area to another during assembly. The group decided that the Gryphon would be assembled using an assembly line approach where the vehicle moves from one station to the next. This will reduce the need to move equipment.

After considering several different building configurations, an assembly building with two parallel assembly lines was chosen. Two independent lines were chosen to allow greater flexibility in launch scheduling. If only one assembly line were used, launches could not be easily conducted in close succession. With two independent assembly lines, the assembly schedules could be staggered to provide one vehicle every two weeks, or two vehicles in close succession if launch windows require it. Having two independent assembly lines also allows for some protection from delays in any step in the assembly process. A problem on one line will not hold up production on the other line. Figure 9.1 on the following page shows the final configuration of the GAB.

9.2.3 The Gryphon Assembly Process

The various components are delivered to the GAB in the Stage Build-up Area and are unloaded using an overhead crane. Each assembly line is equipped with an 80 ton overhead crane that was sized at 80 tons to allow it to move the Castor 120 solid rocket boosters. These boosters weigh approximately 60 tons and are the heaviest component of the Gryphon.

Following completion in the Stage Build-up Area, the components are picked up with the 80 ton overhead crane and placed in position on the trailer in the Stage Integration area. This area of the GAB is equipped with a scaffolding system which can be pushed up close to the Gryphon being assembled to allow easier access to all areas of the booster. A cross sectional sketch of a possible scaffolding system is shown in Figure 9.2 This scaffold system is based on the scaffolding used during construction of the Ariane Launch Vehicle.

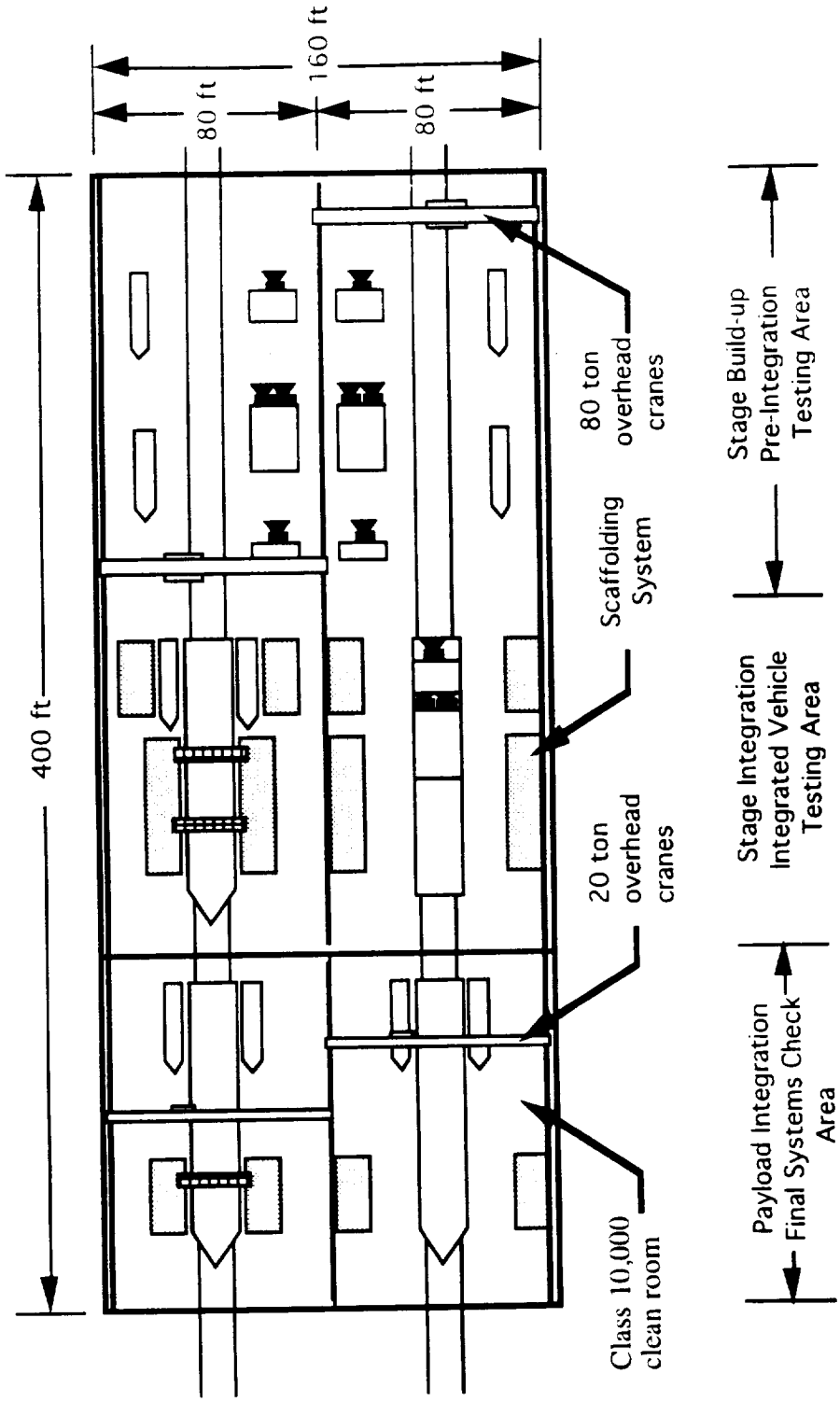

Figure 9.1 Gryphon Assembly Building Layout

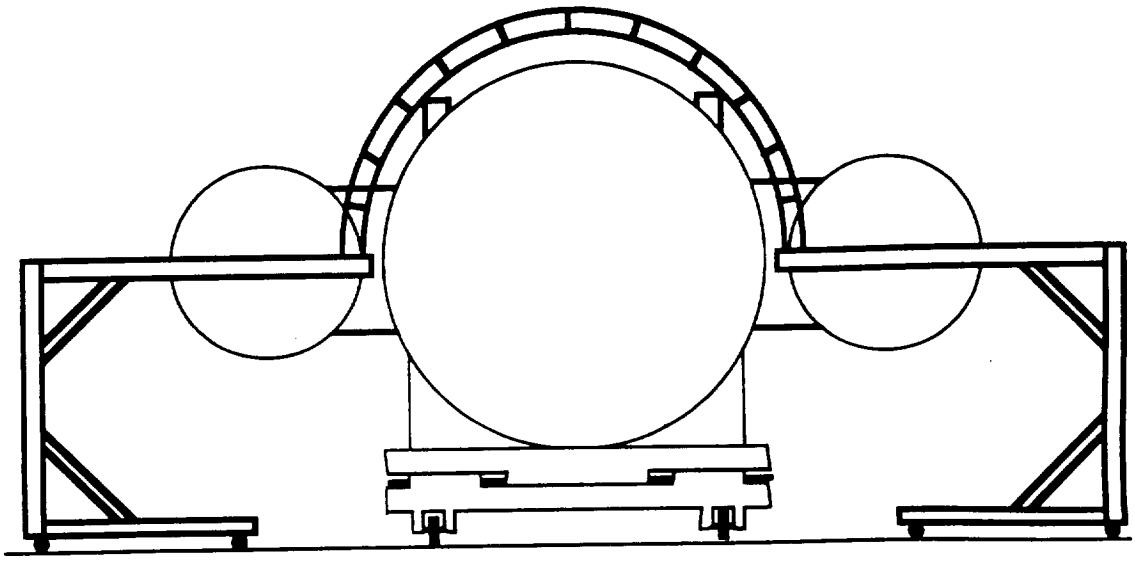

Figure 9.2 Gryphon Stage Integration Scaffolding

Following completion of Stage Integration and Integrated Vehicle Testing, the scaffolds are pushed back and the Gryphon is rolled on its trailer into the Payload Integration and Final Systems Check Area. In each line, this area is sealed off from the rest of the GAB and maintained at a class 10,000 clean room environment. This is necessary to protect the payloads from contamination prior to installation of the fairing. The Payload Integration area of each line is also equipped with a 20 ton overhead crane to be used for hoisting payloads into position for integration with the Gryphon.

Following completion of the payload integration and all final systems checks, the completed Gryphon is rolled out of the GAB and to the waiting Eclipse for attachment.

9.2.4 Ground Facilities Cost Estimates

Cost estimates for construction of the Gryphon Assembly Building were obtained from References 121 and 122. These books provided average construction costs per square foot for various types of buildings. Al Vegter, a local architect, was consulted in how to best estimate costs for this facility. Due to the high ceilings and large roof span required for the GAB, it was decided that aircraft hanger construction costs best represented costs for the GAB. Concrete block bearing walls with steel truss roof structure was determined to be the cheapest construction method. The dimensions and construction costs are shown in Table 9.2.

Table 9.2 Gryphon Assembly Building Cost Estimate

Length	400 ft
Width	160 ft
Height	50 ft
Perimeter Length	1120 ft
Square Foot Area	64,000 ft2
Estimated Cost per Square foot	$53.40
Total Cost Estimate	$3,420,000

Unfortunately a major cost of this facility is not the structure, but the cost of providing a class 10,000 clean room environment for the payload integration area. To determine costs for this part of the facility, reference 73 was contacted. He provided a price estimate of $400-500 per square foot. This high price was due mainly to the high quality clean environment required and high cubic volume space due to the high ceiling. Table 9.3 below shows cost estimates for the clean room environment.

Table 9.3 Class 10,000 Clean Room Costs

Length (ft)	125
Width (ft)	160
Height (ft)	50
Square foot Area (ft^2)	20,000
Estimated Cost per Square foot	$500
Total Cost Estimate	$10,000,000

Costs for the overhead cranes required for assembly of the Gryphon were obtained from Overhead Crane and Service in Romulus, MI.

Table 9.4 Overhead Crane Costs

No.	Item	Cost/Unit	Total Cost
2	80 ton 80' span overhead crane	$180,000	$360,000
2	20 ton 20' span overhead crane	$60,000	$120,000

9.2.5 Gryphon Assembly Labor Cost Estimates

The labor costs associated with construction of one Gryphon booster were based upon the number of people required to construct the Pegasus. The Pegasus requires four people to assemble. Due to the increased size and complexity of the Gryphon, an estimate was made that 12 people would be required to work on each Gryphon during the duration of its 12 week assembly process. Based on this, an estimate of $15 per hour labor costs, and a 40 hour work week the costs were calculated as shown in Table 9.5.

Table 9.5 Assembly Labor Costs

number of workers required	12
number of hours worked per week	40 hours/week
number of weeks worked	12 weeks
labor cost	$15/hour
total labor cost per Gryphon	$86,400

9.3 TRANSPORTING THE GRYPHON

This section deals with transportation of the Gryphon from the Gryphon Assembly Building (GAB) to the Eclipse, attachment of the Gryphon to the Eclipse, and ferrying the Gryphon from the assembly site to the launch site.

9.3.1 The Gryphon Transportation Trailer (GTT)

The main requirements for the design of the Gryphon Transportation Trailer were determined to be the following.

- Support the weight of 500,000 lb Gryphon
- Transport Gryphon (without imparting undue shocks) from the GAB to the Eclipse
- Equipped to allow the Gryphon to be shifted several inches from side to side to allow for proper alignment with the Eclipse during attachment

Based on the preliminary ideas discussed in Sections 9.3.1 and 9.3.2, a drawing of what the GTT could look like is shown in Figures 9.3 and 9.4.

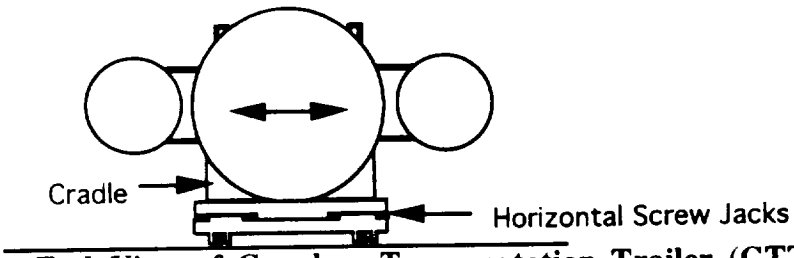

Figure 9.3 End View of Gryphon Transportation Trailer (GTT)

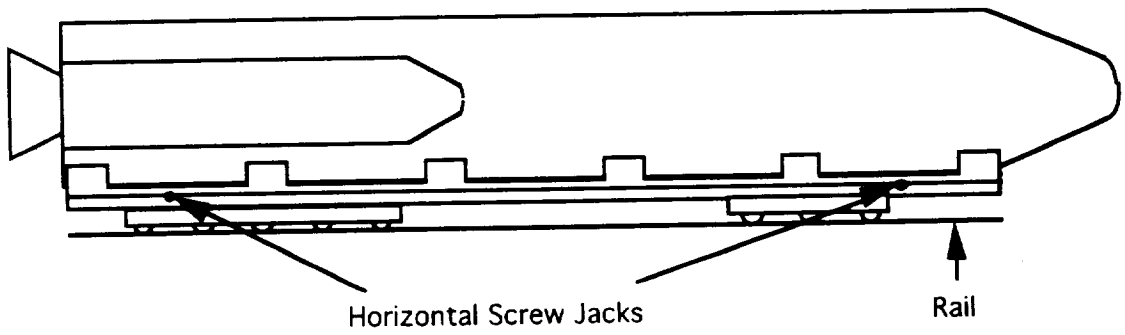

Figure 9.4 Side View of Gryphon Transportation Trailer (GTT)

9.3.2 Type of Trailer

The first step was to determine the method of transportation. The GTT was patterned after the trailer used by Orbital Sciences Corporation to transport the Pegasus from its assembly building to the B-52 drop aircraft. The trailer used to transport the Pegasus is equipped with 24 standard semi-trailer wheels on 6 axles. The Pegasus weighs only 41,000 lb whereas the Gryphon weighs 500,000 lb. By comparison, the GTT would require 73 axles and 292 wheels. It was decided that the GTT should be based on a rail system to support the Gryphon's large weight. This system need not be based on standard rail gauge as it only needs to travel a short distance from the GAB to the Eclipse Attachment Facility. The GTT need not be self propelled and could be pulled by a large aircraft tug.

9.3.3 Method of Alignment

In order to insure proper alignment of the Gryphon with the Eclipse during attachment, the GTT must be able to shift the Gryphon from side to side and also rotate several degrees. To allow for this, it was decided that the Gryphon will be supported in a cradle which rests on top of the trailer. Large screw jacks will be mounted horizontally at the front and rear end of the trailer. By operating the two screw jacks synchronously in either direction the cradle can be moved either left or right. By operating the screw jacks differentially, the cradle can be rotated a few degrees.

9.3.4 Gryphon to Eclipse Attachment Facility

The design requirements for the Gryphon to Eclipse Attachment Facility were as follows:

- The facility should allow for close positioning of the Gryphon and Eclipse prior to the Gryphon being lifted up to the Eclipse
- The facility should be able to lift the 500,000 lb Gryphon and the GTT up to the Eclipse for attachment

The first step in attaching the Gryphon to the Eclipse is positioning. The Eclipse will be positioned within a few inches of the correct location by lining its wheels up with marks on the pavement.

The second step in the attachment process is to roll the Gryphon underneath the Eclipse and align the two precisely. The Gryphon will be brought out from the GAB on its trailer and rolled underneath the Eclipse from the rear. Once it is in position, it will be lifted by four hydraulic lifts (mounted in the ground) up to the Eclipse. The screw jacks on the GTT will then be used to move the Gryphon either to the left or right or to rotate it to achieve proper alignment. If the fore and aft positioning is incorrect, the Eclipse can be pushed forward or backward slightly, or the Gryphon could be lowered, pushed forward or aft on the rails, and lifted up again. Once correct alignment has been achieved, the Gryphon will be raised the last few inches and the hydraulic interface mechanism closed, thus securing the Gryphon to the Eclipse. The GTT can then be lowered back onto its rails and removed.

The last step is to attach the 24 volt electrical connection from the Eclipse to the Gryphon. A sketch of the attachment facility is shown in Figure 9.5.

9.3.5 Gryphon Facility Location

The location of the GAB, GTT rail system, and Gryphon to Eclipse Attachment Facility was determined by the following requirements:

- Availability of rocket fuels on site
- Location close to the equator (desirable for launches to GEO)
- Remote location away from large populations
- Availability of a 10,000 ft runway

Based upon these requirements it was decided that the Kennedy space center was the best place to locate the Gryphon Facility. It was chosen for its close proximity to the equator, long runway used to land the Space Shuttle, and availability of rocket fuels.

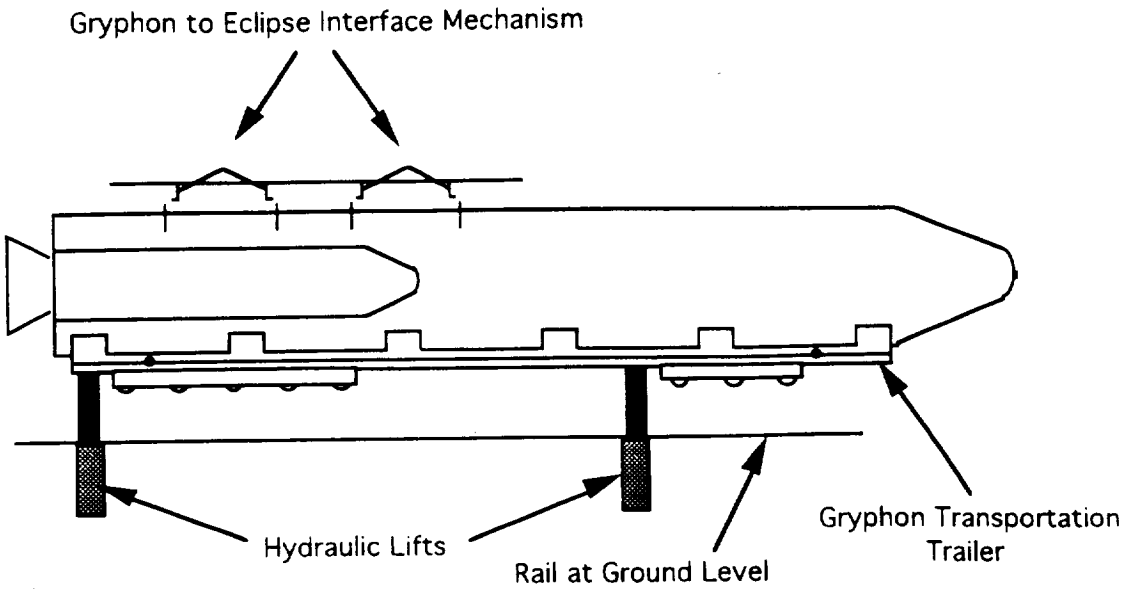

Figure 9.5 Gryphon to Eclipse Attachment Facility

Launches to GEO will be flown directly from Kennedy, thus eliminating the need to ferry the Gryphon from its assembly site to its launch site. However, a small percentage of the launches might be made to very high inclination (polar) orbits. For these orbits, it is desirable to launch from the United States west coast where a northerly launch track can be flown without crossing back over land. Vandenberg Air Force Base was chosen as the launch site for the west coast. It was chosen because of its long runway and the availability of rocket fuel. For these missions, a Gryphon would be ferried unfueled from Kennedy to Vandenberg by the Eclipse. The Gryphon would then be fueled and launched off the west coast.

In order to ferry the Gryphon using the Eclipse from Kennedy to Vandenberg it was necessary to choose several bases at which the Eclipse could stop and refuel in accordance with its 1500 mile range. These bases are shown on the map in Figure 9.6. All bases have the 10,000 ft runway required by the Eclipse. However, some modifications may need to be made to taxi-ways and ramps etc. in order to accommodate the Eclipse's large size and turning radius.

9.4 AIRCRAFT/BOOSTER INTERFACE

The interface attachments between the launch aircraft and booster are of vital importance. There were two designs considered for the Gryphon/Eclipse interface:

- Space Shuttle / Carrier Aircraft attachment
- Orbital Sciences Corporation's Pegasus / L1011 interface

These designs were analyzed and compared to see which would best fit the mission's needs. Some of the design parameters considered were:

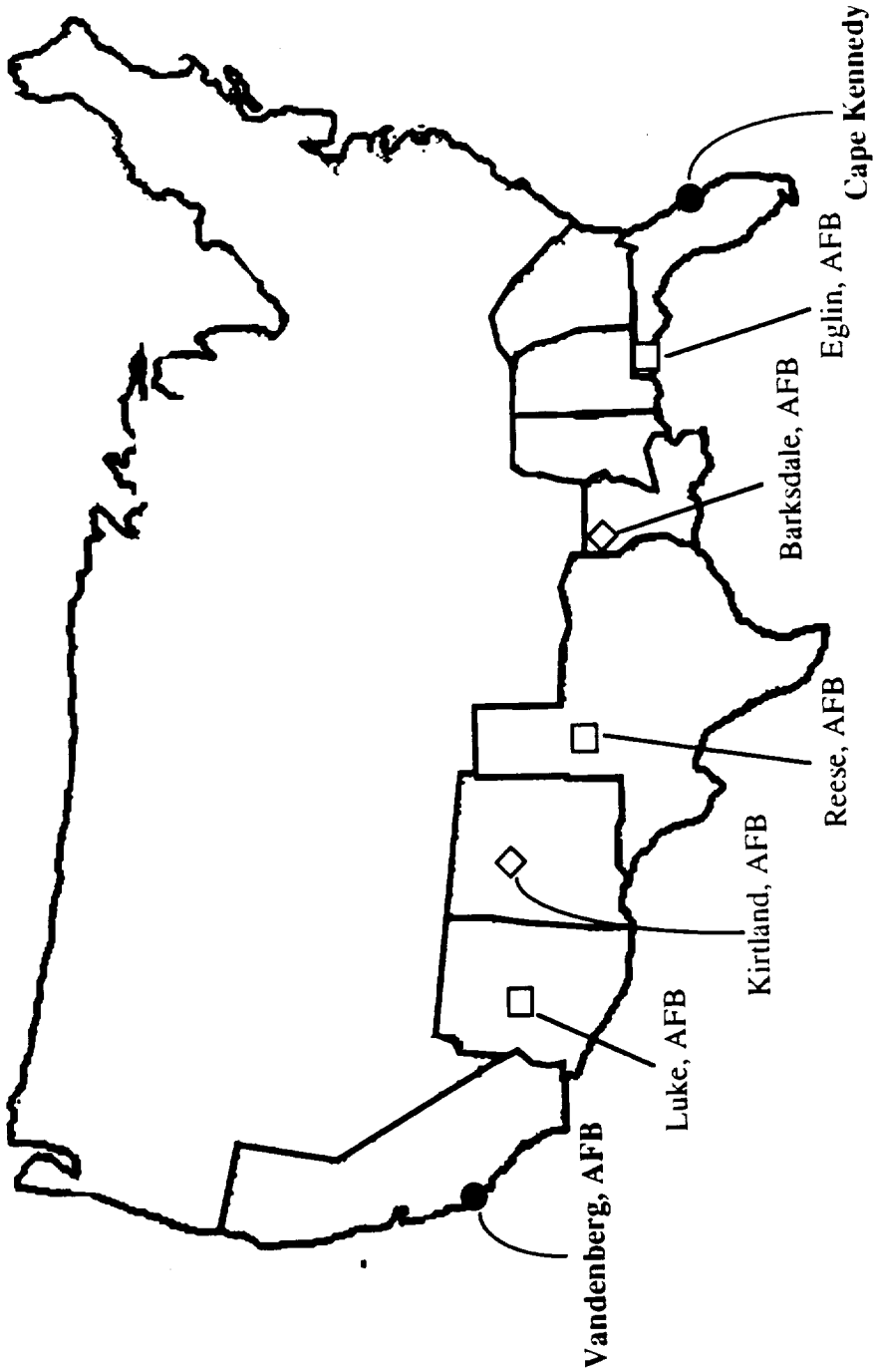

Figure 9.6 Gryphon Launch and Refueling Sites

- Structural Failure Loads
- Pin Layout
- Release Mechanism Geometry
- Hydraulic Power
- Materials
- Smooth Drop Transient
- G-Force Loads
- Environmental Forces
- Reliability and Reuse
- Dynamic Loading

Both designs were considered based on these criteria. It was determined that a design similar to OSC's Pegasus / L1011 interface would be used. This design was chosen because it was similar to our project, proven to work, and easier to analyze. The following sections give overviews of the two designs considered and the specifications of the Gryphon / Eclipse interface attachments. A final section will review the specifics of the overall design and show the layout of the components and costs.

9.4.1 Shuttle / 747 Interface

When the Shuttle needs to be moved across the country, it is placed upon a modified Boeing 747 "piggy-back" style. The attach mechanism used is the same one on the main Shuttle booster. This is a three point configuration that uses struts mounted on the carrier aircraft (see Figure 9.7). The three points have "trailer hitch" rods that are attached inside the Shuttle by collar rings.

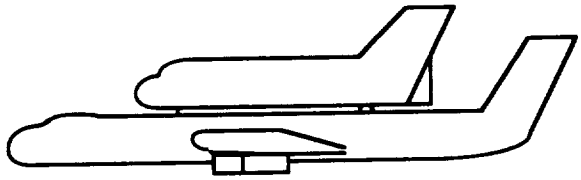

Figure 9.7 Shuttle on Boeing 747 with Three Attach points

9.4.2 Pegasus / L1011 Interface

OSC's Pegasus is launched from a modified L1011 aircraft. The Pegasus hangs from the L1011 from five attach points. The attach mechanism on the L1011 uses lever arms and hooks to attach to the five pins on the Pegasus wing (see Figure 9.8). Four of the points are symmetric about the center of gravity of the Pegasus and the fifth is mounted forward for dynamic stability.

Figure 9.8 L1011 with OSC's Pegasus and Five Attach points

9.4.3 Structural Loading

The structural loading of the Gryphon / Eclipse was an important parameter. Once it was determined to use the Pegasus/L1011 design, the next step was to determine how to modify the configuration for current purposes. The Pegasus II weighs approximately 70,000 lb while the Gryphon weighs just under 500,000 pounds. A structural factor of safety of 1.5 was chosen based on the Pegasus / L1011 design.

9.4.4 Pin Layout

In order to fully analyze the different possibilities, a finite element model was constructed on the CAD program I-DEAS (see Appendix H). It was constructed to run different configurations using finite element models in order to find the best pin layout on the Gryphon. The parameters determining the best pin configuration were:

- Distribution of forces on pins
- Stability of configuration
- Structural Dynamics

Having approximately the same force on each pin would mean only one type of hook and pin combination had to be designed. This would greatly reduce design work and manufacturing costs. Having the same forces on each hook / pin combination would also make the system easier to manufacture. A symmetric system would also help in design and analysis.

Because an infinite number of pin configurations could be run, some of the pin layouts were intuitively determined. First, it was determined to align the center of gravity of the Eclipse and the Gryphon as best as possible. This would ensure some stability and displace the loading on the interface mechanism evenly. Second, the farther apart the pins on the Gryphon, the more stable it would be when hanging off of the Eclipse. This is because the moments created by the hook / pin mechanism would be greater the farther they were from the center of gravity; therefore, it was determined that there would be two pins located as far back as possible. Finally, the Gryphon, unlike the Pegasus, did not have a wing in which the pins could be placed. The pins would have to be placed externally since there was no space to place any type of external structure within the Gryphon. Also, they would have to be placed where extra internal rings could fit or at the booster interstages.

9.4.5 Release Mechanism Geometry

The geometry of the release mechanism was based on the Pegasus/L1011 release mechanism. The release mechanism is very flexible in its operation. The moment arms and control rods are similar to the one used on the Pegasus/L1011 interface except that they are notably larger. This increase is due to the larger weight of the Gryphon and requires the mechanical linkages to be proportionally large to prevent buckling and beam bending. This system, as seen from the picture (see Figure 9.9 and 9.10), will release two pins at the same time. That is, the lever arm rotates the connecting rods evenly. The hook on the right is released when the connecting rod is pulled up by the lever arm. The hook on the left is released when the connecting rod is pulled down by the lever arm. This system can release four hooks simultaneously if two more are place on the main axle of the lever arm.

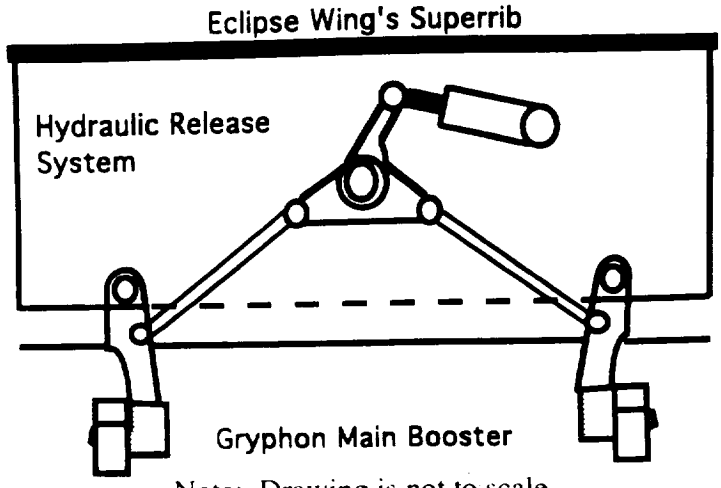

Note: Drawing is not to scale.

Figure 9.9 Side View Layout of Release Mechanism Geometry (Before)

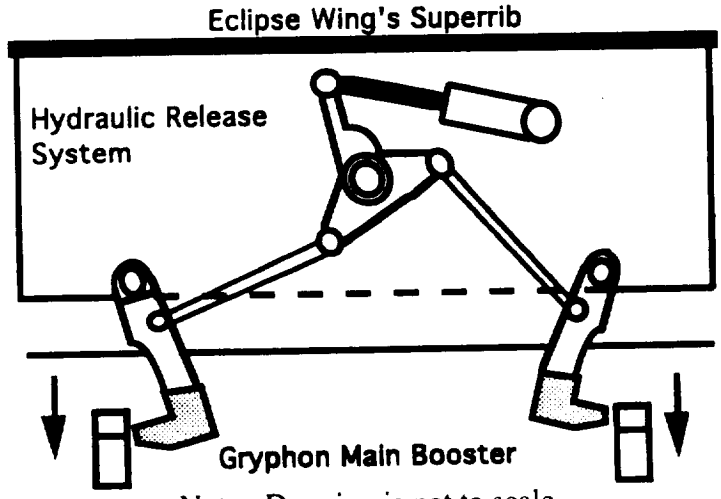

Note: Drawing is not to scale.

Figure 9.10 Side View Layout of Release Mechanism Geometry (After)

9.4.6 Required Hydraulic Force

The hydraulic force to operate the system was calculated using a worst-case-load. The hydraulic force was calculated by using the forces on the pin/hook combination, the friction coefficient between the pin and hook, and the geometry and the lengths of the lever arm and connecting rods. The hydraulic pressure provided by the plane was given at 5000 psi. It was noted that pumps could be added for emergency pressure loss and additional hydraulic force if needed. Using the hydraulic pressure, the pistons were sized by calculating the worst-case load force required. The pistons cross sectional area was found to be 10.54 in^2.

9.4.7 Materials

The material used for the structural members throughout the interface system is a heat treated, quenched and tempered, steel alloy ASTM-A242. The specifics of this material are summarized below (see Table 9.7). This alloy was chosen due to the fact that it is the strongest construction material in yield shear strength.

Table 9.6 Steel Alloy ASTM-A242 Properties

Specific Weight (psi)	0.284
Ultimate Tensile Strength (ksi)	120
Yield Tensile Strength (ksi)	100
Yield Shear Strength (ksi)	55
Modulus of Elasticity (10^6 psi)	29
Modulus of Rigidity (10^6 psi)	11.5
Coefficient of Thermal Exp. (10^{-6}/°F)	6.5
Ductility Percent Elongation (2 in)	18

9.4.8 Drop Transient

Another important consideration involved in air launched vehicles is a smooth drop transient. This involves simultaneous release of all the attachments between the launch and launching vehicle. This was found to be an important consideration from studying OSC's Pegasus launches. In the design of the Gryphon/Eclipse interface, the drop transient was to be as "straight" as possible so it could be dropped without causing damage to the payload or any of the internal components.

9.4.9 G-Force Loads

It was necessary to know the maximum G-Force the Eclipse could perform. This was important so that the Gryphon/Eclipse interface could be designed with a worst-case load. The maximum G-Force was given from the Eclipse Design Team to be 2.5. So, in the design of the interface attachments, the Gryphon was considered 2.5 times its weight for worst-case loading. This would then be multiplied by the structural factor of safety and the dynamic loading coefficient to obtain the overall system factor of safety of 4.

9.4.10 Gryphon / Eclipse System Overview

Taking into account all of the parameters just discussed, the Gryphon / Eclipse Interface Mechanism (GEIM) was designed. The best configuration was found to be two four point, attachment systems on the second stage, symmetric about the center of gravity (Table 9.8 and Figure 9.11). Note, the reference coordinates were taken from the end of the LR91 nozzle. As can be seen, all of the pins lie within the second stage. With the exception of pins 1 and 2, a circular support structure had to be designed at the pin locations. The first two pins were purposefully placed at the interstage between stage 1 and stage 2 due to the structure required there. Pins 5 and 6 are placed at the attach ring required for the struts connecting the two Castor 120 engines. The finite element model solutions for this configuration are in Appendix H. Note that many assumptions were made (i.e. rigid elements, etc.) in this model. However, the purpose was to find the best distribution of

attach points for the statically indeterminate loading. Some of the key aspects of this system are shown below (see Table 9.7).

Table 9.7 Important System Aspects of Gryphon/Eclipse Interface

Hook Cross Sectional Area	16 in^2
Maximum Pin Length	27 in
Total System Weight	11,104.1 lb
Total Pin Weight	1328 lb
System Cost	$472,163.00

The next sections will briefly describe how these system characteristics were calculated and present the final layout via CAD.

Table 9.8 Reference Coordinates of Pins on Gryphon and Loading

Pin Number	X (in)	Y (in)	Z (in)	Z load (kips)
1	171	60	67.08	402
2	171	-60	67.08	402
3	222	60	67.08	402
4	222	-60	67.08	402
5	360	60	67.08	402
6	360	-60	67.08	402
7	411	60	67.08	402
8	411	-60	67.08	402

The pin sizing was determined by the shear force equation for square cross sections:

$$\tau = \frac{3}{2}\frac{F}{A} \qquad \text{(Eq 9.1)}$$

where τ is the shear stress, F is the shear force and A is the cross sectional area. Using the maximum shear force for the steel alloy ASTM-A242 of 55 ksi, and the force per pin from the finite element model of 402 kips (see Appendix H), the cross sectional area was found to be 10.96 in^2 with the system factor of safety of 4. Due to manufacturing constraints and the desire for a simple cross section, this cross section was increased to 16 square inches so that the hook would be 4 inches by 4 inches (see Figure 9.12). The dimensions of the pin were also determined (see Figure 9.13).

The sizing of the hydraulic actuators was determined from the sum of the forces on the lever arm in the equations:

$$\sum M = \mu_f\left(F_{pin1} + F_{pin2}\right)\left(d_{lever}\right) - F_{hydraulic}\left(d_{arm}\right) = 0 \qquad \text{(Eq 9.1)}$$

$$P_{hydraulic} = \frac{F_{hydraulic}}{A} \qquad \text{(Eq 9.2)}$$

ΣM	=	sum of the moments about the lever arm
μ_f	=	static coefficient of friction for steel on steel
$F_{pin1,2}$	=	forces of a pin
d_{conn}	=	distance of the connectors on the lever arm
$F_{hydraulic}$	=	hydraulic force
d_{arm}	=	is the length of the hydraulic arm
$P_{hydraulic}$	=	hydraulic pressure from the plane
A	=	cross sectional area of the hydraulic

After inserting the values for these equations, it was found that the hydraulic needed to have a cross sectional area of 10.3 inches for worst-case loading.

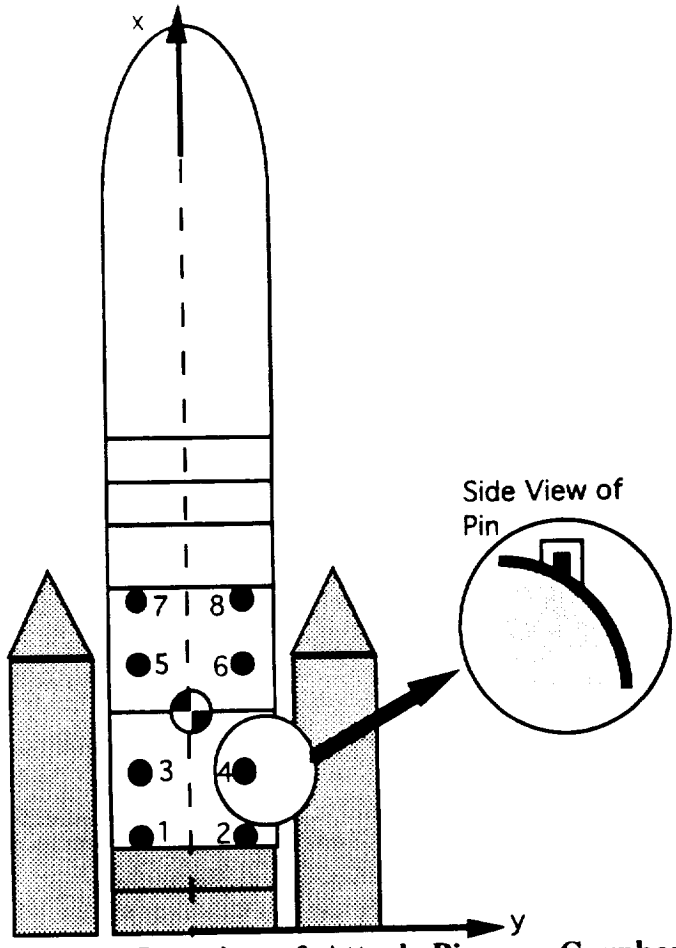

Figure 9.11 Top Down Location of Attach Pins on Gryphon

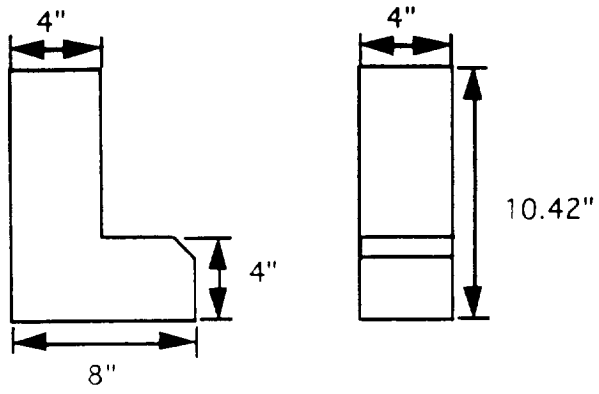

Figure 9.12 Hook dimensions showing side and front views

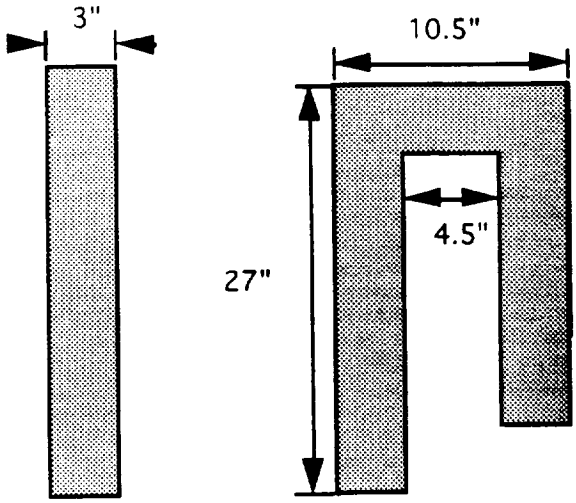

Figure 9.13 Pin dimensions showing side and front views

A summary of the parts costs provided by OSC was found to be a good estimate for our systems costs (see Table 9.9). Note these are the costs of the parts only.

The entire system is shown in the next drawings (see Figure 9.14 - 9.16). Note that the plane is not shown in this figure. The struts are attached to the Eclipse's superrib support structure. Note also that the superribs needed to be extended 3 feet out the back of the wing to support the last two connection points (see Figure 9.17).

Figure 9.14 System Layout of Gryphon/Eclipse Attach Mechanism (Iso-View)

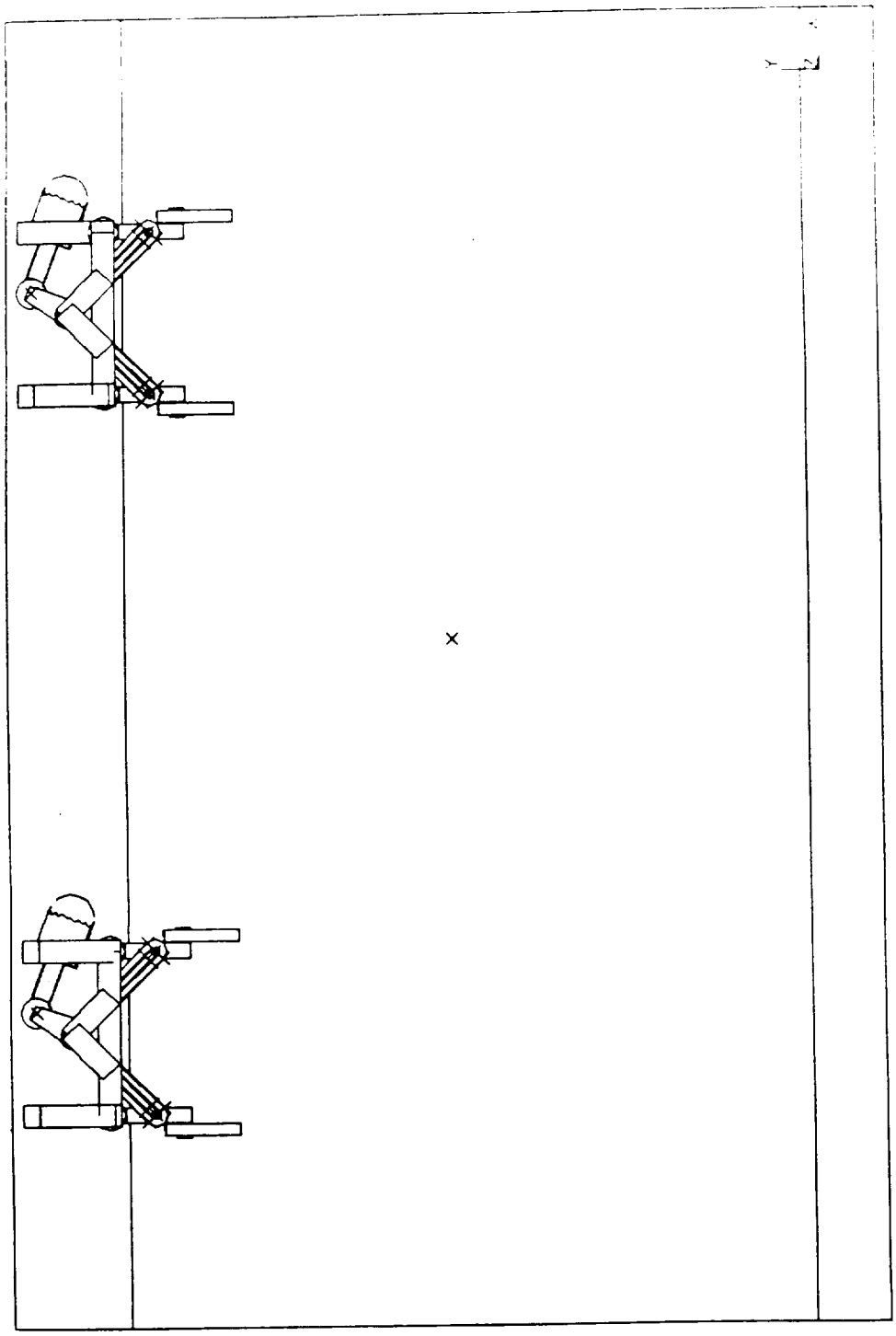

Figure 9.15 System Layout of Gryphon/Eclipse Attach Mechanism (Side View)

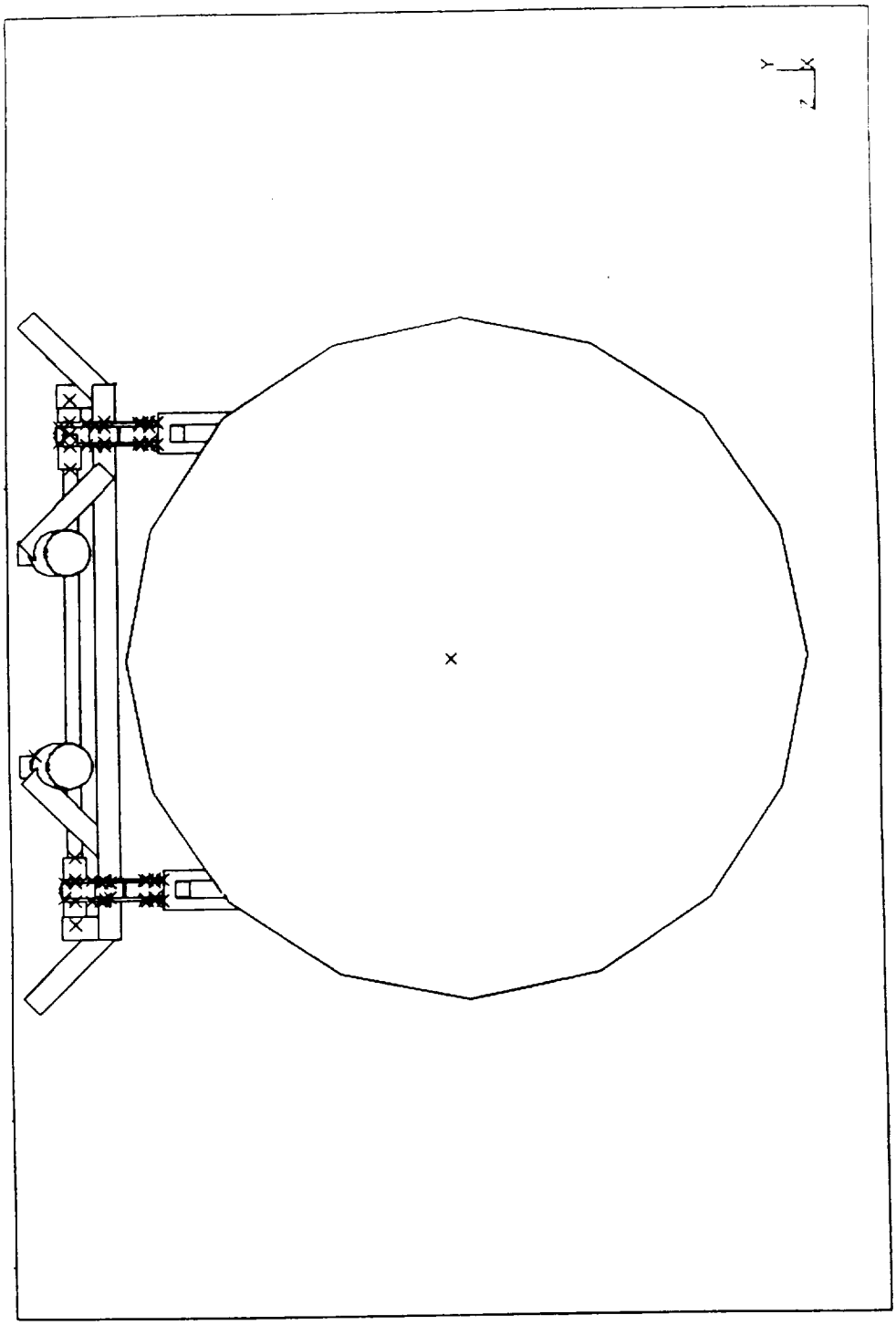

Figure 9.16 System Layout of Gryphon/Eclipse Attach Mechanism (Front View)

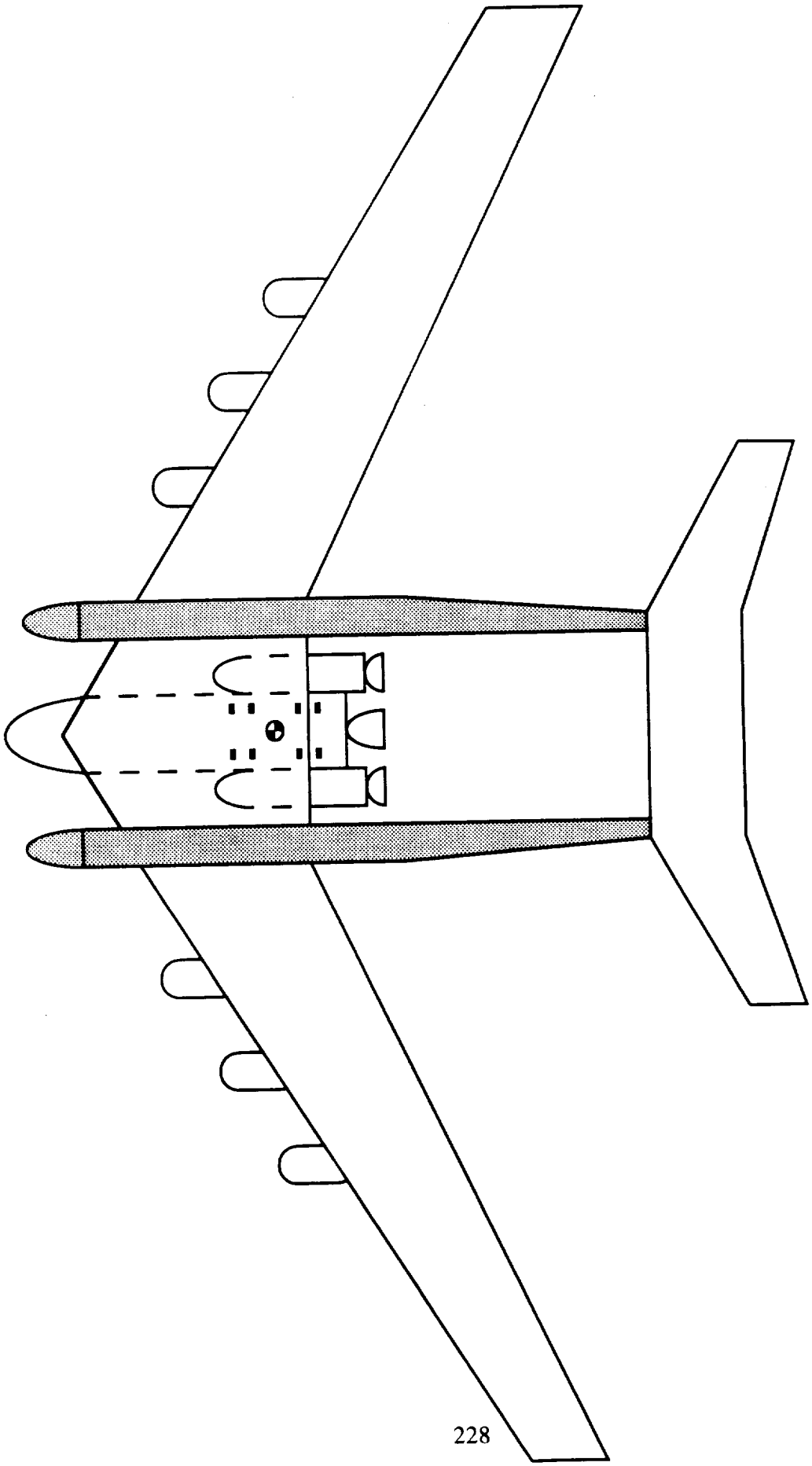

Figure 9.17- Gryphon mounted underneath Eclipse (with attach points)

Table 9.9 Cost Analysis for Gryphon / Eclipse Interface Mechanism

Mechanical Parts	Quantity	Total ($)
Steel		4163.00
Baseplate Assembly	1	10000
Hook Blocks	8	18000
Linkages	8	4800
Overcenter Cam	4	2000
Torque Tube	2	5000
Bearings	8	4000
Locators, Stops, Tongs		1000
Hooks	8	40000
Preload Bolts	8	6000
Preload Shear Pins	8	12000
Hydraulics / Electronics		
Safing Pin Actuators	4	24000
Hydraulic Actuators	4	100000
Microswitches	16	8000
Accumulators	8	120000
Hydraulic Pump	2	30000
Release s/o valves	4	12000
Release flow valves	8	48000
Isolation valve	1	1200
Hand valves		3000
Pressure Transducers	8	8000
Hydraulic lines		3000
Emergency Explosives		8000
Total		472,163.00

9.5 FUELING THE GRYPHON

The Gryphon will be fueled just prior to take-off and after it has been attached to the aircraft. Fueling the Gryphon presented an interesting problem due to the nature of the liquid fuels used for its various stages. The first two stages use storable liquid fuels. The oxidizer is Nitrogen Tetroxide, and the fuel is Aerozine-50 (a 50/50 mixture of Hydrazine and Unsymmetrical Dimethylhydrazine). The third stage uses the cryogenic fuels liquid hydrogen and liquid oxygen. The storable fuels need to be handled with extreme care due to their toxic and corrosive nature, and the cryogenic fuels need to be handled with extreme care due to their low temperatures.

9.5.1 Recommended Safety Precautions

The storable fuels, Nitrogen Tetroxide and Aerozine-50, should be handled with extreme care do to their toxic and corrosive nature. The following is a list of hazards and relative

safety precautions compiled from Ref 42. Since Aerozine-50 is a 50/50 mixture of both Hydrazine and Unsymmetrical Dimethylhydrazine (UDMH), both fuels are listed below.

Nitrogen Tetroxide

Hazards:
- Skin contact causes severe burns
- Breathing of vapor may cause poisoning
- Spills may cause fire and may liberate toxic gas
- Contact with fuels may cause explosions

Safety Precautions:
- The nature and characteristics of nitrogen tetroxide shall be explained to all persons working with this material
- Persons engaged in operations involving handling or transfer of nitrogen tetroxide shall wear approved boots, gloves, acid hood, and protective suit. In addition, a protective mask shall be worn by all persons exposed to the vapors of nitrogen tetroxide
- Operations requiring the handling or use of nitrogen tetroxide shall be performed by groups of two or more persons
- Before beginning to use equipment, make sure the system is not pressurized. Work from above and to one side of an acid line, rather than from below it. Avoid trapping nitrogen tetroxide between closed valves. Do not operate pumps against closed valves. Check lines, valves and the receiving tank before starting to transfer nitrogen tetroxide
- Protective clothing, hand tools, and other equipment shall be flushed with water immediately after contact with nitrogen tetroxide

Hydrazine

Hazards:
- Contact with liquid may cause burns, severe eye damage, and general poisoning
- Breathing vapor may cause lung damage and irritation of the eyes, nose, and throat
- Spills represent an immediate fire and explosion hazard
- Contact with acid causes fire and possibly explosion

Safety Precautions:
- The nature and characteristics of hydrazine shall be explained to all persons working with this material
- Persons handling hydrazine must wear fuel-resistant gloves, shoes, or over-boots, a face shield, wrist and arm protectors, and a rubber-type apron. Where there is a chance of splashing, an approved protective suit must be worn
- Respiratory protection must be available when working in Hydrazine-contaminated atmospheres
- Storage, transfer and operating areas shall be kept clean of organic matter and oxidizers
- Leaks and spills must be immediately flushed away with large amounts of water
- Transfer, handling and storage must be performed by at least two persons

- An atmosphere of nitrogen must be maintained over the hydrazine
- Drums and containers shall be grounded

Unsymmetrical Dimethylhydrazine (UDMH)

Hazards:
- Contact with UDMH may cause eye damage and general poisoning
- Breathing UDMH vapor may cause lung damage and may irritate the eyes, nose and throat
- Spills create immediate fire and explosion hazards
- Contact of UDMH with oxidizing agents causes fire and possibly an explosion

Safety Precautions:
- The nature and characteristics of UDMH shall be explained to all persons working with this material
- Persons handling or transferring UDMH shall wear approved boots, gloves, hood and clothing. In addition, a protective mask shall be worn by all personnel exposed to UDMH vapor
- Operations requiring the handling or use of UDMH shall be performed by persons working in groups of two or more
- Avoid spills of UDMH: the resulting vapors present a fire hazard. Wash all spills with water immediately
- Protective clothing, wrenches, and all other equipment that has been contaminated shall be flushed with water as soon as practical

The cryogenic fuels for the third stage (liquid hydrogen and oxygen) need to be handled with extreme care due to their extremely cold temperatures. The following is a list of hazards and relative safety precautions compiled from Reference 95.

Liquid Oxygen

Hazards:
- Contact with skin causes frostbite and "burns"
- Mixing with fuels causes a dangerous explosion hazard
- Gaseous oxygen from the liquid is absorbed in clothing, and any source of ignition may cause flare burning

Safety Precautions:
- All persons shall be familiar with the nature and characteristics of liquid oxygen
- Personnel engaged in operations involving the handling or transfer of liquid oxygen shall wear the approved goggles or face shields, protective clothing, gloves and boots
- Operations involving the handling of liquid oxygen shall be performed by persons working in groups of two or more
- Extreme caution shall be exercised to prevent any oils, greases, fuels or combustible materials from coming into contact with liquid oxygen
- Care shall be taken to prevent the accumulation of moisture in lines, valves, etc. to avoid freezing and plugging and subsequent pressure ruptures and the trapping of liquid oxygen in unvented sections of the system

Liquid Hydrogen

Hazards:

- Skin contact causes severe frostbite and "burns"
- Extremely flammable
- Explosive hazards are present when-
  - solid air collects in liquid hydrogen
  - gaseous hydrogen is mixed with air in a confined space

Safety Precautions:

- All personnel shall be familiar with the following:
  - Nature and characteristics of liquid hydrogen
  - Safety features of the equipment
  - Proper operating procedures
  - Fire regulations
- Approved clothing, including face shields and gloves shall be worn as specified.
- Allow no ignition source of any kind to be brought into the area.

9.5.2 Procedure for Fueling the Gryphon

The Gryphon is to be fueled just prior to take-off. This is to minimize the time between fueling and launch of the Gryphon due to boil-off of the cryogenic fuels in the third stage.

The minimum safe distance from the Gryphon in the event of an explosion was determined to be 2000 feet. In accordance with this distance, all personnel and equipment not directly involved with fueling the Gryphon should be moved a distance of at least 2000 feet from the Gryphon. In order to minimize the risk of explosion the following precautions should be taken prior to fueling.

- The carrier aircraft Eclipse should be shut down and its engines and APU's should be allowed to cool down sufficiently
- The Eclipse, Gryphon, and any equipment being used during fueling should be grounded
- The area should be swept clean of organic matter to minimize the chance of a fire should Aerozene-50 be spilled
- All possible ignition sources should be removed from the area

In order to minimize the amount of cryogenic fuels lost to boil-off, the storable fuel stages should be fueled first and the cryogenic fuels used in the third stage fueled last. The fueling procedure is as follows:

1. Nitrogen Tetroxide and Aerozene-50 will be transported to the Gryphon in fueling trucks.
2. A water truck and crew should stand by ready to wash away any spill of Nitrogen Tetroxide or Aerozene-50 which might occur.
3. All personnel should work in teams of at least two and should wear approved protective suits and breathing protection.
4. Only after all connections between the Gryphon and the fueling truck have been checked, should fuel transfer begin.
5. Following completion of first and second stage fueling and removal of all associated equipment, fueling of the third stage with cryogenic fuels may proceed.
6. Liquid Hydrogen and Liquid Oxygen will be transported to the Gryphon in fueling trucks.
7. Only after all connections between the Gryphon and the fueling truck have been checked, should fuel transfer begin.
8. Following completion of third stage fueling the Eclipse crew should immediately return to the aircraft and begin launch preparations so as to minimize the amount of cryogenic fuel lost to boil-off.

9.6 POWER AND FUEL CONNECTIONS

Since systems on the Gryphon need an external power supply for the pre-drop phase of the mission, an umbilical power cord is needed to connect the Eclipse and the Gryphon. The umbilical cord will be extending from the underside of the Eclipse next to the right forward most attach point and will be securely attached to the Gryphon. At the point on the umbilical cord closest to the Gryphon there will be placed a cartridge-actuated wire cutter, the most reliable form of wire disconnect available. The cutter consists of a cylindrical housing from steel, a piston cutter blade, an anvil, an end cap, and a cartridge (see Figure 9.14). The piston blade is retained by a shear pin until, after firing within milliseconds,

sufficient pressure develops to shear the pin. At this instant, the blade strikes against the anvil and severs the wire. The device is sealed to prevent gas or flame leakage from causing damage to the Gryphon. After firing, this component can be re-used in future missions by replacing only the piston blade, anvil, and cartridge. The wire cutter is designed to sever a rubber-sheathed electric cable of 16 strands of No. 21 plastic-coated stranded wire of 3/16 in. a diameter of 0.875 in and weighs only 0.12 lb. The wire will be more than needed to carry the 28 V load taken from the Eclipse engines and required by the Gryphon components. This wire cutter was chosen so that for future applications or modifications of the Gryphon, another cutter will not have to be designed to cut a larger wire.

The external structure of the umbilical port on the Gryphon consists of a small "hole" with a flap. After the umbilical cord is severed, the flap will close and latch itself to form a smooth surface for the remainder of the mission.

A fluid line connection was also developed for the Gryphon because at one point it was thought that some coolant would have to be pumped from the Eclipse through the Gryphon in the pre-launch phase of the flight. This line would be a rigid pipe connected to the Gryphon near the left forward most attach point and would be securely connected with a cartridge-actuated release valve. When the release signal is given, the valve will close and detonation will separate the pipe from the Gryphon.

9.7 PLACEMENT OF SUPPORT SYSTEM ON ECLIPSE

On board the Eclipse, it has been determined that one crew member is required. The launch panel operator's (LPU) duties are:

- operate short-range radar and relay information to carrier plane crew
- monitor vehicle status
- switch between external and internal power
- update vehicle IMU prior to release
- prepare and enable vehicle for release
- activate release mechanism
- download and verify mission data
- capture, record, and display data from vehicle and payload

The launch panel console LPC consists of the following equipment: two computers, an inertial measuring unit (IMU), a mass data storage system, the release panel, and three monitors. Two of the monitors will be television screens videoing the forward and aft ends of the Gryphon. The third monitor will be an LCD display used to visually monitor the computers, IMU, and data storage system. Through a keyboard the crew member will be able to manually switch between these displays.

The LPC will be assembled into a desk unit as seen in Figure 9.16. The top shelving unit will consist of three shelves that are 19 inches high. The overall dimensions of the unit are 6' x 5' x 2'. As seen in the figure, all hardware except for the monitors and the keyboard will be placed in the shelving unit. The front of the shelving unit will be covered to prevent equipment from falling out during the mission. The desk unit is approximately 6' x 3' x 6' and will include a swivel chair bolted to the floor. The monitors will be placed at a 45° angle and in a semi-circle on the desk to ensure easy viewing. The keyboard will be located in the middle of the semi-circle. The entire unit (shelving and desk) will be placed directly behind the main cockpit on the Eclipse.

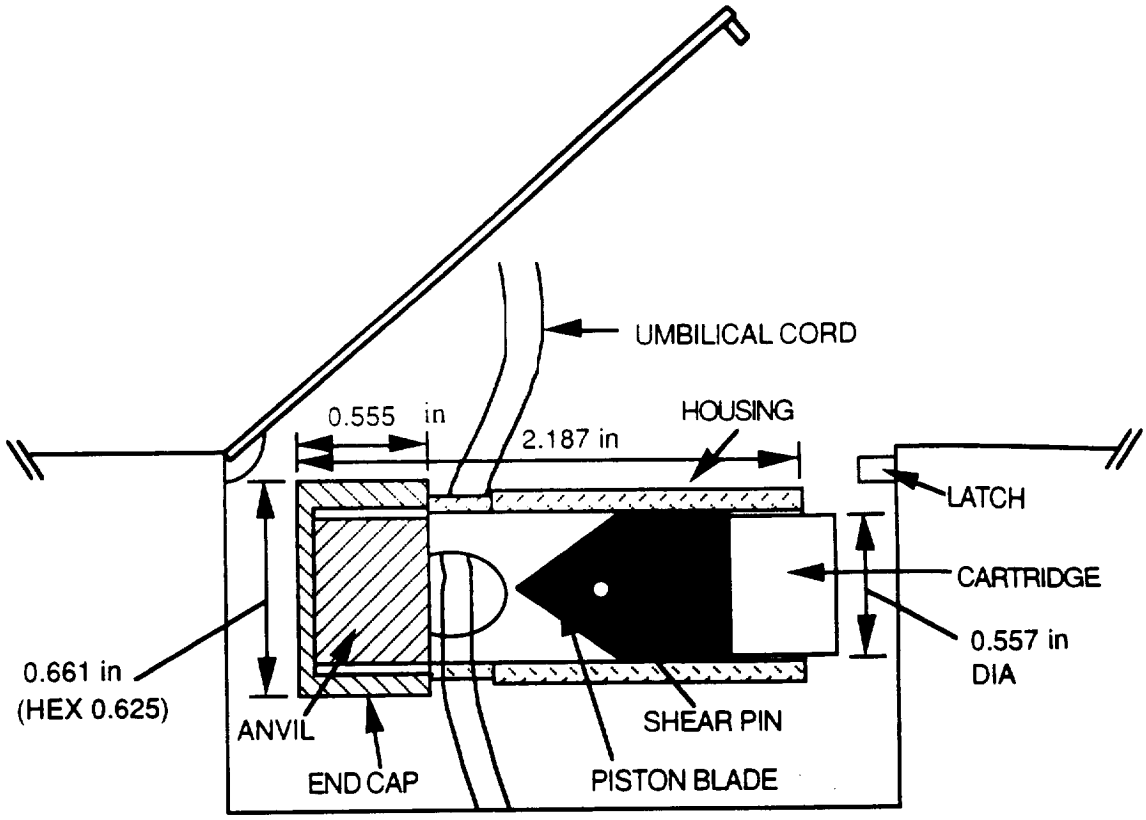

Figure 9.14 Umbilical Cord Cutter

The final piece of equipment that needs to be placed on the Eclipse is a power transformer. The transformer will convert the 110 volt, 400 Hz AC power supply from the Eclipse engines to a 28 volt DC supply that can be used by the Gryphon systems. The transformer unit will be approximately eight inches square and weigh ten pounds. It will be placed in a convenient location between the forward most attach points in order to have easy access to the avionics bay on the Gryphon.

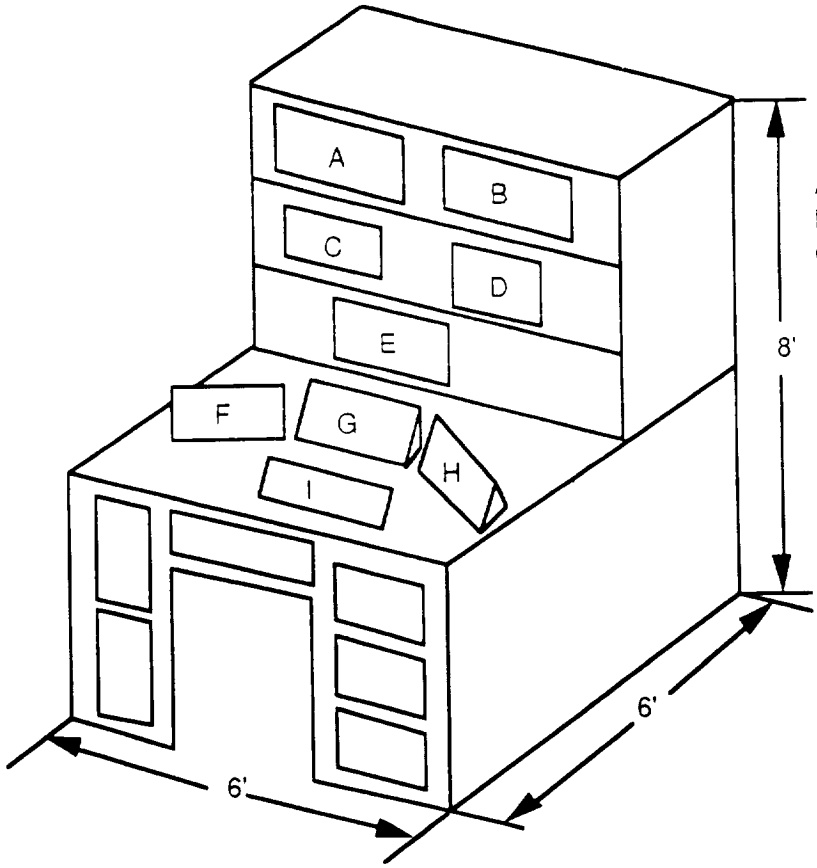

Figure 9.16 Launch Panel Operator

9.8 FUTURE WORK

Due to time constraints, there are some factors that still must be determined. These are:

- Cost analysis
- Refining current system designs
- Force analysis
- Prelaunch checklists

Cost analysis will need to be updated. At the assembly level, more information will be needed to determine a better estimate for the costs of the clean room. Also, cost will need to be determined for the Gryphon Transportation Trailer (GTT) and for the minor assembly equipment (such as wrenches, bolts, etc.). Finally, current estimates for the connections between the Gryphon and Eclipse are based on scaling similar systems between the Pegasus and L10-11 used by OSC, and will need updating.

Further design work will be necessary in some areas. Primarily the GTT and the Gryphon's physical connections. The reason for the redesign of the connection system would be due to the fact that some of the applicable forces still need to be determined.

Undetermined forces will affect the design of the physical connection system. Forces such as drag and side forces, forces due to braking and touchdown (in the event of mission termination), nodal analysis, and forces that will incur when the rigid-body assumption of the Gryphon is removed. A non-rigid finite element model for the Gryphon/connection combination was attempted, but was exceptionally difficult to complete and due to time-constraints was abandoned.

Checklists will be needed from assembly to launch. Starting with Post-Assembly Inspection Checklists to be performed at every sub-level of its completion (for example, after a castor is mounted, all connections and attach struts will be inspected). Then, checklists will be needed for transportation of the booster, mating of the booster to the carrier aircraft, and fueling safety. Finally, a pre-flight checklist and a pre-launch checklist will be necessary.

CONCLUSION & FUTURE WORK

Chapter Ten

10.1 INTRODUCTION

This chapter summarizes the findings of the Gryphon project, identifies the status of the project in the framework of a complete design life cycle, and discusses future work to be performed in a Phase II study.

10.2 SUMMARY

Development of a 500,000 lb air launched space booster as a feasible, profitable commercial space venture has been demonstrated in this report. The increased performance associated with the air-launched system provides twice the payload delivery capability of an identical ground launched system. Coupled with the use of "off-the-shelf" technology and components, the increased payload capability allows the Gryphon to undercut competing space booster systems' cost per pound to orbit by almost 50%.

The Gryphon Air Launched Space Booster can deliver 7,900 lb of payload to Geosynchronous Earth Orbit (GEO). The vehicle is released from the Eclipse carrier aircraft at an altitude of 44,000 ft at the start of its trajectory. Based on the investment necessary to develop such a system in addition to per-mission costs and financing, the Gryphon can deliver its payload at a cost of $6,200 per pound to GEO.

10.3 DESIGN STATUS

The process of developing a large-scale engineering project, such as the Gryphon, can be divided into the following categories.

Phase I: Preliminary Design

- Feasibility study
- Cost analysis
- Preliminary analysis

Phase 2: Detailed Design

- In-depth analysis of system
- Comprehensive integration of sub-systems

Phase 3: Development

- Sub-system testing
- Prototype development
- Testing of prototype

Phase 4: Realization

- Manufacturing
- Operation

This report represents the Phase I design of a 500,000 lb air launched space booster. Although a substantial amount of preliminary analysis was performed for this system, the time constraints imposed by the academic semester halted the design process prior to a Phase II study. The feasibility study and cost analysis performed in the design of the Gryphon present strong motivation to continue the project through the realization stage.

10.4 FUTURE WORK

A brief listing of items that would need to be addressed in a Phase II study are presented below.

Identification of Secondary Structural Masses

The weight of the booster is a vital parameter that must be constantly monitored and modified to ensure its payload delivery capability. Currently the design accounts for all primary masses: i.e. support structures, fuel tanks, engines, and avionics. The amount of secondary mass introduced in the form of wires, fasteners, conduit, etc. must be identified and accounted for.

Optimization of Trajectory

Although all effort has been made to produce an efficient trajectory for placing payloads in orbit, optimization of this trajectory must be performed in order to minimize fuel used and maximize payload weight.

Detailed Analysis of Orbit

The primary mission for the Gryphon is placing communications satellites in Geosynchronous Transfer Orbit. All payload weights and trajectory analysis was computed for this orbit. The secondary goal of the booster is the placement of scientific payloads into Low Earth Orbit and resupply of Space Station Freedom. An analysis must be done of these low orbits to identify the variation of payload delivery capability with orbital altitude and inclination angle.

Stability Analysis of Vehicle

A stability analysis of the vehicle must be performed in order to develop a more complete attitude control system. The vehicle is currently equipped with Reaction Control Thrusters and a Vertical tail to provide control during the unpowered portion of the launch, however, time constraints did not allow determination of the actual vehicle stability characteristics.

Aft Nozzle Cover Design

The need for an Aft Nozzle Cover was identified to reduce aerodynamic drag during captive carry of the booster. Although the shape of this cover was designed, no attempt was made to perform a structural analysis of the ANC or to design a mechanism to separate the ANC from the booster. The actual design of this component must minimize both weight and cost since the cover does not play an integral part in the Gryphon's mission.

Design of an Orbital Maneuvering System

Resupply of Space Station Freedom was selected as a secondary mission for the Gryphon. The delivery of payloads to the Space Station will require precise maneuvers to ensure payload-station rendezvous. This maneuvering system would have to be included in any resupply payload.

SPACECRAFT INTEGRATION

Appendix A

A.1 EXPENSE REPORT

Appendix A.1 contains a complete expense report for the Gryphon. Where uncertainty existed, costs were overestimated. Still, there is a great uncertainty in the cost to build and operate the Eclipse airplane.

Table A.1 Gryphon Expenses

	Low Estimate	High Estimate
Airplane Costs		
1.5 Airplanes	$ 750 million*	$ 1 billion*
Operating Costs	$ 1 million	$ 2 million
Aircraft Integration		
and Ground Support		
Hanger	$ 32 million*	$ 32 million*
Assembly Building	$ 13.4 million*	$ 13.4 million*
Assembly Cost	$ 81 thousand	$ 81 thousand
Rail System	$ 10 million*	$ 10 million*
Attach Mechanism		
Steel Material Cost	$ 4.163 million	$ 4.163 million
Base Plate	$ 10 thousand	$ thousand
8 Hook Blocks	$ 18 thousand	$ 18 thousand
8 Linkages	$ 4.8 thousand	$ 4.8 thousand
4 Overcenter Cams	$ 2 thousand	$ 2 thousand
2 Torque Tubes	$ 5 thousand	$ 5 thousand
8 Bearings	$ 4 thousand	$ 4 thousand
Locator, Stops, Tongs	$ 1 thousand	$ 1 thousand
8 Hooks	$ 40 thousand	$ 40 thousand
8 Preload Bolts	$ 6 thousand	$ 6 thousand
8 Preload Sheer Pins	$ 12 thousand	$ 12 thousand
4 Pin Actuators	$ 24 thousand	$ 24 thousand
4 Hydraulic Actuators	$ 100 thousand	$ 100 thousand
16 Microswitches	$ 8 thousand	$ 8 thousand
8 Accumulators	$ 120 thousand	$ 120 thousand
2 Hydraulic Pumps	$ 30 thousand	$ 30 thousand
4 Release Valves	$ 12 thousand	$ 12 thousand
8 Release Flow Valves	$ 48 thousand	$ 48 thousand
Isolation Valve	$ 1.2 thousand	$ 1.2 thousand
Hand Valves	$ 3 thousand	$ 3 thousand
8 Pressure Transducers	$ 8 thousand	$ 8 thousand
Hydraulic Lines	$ 3 thousand	$ 3 thousand
Emergency Explosives	$ 8 thousand	$ 8 thousand

Mission Control		
Computers and Software	$ 2 million	$ 2 million
GPS Receiver	$ 14 thousand	$ 14 thousand
IMU	$ 100 thousand	$ 100 thousand
Transmitters & Receivers	$ 50 thousand	$ 50 thousand
Mission Cont. Employees	$ 500 thousand*	$ 500 thousand*
Ground Station Use	$ 75 thousand	$ 75 thousand
Plane Modification	$ 340 thousand	$ 340 thousand
Inertial Navigation	$ 50 thousand	$ 50 thousand
Power/Thermal		
Thermal Control System	$ 4.9 thousand	$ 4.9 thousand
Lithium Chlorate Battery	$ 2.5 thousand	$ 2.5 thousand
Silver Zinc Battery	$ 1 thousand	$ 1 thousand
Attitude Control Thrusters	$ 3.9 thousand	$ 3.9 thousand
Venting System	$ 800	$ 800
Propulsion		
1 RL10A-4 (GTO only)	$ 225 thousand	$ 250 thousand
RL10 Fuel	$ 12 thousand	$ 12 thousand
2 Castor 120's	$ 8.4 million	$ 9 million
3 LR91's	$ 3.6 million	$ 3.6 million
LR91 Fuel	$ 2.5 million	$ 2.5 million
Structures		
Stage II Fuel Tank	$ 1 million	$ 4 million
Stage III Fuel Tank	$ 100 thousand	$ 500 thousand
Payload Interface Ring	$ 100 thousand	$ 500 thousand
Attach Struts	$ 500	$ 1 thousand
Fairings	$ 100 thousand	$ 500 thousand
Main Shroud	$ 1 million	$ 2 million
Payload Shroud	$ 1 million	$ 1 million
Aft Nozzle Cover	$ 20 thousand	$ 50 thousand
Vertical Tail	$ 500 thousand	$ 1 million

* indicates a one time cost

A.2 WEIGHT AND CENTER OF MASS CALCULATIONS

The spreadsheet below tabulates individual component weights and center of mass locations on the Gryphon. The origin is located at the center of the Stage One LR-91 engine nozzle exit (See Figure 2.6A). The x-axis then runs up the center line of the booster and the y-axis points out towards the left Castor. The center of mass is assumed to lie on the x-axis for each configuration. This is an approximation since the Gryphon is not perfectly symmetrical about this axis because of the non symmetrical Stage One

propellant tanks, power/avionics bay configuration, and the internal cabling and piping. However, this assumption should be accurate because of the large ratio of (x-axis) symmetrical masses to (x-axis) non symmetrical masses.

The center of mass is calculated by using the relation,

$$\frac{\sum m r}{\sum m} \qquad \text{(Eq A.1)}$$

where m is the mass of each component and r is the distance from the yz-plane. The centers of mass were calculated for each stage individually and then added using the above formula to find the configuration's center of mass.

The moments of inertia for each component are determined by modeling each as a simple geometric shape. The parallel axis theorem,

$$I = I_i + m r^2 \qquad \text{(Eq A.2)}$$

was then used to transfer each component's moment of inertia (I_i) about its center of mass to its moment of inertia (I) a distance r from the center of mass of each stage. Then, these moments of inertia were added together to find the three principle values (I_{xx}, I_{yy}, I_{zz}) for each stage. A configuration of stages' moments of inertia were then calculated, again from the parallel axis theorem and the center of mass formula above. These values are tabulated in Table A.2. For light components, such as the 2 lb radar transponder, individual moments of inertia were not calculated since they would be insignificant compared to much heavier items. However, the item was used as a point mass in the parallel axis theorem.

Table A.2 also includes moments of inertia for half full and empty propellant tanks. To do this, the masses of the oxidizer and fuel were modified along with their respective center of mass locations and individual moments of inertia. The method described above was then used to calculate the configuration's moments of inertia.

Table A.2 Component Weights, Centers of Mass, and Moments of Inertia

	GTO OPTION				LEO OPTION	
	Weight	CM from yz-plane	CM from xz-plane	CM from xy-plane	Weight	CM from yz-plane
	(lb)	(in)	(in)	(in)	(lb)	(in)
Stage 1						
Castor Left						
Propellant	109000	210	148	0	109000	210
Engine	0	62	148	0	0	62
Nozzle	3000	24	148	0	3000	24
Fuel Tanks	5687	210	148	0	5687	210
Front Attachment	200	360	97	0	200	360
Rear Attachment	200	65	97	0	200	65
Fairing Attach Ring	20	360	148	0	20	360
Fairing	55	396	148	0	55	396

Castor Right						
Propellant	109000	210	148	0	109000	210
Engine	0	62	148	0	0	62
Nozzle	3000	24	148	0	3000	24
Fuel Tanks	5687	210	148	0	5687	210
Front Attachment	200	360	97	0	200	360
Rear Attachment	200	65	97	0	200	65
Fairing Attach Ring	20	360	148	0	20	360
Fairing	55	396	148	0	55	396
LR-91						
Engine	500	93	0	0	500	93
Nozzle	800	36	0	0	800	36
Fuel	8365	164	26	0	8365	164
Oxidizer	15559	164	-38	0	15559	164
External Skin	545	130	0	0	545	130
Bottom Support Ring	525	63	0	0	525	63
Plane Attach Ring 1	358	171	0	0	358	171
Gryp-Eclipse Rings 1&2	334	171	0	67	334	171
Engine Mount	349	129	0	0	349	129
Fuel Tank	395	164	26	0	395	164
Oxidizer Tank	280	164	-38	0	280	164
Payload Shroud	6200	1000	0	0	6200	762
Vertical Tail	1500	62	0	153	1500	62
Interstage	675	238	0	0	675	238
Interstage Ring	80	275	0	0	80	275
Aft Nozzle Cover (ANC)	5800	-184	0	0	5800	-184
Stage 2						
LR-91 (2)						
Right Engine	500	295	42	0	500	295
Right Nozzle	800	235	42	0	800	235
Left Engine	500	295	-42	0	500	295
Left Nozzle	800	235	-42	0	800	235
Fuel	58777	385	0	0	58777	382
Oxidizer	109324	487	0	0	109324	487
Plane Attach Ring 2	358	222	0	0	358	222
Gryp-Eclipse Rings 3&4	334	222	0	67	334	222
Plane Attach Ring 3	358	360	0	0	358	360
Gryp-Eclipse Rings 5&6	334	360	0	67	334	360
Plane Attach Ring 4	358	411	0	0	358	411
Gryp-Eclipse Rings 7&8	334	411	0	67	334	411
External Skin	1730	429	0	0	1730	429
Strut Support Ring	525	360	0	0	525	360
Engine Mount	646	325	0	0	646	325
Fuel Tank	1120	382	0	0	1120	382
Oxidizer Tank	1380	487	0	0	1380	487
Interstage Ring 1	80	279			80	279
Interstage Ring 2	80	543	0	0	80	543

Stage 3						
RL-10 (1)						
Interstage Ring	80	547	0	0	80	547
Payload Interface Attach	210	783	0	0	210	545
Engine	112	602	0	0		
Nozzle	175	560	0	0		
Fuel	1510	730	0	0		
Oxidizer	7547	658	0	0		
External Skin	860	664	0	0		
Structure Mount	207	582	0	0		
Fuel Tank	350	730	0	0		
Oxidizer Tank	260	658	0	0		
Helium	10	685	50	0	10	553
Helium Tank	45	685	50	0	45	553
Engine Attach	27	619	0	0		
Power/Avionics Ring	221	807	0	0	221	569
Power/Thermal						
Cabling	150	795	0	0	150	557
Hydrazine/Oxidizer & Tanks	800	795	0	0	500	557
Control Thrusters	13	810	0	0	13	572
Venting System	15	795	0	0	15	557
Thermal Control	1000	795	30	0	1000	557
Batteries	600	795	-20	0	160	557
Mission Control						
CPUs	10	795	0	0	10	557
Radar Transponder	2	795	0	0	2	557
Telemetry Transmitters	3	795	0	0	3	557
GPS	3	795	0	0	3	557
Inertial Guidance (IMU)	19	795	0	0	19	557
GTO Payload	6553	957	0	0	0	0
LEO Payload	0	0	0	0	15653	719
Payload Interface	1347	890	0	0	1347	652

A.3 FINANCIAL SCHEDULE

Table A.3 Financial Schedule for Minimum Launch Price

Year	1	2	3	4	5	6	7
Revenue ($)	0.000	0.000	0.000	130.352	260.704	391.056	391.056
Total Expenses ($)	53.125	53.125	89.829	113.104	226.208	339.313	339.313
Before Tax Profit ($)	-53.125	-53.125	-89.829	17.248	34.496	51.743	51.743
Income Tax ($)	-19.125	-19.125	-32.338	6.209	12.418	18.628	18.628
After Tax Profit ($)	-34.000	-34.000	-57.491	11.039	22.077	33.116	33.116
Indebtedness ($)	39.502	85.398	166.012	180.054	183.543	174.771	164.580

Year	8	9	10	11	12	13
Revenue ($)	456.232	456.232	456.232	456.232	456.232	456.232
Total Expenses ($)	395.865	395.865	395.865	395.865	395.865	395.865
Before Tax Profit ($)	60.367	60.367	60.367	60.367	60.367	60.367
Income Tax ($)	21.732	21.732	21.732	21.732	21.732	21.732
After Tax Profit ($)	38.635	38.635	38.635	38.635	38.635	38.635
Indebtedness ($)	146.327	125.120	100.482	71.855	38.596	-0.045

MISSION ANALYSIS

Appendix B

B.1 ASCENT TRAJECTORY

Table B.1 Ascent Trajectory Data

	Time (seconds)	Altitude (feet)	Angle of Attack	Flgt Path Angle	Velocity (ft/s)	Weight (lbs)	Latitude (°N)	Long. (°W)	Range Dis (nm)
Drop	0	40,000	0	0	733.3	480,403	12.5	118.0	0
Jettison ANC	3.5	39,813	8.32	-8.30	741.0	474,603	12.5	118.0	0.4
Stage 1 Ignition	7.5	39,141	17.37	-17.32	768.2	474,603	12.5	118.0	0.9
	12.5	37,636	22.47	-19.89	1,081	459,090	12.5	118.0	1.6
	17.5	35,547	28.31	-19.44	1,364	443,578	12.5	118.0	2.6
	22.5	33,229	25.86	-16.96	1,597	428,066	12.5	117.9	3.7
	47.5	33,681	25.17	18.34	2,033	350,503	12.5	117.8	11.3
	67.5	53,683	13.92	29.78	2,718	288,453	12.5	117.7	18.1
Stage 2 Ignition	85.5	84,701	11.18	32.73	3,985	208,614	12.5	117.6	26.4
Shroud Separation	144.3	200,000	22.67	21.75	4,964	169,550	12.5	116.9	63.8
	175.5	257,861	26.20	18.78	5,887	142,004	12.5	116.5	89.6
	205.5	316,698	18.36	16.74	7,024	122,067	12.5	116.0	119.4
	235.5	378,841	11.01	14.32	8,528	102,130	12.5	115.3	155.7
	265.5	442,403	4.11	11.56	10,508	82,194	12.5	114.6	200.4
	295.5	503,840	-2.28	8.53	13,170	62,257	12.4	113.6	256.3
Stage 2 Burnout	338.4	573,901	-10.19	3.39	19,219	33,713	12.4	111.8	365.1

B.2 SUBSONIC AERODYNAMIC DATA

See Section 3.6.1 for details of the analysis

Table B.2 Data for Computation of Drag in Axial Direction

Gryphon Fuselage			
Pressure	393.12 lbf/ft^2	Re #	1.49E+08
Temp	389.99°R		
Gas Constant	1716	R_{wf}	1.105
Density	0.000587 $slug/ft^3$	C_f mid	0.00189
Viscosity	2.97E-7 $slug/ft \cdot s^2$	S_{wet} mid	5026.5 ft^2
Speed	733.3 ft/s		
Mach #	0.78	C_{do} mid	0.0081088
Length	92 ft		
Diameter	15 ft	C_{dl} mid	0.0003512
Weight per ref. area	333.3 lbf/ft^2		
Dynamic Pressure	167.4 lbf/ft^2		
Ref. area	1500 ft^2	C_d mid	0.00846

Table B.3 Coefficient of drag for Gryphon modeled as cylinders

Altitude 40,000 ft
Density 0.000587 slug/ft^3
Viscosity 2.97E-7 slug/ft·s^2

SRBs			
Velocity (ft/s)	Re number	C_d per unit length	C_d with 15% interference
1	1.68E+04	1.2	1.38
2	3.36E+04	1.2	1.38
3	5.04E+04	1.2	1.38
4	6.72E+04	1.2	1.38
5	8.40E+04	1.2	1.38
10	1.68E+05	1.2	1.38
15	2.52E+05	1	1.15
20	3.36E+05	0.98	1.127
25	4.20E+05	0.8	0.92
30	5.04E+05	0.35	0.4025
35	5.88E+05	0.36	0.414
40	6.72E+05	0.37	0.4255
50	7.56E+05	0.37	0.4255
55	8.40E+05	0.38	0.437
60	9.24E+05	0.39	0.4485
70	1.01E+06	0.39	0.4485

Fuselage			
Velocity (ft/s)	Re number	C_d per unit length	
1	2.96E+04	1.2	
2	5.93E+04	1.2	
3	8.89E+04	1.2	
4	1.19E+05	1.2	
5	1.48E+05	1.1	
10	2.96E+05	1	
15	4.45E+05	0.35	
20	5.93E+05	0.35	
25	7.41E+05	0.37	
30	8.89E+05	0.38	
35	1.04E+06	0.39	
40	1.19E+06	0.39	
45	1.33E+06	0.39	
50	1.48E+06	0.39	
55	1.63E+06	0.39	
60	1.78E+06	0.39	
65	1.93E+06	0.39	

B.3 SUPERSONIC AERODYNAMIC DATA

The equations used to compute data in this section are:

$$L = \rho M^2 a^2 S_b \alpha \qquad \text{(Eq B.1)}$$

$$D = \tfrac{1}{2}\rho M^2 a^2 \left[S_b (X + \alpha^2) + S_{Tail} \left(\frac{4}{\sqrt{M^2 - 1}} \left(\frac{t_m}{c} \right)^2 \right) \right] * 1.2 \qquad \text{(Eq B.2)}$$

See section 3.6.2 for details.

Table B.4 Lift (in pounds) at 50,000 ft

Angle of Attack (degrees)

Mach	2	4	6	8	10	12	14	16	18
1.5	7.21E+03	1.44E+04	2.16E+04	2.88E+04	3.60E+04	4.32E+04	5.05E+04	5.77E+04	6.49E+04
2	1.28E+04	2.56E+04	3.84E+04	5.13E+04	6.41E+04	7.69E+04	8.97E+04	1.03E+05	1.15E+05
3	2.88E+04	5.77E+04	8.65E+04	1.15E+05	1.44E+05	1.73E+05	2.02E+05	2.31E+05	2.59E+05
4	5.13E+04	1.03E+05	1.54E+05	2.05E+05	2.56E+05	3.08E+05	3.59E+05	4.10E+05	4.61E+05
5	8.01E+04	1.60E+05	2.40E+05	3.20E+05	4.00E+05	4.81E+05	5.61E+05	6.41E+05	7.21E+05
6	1.15E+05	2.31E+05	3.46E+05	4.61E+05	5.77E+05	6.92E+05	8.07E+05	9.23E+05	1.04E+06
7	1.57E+05	3.14E+05	4.71E+05	6.28E+05	7.85E+05	9.42E+05	1.10E+06	1.26E+06	1.41E+06
8	2.05E+05	4.10E+05	6.15E+05	8.20E+05	1.03E+06	1.23E+06	1.44E+06	1.64E+06	1.85E+06

Table B.5 Lift (in pounds) at 75,000 ft

Angle of attack (degrees)

Mach	2	4	6	8	10	12	14	16	18
1.5	2.21E+03	4.41E+03	6.62E+03	8.82E+03	1.10E+04	1.32E+04	1.54E+04	1.76E+04	1.99E+04
2	3.92E+03	7.84E+03	1.18E+04	1.57E+04	1.96E+04	2.35E+04	2.75E+04	3.14E+04	3.53E+04
3	8.82E+03	1.76E+04	2.65E+04	3.53E+04	4.41E+04	5.29E+04	6.18E+04	7.06E+04	7.94E+04
4	1.57E+04	3.14E+04	4.71E+04	6.28E+04	7.84E+04	9.41E+04	1.10E+05	1.26E+05	1.41E+05
5	2.45E+04	4.90E+04	7.35E+04	9.80E+04	1.23E+05	1.47E+05	1.72E+05	1.96E+05	2.21E+05
6	3.53E+04	7.06E+04	1.06E+05	1.41E+05	1.76E+05	2.12E+05	2.47E+05	2.82E+05	3.18E+05
7	4.80E+04	9.61E+04	1.44E+05	1.92E+05	2.40E+05	2.88E+05	3.36E+05	3.84E+05	4.32E+05
8	6.28E+04	1.26E+05	1.88E+05	2.51E+05	3.14E+05	3.77E+05	4.39E+05	5.02E+05	5.65E+05

Table B.6 Lift (in pounds) at 100,000 ft

Angle of attack (degrees)

Mach	2	4	6	8	10	12	14	16	18
1.5	6.66E+02	1.33E+03	2.00E+03	2.66E+03	3.33E+03	4.00E+03	4.66E+03	5.33E+03	5.99E+03
2	1.18E+03	2.37E+03	3.55E+03	4.74E+03	5.92E+03	7.10E+03	8.29E+03	9.47E+03	1.07E+04
3	2.66E+03	5.33E+03	7.99E+03	1.07E+04	1.33E+04	1.60E+04	1.86E+04	2.13E+04	2.40E+04
4	4.74E+03	9.47E+03	1.42E+04	1.89E+04	2.37E+04	2.84E+04	3.31E+04	3.79E+04	4.26E+04
5	7.40E+03	1.48E+04	2.22E+04	2.96E+04	3.70E+04	4.44E+04	5.18E+04	5.92E+04	6.66E+04
6	1.07E+04	2.13E+04	3.20E+04	4.26E+04	5.33E+04	6.39E+04	7.46E+04	8.52E+04	9.59E+04
7	1.45E+04	2.90E+04	4.35E+04	5.80E+04	7.25E+04	8.70E+04	1.02E+05	1.16E+05	1.31E+05
8	1.89E+04	3.79E+04	5.68E+04	7.58E+04	9.47E+04	1.14E+05	1.33E+05	1.52E+05	1.70E+05

Table B.7 Drag (in pounds) at 50,000 ft

Angle of attack (degrees)

Mach	2	4	6	8	10	12	14	16	18
1.5	1.13E+05	1.14E+05	1.15E+05	1.16E+05	1.17E+05	1.19E+05	1.21E+05	1.23E+05	1.26E+05
2	1.46E+05	1.46E+05	1.48E+05	1.50E+05	1.52E+05	1.55E+05	1.58E+05	1.62E+05	1.67E+05
3	3.01E+05	3.03E+05	3.06E+05	3.10E+05	3.15E+05	3.22E+05	3.30E+05	3.39E+05	3.49E+05
4	5.16E+05	5.19E+05	5.24E+05	5.32E+05	5.42E+05	5.53E+05	5.67E+05	5.83E+05	6.02E+05
5	7.63E+05	7.69E+05	7.77E+05	7.89E+05	8.04E+05	8.22E+05	8.44E+05	8.69E+05	8.98E+05
6	1.10E+06	1.11E+06	1.12E+06	1.13E+06	1.16E+06	1.18E+06	1.21E+06	1.25E+06	1.29E+06
7	1.49E+06	1.50E+06	1.52E+06	1.54E+06	1.57E+06	1.61E+06	1.65E+06	1.70E+06	1.76E+06
8	1.95E+06	1.96E+06	1.98E+06	2.01E+06	2.05E+06	2.10E+06	2.16E+06	2.22E+06	2.29E+06

Table B.8 Drag (in pounds) at 75,000 ft

Angle of attack (degrees)

Mach	2	4	6	8	10	12	14	16	18
1.5	3.47E+04	3.49E+04	3.51E+04	3.54E+04	3.58E+04	3.64E+04	3.70E+04	3.77E+04	3.84E+04
2	4.46E+04	4.48E+04	4.52E+04	4.58E+04	4.65E+04	4.74E+04	4.85E+04	4.97E+04	5.11E+04
3	9.21E+04	9.26E+04	9.36E+04	9.49E+04	9.65E+04	9.86E+04	1.01E+05	1.04E+05	1.07E+05
4	1.58E+05	1.59E+05	1.61E+05	1.63E+05	1.66E+05	1.69E+05	1.74E+05	1.79E+05	1.84E+05
5	2.34E+05	2.35E+05	2.38E+05	2.41E+05	2.46E+05	2.52E+05	2.58E+05	2.66E+05	2.75E+05
6	3.36E+05	3.38E+05	3.42E+05	3.47E+05	3.54E+05	3.62E+05	3.72E+05	3.83E+05	3.95E+05
7	4.57E+05	4.60E+05	4.65E+05	4.72E+05	4.81E+05	4.92E+05	5.05E+05	5.21E+05	5.38E+05
8	5.97E+05	6.01E+05	6.07E+05	6.17E+05	6.28E+05	6.43E+05	6.60E+05	6.80E+05	7.02E+05

Table B.9 Drag (in pounds) at 100,000 ft

Angle of attack (degrees)

Mach	2	4	6	8	10	12	14	16	18
1.5	1.05E+04	1.05E+04	1.06E+04	1.07E+04	1.08E+04	1.10E+04	1.12E+04	1.14E+04	1.16E+04
2	1.34E+04	1.35E+04	1.36E+04	1.38E+04	1.40E+04	1.43E+04	1.46E+04	1.50E+04	1.54E+04
3	2.78E+04	2.80E+04	2.82E+04	2.86E+04	2.91E+04	2.98E+04	3.05E+04	3.13E+04	3.23E+04
4	4.77E+04	4.80E+04	4.85E+04	4.92E+04	5.00E+04	5.11E+04	5.24E+04	5.39E+04	5.56E+04
5	7.05E+04	7.10E+04	7.18E+04	7.29E+04	7.43E+04	7.60E+04	7.80E+04	8.03E+04	8.29E+04
6	1.01E+05	1.02E+05	1.03E+05	1.05E+05	1.07E+05	1.09E+05	1.12E+05	1.16E+05	1.19E+05
7	1.38E+05	1.39E+05	1.40E+05	1.43E+05	1.45E+05	1.49E+05	1.53E+05	1.57E+05	1.62E+05
8	1.80E+05	1.81E+05	1.83E+05	1.86E+05	1.90E+05	1.94E+05	1.99E+05	2.05E+05	2.12E+05

B.4 AFT NOZZLE COVER

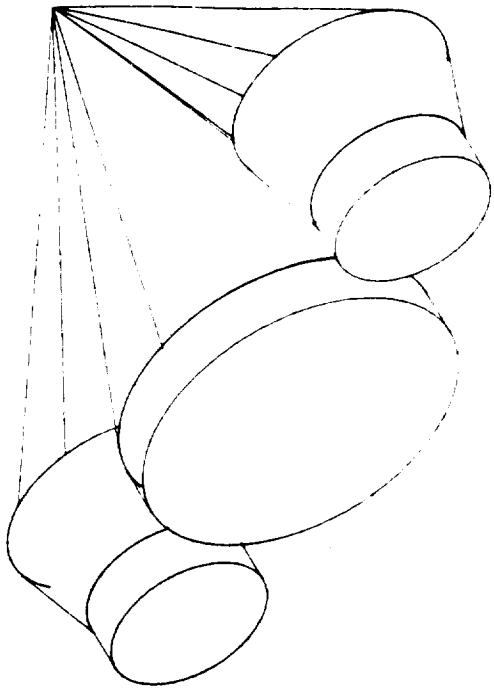

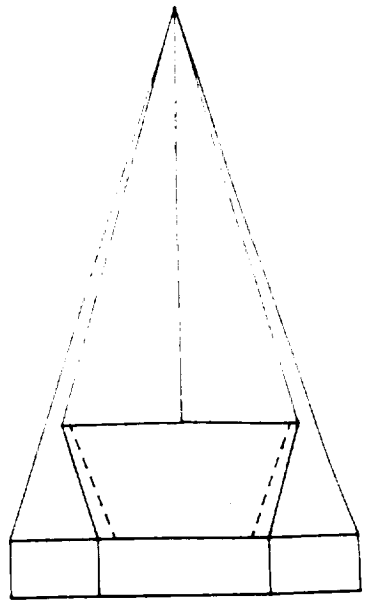

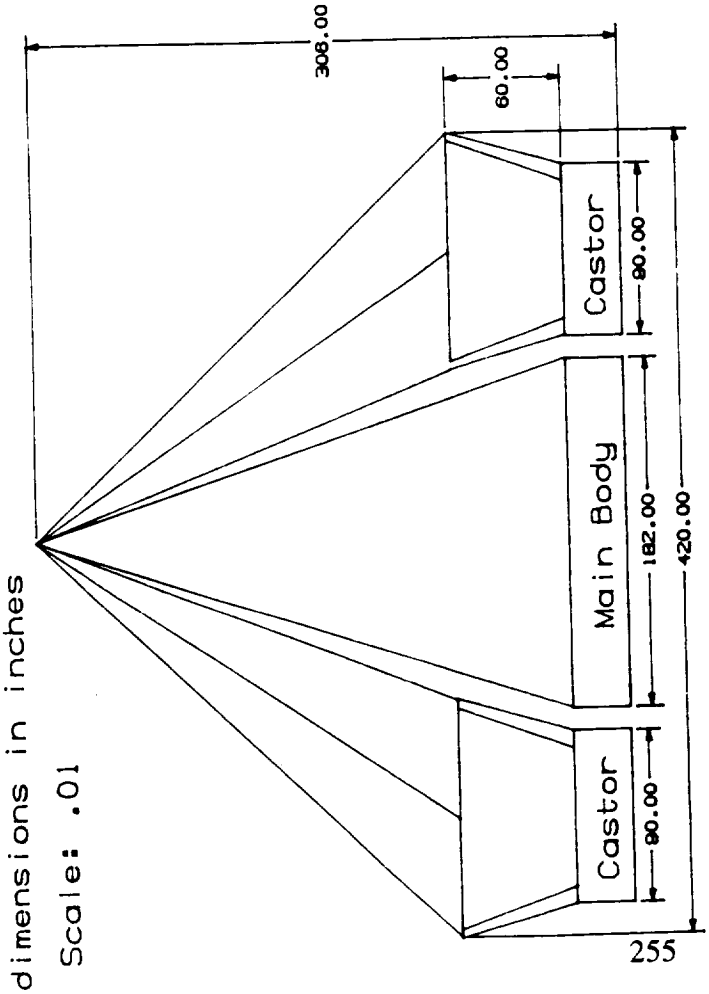

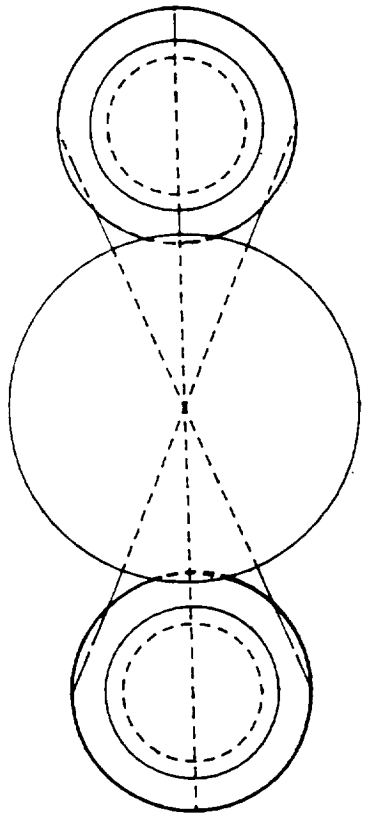

B.5 MISSION TIME LINE

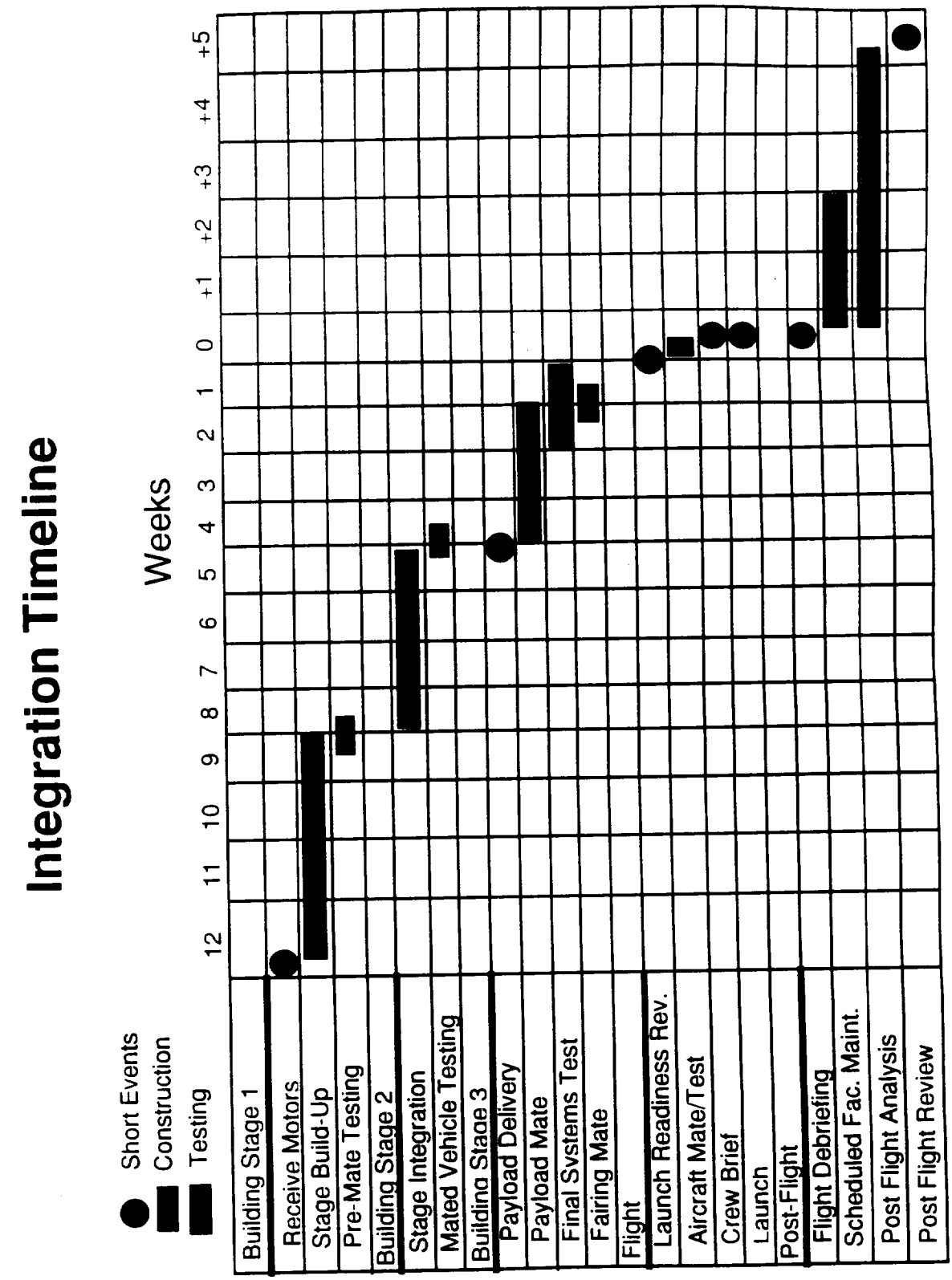

B.5.1 Trajectory Program Data

The following programs were written on MATLAB software. The first program calculates the function arguments in Table 3.4 that are used to find the sine and cosine integrals. Once the values of the sine and cosine integrals are calculated using MAPLE V, the second program evaluates (Eqs 3.26-56), except (Eqs 3.28-29, 3.32-33, 3.36-37).

Program 1

```
ri=21033297;
hi=130397;
edot=.075;
rs=21147847;
gs=31.45;
pf=.1619;
cs=10175.2;
n=1.05784;
nu=(70+((cs*edot)/(n*gs)))/57.3;
s=-((cs*edot)/(n*gs))/57.3;
c=(cs^2)/(n*gs);
X=(c/cs)*(sqrt(gs/rs));
one=s+X
two=(s+X)*pf
three=s-X
four=(s-X)*pf
```

Program 2

```
cione=-3.02384;
sione=-.0272989;
citwo=-4.84894;
sitwo=-.0043999;
cithree=.174305;
sithree=-.748066;
cifour=-1.50454;
sifour=-.125091;
E=(citwo-cione)+(cifour-cithree);
F=(sitwo-sione)+(sifour-sithree);
G=(citwo-cione)-(cifour-cithree);
H=(sitwo-sione)-(sifour-sithree);
A=.5*(E*cos(nu) - F*sin(nu));
B=.5*(G*sin(nu) + H*cos(nu));
C=.5*(E*sin(nu) + F*cos(nu));
D=.5*(-G*cos(nu) + H*sin(nu));
imz=A*sin(X*pf) - B*cos(X*pf);
rz=A*cos(X*pf) + B*sin(X*pf);
imw=C*sin(X*pf) - D*cos(X*pf);
rw=C*cos(X*pf) +D*sin(X*pf);
y=(c/X)*((imz+(yi/cs)*sin(X*(1-pf))) +(ri*cos(X*(1-pf)));
x=(c/X)*(imw+(xi/cs)*sin(X*(1-pf)));
ydot=-cs*(rz+((ri*X)/c)*sin(X*(1-pf))) + yi*cos(X*(1-pf));
```

```
xdot=-cs*(rw) + xi*cos(X*(1-pf));
hf=(sqrt(x^2 +y^2))-ri+hi
vf=sqrt(xdot^2+ydot^2)
bet=(x*xdot +y*ydot)/sqrt((x^2+y^2)*(xdot^2+ydot^2))
```

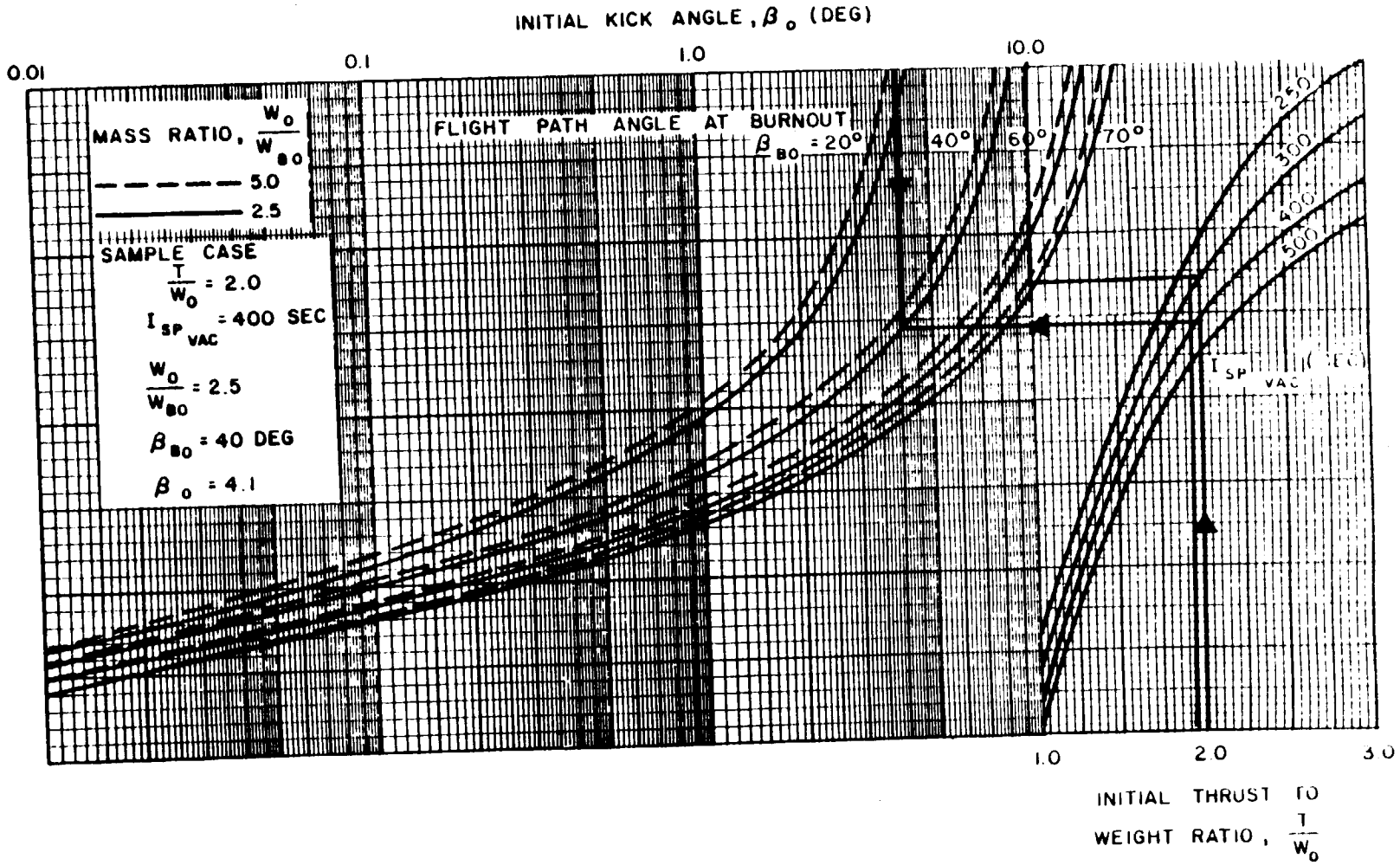

Figure B.1

Figure 52. First-Stage Burnout Angle Nomograph

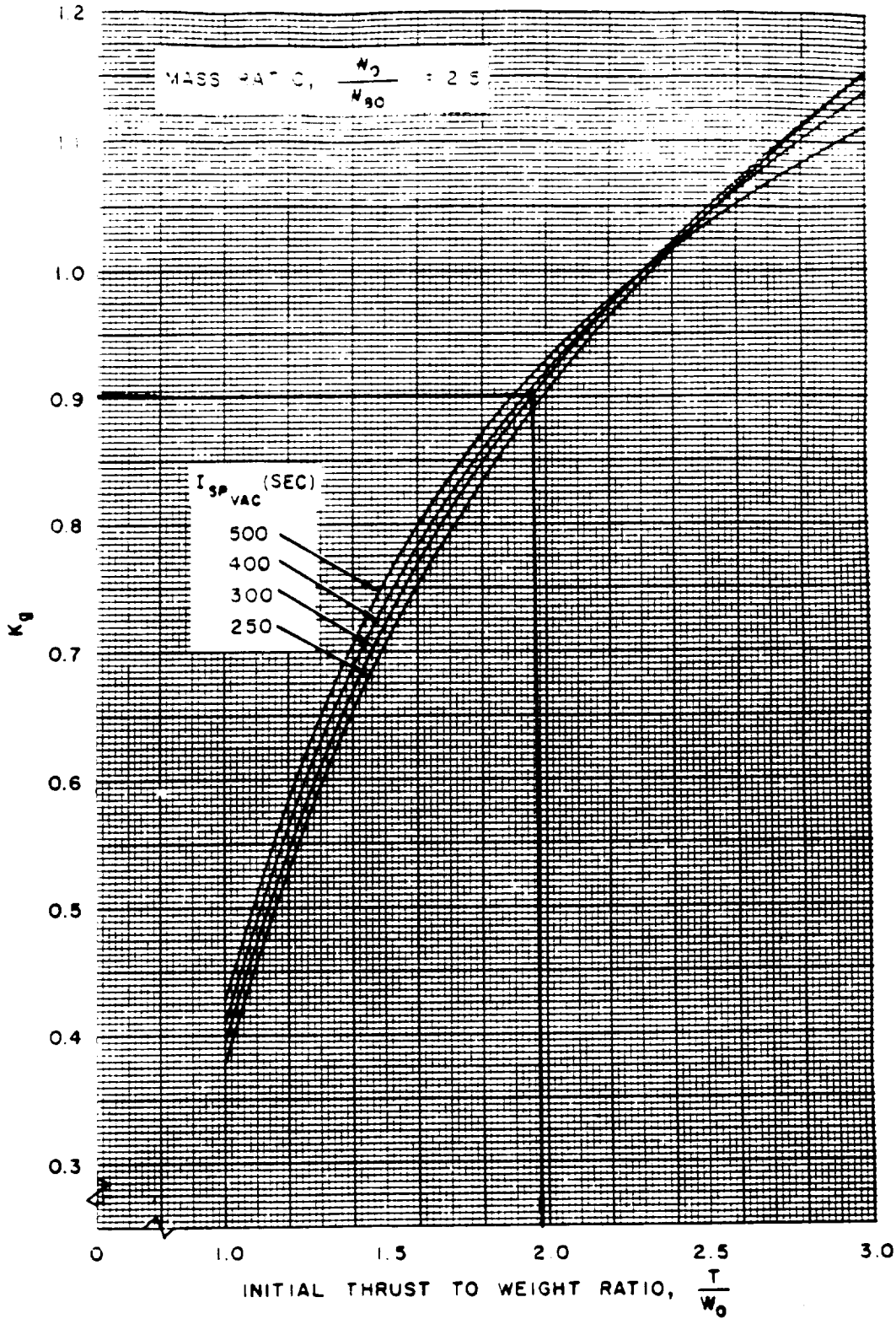

Figure 63. First-Stage Gravity-Loss Constant

Figure B.2

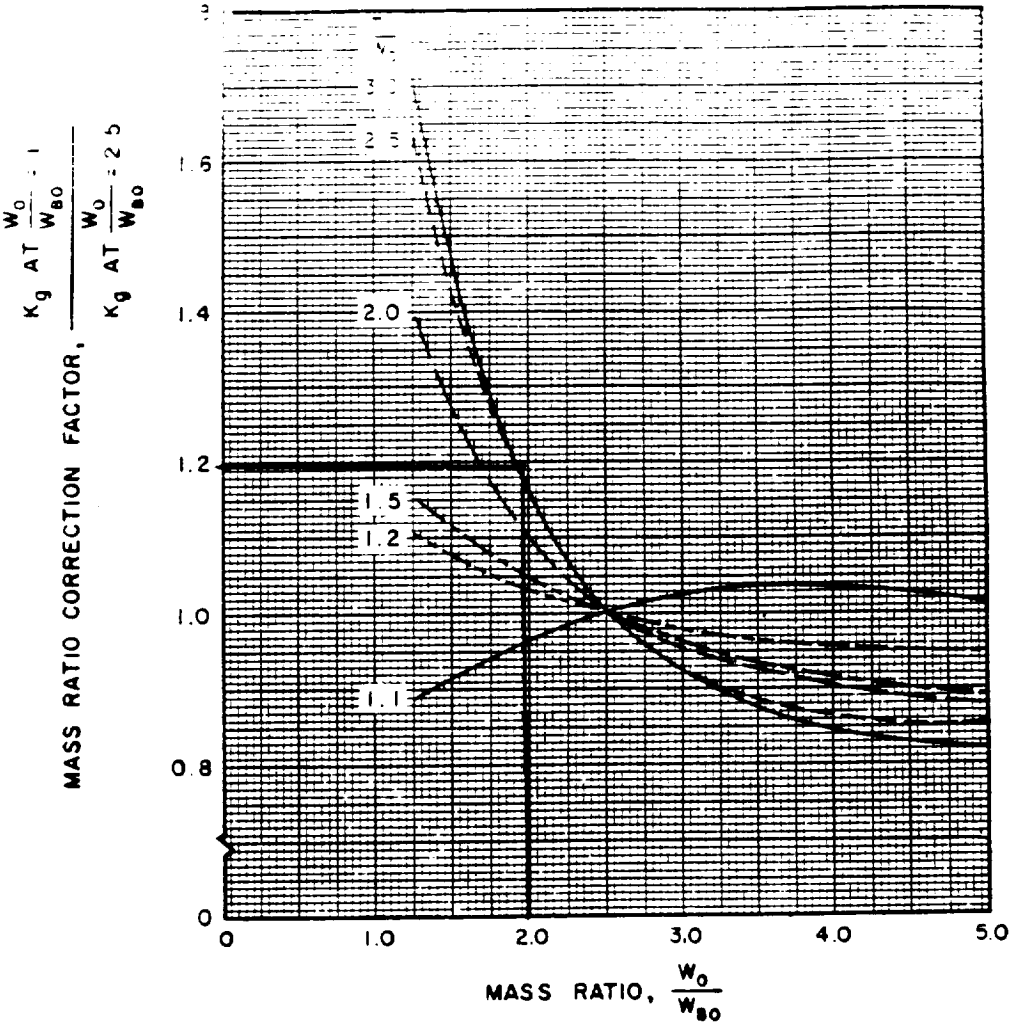

Figure 65. First-Stage Mass Ratio Correction Factor

Figure B.3

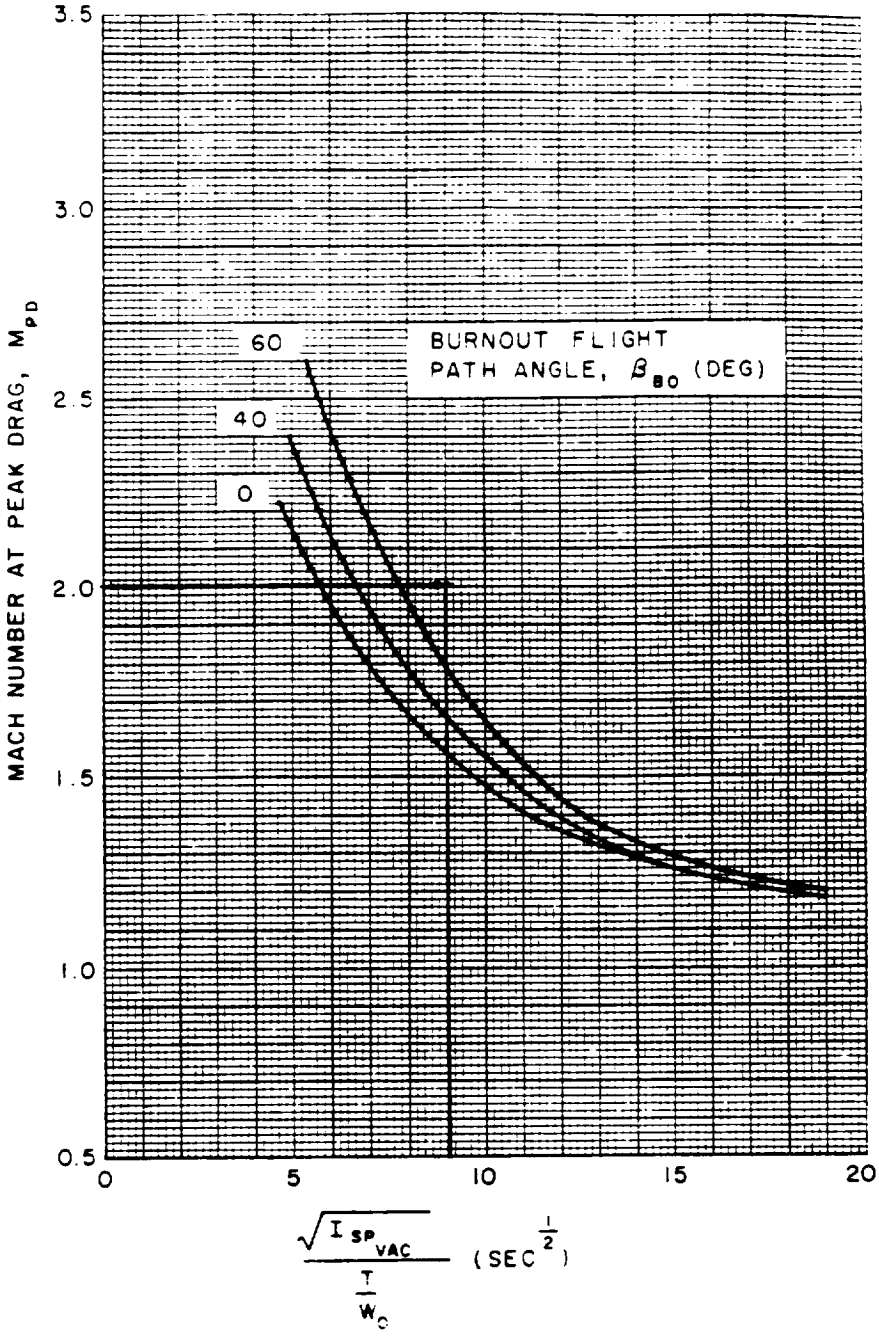

Figure 66. First-Stage Mach Number at Peak Drag

Figure B.4

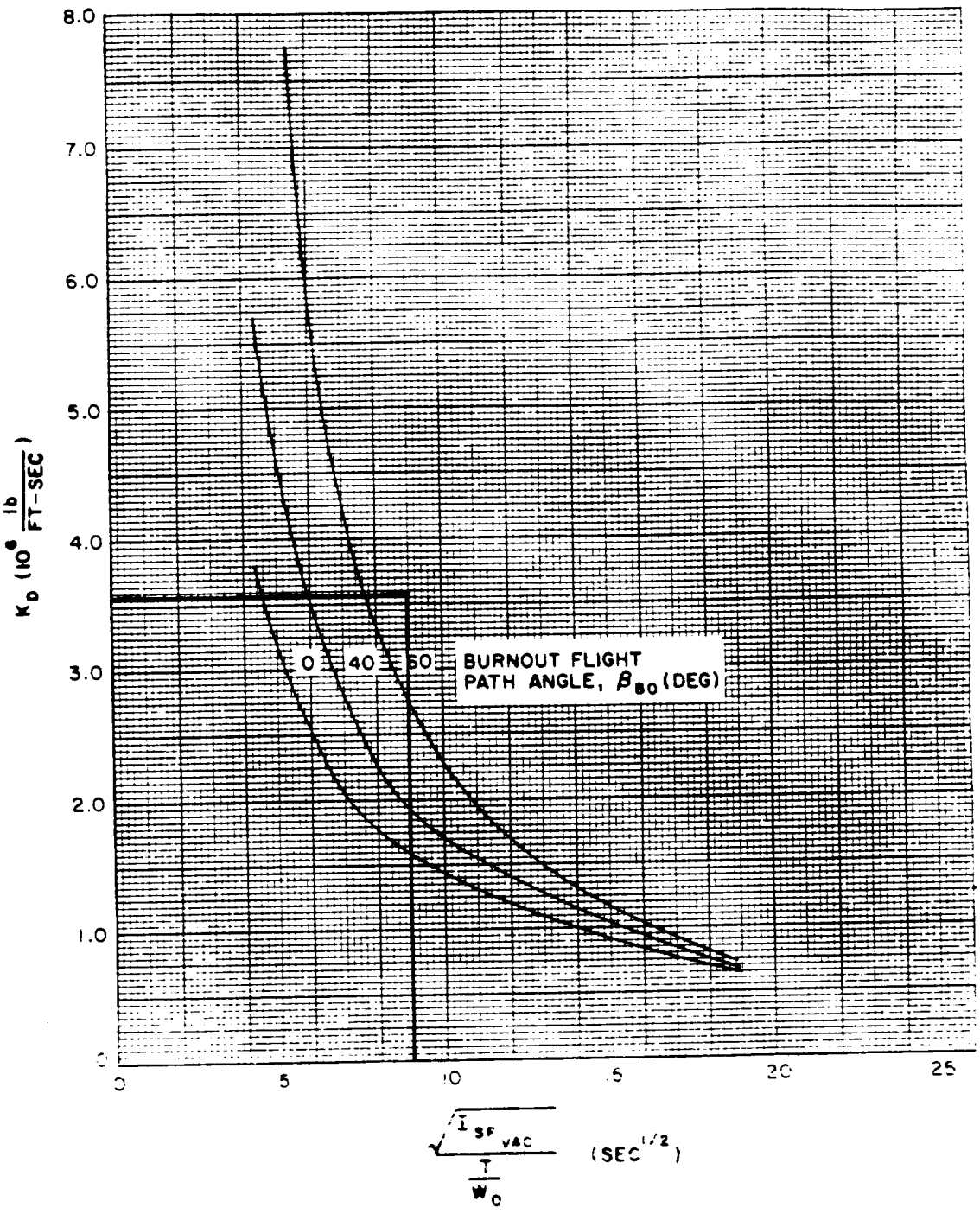

Figure 67. First-Stage Drag-Loss Constant

Figure B.5

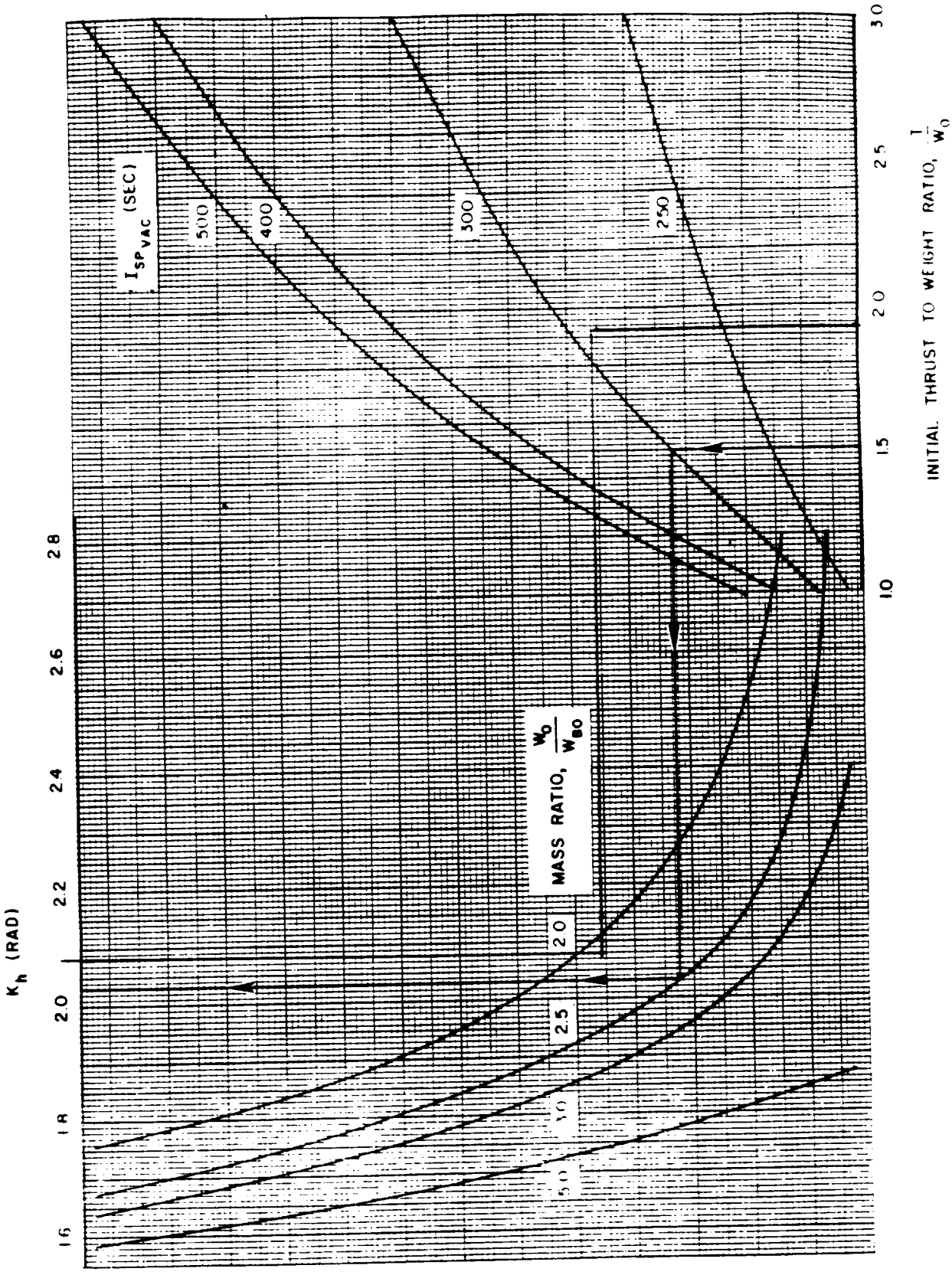

Figure 69. First-Stage Burnout Altitude Constant

Figure B.6

PROPULSION

Appendix C

C.1 ENGINE SPECIFICATIONS

Table C.1 Engine Comparison Data

Engine	Weight (lb)	Isp (sec)	Fuel	Max Thrust (lb)
Orbus 7s	7820	285	Solid	34,500
Orbus 21	22,700	294	Solid	44,700
Castor XX	34,900	295	Solid	107,880
RL10A-3-3A	310	444	Cryogenic	16,500
RL10A-4	370	449	Cryogenic	20,800
J-2	3350	425	Cryogenic	230,000

C.2 LR91-AJ-11 ENGINE DIAGRAMS

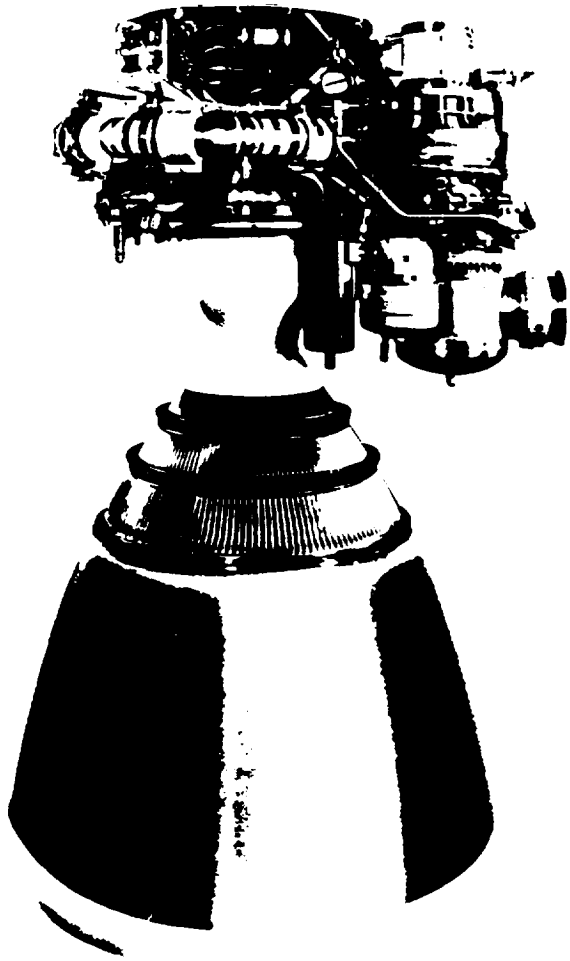

Figure C.1 Full View: LR91-AJ-11

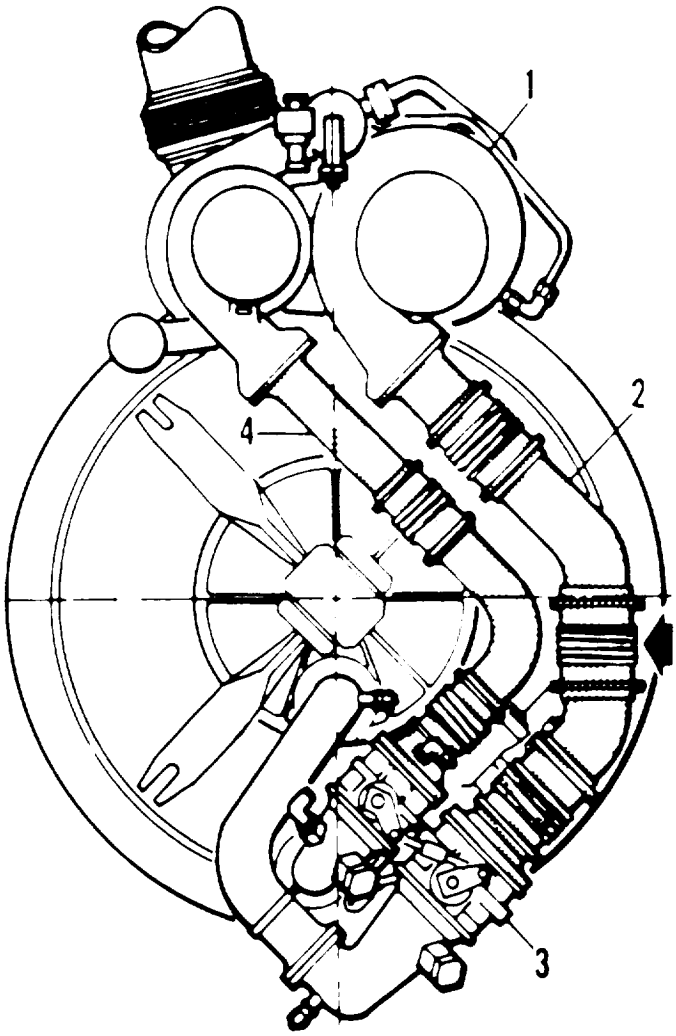

1. Turbopump Assembly
2. Oxidizer Discharge Line
3. Thrust Chamber Valves
4. Fuel Discharge Line

Figure C.2 LR91-AJ-11 Propellant Lines

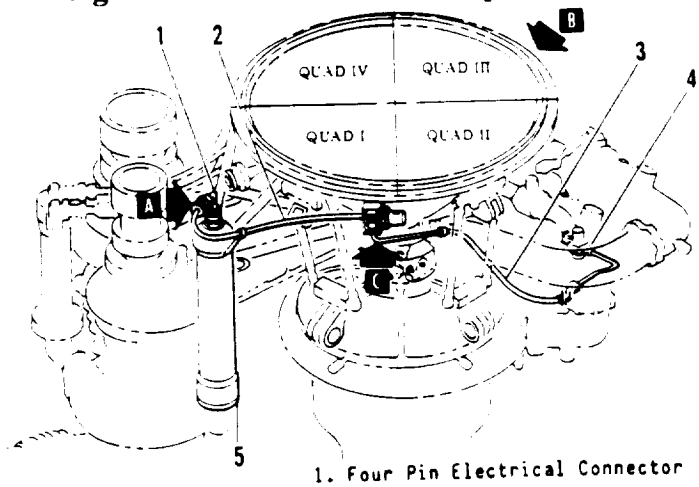

1. Four Pin Electrical Connector
2. Conduit
3. Conduit
4. FCPSV(OR) (Ref)
5. Start Cartridge (Ref)

Figure C.3 LR91-AJ-11 Engine Electrical Control

C.3 STAGING CALCULATIONS

Table C.2 Spreadsheet Program

Stage 3							
Payload & Interface	7900	lb					
Engine	360	lb	Isp	449	s	g*Tb	
Inert	2300	lb	E	0.239		5283	ft/s
Propellant	8460	lb	Tb	190.1	s	Angle	
Unused Fuel (2.5%)	212	lb				86	°
Final Weight	10772	lb	R	1.79		Loss	
Initial Weight	19232	lb	ΔV ideal	8374	ft/s	-347	ft/s

Stage 2							
Payload	19232	lb					
Engine	2600	lb	Isp	316	s	g*Tb	
Inert	5850	lb	E	0.050		7695	ft/s
Propellant	160000	lb	Tb	239.2	s	Angle	
Unused Fuel (2.5%)	4000	lb				86	°
Final Weight	31682	lb	R	6.18		Loss	
Initial Weight	191682	lb	ΔV ideal	18514	ft/s	-460	ft/s

Stage 1							
Payload	191682	lb					
Engines	18372	lb	Isp	295	s	g*Tb	
Inert	10500	lb	E	0.109		2510	ft/s
Propellant	242226	lb	Tb	78	s	Angle	
Unused Fuel (2.5%)	651	lb				76	°
Final Weight	220780	lb	R	2.14		Loss	
Initial Weight	473353	lb	ΔV ideal	7239	ft/s	-607	ft/s

Velocity Losses & Gains		
Drag	-261	ft/s
Earth rotation	1342	ft/s
Air launch	733	ft/s
Gravity	1740	ft/s

Velocity Reqiurements		
Velocity for GTO	7934	ft/s
Velocity for LEO	24934	ft/s
Final Velocity	32868	ft/s

Velocity Achieved		
V GTO	8026	ft/s
V LEO	26500	ft/s
V Total	37681	ft/s

PAYLOADS

Appendix D

D.1 SPACE STATION FREEDOM RESUPPLY MODULES

courtesy of Reference 94

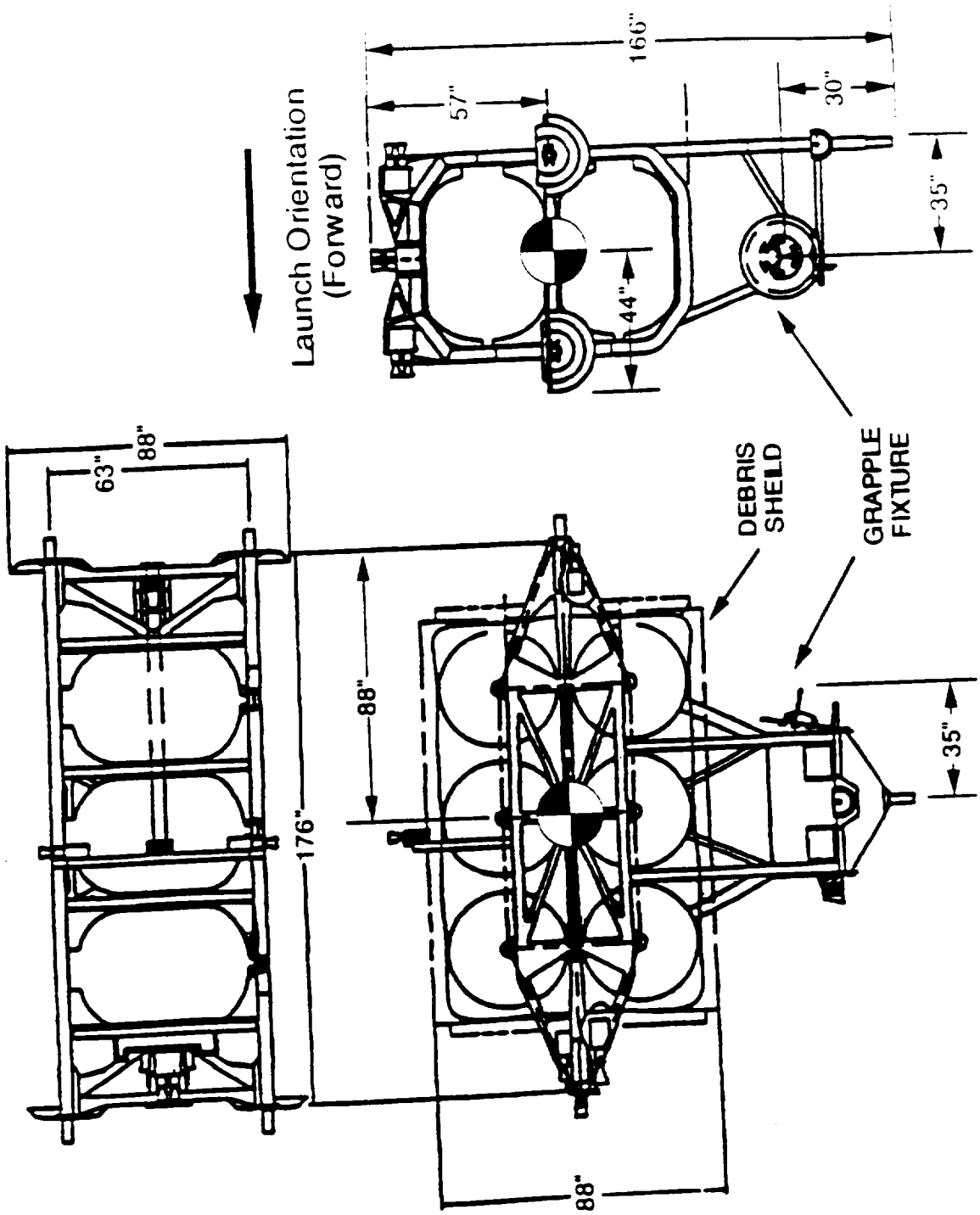

Dry Cargo Carrier

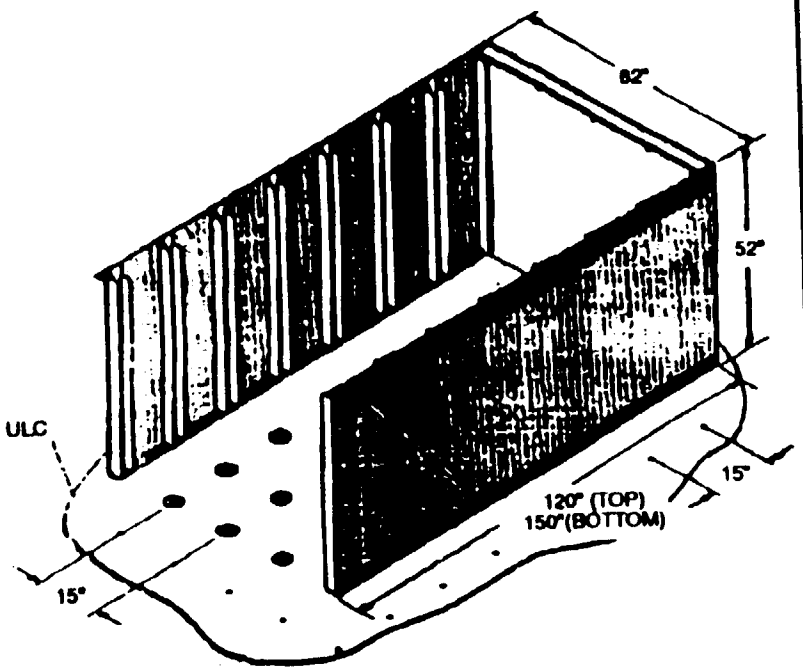

DCC STRUCTURE ONLY

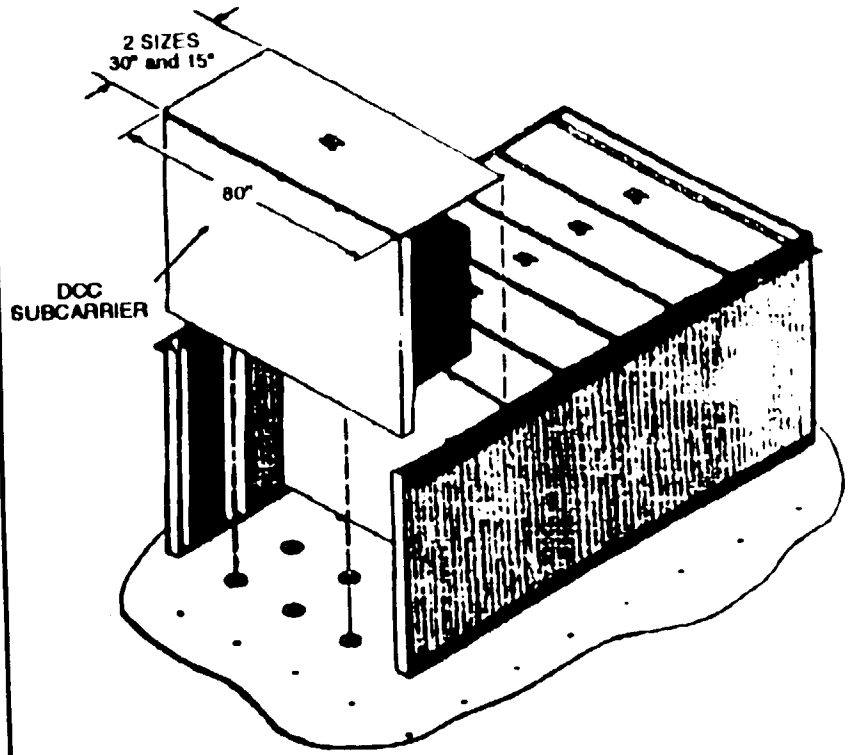

DCC STRUCTURE WITH SUBCARRIERS

- Center of Gravity (with cargo) located at center of volume

Cryogenic Fluid Carrier

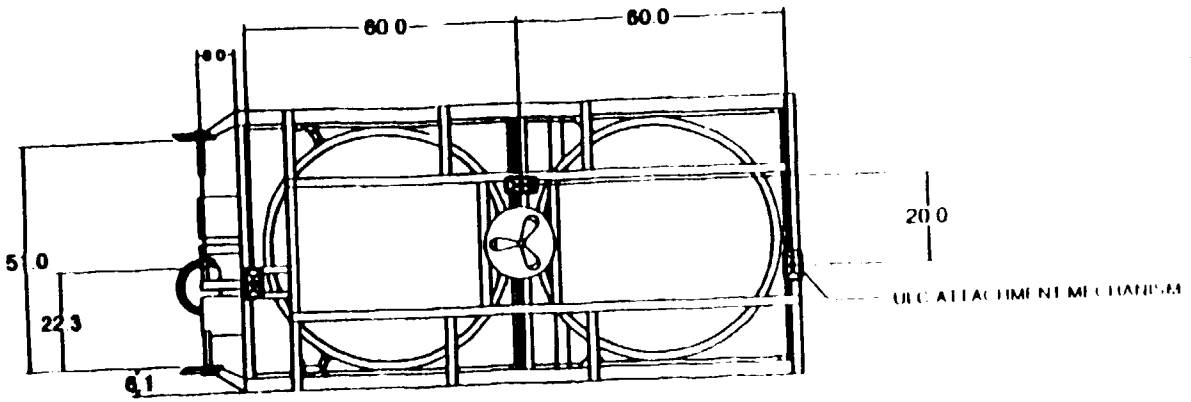

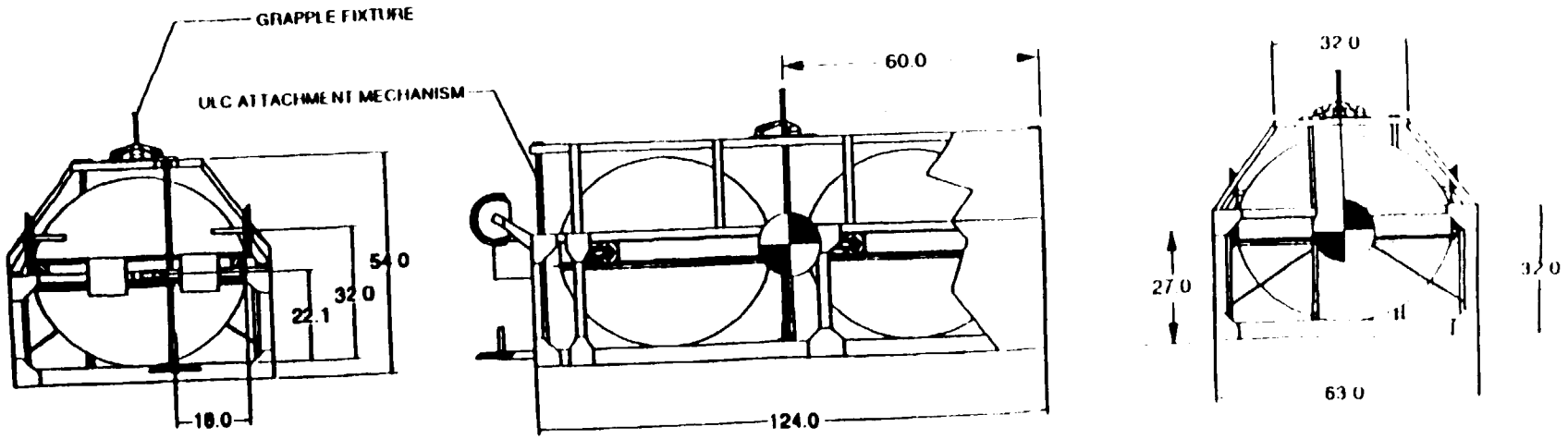

Note: All dimensions in inches

Unpressurized Logistics Carrier

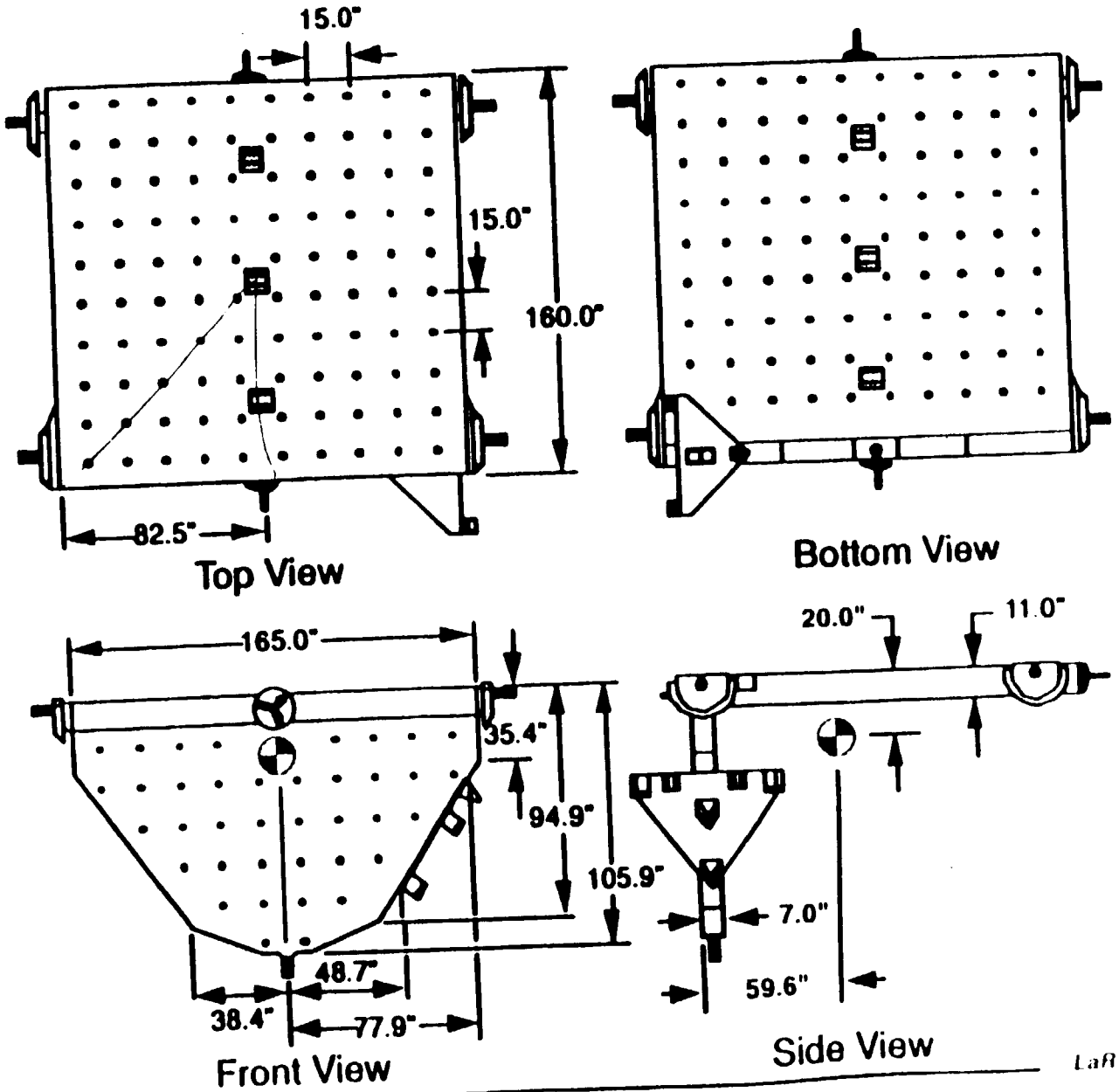

Mini-Pressurized Logistics Module

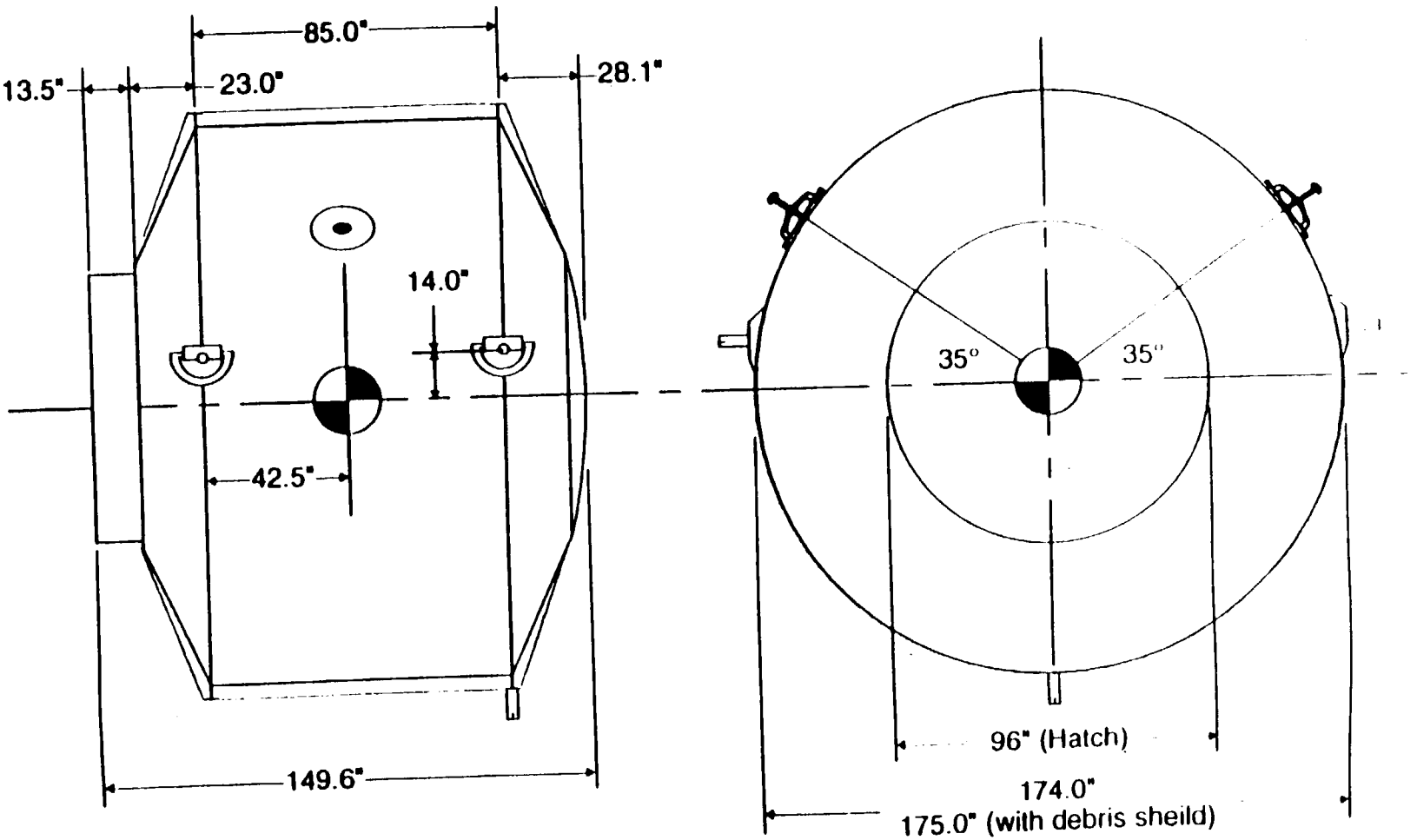

Pressurized Logistics Module

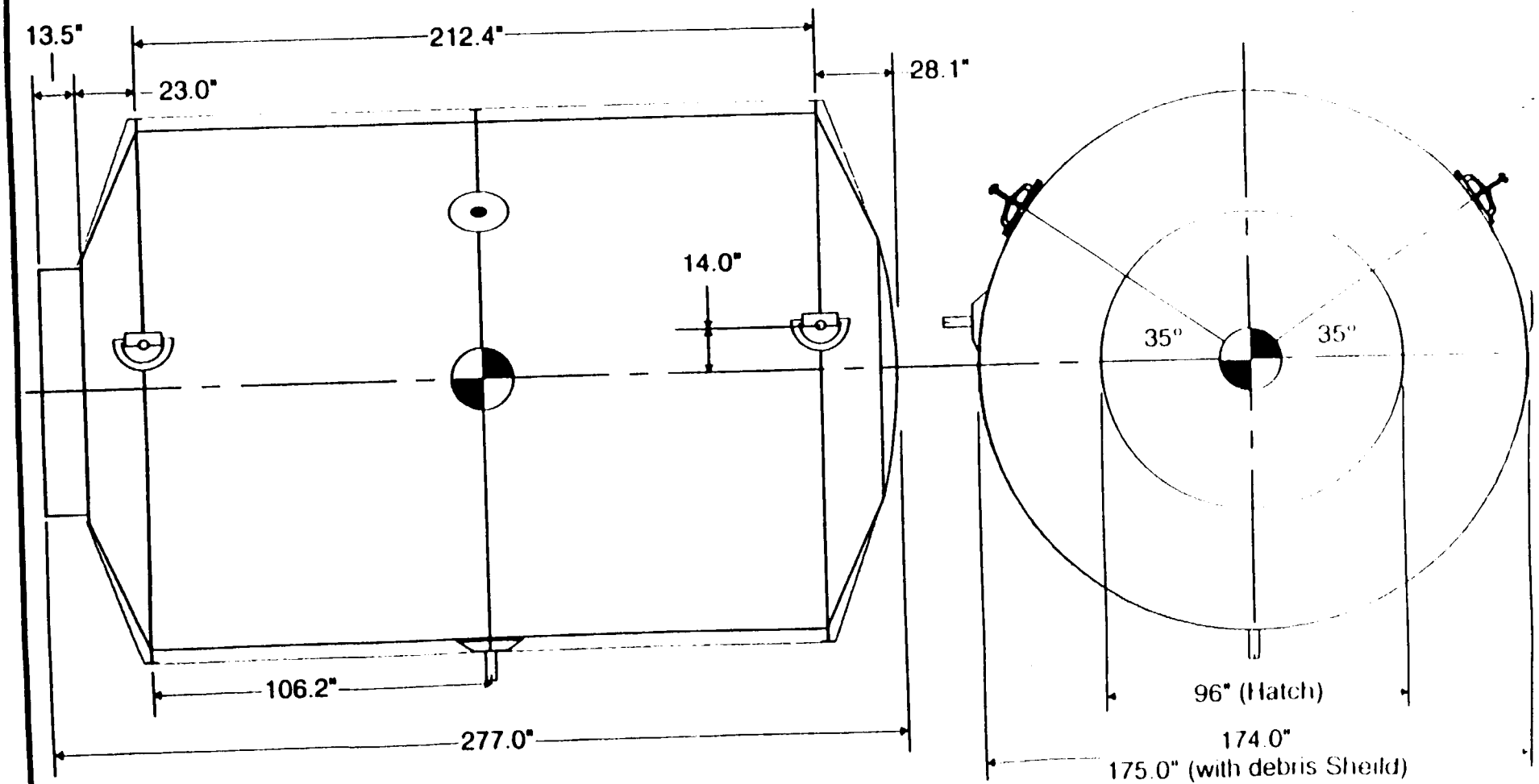

Pressurized Logistics Module

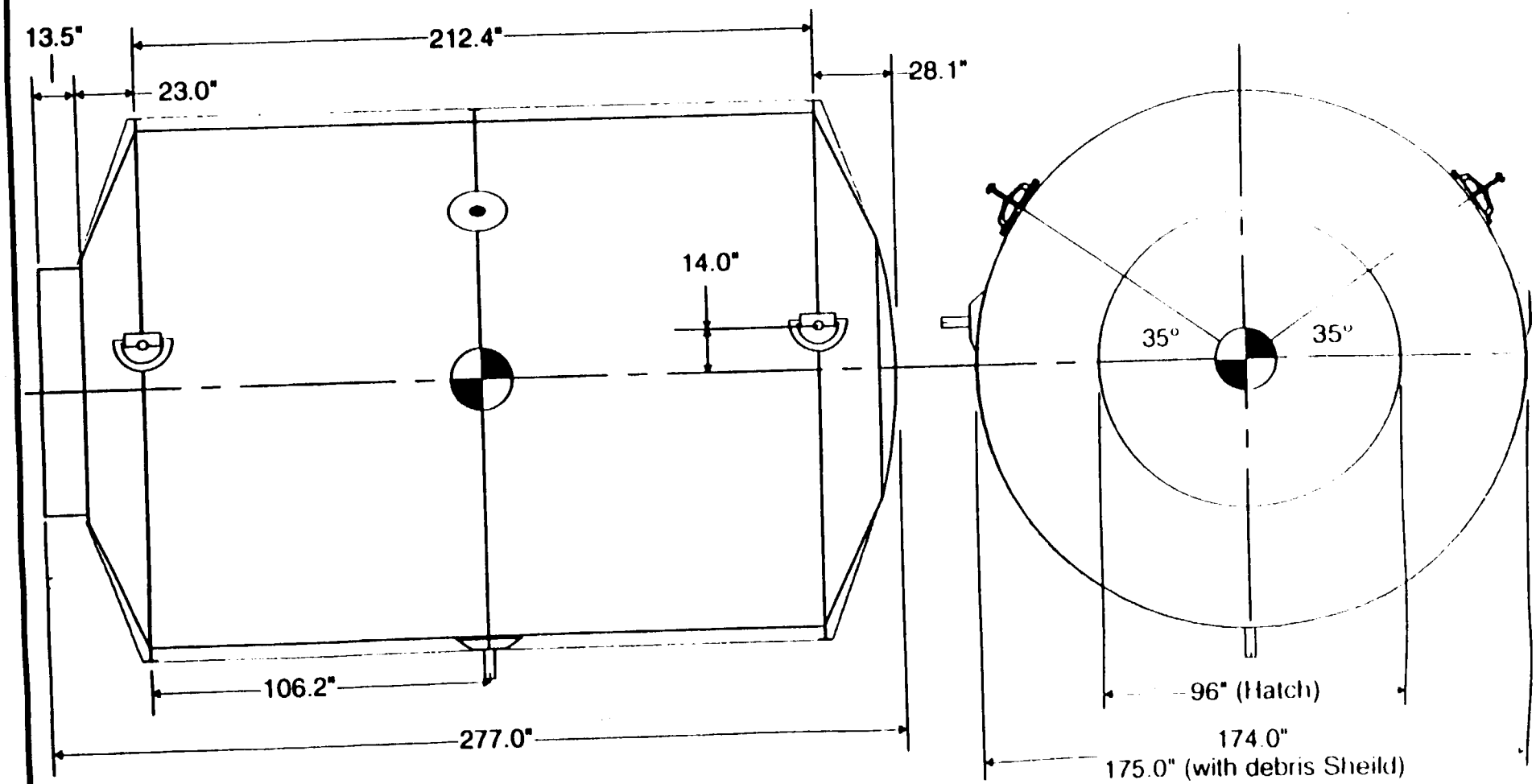

MISSION CONTROL

Appendix E

E.1 DATA RATE DETERMINATION

Data rate is defined as the quantity of data being relayed from the space craft to the ground. A high data rate indicates a large quantity of data transmitted with high accuracy. The major characteristics involved in calculating the required data rate are the number of bits per sample and the sampling period. Generally the greater the number of bits per sample the more accurately the word represents the data measurement. (See Table E.1)

Table E.1 Required Bits per Sample

Number of Bits per Sample	Maximum Quantization Error (%)
3	6.25
4	3.13
5	1.56
6	0.79
7	0.39
8	0.20
9	0.10
10	0.05
11	0.02
12	0.01

The sample rate for the telemetry data varies with measurement types. Parameters which change slowly need to be sampled at lower frequencies (once every 10 seconds) while critical or rapidly changing parameters need to be sampled at higher frequencies (10+ times per second). Table E.2 lists some typical sample frequencies. For telemetry, the sampling rate is calculated with:

f_s = sample rate (samples/seconds)
n = number of measurements (samples)
T_s = sampling period (seconds)

After determining these two factors, the data rate is determined by:

$$R = \text{Bits} \times f_s \qquad \text{(Eq E.1)}$$

where R is the data rate.

Table E.2 Typical Sampling Frequency Required to Transmit Analog Information Over Digital Communication Links

Analog Information	Frequency (Hz)	Frequency (samples/sec)
Voice (PCM*)	3600	8000
Voice (Delta PCM**)	3600	8000
Color Television (Commercial Quality)	4.0 M	8.8 M
Color Television (Broadcast Quality)	4.2 M	9.25 M
Low Rate Telemetry	---	10 samples / 1 sec
High Rate Telemetry	---	1000 samples /.1 sec

* digitized, or Pulse Code Modulated

** technique of reducing the bit rate of digitized voice by transmitting only the changes in amplitude between consecutive samples

For maximum accuracy and maximum quantity of data transmitted, the highest number of bits per sample and the high rate telemetry sampling rate were chosen.

With: Bits = 12 (bits per sample)
f_s = 1000 (samples per second)

The calculated data rate per transmitter is 12 kbps (kilobits per second). The Gryphon will carry one transmitter and one transponder (transmitter-receiver) for a system data rate of 24 kbps.

Communications Link Characteristics Calculations

Two important parameters in designing a communications subsystem are the power consumed and the mass. The link design process allows rough estimates for power and mass to be determined. The equation for determining the power needed by the transmitter is:

$$P = \frac{E_b}{N_0} - L_l - G_t - L_s - L_a - G_r - 228.6 + 10\log_{10}(T) + 10\log_{10}(R_0) \quad \text{(Eq E.2)}$$

where:

P	=	transmitter power (dBW)
$\frac{E_b}{N_0}$	=	signal-to-noise ratio (dB)
L_l	=	line loss (dB)
G_t	=	transmitting antenna gain (dB)
L_s	=	space loss (dB)
L_a	=	attenuation loss (dB)
G_r	=	receiving antenna gain (dB)
T	=	system noise temperature (K)
R_0	=	data rate (bps) = 24 kbps

The relation:

$$A = 10\log_{10}(A)$$

converts a quantity into decibels (dB).

Signal-to-Noise Ratio

Signal-to-noise ratio (SNR) can be predetermined by specifying the desired Bit Error Rate (BER). BER is the probability of receiving erroneous bits in the signal. For highly accurate data a BER of 10^{-6} (1 error per million bits) is an acceptable estimation. The higher the SNR the better the quantity of the received signal. From curves of various modulation techniques plus the fact that an additional 1 to 3 dB must be added to the final SNR value for error correction, a value for SNR can be estimated. For better signal quality choose:

$$SNR = \frac{E_b}{N_o} \approx 14 \qquad \text{(Eq E.4)}$$

Line Loss

Line loss accounts for the transmitter to antenna reduction in power. The value is usually between -1 and -3 dB when estimated conservatively:

$$L_l = -3\text{dB}$$

Transmitting Antenna Gain

The transmitting antenna gain can be calculated from:

$$G = \frac{\pi^2 D^2 \eta}{\lambda^2} \qquad \text{(Eq E.5)}$$

where:

	G	=	antenna gain (dB)
	D	=	aperture diameter (cm)
	η	=	antenna efficiency (.55 - .70)
	λ	=	signal wavelength (cm)

The aperture diameter is determined by first choosing the antenna type. An omni-directional antenna was chosen to spare the weight of the attitude control system necessary for a directional antenna and for flight planning flexibility. For the omen-directional antenna types, two options were available: (1) biconical horn and (2) quad-helix. The biconical horn (one horn each for S and C bands) assembly was investigated. The aperture diameter was determined from:

$$D = \frac{225\lambda}{\theta_b \pi} \qquad \text{(Eq E.6)}$$

where: λ = band wavelength
= 11.5 cm for S band (2.6 GHz)
= 0.6 cm for C band (5 GHz)
θ_b = beam width (angle within which the signal is concentrated)

and:
$$\tan\frac{\theta}{2} = \frac{R}{h} \qquad \text{(Eq E.7)}$$

R_e = earth radius ≈ 4144 miles
h = operating altitude ≈ 23000 miles (GTO orbit)

With these values the aperture diameters:

$D_{S\text{-band horn}}$ = 40 cm
$D_{C\text{-band horn}}$ = 2.1 cm

Assume a conservative antenna efficiency:

$$\eta = 0.55$$

The antennae gains are:

$G_{S\text{-band}}$ = 65.6 dB
$G_{C\text{-band}}$ = 66.43 dB

Space Loss

Space loss represents the loss of power due to signal path length. It is estimated from:

$$L_s = \frac{c}{4\pi l f} \qquad \text{(Eq E.8)}$$

where: L_s = space loss (dB)
c = speed of light (cm/s)
l = path length from receiver to transmitter (cm)
f = frequency of transmitted signal (Hz)

path length, l, was determined to be:

$$l = \left[x^2 + h^2\right]^{\frac{1}{2}} \qquad \text{(Eq E.9)}$$

where: x = operating radius = 1500 miles
h = operating altitude = 23000 miles (GTO orbit)

The space loss was determined to be:

$$L_{s,\,S\text{-band}} = 2.47 \times 10^{-10} \approx 0$$
$$L_{s,\,C\text{-band}} = 1.29 \times 10^{-10} \approx 0$$

Attenuation Loss

The antenna loss is mainly due to rain attenuation. This value was approximated with the Crane Model which determines antenna loss given a certain signal frequency. It predicts no antenna loss:

$$L_a = 0$$

for both S-band and C-band frequencies.

Receiving Antenna Gain

The receiving antenna gain will be identical to the transmitting antenna gain.

System Noise Temperature

The system noise contributes to overall degradation of the signal. It embodies antenna noise, line noise, and receiver noise. From tables of typical noise temperatures for various downlink frequencies:

$$T = 552\ K$$

Power

From the above factors the input power needed for each transmitter is:

$$P \approx 275\ W$$

Thus a total system power requirement of:

$$P_{total} \approx 550\ W$$

System Mass Estimate

The system mass was estimated at:

$$\text{System Mass} \approx 50\ kg$$

for each transmitter. Thus a total system mass of:

$$\text{Total System Mass} \approx 220\ LB$$

STRUCTURES

Appendix F

Appendix F.1 Main Booster Element Forces

SDRC I-DEAS VI: FE_Modeling_&_Analysis

10-APR-93 18:48:29

Database: junk
View : No stored View
Task: Post Processing
Model: 1-FE MODEL1

Units : IN
Display : No stored Option
Model Bin: 1-MAIN
Associated Workset: 1-WORKING_SET1

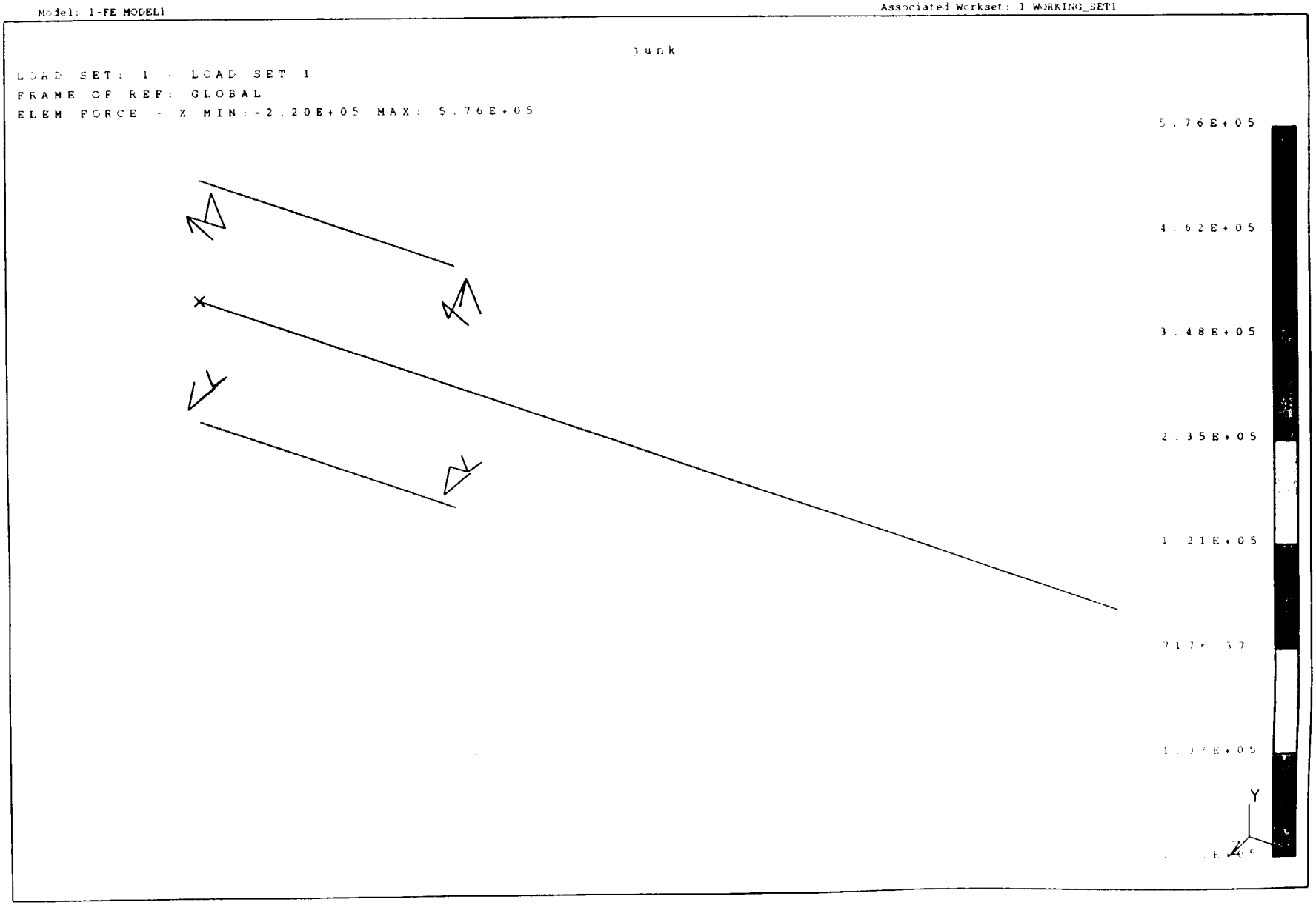

SDRC I-DEAS VI: FE_Modeling_&_Analysis

10-APR-93 15:49:56
Units : IN

Database: junk
View : No stored View
Task: Post Processing
Model: 1-FE MODEL1

Display : No stored option
Model Bin: 1-MAIN
Associated Workset: 1-WORKING SET1

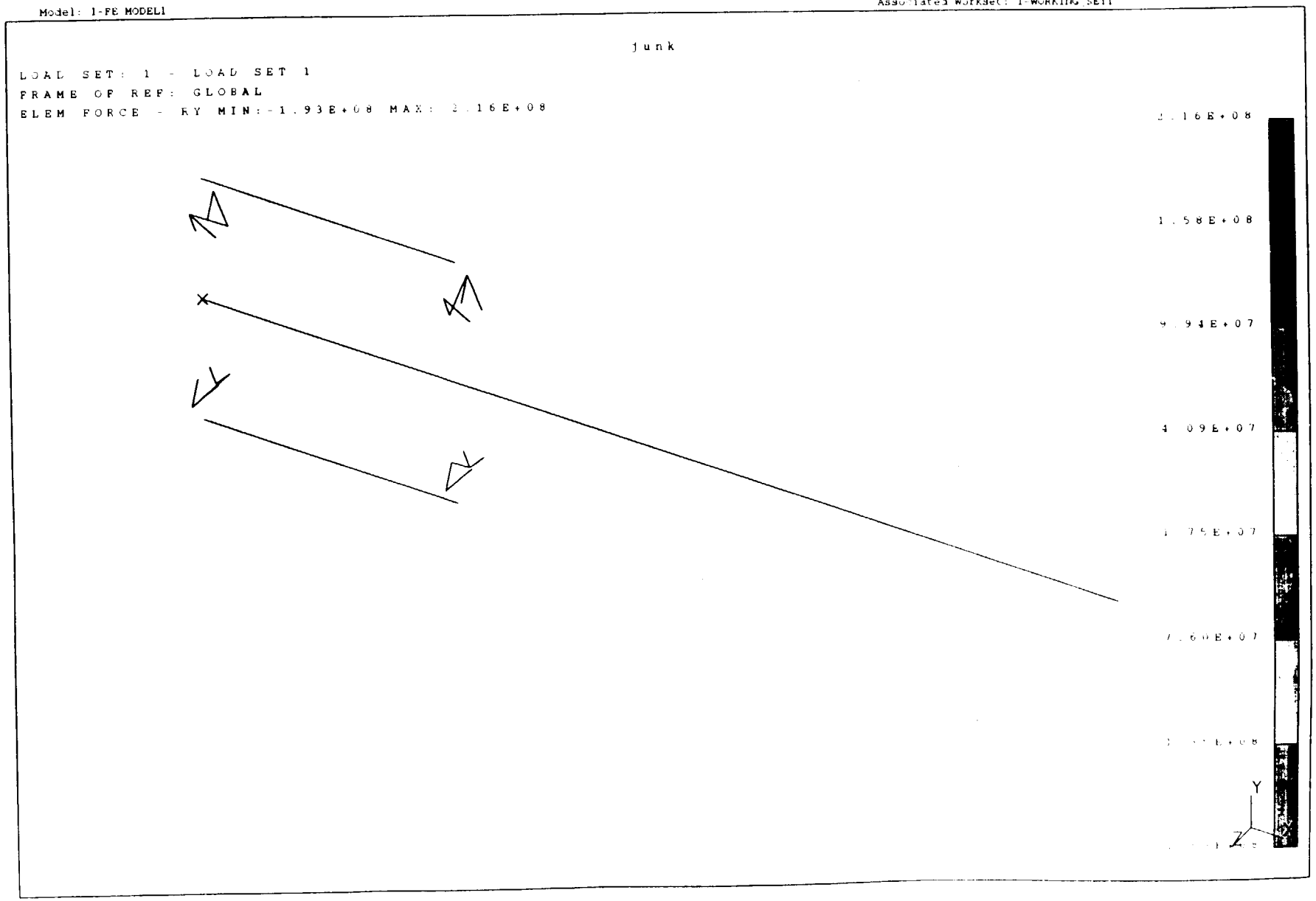

F.2 MOMENT AND SHEAR DIAGRAM CALCULATIONS

To analyze this structure shear and moment diagrams were needed. To create these diagrams, it was necessary to compute all of the external loading on the Gryphon. The body of the Gryphon was split into three separate 'effective' masses. This was done to allow a separate calculation of mass at each of the three stages, and to obtain a more accurate distributed loading for the lateral and longitudinal calculations. The model of this system is shown in Figure F.1. To calculate the values for shear and moment, the five different points shown in Figure F.1 were used. These points correspond to the center of mass, the total center of mass and the center of pressure for stages the 1,2 and 3

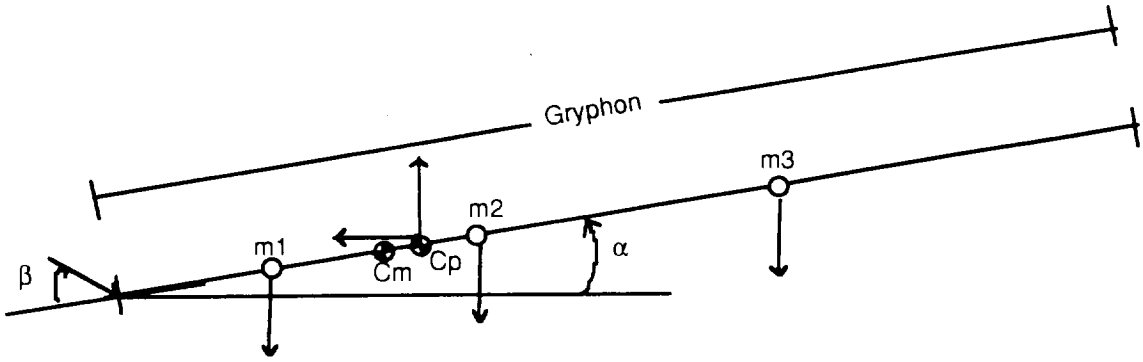

Figure F.1 Diagram of model used to do analysis on Gryphon.

The effective center of pressure (C_p) was calculated by mission analysis and found to be at 31 feet from the bottom of the first stage nozzle. From the mission analysis trajectory, a lateral load of twice the amount of Earth's gravity (2g's) was used. In this analysis, the 'worst' case loading scenarios of lift (L), drag (D) and nozzle gimbal angle (β) were used. Lateral and Longitudinal loading values are given in Table F.1 and the total loading for this model is given in Table F.2. These are the numbers used in calculating the moment and shear.

Table F.1 Lateral and Longitudinal loading values for Gryphon

	mass (lb_m)	accel. ($\frac{ft}{s^2}$)	Force (lb_f)
Lateral	$m_1 = 8217$	a = 2(32.2)	F = 529200
	$m_2 = 5348$	a = 2(32.2)	F = 344380
	$m_3 = 801$	a = 2(32.2)	F = 51584
Longitudinal	$m_1 = 8217$	a = 32.2	F = 264600
	$m_2 = 5348$	a = 32.2	F = 172190
	$m_3 = 801$	a = 32.2	F = 25792

Table F.2 Total loading values for Gryphon

Totals:	$F_1 = 926100\ lb_f$
	$F_2 = 602665\ lb_f$
	$F_3 = 90272\ lb_f$
	$D = 165000\ lb_f$
	$L = 12800\ lb_f$

Based on information given by mission analysis, the maximum aerodynamic loading was used.

Having calculated all of the loading on the Gryphon it was possible to calculate the shear and moment at any point along the structure. Using various angle of attacks and nozzle gimbal angles it was found through trial and error that an α of 0 and a β of 10 made the moment maximum. This maximum moment acts (as it should in theory) at the center of mass of the entire structure. The shear and moment diagrams are givenin Figure F.2 and F.3. It is seen that the maximum moment is located at the center of mass of the Gryphon and its value is $-14.6 \times 10^6\ lb_f$-ft. The moment diagram was used to calculate the maximum stress at each stage and interstage. Some stages could be designed to take a lesser load, and therefore, save weight, because the highest moment on that stage was less than the maximum moment at the center of mass.

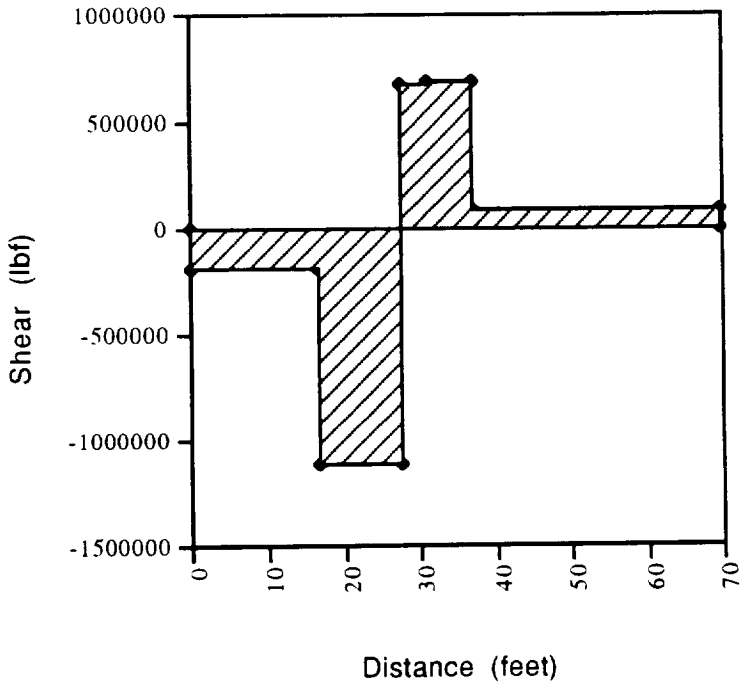

Figure F.2 Shear diagram of Gryphon

This preliminary model gave us the shears and moments along the body of the Gryphon. This lead to current configurations and design for the finite element model done on IDEAS.

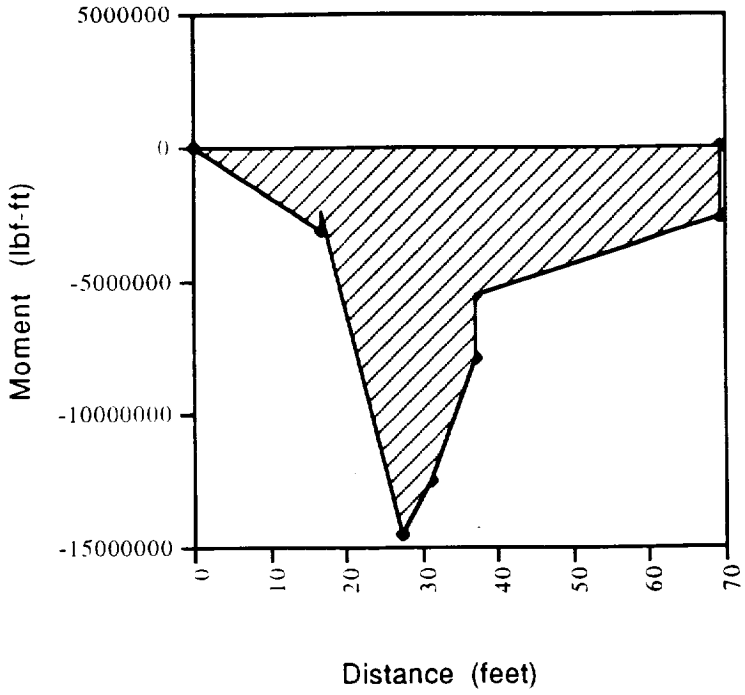

Figure F.3 Moment diagram of Gryphon

Appendix F.3 Main Booster Buckling Modes

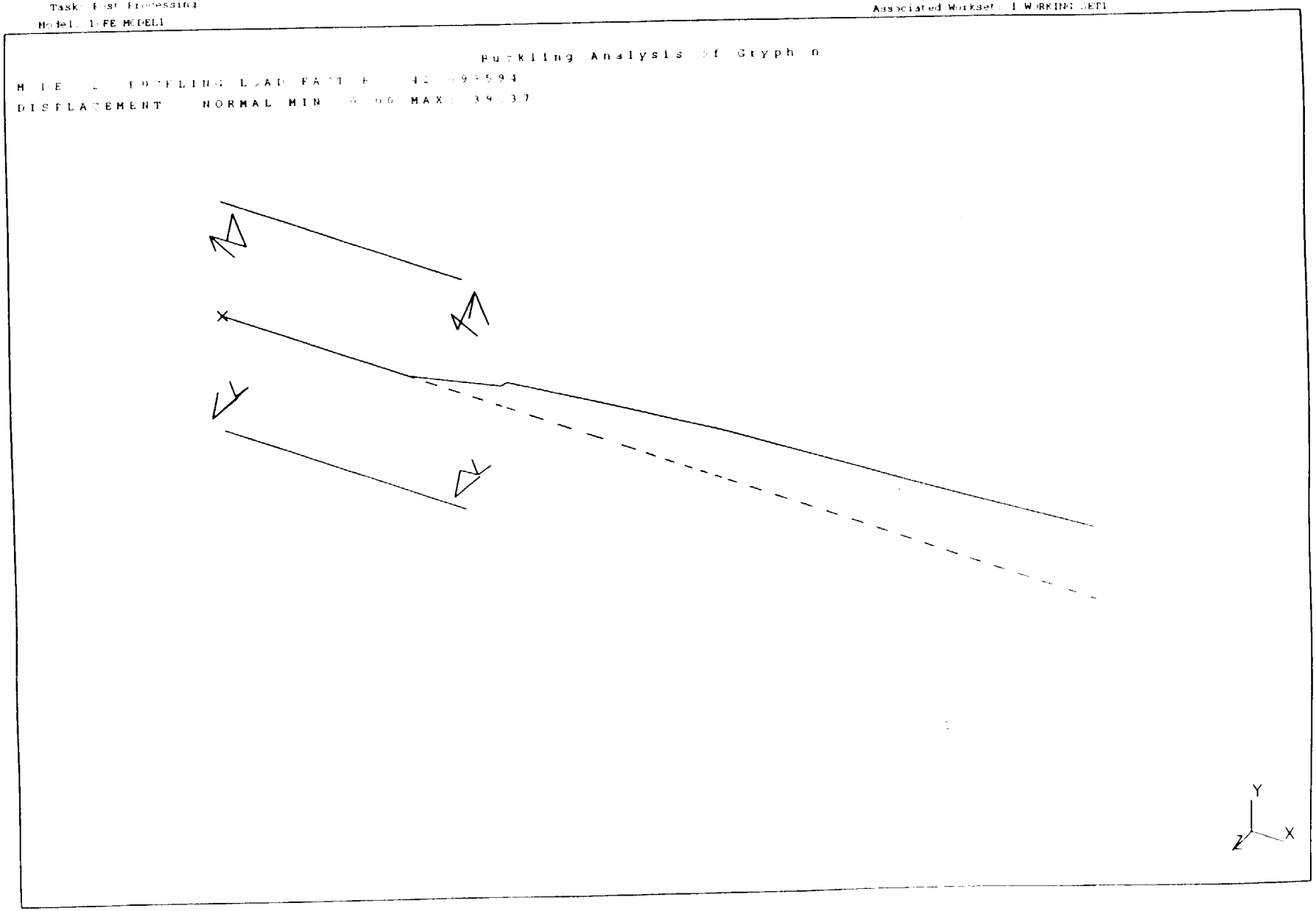

Buckling Analysis of Gryphon

MODE : BUCKLING LOAD FACTOR : 1.94E+08

DISPLACEMENT NORMAL MIN : 0.00 MAX : 39.37

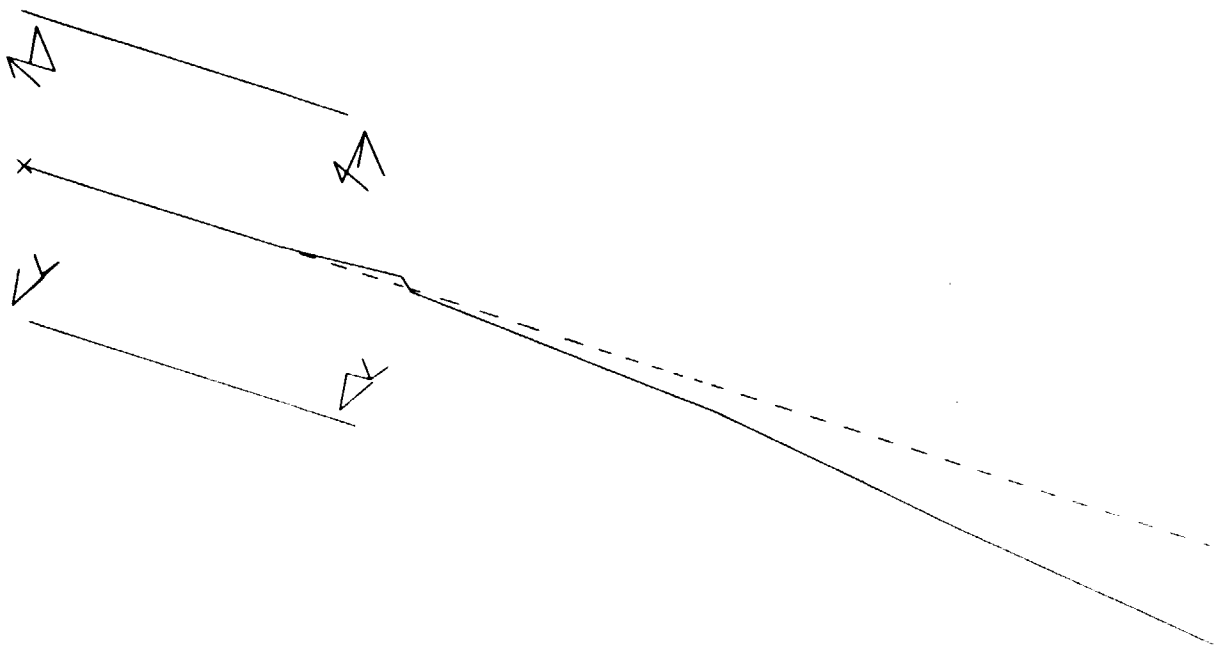

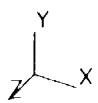

Appendix F.4 Main Booster Free Vibration Modes

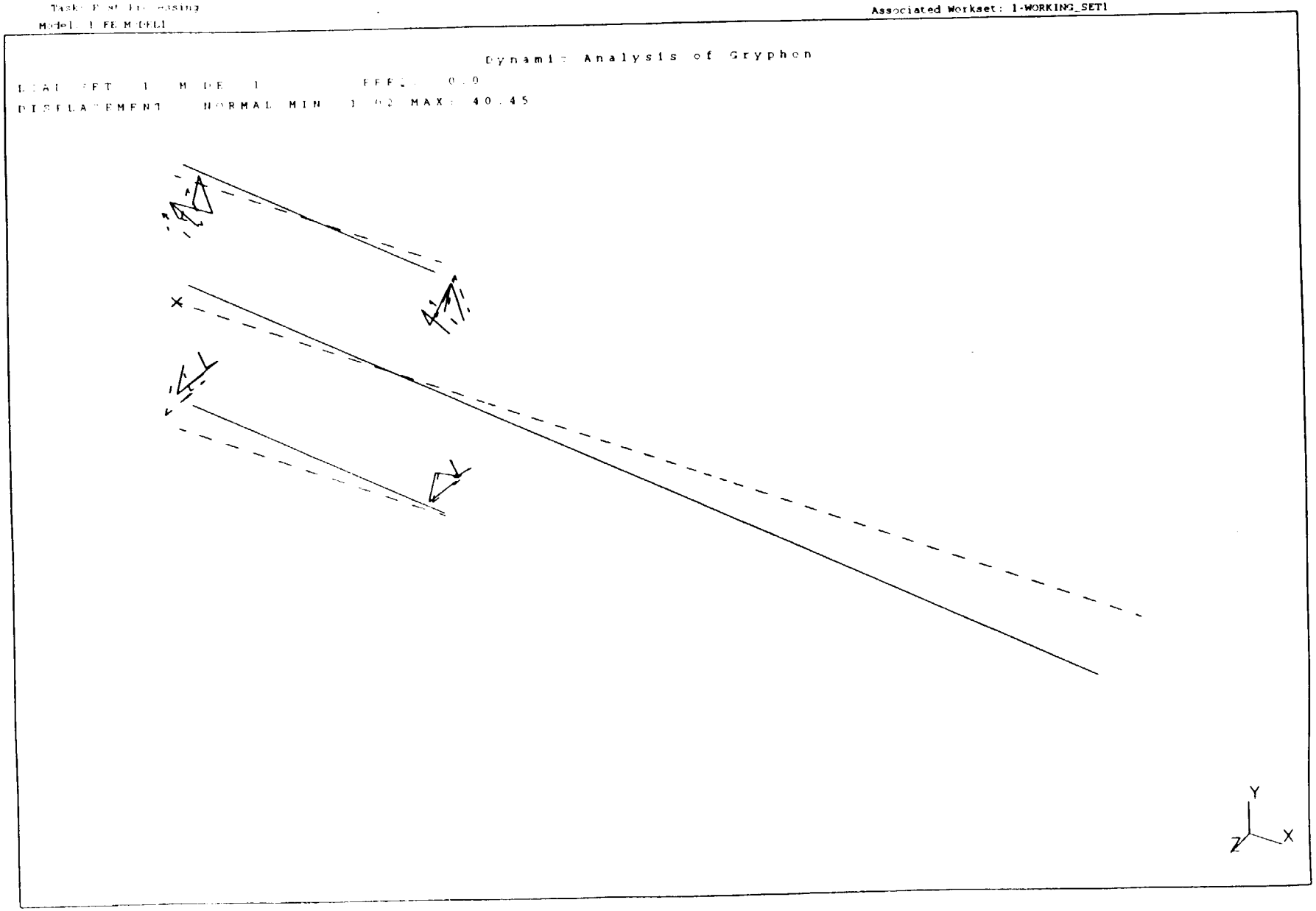

Dynamic Analysis of Gryphon

DISPLACEMENT NORMAL MIN: 4.99 MAX: 40.26

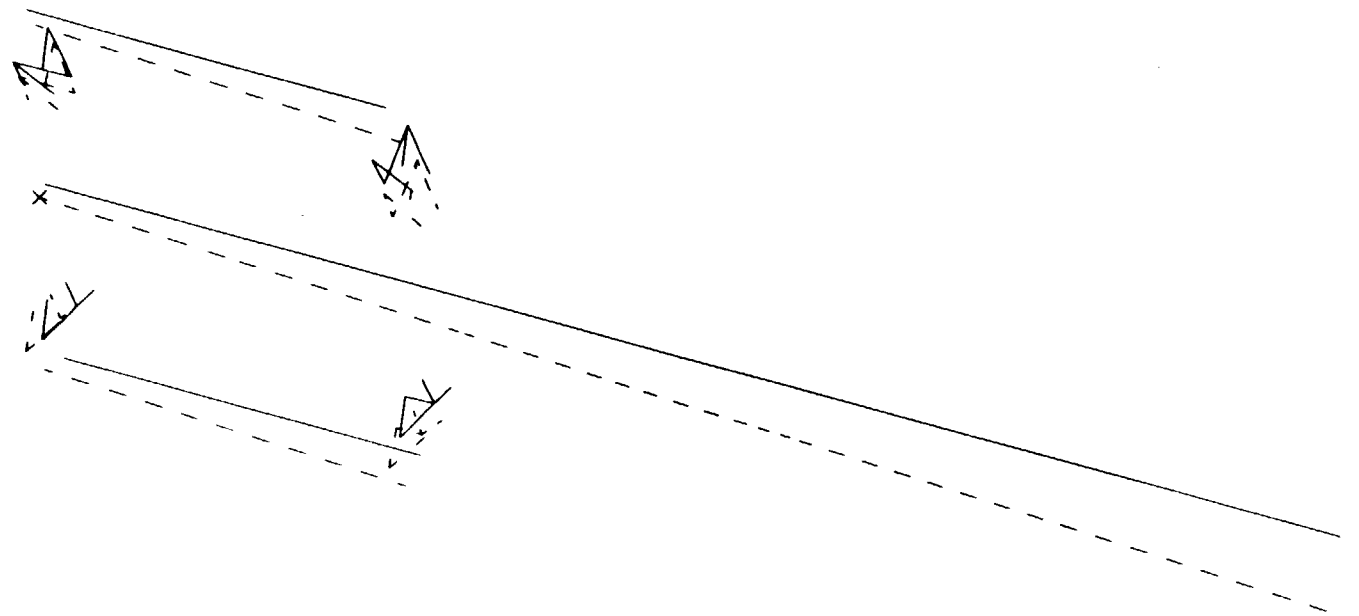

10 APR 93 19:15:08

Units : IN

Database: Dynamic Analysis of Gryphon
View : No stored View
Task: Post FE Processing
Model: 1-FE MODEL1

Display : No stored Option
Model Bin: 1-MAIN
Associated Workset: 1-WORKING_SET1

Dynamic Analysis of Gryphon

LOAD SET: 1 MODE: 4 FREQ: 9.9
DISPLACEMENT NORMAL MIN: 1.07 MAX: 43.46

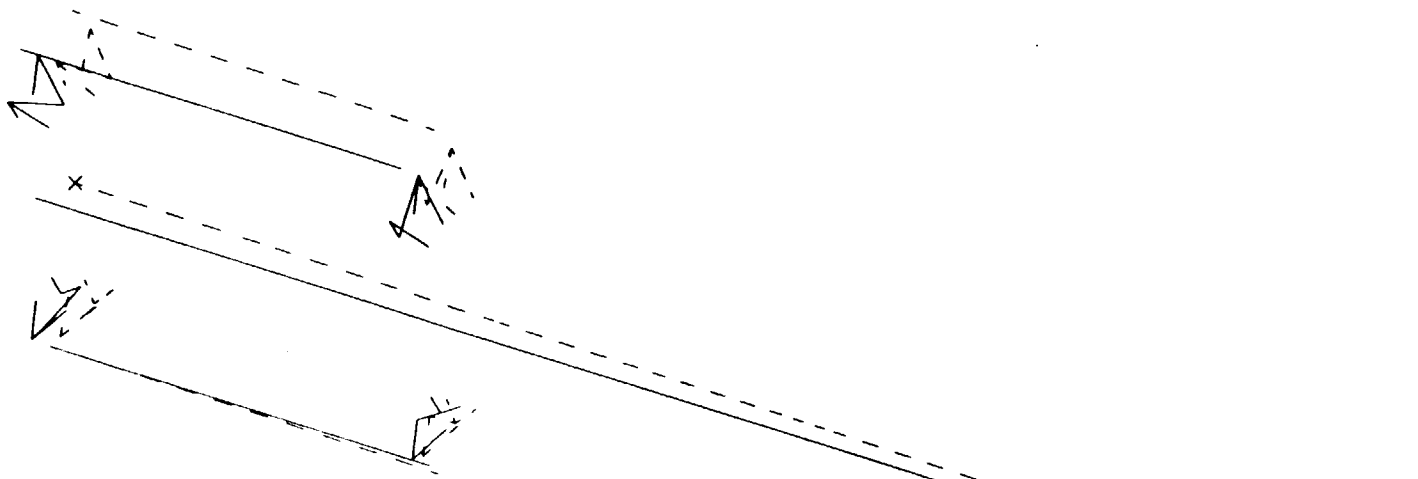

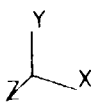

Dynamic Analysis of Gryphon

LOAD SET 5 MODE 5 FREQ: 0.0
DISPLACEMENT NORMAL MIN: 35.52 MAX: 42.20

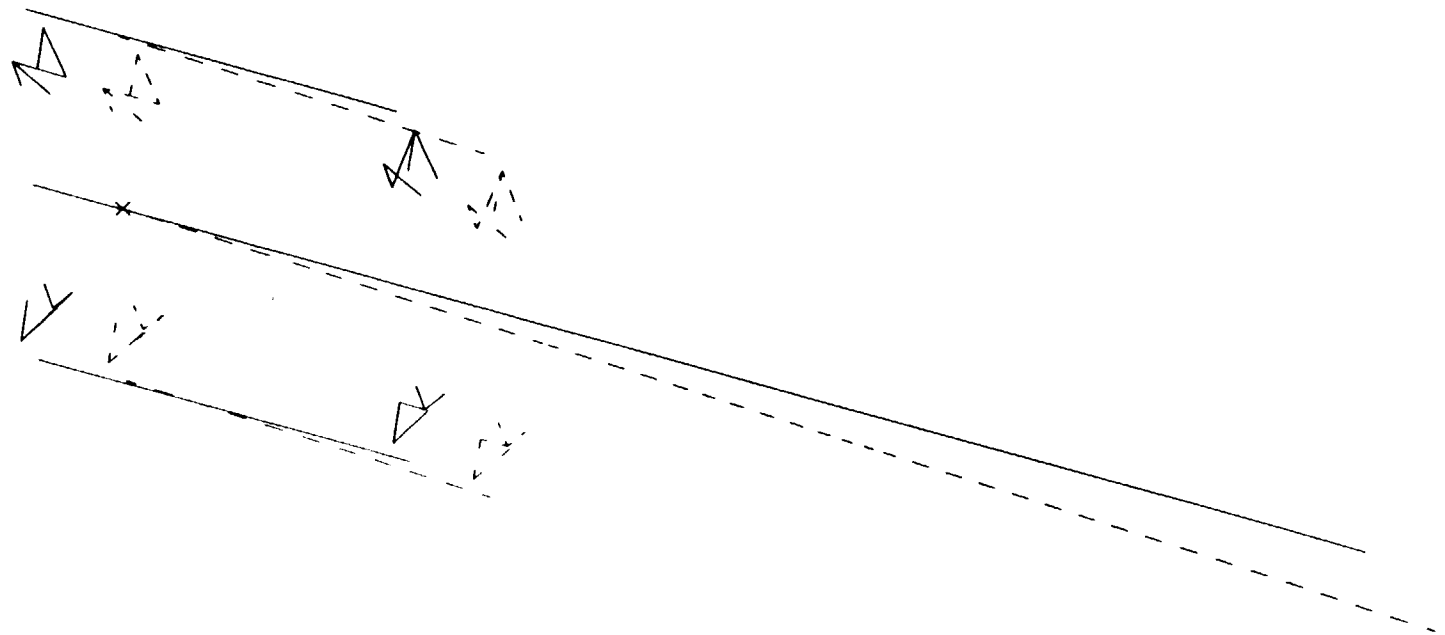

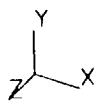

Database: Dynamic Analysis of Gryphon
View : No stored View
Task: Post Processing
Model: 1-FE MODEL1

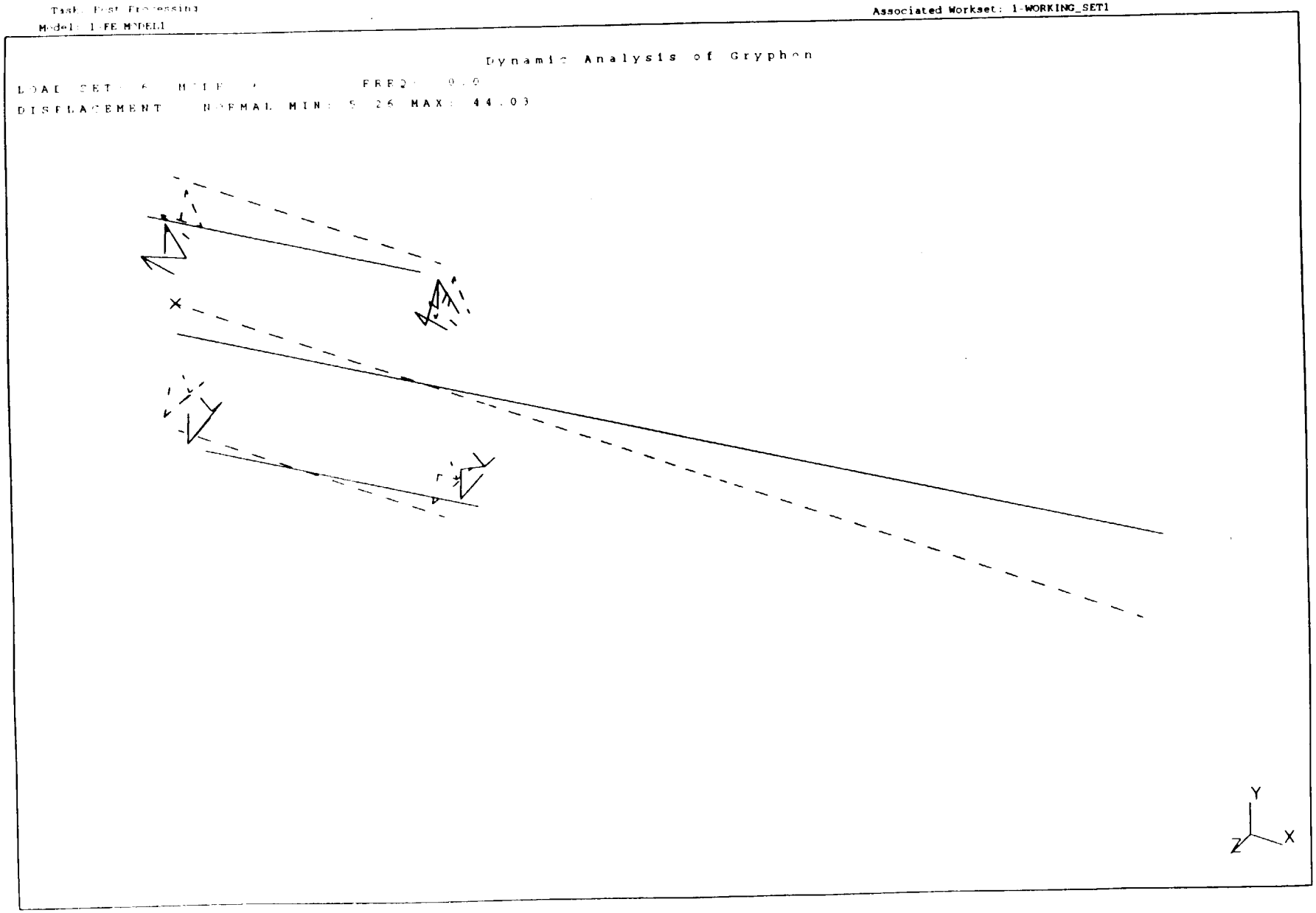

SDRC I DEAS VI: FE_Modeling_&_Analysis 10-APR-93 19:18:48

Database: Dynamic Analysis of Gryphon
View : No stored View
Task: Post Processing
Model: 1-FE MODEL1

Units : IN
Display : No stored Option
Model Bin: 1-MAIN
Associated Workset: 1-WORKING_SET1

Dynamic Analysis of Gryphon

LOAD SET: 7 MODE: 7 FREQ: 4.245739
DISPLACEMENT - NORMAL MIN: 0.045136 MAX: 39.37

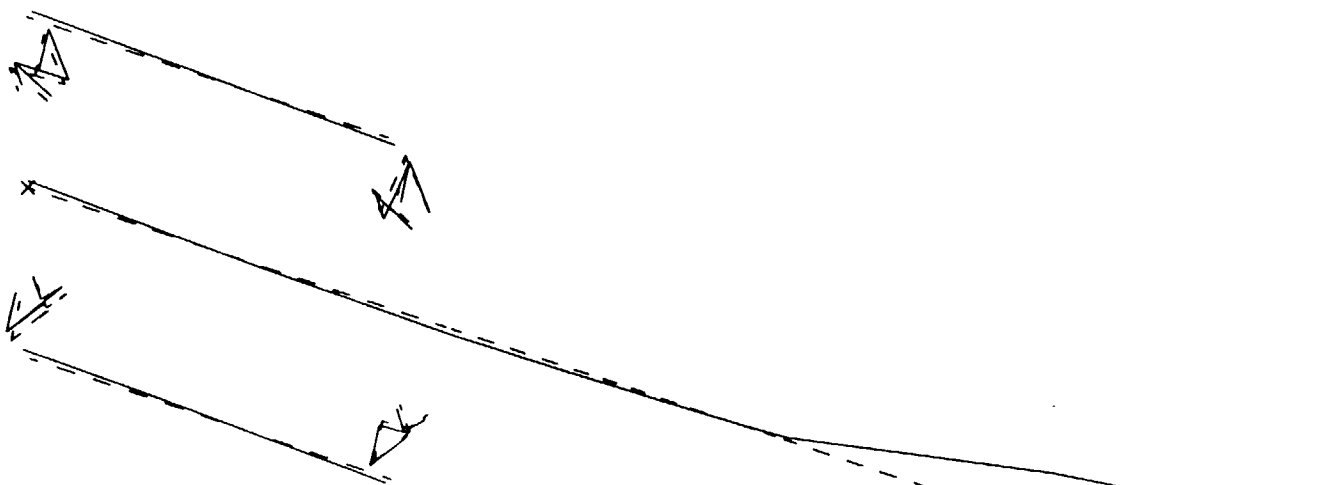

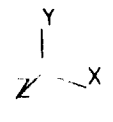

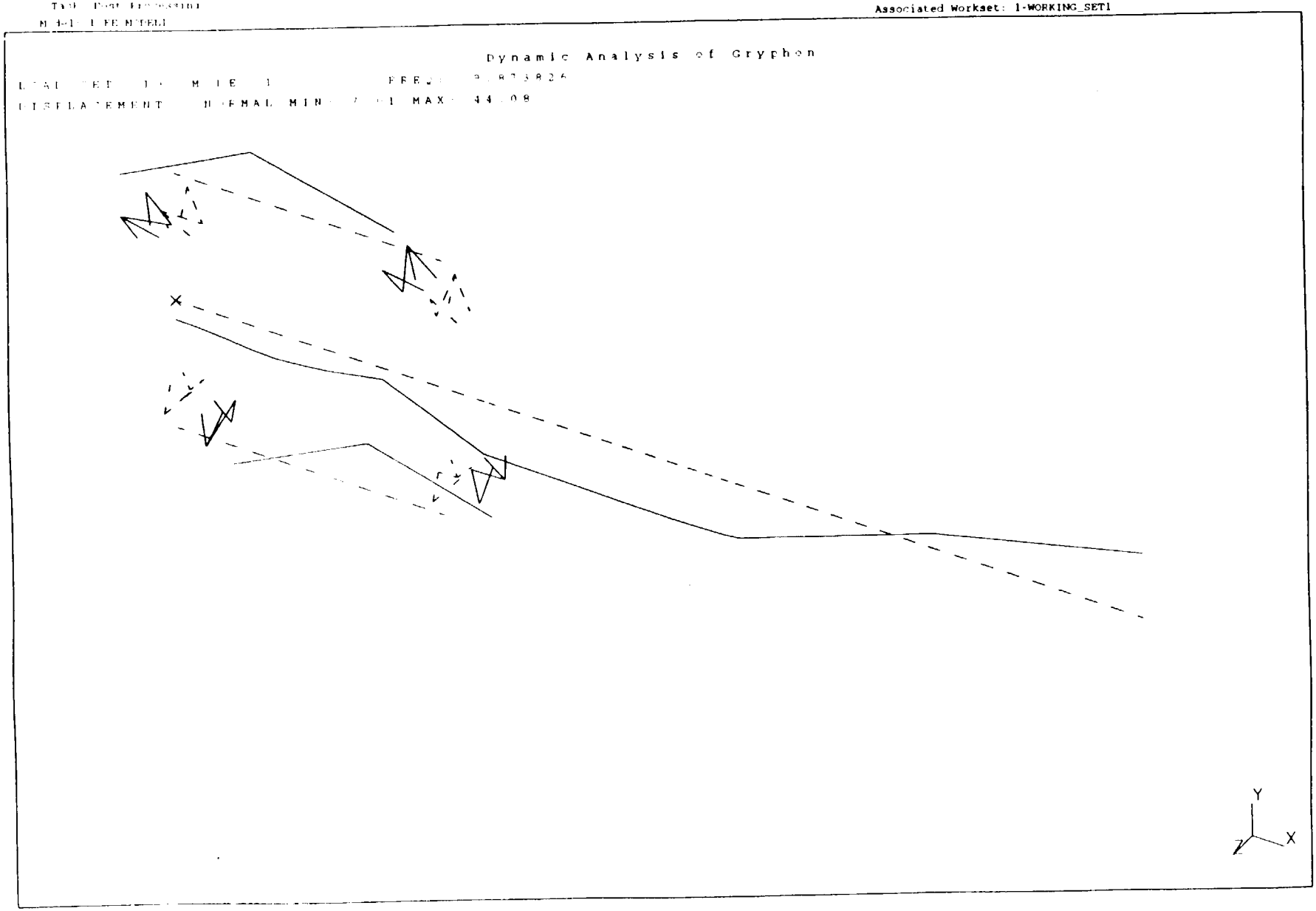

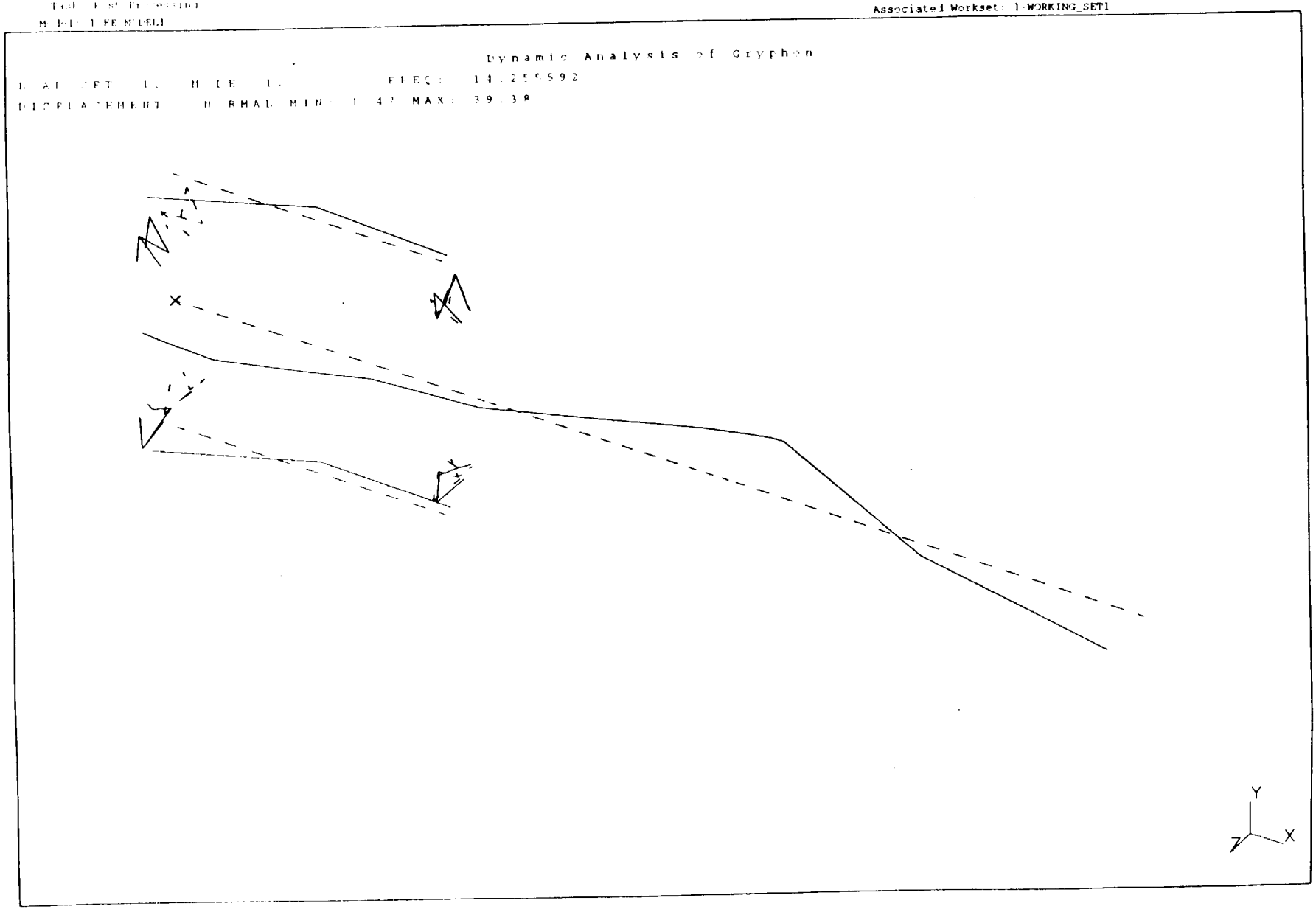

Appendix F.5 Composite FORTRAN Program

```
C       ......THIS PROGRAM COMPUTES THE A,B,D MATRICES.....
C       ......FOR A LAMINATE WITH ORTHOTROPIC LAMINAE.....
C       ........OF UP TO 10 MATERIAL PROPERTY TABLES.....
C
C       THE DATA FILE MUST CONTAIN:
C          1. Code specifying type of material data:
C               1=Use Engineering Props -
C                  E11,E22,NU12,NU21,G12
C               2=Use Q-Matrix
C                  Q11,Q12,Q22,Q33
C             *note that data for each must be present
C          2. The total number of plies (n)
C          3. The total number of material properties (m)
C          4. The engineering properties for each mater (5)
C          5. The Q matrix for each material
C          6. A table of plies listing information f/top
C             to bottom of laminate:
C               a. Material Number
C               b. Height to upper/lower surface (down=+)
C               c. Ply orientation


C       ..... Init and Read File ....

        dimension q(6,6), qbar(6,6), a(6,6), b(6,6), d(6,6)
        dimension angle(100),height(100),mat(100),g12(10)
        dimension e11(10),e22(10),q11(10),q12(10),q22(10),q33(10)
        real nu21(10),nu12(10)
        double precision qbar,q,a,b,d,height,
     1                   angle,theta,c4,s4,s1c3,s2c2,s3c1,
     2                   q11,q12,q22,q33,qt11,qt12,qt22,qt33,pi,
     3                   exx,e11,e22,g12

        open(5,file='composite.dat')
        open(6,file='composite.out')

        read(5,*) icode, n, m,
     1          (e11(i),e22(i),nu12(i),nu21(i), g12(i),i=1,m),
     2          (q11(j),q12(j),q22(j),q33(j),j=1,m),
     3          (mat(k),height(k),angle(k),k=0,n)


C       .....Compute matrix properties .....

        do 10 k=1,n

C       .....Compute Q matrix from Material Values if needed....

        if (icode .eq. 1) then
          q(1,1)= e11(mat(k-1))/(1-nu12(mat(k-1))*nu21(mat(k-1)))
          q(1,2)= nu12(mat(k-1))*e22(mat(k-1))/(1-nu12(mat(k-1))
     1              *nu21(mat(k-1)))
          q(2,2)= e22(mat(k-1))/(1-nu12(mat(k-1))*nu21(mat(k-1)))
          q(3,3)= g12(mat(k-1))
        endif

C       .....Assign Material Values to Q matrix if q entered....

        if (icode .eq. 2) then
            q(1,1)=q11(mat(k-1))
```

```
            q(1,2)=q12(mat(k-1))
            q(2,2)=q22(mat(k-1))
            q(3,3)=q33(mat(k-1))
          endif

C         .....Compute values for qbar matrix.....

            pi=3.14159
            theta=angle(k-1)*pi/180
            c4=cos(theta)**4
            s4=sin(theta)**4
            s1c3=sin(theta)*cos(theta)**3
            s2c2=sin(theta)**2*cos(theta)**2
            s3c1=sin(theta)**3*cos(theta)

            qt11=q(1,1)
            qt12=q(1,2)
            qt22=q(2,2)
            qt33=q(3,3)

            qbar(1,1)= qt11*c4 + 2*(qt12+2*qt33)*s2c2 + qt22*s4
            qbar(1,2)=(qt11+qt22-4*qt33)*s2c2 + qt12*(s4+c4)
            qbar(1,3)=(qt11-qt12-2*qt33)*s1c3+(qt12-qt22+2*qt33)*s3c1
            qbar(2,1)=qbar(1,2)
            qbar(2,2)= qt11*s4 + 2*(qt12+2*qt33)*s2c2 + qt22*c4
            qbar(2,3)=(qt11-qt12-2*qt33)*s3c1+(qt12-qt22+2*qt33)*s1c3
            qbar(3,1)=qbar(1,3)
            qbar(3,2)=qbar(2,3)
            qbar(3,3)=(qt11+qt22-2*qt12-2*qt33)*s2c2 + qt33*(s4+c4)


C         .... Compute A,B,and D matrices....

           do 20 i=1,3
            do 30 j=1,3

            a(i,j)=a(i,j) + qbar(i,j)*(height(k)-height(k-1))
            b(i,j)=b(i,j) +(qbar(i,j)*(height(k)**2-height(k-1)**2))/2
            d(i,j)=d(i,j) +(qbar(i,j)*(height(k)**3-height(k-1)**3))/3

   30     continue
   20     continue
   10     continue


C         ....Adjust nil values of variables....

          do 89 i=1,3
            do 90 j=1,3
              if(abs(a(i,j)) .lt. .00001) then
                  a(i,j)=0
                  endif
              if(abs(b(i,j)) .lt. .00001) then
                  b(i,j)=0
                  endif
              if(abs(d(i,j)) .lt. .00001) then
                  d(i,j)=0
                  endif
   90       continue
   89     continue
```

```
C       .... Process output .....

        write(6,*)' The A-Matrix is:'
        do 60 i=1,3
          write(6,100) a(i,1),a(i,2),a(i,3)
  60    continue

        write(6,*)
        write(6,*)' The B-Matrix is:'
        do 70 i=1,3
          write(6,100) b(i,1),b(i,2),b(i,3)
  70    continue

        write(6,*)
        write(6,*)' The D-Matrix is:'
        do 80 i=1,3
          write(6,100) d(i,1),d(i,2),d(i,3)
  80    continue

  100   format(5x, e10.4,2x,e10.4,2x,e10.4)

C       .... Compute equivalent Ex ....

        exx=(a(1,1)-a(1,2)**2/a(2,2))/(height(n)-height(0))
        write(6,*)
        write(6,*)
        write(6,110) exx

  110   format(' The equivalent Ex for this layup is: ',e10.4)
  999   end
```

Appendix F.6 Buckling FORTRAN Program

```
C       THIS PROGRAM COMPUTES A BUCKLING LOAD OF A COMPOSITE TUBE WITH THE
C       FOLLOWING ASSUMPTIONS (FORCE/CIRCUMFERENCE):
C                       1.  MATRIX VALUES ENTERED FROM IDEAS
C                       2.  LOCAL BUCKLING FACTOR
C                       3.  EULER BUCKLING FACTOR
C
C       THE FOLLOWING ARE ENTERED FROM THE DATA FILE:
C               1.  MATRIX A (11,12,22,66)
C               2.  MATRIX D (11,12,22)
C               3.  INNER DIAMETER OF INTEREST
C               4.  OUTER DIAMETER OF INTEREST
C               5.  MAX LENGTH OF INTEREST
C               6.  #OF LENGTH DIVISIONS OF INTEREST
C       THE PROGRAM WILL RUN EACH COMPOSITE FOR LENGTHS IN STEPS
C       OF THE MAX LENGTH DIVIDED BY EACH DIVISION
C


        IMPLICIT REAL*8(A-H,O-Z)
        REAL*8 LEN, MAX

        OPEN(5, FILE='buckle.dat')
        OPEN(6, FILE='buckle.out')

C       READ VALUES

 1      READ(5,*,END=999) A11,A12,A22,A66,D11,D12,D22,
     1                    DIAI,DIAO,MAX,IDIV

        WRITE(6,301) DIAI
        WRITE(6,302) DIAO

  301   FORMAT('MATERIAL INNER DIAMETER:',F9.2)
  302   FORMAT('MATERIAL OUTER DIAMETER:',F9.2)
        WRITE(6,*)

C       START LOOP AT DIFF LENGTHS

        WRITE(6,103)
  103   FORMAT(5X,'LENGTH USED',10X,'EULER PCR',4X,'LOCAL PCR (P/CIRC)',
     1         4X,'SIGMA CR')
        WRITE(6,*)

        DO 70 J=1,IDIV
          LEN=MAX/J
          R=DIAI/2

C       CALCULATION OF EULER BUCKLING LOAD

          PI=3.14159
          RMOFI = PI/64*(DIAO**4-DIAI**4)
          EX = (A11-A12**2/A22)/((DIAO-DIAI)/2)
          PCRE=PI**2*EX*RMOFI/LEN**2


C       CALCULATION OF LOCAL BUCKLING LOAD

          pcr=99999999.
          PULCR=9999999.
```

```
      DO 20 N=1,10
        DO 30 M=1,100
              BETA=N*LEN/PI/R/M
              PHI=1./29.8*DSQRT(R/DSQRT(d11*d22/a11/a22))
              GAMMA=1.0-.901*(1-DEXP(-phi))
              TERM1=M**2*(1.0+2*d12/d11*BETA**2+d22/d11*BETA**4)
              TERM2=GAMMA**2*LEN**4/PI**4/M**2/d11/R**2
              STUFF=(A11*A22-A12**2)/A66 - 2*A12
              TERM3=(A11*A22-A12**2)/(A11+STUFF*BETA**2 + A22*BETA**4)

              P=PI**2*d11/LEN**2*(TERM1 + TERM2*TERM3)
              if (p .lt. pcr) then
                pcr=p
                mcr=m
                endif

30            CONTINUE

        IF (PCR .LT. PULCR) THEN
              NCR=N
              PULCR=PCR
              MULCR=MCR
        ENDIF

      pcr=9999999.

20    CONTINUE

      SCR = PULCR*2/(DIAO-DIAI)

      WRITE (6,102) LEN,PCRE,PULCR,SCR
102   FORMAT(4X,F10.2,5X,F15.2,6X,F10.2,9X,F10.2)
70    CONTINUE

      WRITE(6,*)
      WRITE(6,*)
      WRITE(6,*)

      GOTO 1
999   STOP

      END
```

POWER/THERMAL ATTITUDE CONTROL

Appendix G

G.1 APPENDIX FOR ATTITUDE CONTROL AND POWER SYSTEMS

This appendix presents the detailed calculations involved in the design of the attitude control and power systems. (See next pages).

G.2 ATTITUDE CONTROL SYSTEM

The following section details the method used to analyze the pitch-up maneuver for the booster's free fall. Section G.2.2 explains the calculations involved in sizing the Hydrazine thrusters.

G.2.1 Analysis of Booster Pitch-up Aerodynamics During Free Fall

The analysis of the pitch-up maneuver involved the study of the forces and moments imparted to the booster during the duration of its free fall. The instantaneous forces and moments on the booster are a function of the booster's velocity and its angular orientation. To complicate matters, these forces and moments affect the velocity and orientation of the booster in the subsequent time period.

Because of the time-varying nature of this problem, the total duration of the free fall was first divided into small 0.25 second intervals. The assumption was then made that the forces and moments on the booster are constant during these intervals. Thus, once the forces and moments were determined for a particular interval, the linear and angular accelerations of the booster could be found for this interval using Newton's Second Law:

$$a_x = \frac{F_x}{m} \qquad \text{(Eq G.1)}$$

$$a_y = \frac{F_y}{m} \qquad \text{(Eq G.2)}$$

$$\ddot{\theta}_y = \frac{M_y}{I_{yy}} \qquad \text{(Eq G.3)}$$

In the above equation, a_x and a_y denote the accelerations in the horizontal and vertical directions, respectively. $\ddot{\theta}_y$ denotes the angular acceleration of the booster about the pitch axis. F_x and F_y are the aerodynamic forces on the booster in the horizontal and vertical directions, respectively. M_y is the moment applied to the booster along the pitch axis. Finally, m is the mass of the booster, and I_{yy} is the moment of inertia of the booster about the pitch axis.

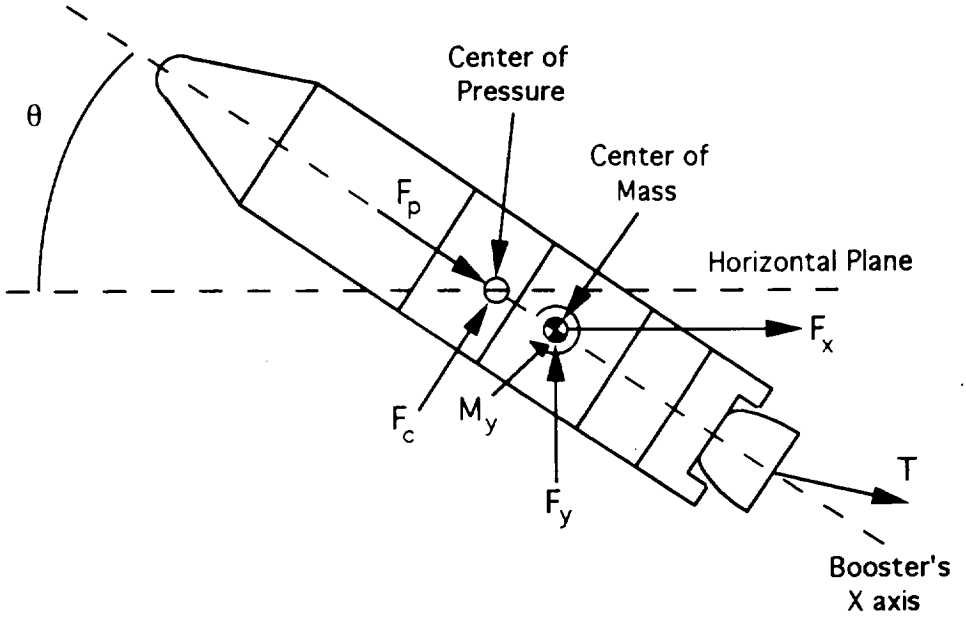

Figure G.1: Forces and Moments on the Booster During Free Fall

In order to use to the above equations to find the boosters' accelerations, the relations governing the aerodynamic forces and moments on the booster were derived. The instantaneous velocity was first decomposed into components perpendicular and parallel to the booster's X axis (see Figure G.1 above). The aerodynamic forces on the booster were then calculated using these component velocities. For the force along the booster's X axis, each of the three sections (the two Castor engines and the main section) was modeled as a conical shell followed by a cylinder. This approximation facilitated the calculation of drag force along the booster's X axis using standardized experimental data. For this analysis, the coefficient of drag along the booster's X axis was assumed to be constant at 0.0199. Thus, the drag force along the booster's X axis was computed as follows:

$$F_p = C_{d_p}\left(\frac{1}{2}\rho V_p^2\right)(S_p) \qquad \text{(Eq G.4)}$$

In the above equation, F_p is the force on the booster, in pounds, along the booster's X axis, C_{d_p} is the coefficient of drag along the booster's X axis (0.0199), ρ is the air density at the drop altitude (5.87×10^{-4} slug/ft^3), V_p is the component of the booster's velocity along the booster's X axis in ft/s, and S_p is the frontal surface area of the three cylinders (534.09 ft^2).

The booster was modeled as three cylinders placed side by side to facilitate the computation of the force perpendicular to the booster's X axis. The drag force was computed for each of the cylinders using standard curves giving drag versus Reynolds

number for a cylinder. The drag forces on the two Castor engines were increased by 15% to account for interference effects with the main body of the booster. The total drag in this direction was then the sum of these three cylinder drag forces. Thus, the force perpendicular to the X axis of the booster was found as follows:

$$F_c = \frac{1}{2}\rho V_c^2 \times \left[\left(1.15 \times C_{d_1} S_{c_1}\right) + C_{d_2} S_{c_2}\right] \qquad \text{(Eq G.5)}$$

In the above equation, F_c is the total force perpendicular to the booster's X axis in pounds, C_{d_1} is the coefficient of drag perpendicular to the booster's X axis on the Castor engines, C_{d_2} is the coefficient of drag perpendicular to the booster's X axis on the main cylinder, V_c is the component of the booster's velocity perpendicular to the booster's X axis in ft/s, S_{c_1} is the combined planform area of the Castor engines (495 ft^2), and S_{c_2} is the planform area of the main cylinder (1281 ft^2).

By finding the forces on the booster in this manner, it was inherently assumed that the Gryphon's profile provides no aerodynamic lift force; all forces are derived from drag terms. The moment applied to the booster was simply the perpendicular drag force multiplied by the distance between the center of mass and the center of pressure (Δx):

$$M_y = F_c \times \Delta x \qquad \text{(Eq G.6)}$$

The forces in the x and y directions were then found from the forces parallel and perpendicular to the booster's X axis as follows:

$$F_x = F_c \sin\theta + F_p \cos\theta \qquad \text{(Eq G.7)}$$

$$F_y = F_c \cos\theta - F_p \sin\theta \qquad \text{(Eq G.8)}$$

In the above equations, θ is the booster's angle of inclination with respect to horizontal.

The moment given in equation G.6 and the forces given in equations G.7 and G.8 were then substituted into equations G.1 through G.3 to find the corresponding accelerations of the booster. By integrating these accelerations with respect to time, the changes in position and orientation over the given interval were determined. From these position and orientation changes, new positions, velocities, and orientations were found for the beginning of the next interval. These values were then used to find new aerodynamic forces on the booster, which in turn led to new accelerations, etc. The process repeated through each of the intervals, until the end of the time period in question. In this way, the position and orientation of the booster was calculated for each 0.25 second interval.

The above method was implemented in a spreadsheet. Tables G.1 and G.2 on the following four pages are printouts of the runs used to find the behavior for the LEO and GTO configurations. The spreadsheet is set up to calculate values from left to right and from top to bottom, thus ensuring an orderly calculation of values, and eliminating any potential data management problems.

The user may enter values for the booster's aerodynamic moment arm, moment of inertia along the pitch axis, weight, drag coefficients in the direction perpendicular to the X axis, initial angle of inclination, and initial velocity. Given these quantities, the spreadsheet computes forces, moments, positions, velocities, accelerations, angular

orientations, and distances from the airplane for each 0.25 second time interval of free fall. In addition, given a particular first stage engine configuration, the moments and forces generated by these engines may be added to the spreadsheet. Thus, the engine's ability to regain control of the booster at the conclusion of the pitch-up maneuver may be determined. Please refer to Section 8.2 in the text for a discussion of the results.

G.2.2 Hydrazine Thruster Sizing

For coast periods, forces caused by solar pressure, aerodynamic effects and misaligned thrust forces are negligible. Only gravity-gradient disturbances are included (Reference 124):

$$T = \frac{3m}{R_o^3}(I_{xx} - I_{yy})a_{zx}a_{zy} \qquad \text{(Eq G.9)}$$

where T is the torque, a_{zx} and a_{zy} are equal direction cosines of angles between the spacecraft axes with a maximum value of ± 0.5, m is the mass of the booster, I_{xx} and I_{yy} are the booster's moments of inertia about the corresponding axes, and R_o^3 equals the Earth's gravitational constant (3.986×10^4 m^3/sec^2). This disturbance torque equals 220 lb.

This must be countered by a restoring force created by the thrusters:

$$T = F \times L \qquad \text{(Eq G.10)}$$

Where T is the torque, F is the thrust, and L equals the lever arm.

$$(F)(L) = I\frac{\partial^2\theta}{\partial t^2} \qquad \text{(Eq G.11)}$$

In the above equation, I is the moment of inertia and θ is the angle of the spacecraft.

However, the main design parameters stems from the first spin-up of the payload and the reorientation before entering GTO. For spin:

$$T_{req} = \frac{\frac{1}{2}w_t^2 I_{ms}}{\theta_{max}} \qquad \text{(Eq G.12)}$$

In the above equation, w_t^2 is the desired spin rate, I_{ms} is the moment of inertia about the spin axis, and θ_{max} is the maximum angle through which the acceleration can take place.

The thrusters provide 100 lb of thrust each. Therefore, the tip-off rate imparted to the satellite can be determined. The first payload can be released at a w_t^2 of 3.37 radians per second. The next two payloads can be released with a higher w_t^2 since the moment of inertia decreases.

Fuel Requirement

$$M_{spin} = I_{m_{ss}} \Omega_s \left(L\ g\ I_{sp} \right) \qquad \text{(Eq G.13)}$$

In the above equation, M_{spin} is the fuel mass required for spin-up, Ω_s is the spin rate, L is the moment arm of the thruster, g is the accleration due to gravity, and I_{sp} is the specific impulse of the fuel. Using the spin rate and moments of inertia for each of the payloads, the total propellant mass for the spinup/despin manuevers equals 63 lb. This amount of fuel will allow for three spinups and two full despins (down to zero rpm).

Attitude Control

$$M_p = \frac{F_t}{I_{sp}\ g} \quad \text{or} \quad M_{att\ man} = \frac{4\ I_c\ \theta_m}{T\ L\ g\ I_{sp}} \qquad \text{(Eq G.14)}$$

In the above equations, M_p is the propellant mass, t is the time that the thruster is firing, $M_{att\ man}$ is the fuel mass required for a given attitude control maneuver, θ_m is the angle of the maneuver, T is torque, F is thrust, I_c is the spacecraft's moment of inertia about the maneuver axis, g is the acceleration due to gravity, and L is the moment arm of the thruster.

The oxidizer weight is calculated from the propellant weight by using the mixing ratio. Tables used to acquire the mixing ratios can be located in Sutton (115).

Since the thrusters should not continually fire, it is required that the error in attitude must past through some angle θ_d, referred to as the dead zone (radians). Within this region, even if the Gryphon does not point at the correct angle, the thrusters will not fire, nor will the main rocket nozzles gimbal. When the RCS is employed, it will compensate for this delay by either firing a longer period of time, or gimballing through a larger angle for a quicker response time. The value for θ_d was chosen to be 3°. In addition, fuel is needed to accomodate three-axis attitude control. The thrusters require aprroximately 5 lb of fuel for a one time use. Assuming that the impulse time of a thruster may fluctuate from 3 to 5 seconds, and designing for unforeseen emergencies and payload reorientation, the total fuel and oxidizer weight equals 450 lb.

G.3 POWER SYSTEM

Determining the power losses in the cabling had the following assumpings:

- 150 ft of 2 gage cable
- resistance of .008658 Ω
- 5 amp current

Then:

$$P = I^2R = 0.216\ W \qquad \text{(Eq G.15)}$$

Therefore, a maximum of 0.216 W would be lost in the cabling.

Table G.1 - LEO Free Fall

Time at begin of interval (s)	Aero mom arm (ft) - pos =CP ahead of CM	Mom of Inertia Iyy (lb*ft^2)	Weight of Booster (lb)	Angle of Inclination (rad) + is initial nose up	Vy (ft/s) + is down halfway thru interval	Vx (ft/s) + is along plane's initial direct halfway thru interval	V perp to booster (ft/s pos is toward booster halfway thru interval	V par to booster (ft/s pos is toward booster halfway thru interval	Coeff of Drag 1 Castor const thru interval	Coeff of Drag Main Section const thru interval	Force perp to booster (lb) pos is toward booster constant thru interval	Force par to booster (lb) pos is toward booster constant thru interval	Force in Y dir (lb) + is up constant thru interval	Force in X dir (lb) + is opp direction of plane's initial dir constant thru interval	Y position (ft) pos is distance down from drop end of interval	X position (ft) pos is distance ahead of drop end of interval
00	4.48	174159614	477365	0.00000	4.03	733.33	4.03	733.33	1.38	1.20	10.57	1674.26	10.57	1674.26	2.01	183.33
25	4.48	174159614	477365	0.00000	12.08	733.30	12.08	733.30	1.29	0.74	67.90	1674.13	67.90	1674.13	6.04	366.65
50	4.48	174159614	477365	0.00000	20.13	733.27	20.13	733.27	1.13	0.35	119.78	1674.00	119.77	1674.00	12.08	549.97
75	4.48	174159614	477365	0.00001	28.18	733.25	28.18	733.25	0.61	0.38	183.80	1673.87	183.78	1673.87	20.13	733.27
1.00	4.48	174159614	477365	0.00002	36.22	733.22	36.24	733.22	0.42	0.39	272.64	1673.74	272.60	1673.75	30.19	916.57
1.25	4.48	174159614	477365	0.00005	44.27	733.19	44.30	733.19	0.43	0.39	410.34	1673.60	410.26	1673.63	42.26	1099.87
1.50	4.48	174159614	477365	0.00010	52.31	733.16	52.38	733.16	0.44	0.39	577.55	1673.46	577.39	1673.52	56.35	1283.15
1.75	4.48	174159614	477365	0.00017	60.35	733.13	60.47	733.12	0.45	0.39	775.09	1673.31	774.81	1673.44	72.44	1466.43
2.00	4.48	174159614	477365	0.00027	68.39	733.10	68.59	733.09	0.45	0.39	997.04	1673.14	996.59	1673.41	90.54	1649.71
2.25	13.64	167776858	471565	0.00042	76.42	733.08	76.73	733.04	0.45	0.39	1247.88	1672.95	1247.17	1673.48	110.65	1832.97
2.50	13.64	167776858	471565	0.00070	84.45	733.05	84.96	732.99	0.45	0.39	1530.04	1672.70	1528.87	1673.77	132.76	2016.23
2.75	13.64	167776858	471565	0.00121	92.48	733.02	93.36	732.91	0.45	0.39	1847.33	1672.33	1845.31	1674.56	156.89	2199.48
3.00	13.64	167776858	471565	0.00199	100.49	732.99	101.95	732.79	0.45	0.39	2203.01	1671.79	2199.68	1676.17	183.01	2382.73
3.25	13.64	167776858	471565	0.00310	108.51	732.96	110.78	732.62	0.45	0.39	2601.07	1671.03	2595.87	1679.09	211.14	2565.96
3.50	13.64	167776858	471565	0.00461	116.51	732.93	119.89	732.39	0.45	0.39	3046.43	1669.96	3038.70	1683.99	241.27	2749.19
3.75	13.64	167776858	471565	0.00658	124.51	732.90	129.33	732.07	0.45	0.39	3545.05	1668.51	3533.99	1691.80	273.39	2932.41
4.00	13.64	167776858	471565	0.00909	132.50	732.88	139.15	731.64	0.45	0.39	4104.13	1666.56	4088.82	1703.78	307.51	3115.63
4.25	13.64	167776858	471565	0.01222	140.48	732.85	149.42	731.08	0.45	0.39	4732.38	1663.98	4711.69	1721.69	343.63	3298.84
4.50	13.64	167776858	471565	0.01608	148.45	732.82	160.21	730.34	0.45	0.39	5440.28	1660.62	5412.88	1747.86	381.74	3482.04
4.75	13.64	167776858	471565	0.02077	156.41	732.79	171.59	729.38	0.45	0.39	6240.45	1656.28	6204.71	1785.50	421.83	3665.23
5.00	13.64	167776858	471565	0.02641	164.35	732.76	183.64	728.16	0.45	0.39	7148.08	1650.74	7102.00	1838.93	463.91	3848.42
5.25	13.64	167776858	471565	0.03315	172.28	732.73	196.47	726.61	0.45	0.39	8181.49	1643.73	8122.52	1913.99	507.97	4031.59
5.50	13.64	167776858	471565	0.04114	180.19	732.69	210.17	724.66	0.45	0.39	9362.76	1634.91	9287.59	2018.64	554.00	4214.76
5.75	13.64	167776858	471565	0.05057	188.08	732.66	224.88	722.21	0.45	0.39	10718.55	1623.89	10622.76	2163.65	602.01	4397.92
6.00	13.64	167776858	471565	0.06164	195.95	732.62	240.71	719.16	0.45	0.39	12281.09	1610.18	12158.57	2363.70	651.98	4581.07
6.25	13.64	167776858	471565	0.07460	203.79	732.58	257.82	715.36	0.45	0.39	14089.34	1593.19	13931.42	2638.82	703.90	4764.21
6.50	13.64	167776858	471565	0.08971	211.61	732.54	276.38	710.63	0.45	0.39	16190.44	1572.23	15964.48	3016.37	757.77	4947.34
6.75	13.64	167776858	471565	0.10730	219.38	732.48	296.56	704.78	0.45	0.39	18641.30	1546.43	18358.50	3533.83	813.59	5130.45
7.00	13.64	167776858	471565	0.12773	227.12	732.42	318.57	697.53	0.45	0.39	21510.53	1514.76	21142.32	4242.56	871.33	5313.55
7.25	13.64	167776858	471565	0.15145	234.81	732.35	342.61	688.54	0.45	0.39	24880.32	1475.99	24372.81	5212.95	930.98	5496.63
7.50	13.64	167776858	471565	0.17897	242.44	732.26	368.92	677.41	0.45	0.39	28848.36	1428.65	28133.25	6541.34	992.54	5679.68
7.75	13.64	167776858	471565	0.21088	250.01	732.15	397.73	663.60	0.45	0.39	33529.07	1370.99	32499.30	8359.06	1055.98	5862.70
8.00	13.64	167776858	471565	0.24790	257.51	732.01	429.24	646.45	0.45	0.39	39053.33	1301.04	37540.24	10843.68	1121.28	6045.68
8.25	13.64	167776858	471565	0.29085	264.92	731.82	463.65	625.12	0.45	0.39	45565.11	1216.60	43302.50	14232.12	1188.43	6228.60
8.50	13.64	167776858	471565	0.34073	272.23	731.58	501.05	598.55	0.45	0.39	53212.04	1115.40	49780.26	18833.25	1257.38	6411.46
8.75	13.64	167776858	471565	0.39745	279.43	731.26	540.69	566.10	0.45	0.39	61965.42	997.73	56749.07	24904.86	1328.13	6594.22
9.00	13.64	167776858	471565	0.45990	286.51	730.83	581.13	527.73	0.45	0.39	71579.72	867.05	63757.43	32548.41	1400.62	6776.86
9.25	13.64	167776858	471565	0.52712	293.47	730.28	621.00	483.52	0.45	0.39	81738.98	727.87	70277.44	41747.71	1474.85	6959.34
9.50	13.64	167776858	471565	0.59826	300.32	729.57	659.05	433.71	0.45	0.39	92064.66	585.63	75744.59	52335.48	1550.77	7141.62
9.75	13.64	167776858	471565	0.67254	307.08	728.67	694.15	378.70	0.45	0.39	102131.13	446.49	79613.16	63974.31	1628.38	7323.65
10.00	13.64	167776858	471565	0.74731	313.77	727.58	724.67	320.44	0.45	0.39	111307.80	319.68	81429.41	75886.62	1707.65	7505.38
10.25	13.64	167776858	471565	0.81798	320.43	726.28	749.09	262.72	0.45	0.39	118938.45	214.89	81160.60	86944.57	1788.59	7686.77
10.50	13.64	167776858	471565	0.88287	327.09	724.80	767.64	207.51	0.45	0.39	124899.64	134.06	79200.00	96577.93	1871.20	7867.76
10.75	13.64	167776858	471565	0.94307	333.79	723.15	781.33	154.56	0.45	0.39	129395.34	74.37	75934.71	104771.56	1955.49	8048.33
11.00	13.64	167776858	471565	0.99944	340.54	721.36	790.94	103.64	0.45	0.39	132599.54	33.44	71678.13	111556.65	2041.48	8228.43
11.25	13.64	167776858	471565	1.05262	347.37	719.46	797.06	54.58	0.45	0.39	134658.59	9.28	66688.37	116985.45	2129.19	8408.04
11.50	13.64	167776858	471565	1.10302	354.28	717.46	800.13	7.28	0.45	0.39	135698.48	0.17	61186.11	121121.17	2218.64	8587.15
11.75	13.64	167776858	471565	1.15092	361.29	715.39	800.53	-38.27	0.45	0.39	135833.78	4.56	55368.18	124037.02	2309.85	8765.73
12.00	13.64	167776858	471565	1.19640	368.39	713.28	798.59	-82.02	0.45	0.39	135176.17	20.94	49416.17	125819.87	2402.85	8943.78
12.25	13.64	167776858	471565	1.23942	375.60	711.13	794.64	-123.80	0.45	0.39	133841.50	47.71	43500.03	126575.26	2497.66	9121.30
12.50	13.64	167776858	471565	1.27981	382.91	708.97	788.02	-163.41	0.45	0.39	131954.66	83.13	37777.65	126431.36	2594.31	9298.27
12.75	13.64	167776858	471565	1.31732	390.31	706.81	782.10	-200.59	0.45	0.39	129651.86	125.27	32391.63	125540.45	2692.83	9474.70
13.00	13.64	167776858	471565	1.35160	397.81	704.67	774.31	-235.08	0.45	0.39	127080.06	172.02	27465.10	124076.75	2793.23	9650.60
13.25	13.64	167776858	471565	1.38225	405.39	702.55	766.08	-266.52	0.45	0.39	124393.90	221.16	23097.90	122230.84	2895.53	9825.98
13.50	13.64	167776858	471565	1.40884	413.05	700.46	757.90	-294.69	0.45	0.39	121750.73	270.37	19364.79	120201.15	2999.76	10000.84
13.75	13.64	167776858	471565	1.43094	420.77	698.41	750.25	-319.30	0.45	0.39	119304.37	317.41	16316.30	118183.81	3105.92	10175.19
14.00	13.64	167776858	471565	1.44813	428.54	696.39	743.59	-340.11	0.45	0.39	117198.63	360.13	13982.47	116362.10	3214.03	10349.04
14.25	13.64	167776858	471565	1.46004	436.35	694.41	738.38	-356.92	0.45	0.39	115561.19	396.61	12378.82	114896.96	3324.10	10522.40
14.50	13.64	167776858	471565	1.46636	444.19	692.44	734.98	-369.58	0.45	0.39	114498.47	425.24	11513.47	113918.92	3436.13	10695.26

Config LEO - ANC off at 2.25 s gives 20 deg at seperation distance of 2994 ft (8.50 sec) - Recov. starts Engine recovery (0 ang vel) at 14.50 sec (final ang = 84.0 deg)

Table G 1 - LEO Free Fall

Y position (ft) of PLANE Pos is distance down from drop End of interval	X position (ft) of PLANE Pos is distance ahead of drop End of interval	Z position (ft) of PLANE Pos is away from booster End of interval	Absolute distance between plane and booster (ft) End of interval	Mom applied by aero loads (ft*lb) + will tilt booster up from horiz const thru interval	Mom applied by control mech (ft*lb) pos will tilt booster up from horiz constant thru interval	Ang accel of booster (rad/s^2) pos will tilt nose up dir end of interval	Ang vel of booster (rad/s) pos is initial nose up dir end of interval	Ang inclinatio of booster (rad) + is initial nose up dir end of interval	Ang velocity of booster (deg/s) + is initial nose up dir end of interval	Ang inclinatio of booster (degrees) + is initial nose up dir end of interval	Time at begin of interval (s)
-10 13	187 99	2 30	13 21	47 34	0 00	0 00001	0 00000	0 00000	0 00013	0 000	00
-20 25	375 88	9 21	29 34	304 19	0 00	0 00006	0 00002	0 00000	0 00093	0 000	25
-30 38	563 53	20 72	49 15	536 61	0 00	0 00010	0 00004	0 00001	0 00235	0 001	50
-40 50	750 85	36 82	73 08	823 40	0 00	0 00015	0 00008	0 00002	0 00453	0 001	75
-50 63	937 72	57 51	101 42	1221 41	0 00	0 00023	0 00014	0 00005	0 00777	0 003	1 00
-60 75	1124 02	82 76	134 33	1838 33	0 00	0 00034	0 00022	0 00010	0 01264	0 006	1 25
-70 88	1309 65	112 58	171 93	2587 44	0 00	0 00048	0 00034	0 00017	0 01949	0 010	1 50
-81 00	1494 49	146 93	214 29	3472 39	0 00	0 00064	0 00050	0 00027	0 02868	0 016	1 75
-91 13	1678 44	185 80	261 44	4466 75	0 00	0 00083	0 00071	0 00042	0 04051	0 024	2 00
-101 25	1861 38	229 17	313 41	17021 05	0 00	0 00327	0 00152	0 00070	0 08731	0 040	2 25
-111 38	2043 20	277 00	370 22	20869 76	0 00	0 00401	0 00253	0 00121	0 14468	0 069	2 50
-121 50	2223 79	329 27	431 87	25197 64	0 00	0 00484	0 00373	0 00199	0 21395	0 114	2 75
-131 63	2403 05	385 95	498 37	30049 03	0 00	0 00577	0 00518	0 00310	0 29655	0 178	3 00
-141 75	2580 87	447 01	569 71	35478 63	0 00	0 00681	0 00688	0 00461	0 39409	0 264	3 25
-151 88	2757 14	512 40	645 90	41553 34	0 00	0 00797	0 00887	0 00658	0 50832	0 377	3 50
-162 00	2931 76	582 10	726 91	48354 45	0 00	0 00928	0 01119	0 00909	0 64125	0 521	3 75
-172 13	3104 61	656 05	812 76	55980 33	0 00	0 01074	0 01388	0 01222	0 79514	0 700	4 00
-182 25	3275 60	734 21	903 41	64549 65	0 00	0 01239	0 01698	0 01608	0 97260	0 921	4 25
-192 38	3444 63	816 53	998 87	74205 39	0 00	0 01424	0 02054	0 02077	1 17659	1 190	4 50
-202 50	3611 58	902 98	1099 11	85119 70	0 00	0 01634	0 02462	0 02641	1 41059	1 513	4 75
-212 63	3776 37	993 48	1204 12	97499 83	0 00	0 01871	0 02930	0 03315	1 67862	1 899	5 00
-222 75	3938 90	1088 00	1313 88	111595 56	0 00	0 02142	0 03465	0 04114	1 98541	2 357	5 25
-232 88	4099 05	1186 47	1428 38	127708 08	0 00	0 02451	0 04078	0 05057	2 33649	2 898	5 50
-243 00	4256 75	1288 83	1547 60	146201 08	0 00	0 02806	0 04779	0 06164	2 73840	3 532	5 75
-253 13	4411 90	1395 03	1671 51	167514 10	0 00	0 03215	0 05583	0 07460	3 19891	4 274	6 00
-263 25	4564 39	1505 00	1800 09	192178 67	0 00	0 03688	0 06505	0 08971	3 72722	5 140	6 25
-273 38	4714 15	1618 66	1933 32	220837 59	0 00	0 04238	0 07565	0 10730	4 33432	6 148	6 50
-283 50	4861 07	1735 97	2071 17	254267 38	0 00	0 04880	0 08785	0 12773	5 03332	7 319	6 75
-293 63	5005 08	1856 83	2213 62	293403 56	0 00	0 05631	0 10193	0 15145	5 83991	8 678	7 00
-303 75	5146 09	1981 19	2360 63	339367 52	0 00	0 06513	0 11821	0 17897	6 77285	10 254	7 25
-313 88	5284 00	2108 97	2512 17	393491 64	0 00	0 07552	0 13709	0 21088	7 85458	12 083	7 50
-324 00	5418 75	2240 08	2668 22	457336 51	0 00	0 08777	0 15903	0 24790	9 11183	14 204	7 75
-334 13	5550 24	2374 46	2828 73	532687 43	0 00	0 10223	0 18459	0 29085	10 57623	16 665	8 00
-344 25	5678 40	2512 02	2993 67	621508 12	0 00	0 11928	0 21441	0 34073	12 28480	19 522	8 25
-354 38	5803 15	2652 67	3162 98	725812 28	-205336 43	0 09989	0 23938	0 39745	13 71562	22 772	8 50
-364 50	5924 42	2796 34	3336 64	845208 34	-410672 86	0 08340	0 26023	0 45990	14 91019	26 350	8 75
-374 63	6042 13	2942 94	3514 57	976347 37	-616009 29	0 06916	0 27752	0 52712	15 90078	30 202	9 00
-384 75	6156 22	3092 38	3696 74	1114919 67	-821345 72	0 05634	0 29161	0 59826	16 70783	34 278	9 25
-394 88	6266 61	3244 56	3883 09	1255762 01	-1026682 16	0 04397	0 30260	0 67254	17 33759	38 534	9 50
-405 00	6373 24	3399 41	4073 56	1393068 58	-1540023 23	-0 02820	0 29555	0 74731	16 93360	42 817	9 75
-415 13	6476 04	3556 82	4268 10	1518238 36	-2053364 31	-0 10270	0 26987	0 81798	15 46250	46 867	10 00
-425 25	6574 96	3716 70	4466 67	1622320 49	-2053364 31	-0 08273	0 24919	0 88287	14 27754	50 584	10 25
-435 38	6669 93	3878 96	4669 20	1703631 02	-2053364 31	-0 06712	0 23241	0 94307	13 31610	54 034	10 50
-445 50	6760 90	4043 50	4875 67	1764952 44	-2053364 31	-0 05535	0 21857	0 99944	12 52323	57 264	10 75
-455 63	6847 81	4210 21	5086 02	1808657 78	-2053364 31	-0 04696	0 20683	1 05262	11 85052	60 310	11 00
-465 75	6930 61	4379 01	5300 21	1836743 10	-2053364 31	-0 04157	0 19644	1 10302	11 25501	63 198	11 25
-475 88	7009 24	4549 78	5518 21	1850927 23	-2053364 31	-0 03885	0 18672	1 15092	10 69850	65 943	11 50
-486 00	7083 68	4722 42	5739 98	1852772 81	-2053364 31	-0 03850	0 17710	1 19640	10 14706	68 548	11 75
-496 13	7153 86	4896 84	5965 48	1843802 99	-2053364 31	-0 04022	0 16705	1 23942	9 57096	71 013	12 00
-506 25	7219 74	5072 93	6194 67	1825508 00	-2053364 31	-0 04371	0 15612	1 27981	8 94481	73 328	12 25
-516 38	7281 30	5250 58	6427 53	1799861 58	-2053364 31	-0 04865	0 14395	1 31732	8 24792	75 477	12 50
-526 50	7338 48	5429 68	6664 00	1768451 43	-2053364 31	-0 05468	0 13028	1 35160	7 46467	77 441	12 75
-536 63	7391 26	5610 12	6904 06	1733371 99	-2053364 31	-0 06141	0 11493	1 38225	6 58499	79 197	13 00
-546 75	7439 60	5791 81	7147 67	1696732 77	-2053364 31	-0 06845	0 09782	1 40884	5 60459	80 721	13 25
-556 88	7483 48	5974 63	7394 79	1660679 92	-2053364 31	-0 07536	0 07898	1 43094	4 52507	81 987	13 50
-567 00	7522 86	6158 47	7645 38	1627311 63	-2053364 31	-0 08177	0 05854	1 44813	3 35383	82 972	13 75
-577 13	7557 73	6343 21	7899 41	1598589 31	-2053364 31	-0 08728	0 03672	1 46004	2 10362	83 654	14 00
-587 25	7588 08	6528 76	8156 82	1576254 61	-2053364 31	-0 09157	0 01382	1 46636	0 79201	84 016	14 25
-597 38	7613 84	6714 99	8417 58	1561759 15	-2053364 31	-0 09435	-0 00976	1 46686	-0 55945	84 045	14 50

Table G 2 - GTO Free Fall

Time at begin of interval (s)	Aero. mom. arm (ft) - pos =CP ahead of CM	Mom. of Inertia Iyy (lb*ft^2)	Weight of Booster (lb)	Angle of Inclination (rad) + is initial nose up	Vy (ft/s) + is down halfway thru interval	Vx (ft/s) + is along plane's initial direct halfway thru interval	V perp to booster (ft/s pos is toward halfway thru interval	V par to booster (ft/s pos. is toward halfway thru interval	Coeff of Drag 1 Castor const. thru interval	Coeff of Drag Main Section const thru interval	Force perp to booster (lb) pos is toward booster constant thru interval	Force par to booster (lb) pos is toward booster constant thru interval	Force in Y dir (lb) + is up constant thru interval	Force in X dir (lb) + is opp direction of plane's initial dir constant thru interval	Y position (ft) pos is distanc down from drop end of interval	X position (ft) pos is distanc ahead of drop end of interval
Config GTO :				dir begin of												
ANC off at 2.25 s gives 20 deg at																
seperation distance of 3,163 ft (8.75 sec) - Recov starts				interval												
Engine recovery (0 ang vel) at 14.25 sec (final ang = 62.5 deg)																
00	3.82	191098196	478413	0.00000	4.03	733.33	4.03	733.33	1.38	1.20	10.57	1674.26	10.57	1674.26	2.01	183.33
25	3.82	191098196	478413	0.00000	12.08	733.30	12.08	733.30	1.29	0.74	67.90	1674.13	67.90	1674.13	6.04	366.65
50	3.82	191098196	478413	0.00000	20.13	733.27	20.13	733.27	1.13	0.35	119.77	1674.00	119.77	1674.00	12.08	549.97
75	3.82	191098196	478413	0.00001	28.18	733.25	28.18	733.25	0.61	0.38	183.77	1673.87	183.76	1673.87	20.13	733.27
1.00	3.82	191098196	478413	0.00002	36.22	733.22	36.23	733.22	0.42	0.39	272.58	1673.74	272.54	1673.75	30.19	916.57
1.25	3.82	191098196	478413	0.00004	44.27	733.19	44.30	733.19	0.43	0.39	410.19	1673.61	410.12	1673.62	42.26	1099.87
1.50	3.82	191098196	478413	0.00007	52.31	733.16	52.36	733.16	0.44	0.39	577.21	1673.47	577.08	1673.51	56.35	1283.15
1.75	3.82	191098196	478413	0.00013	60.35	733.13	60.44	733.13	0.45	0.39	774.39	1673.32	774.18	1673.42	72.44	1466.43
2.00	3.82	191098196	478413	0.00021	68.39	733.10	68.54	733.09	0.45	0.39	995.76	1673.17	995.40	1673.38	90.54	1649.71
2.25	12.97	184495795	472613	0.00033	76.42	733.08	76.66	733.05	0.45	0.39	1245.64	1672.99	1245.09	1673.40	110.65	1832.97
2.50	12.97	184495795	472613	0.00055	84.45	733.05	84.85	733.00	0.45	0.39	1526.15	1672.76	1525.23	1673.60	132.76	2016.23
2.75	12.97	184495795	472613	0.00097	92.48	733.02	93.19	732.93	0.45	0.39	1840.61	1672.43	1838.98	1674.22	156.89	2199.48
3.00	12.97	184495795	472613	0.00163	100.49	732.99	101.69	732.83	0.45	0.39	2191.80	1671.96	2189.06	1675.54	183.01	2382.73
3.25	12.97	184495795	472613	0.00258	108.51	732.96	110.39	732.68	0.45	0.39	2583.11	1671.29	2578.79	1677.95	211.14	2565.96
3.50	12.97	184495795	472613	0.00386	116.51	732.93	119.34	732.48	0.45	0.39	3018.71	1670.37	3012.23	1682.02	241.27	2749.19
3.75	12.97	184495795	472613	0.00554	124.51	732.91	128.57	732.20	0.45	0.39	3503.60	1669.12	3494.30	1688.51	273.39	2932.42
4.00	12.97	184495795	472613	0.00768	132.50	732.88	138.12	731.84	0.45	0.39	4043.83	1667.45	4030.90	1698.46	307.52	3115.63
4.25	12.97	184495795	472613	0.01036	140.48	732.85	148.06	731.35	0.45	0.39	4646.61	1665.25	4629.12	1713.28	343.63	3298.84
4.50	12.97	184495795	472613	0.01364	148.45	732.82	158.44	730.73	0.45	0.39	5320.60	1662.39	5297.42	1734.82	381.74	3482.04
4.75	12.97	184495795	472613	0.01764	156.41	732.79	169.31	729.92	0.45	0.39	6076.09	1658.71	6045.89	1765.62	421.84	3665.23
5.00	12.97	184495795	472613	0.02244	164.36	732.76	180.76	728.89	0.45	0.39	6925.39	1654.03	6886.54	1809.00	463.92	3848.42
5.25	12.97	184495795	472613	0.02816	172.29	732.73	192.85	727.59	0.45	0.39	7883.19	1648.14	7833.66	1869.43	507.98	4031.60
5.50	12.97	184495795	472613	0.03493	180.21	732.70	205.68	725.96	0.45	0.39	8966.98	1640.76	8904.22	1952.88	554.02	4214.77
5.75	12.97	184495795	472613	0.04289	188.11	732.66	219.34	723.93	0.45	0.39	10197.70	1631.59	10118.37	2067.29	602.04	4397.93
6.00	12.97	184495795	472613	0.05220	195.99	732.63	233.94	721.40	0.45	0.39	11600.33	1620.25	11499.99	2223.31	652.01	4581.08
6.25	12.97	184495795	472613	0.06306	203.84	732.59	249.60	718.29	0.45	0.39	13204.77	1606.29	13077.30	2435.20	703.95	4764.22
6.50	12.97	184495795	472613	0.07567	211.67	732.55	266.44	714.45	0.45	0.39	15046.75	1589.17	14883.56	2722.11	757.84	4947.36
6.75	12.97	184495795	472613	0.09028	219.46	732.50	284.61	709.73	0.45	0.39	17168.99	1568.25	16957.69	3109.77	813.68	5130.47
7.00	12.97	184495795	472613	0.10717	227.23	732.45	304.26	703.94	0.45	0.39	19622.46	1542.76	19344.87	3632.80	871.45	5313.58
7.25	12.97	184495795	472613	0.12666	234.95	732.39	325.58	696.84	0.45	0.39	22467.79	1511.79	22096.84	4337.86	931.15	5496.67
7.50	12.97	184495795	472613	0.14913	242.62	732.31	348.73	688.14	0.45	0.39	25776.71	1474.26	25271.57	5287.74	992.76	5679.73
7.75	12.97	184495795	472613	0.17501	250.24	732.22	373.91	677.47	0.45	0.39	29633.37	1428.90	28931.90	6566.82	1056.26	5862.77
8.00	12.97	184495795	472613	0.20481	257.80	732.11	401.31	664.38	0.45	0.39	34135.07	1374.22	33142.12	8288.04	1121.64	6045.79
8.25	12.97	184495795	472613	0.23913	265.28	731.97	431.10	648.31	0.45	0.39	39391.95	1308.55	37961.13	10601.43	1188.89	6228.76
8.50	12.97	184495795	472613	0.27864	272.69	731.79	463.44	628.56	0.45	0.39	45524.22	1230.05	43430.05	13703.96	1257.98	6411.67
8.75	12.97	184495795	472613	0.32416	280.00	731.56	498.42	604.28	0.45	0.39	52655.34	1136.82	49550.88	17849.03	1328.88	6594.52
9.00	12.97	184495795	472613	0.37551	287.20	731.25	535.37	574.97	0.45	0.39	60751.60	1029.24	56141.09	23237.79	1401.56	6777.29
9.25	12.97	184495795	472613	0.43151	294.30	730.86	572.99	540.77	0.45	0.39	69590.71	910.45	62830.77	29933.11	1476.01	6959.94
9.50	12.97	184495795	472613	0.49114	301.28	730.35	610.12	501.93	0.45	0.39	78900.00	784.34	69203.62	37903.61	1552.19	7142.44
9.75	12.97	184495795	472613	0.55344	308.15	729.70	645.69	458.81	0.45	0.39	88367.80	655.37	74832.01	47004.97	1630.07	7324.77
10.00	12.97	184495795	472613	0.61748	314.92	728.90	678.79	411.97	0.45	0.39	97660.65	528.38	79320.45	56974.97	1709.64	7506.87
10.25	12.97	184495795	472613	0.68069	321.62	727.93	708.05	363.30	0.45	0.39	106262.22	410.91	82321.74	67193.46	1790.87	7688.71
10.50	12.97	184495795	472613	0.73873	328.27	726.79	732.08	316.30	0.45	0.39	113595.51	311.47	83774.47	76719.46	1873.77	7870.25
10.75	12.97	184495795	472613	0.78991	334.89	725.48	751.03	272.80	0.45	0.39	119555.27	231.69	83991.07	85082.41	1958.32	8051.43
11.00	12.97	184495795	472613	0.83520	341.51	724.03	765.98	232.64	0.45	0.39	124361.20	168.50	83325.27	92318.12	2044.53	8232.24
11.25	12.97	184495795	472613	0.87534	348.14	722.46	777.74	195.62	0.45	0.39	128209.09	119.14	82056.97	98510.09	2132.39	8412.65
11.50	12.97	184495795	472613	0.91094	354.79	720.78	786.96	161.52	0.45	0.39	131267.99	81.23	80403.06	103762.42	2221.93	8592.62
11.75	12.97	184495795	472613	0.94251	361.47	719.01	794.17	130.16	0.45	0.39	133681.68	52.75	78530.08	108184.20	2313.13	8772.15
12.00	12.97	184495795	472613	0.97042	368.19	717.17	799.76	101.37	0.45	0.39	135571.82	31.99	76565.63	111881.30	2406.02	8951.20
12.25	12.97	184495795	472613	0.99497	374.93	715.26	804.08	75.01	0.45	0.39	137041.39	17.52	74607.75	114952.28	2500.60	9129.77
12.50	12.97	184495795	472613	1.01642	381.71	713.31	807.41	50.96	0.45	0.39	138177.93	8.08	72732.20	117486.88	2596.88	9307.85
12.75	12.97	184495795	472613	1.03493	388.52	711.30	809.97	29.12	0.45	0.39	139056.23	2.64	70997.93	119565.59	2694.87	9485.42
13.00	12.97	184495795	472613	1.05086	395.36	709.27	811.96	9.43	0.45	0.39	139740.51	0.28	69451.06	121259.89	2794.57	9662.48
13.25	12.97	184495795	472613	1.06371	402.23	707.20	813.55	-8.17	0.45	0.39	140286.05	0.21	68127.77	122632.71	2895.99	9839.02
13.50	12.97	184495795	472613	1.07417	409.12	705.11	814.86	-23.73	0.45	0.39	140740.36	1.75	67056.41	123738.78	2999.13	10015.03
13.75	12.97	184495795	472613	1.08211	416.03	703.01	816.03	-37.29	0.45	0.39	141144.10	4.33	66258.92	124625.09	3104.00	10190.52
14.00	12.97	184495795	472613	1.08759	422.95	700.88	817.15	-48.88	0.45	0.39	141531.60	7.44	65751.85	125331.12	3210.61	10365.47
14.25	12.97	184495795	472613	1.09067	429.88	698.75	818.30	-58.53	0.45	0.39	141931.30	10.67	65547.12	125889.12	3318.94	10539.89
14.50	12.97	184495795	472613	1.09141	436.81	696.60	819.58	-66.27	0.45	0.39	142366.03	13.67	65652.43	126324.36	3429.01	10713.77

Table G 2 - GTO Free Fall

Y position (ft) of PLANE Pos is distance down from drop End of interval	X position (ft) of PLANE Pos distance ahead of drop End of interval	Z position (ft) of PLANE Pos is away from booster End o interval	Absolute distan between plane and booster (ft) End of interval	Mom applied by aero loads (ft*lb) + will tilt booster up from horiz const thru interval	Mom applied by control mech (ft*lb) pos will tilt booster up fron horiz constant thru interval	Ang accel of booster (rad/s^2) pos will tilt booster up fron horiz constant thru interval	Ang vel of booster (rad/s pos is initial nose up dir end of interval	Ang inclinatio of booster (rad) + is initial nose up dir end of interval	Ang velocity of booster (deg/s) + is initial nose up dir end of interval	Ang inclinatio of booster (degrees) + is initial nose up dir end of interval	Time at begin of interval (s)
-10 13	187 99	2 30	13 21	40 37	0 00	0 00001	0 00000	0 00000	0 00010	0 000	00
-20 25	375 88	9 21	29 34	259 37	0 00	0 00004	0 00001	0 00000	0 00072	0 000	25
-30 38	563 53	20 72	49 15	457 53	0 00	0 00008	0 00003	0 00001	0 00183	0 000	50
-40 50	750 85	36 82	73 08	702 02	0 00	0 00012	0 00006	0 00002	0 00352	0 001	75
-50 63	937 72	57 51	101 41	1041 24	0 00	0 00018	0 00011	0 00004	0 00604	0 002	1 00
-60 75	1124 02	82 76	134 33	1566 91	0 00	0 00026	0 00017	0 00007	0 00982	0 004	1 25
-70 88	1309 65	112 58	171 93	2204 94	0 00	0 00037	0 00026	0 00013	0 01514	0 007	1 50
-81 00	1494 49	146 93	214 29	2958 18	0 00	0 00050	0 00039	0 00021	0 02228	0 012	1 75
-91 13	1678 44	185 80	261 44	3803 79	0 00	0 00064	0 00055	0 00033	0 03146	0 019	2 00
-101 25	1861 38	229 17	313 41	16155 91	0 00	0 00282	0 00125	0 00055	0 07185	0 032	2 25
-111 38	2043 20	277 00	370 22	19794 20	0 00	0 00345	0 00212	0 00097	0 12133	0 056	2 50
-121 50	2223 79	329 27	431 87	23872 77	0 00	0 00417	0 00316	0 00163	0 18101	0 094	2 75
-131 63	2403 05	385 95	498 37	28427 61	0 00	0 00496	0 00440	0 00258	0 25208	0 148	3 00
-141 75	2580 87	447 01	569 71	33502 95	0 00	0 00585	0 00586	0 00386	0 33584	0 221	3 25
-151 88	2757 14	512 40	645 90	39152 63	0 00	0 00683	0 00757	0 00554	0 43372	0 317	3 50
-162 00	2931 76	582 10	726 91	45441 72	0 00	0 00793	0 00955	0 00768	0 54732	0 440	3 75
-172 13	3104 61	656 05	812 76	52448 46	0 00	0 00915	0 01184	0 01036	0 67844	0 593	4 00
-182 25	3275 60	734 21	903 41	60266 59	0 00	0 01052	0 01447	0 01364	0 82910	0 782	4 25
-192 38	3444 63	816 53	998 87	69008 15	0 00	0 01204	0 01748	0 01764	1 00162	1 011	4 50
-202 50	3611 58	902 98	1099 11	78806 89	0 00	0 01375	0 02092	0 02244	1 19863	1 286	4 75
-212 63	3776 37	993 48	1204 13	89822 36	0 00	0 01568	0 02484	0 02816	1 42318	1 613	5 00
-222 75	3938 90	1088 00	1313 89	102244 92	0 00	0 01784	0 02930	0 03493	1 67879	2 001	5 25
-232 88	4099 05	1186 47	1428 40	116301 73	0 00	0 02030	0 03437	0 04289	1 96954	2 457	5 50
-243 00	4256 75	1288 83	1547 62	132264 12	0 00	0 02308	0 04015	0 05220	2 30019	2 991	5 75
-253 13	4411 90	1395 03	1671 53	150456 27	0 00	0 02626	0 04671	0 06306	2 67632	3 613	6 00
-263 25	4564 39	1505 00	1800 12	171265 85	0 00	0 02989	0 05418	0 07567	3 10448	4 336	6 25
-273 38	4714 15	1618 66	1933 36	195156 38	0 00	0 03406	0 06270	0 09028	3 59236	5 173	6 50
-283 50	4861 07	1735 97	2071 22	222681 86	0 00	0 03886	0 07241	0 10717	4 14905	6 140	6 75
-293 63	5005 08	1856 83	2213 69	254503 36	0 00	0 04442	0 08352	0 12656	4 78530	7 257	7 00
-303 75	5146 09	1981 19	2360 72	291407 26	0 00	0 05086	0 09623	0 14913	5 51380	8 544	7 25
-313 88	5284 00	2108 97	2512 29	334323 99	0 00	0 05835	0 11082	0 17501	6 34959	10 027	7 50
-324 00	5418 75	2240 08	2668 38	384344 79	0 00	0 06708	0 12759	0 20481	7 31044	11 735	7 75
-334 13	5550 24	2374 46	2828 94	442731 89	0 00	0 07727	0 14691	0 23913	8 41724	13 701	8 00
-344 25	5678 40	2512 02	2993 93	510913 54	0 00	0 08917	0 16920	0 27864	9 68450	15 965	8 25
-354 38	5803 15	2652 67	3163 33	590449 15	0 00	0 10305	0 19496	0 32416	11 17059	18 573	8 50
-364 50	5924 42	2796 34	3337 08	682939 75	-205336 43	0 08336	0 21580	0 37551	12 36458	21 515	8 75
-374 63	6042 13	2942 94	3515 14	787948 30	-410672 86	0 06585	0 23226	0 43151	13 30775	24 724	9 00
-384 75	6156 22	3092 38	3697 46	902591 54	-616009 29	0 05002	0 24477	0 49114	14 02419	28 140	9 25
-394 88	6266 61	3244 56	3883 98	1023332 95	-821345 72	0 03525	0 25358	0 55344	14 52914	31 710	9 50
-405 00	6373 24	3399 41	4074 67	1146130 31	-1026682 16	0 02085	0 25879	0 61748	14 82776	35 379	9 75
-415 13	6476 04	3556 82	4269 45	1266658 65	-1540023 23	-0 04771	0 24687	0 68069	14 14436	39 001	10 00
-425 25	6574 96	3716 70	4468 28	1378221 01	-2053364 31	-0 11783	0 21741	0 73873	12 45654	42 326	10 25
-435 38	6669 93	3878 96	4671 11	1473333 76	-2053364 31	-0 10123	0 19210	0 78991	11 00649	45 259	10 50
-445 50	6760 90	4043 50	4877 88	1550631 86	-2053364 31	-0 08774	0 17016	0 83520	9 74969	47 853	10 75
-455 63	6847 81	4210 21	5088 55	1612964 77	-2053364 31	-0 07686	0 15095	0 87534	8 64871	50 153	11 00
-465 75	6930 61	4379 01	5303 06	1662871 87	-2053364 31	-0 06815	0 13391	0 91094	7 67250	52 193	11 25
-475 88	7009 24	4549 78	5521 39	1702545 79	-2053364 31	-0 06123	0 11860	0 94251	6 79547	54 002	11 50
-486 00	7083 68	4722 42	5743 46	1733851 42	-2053364 31	-0 05576	0 10466	0 97042	5 99670	55 601	11 75
-496 13	7153 86	4896 84	5969 25	1758366 53	-2053364 31	-0 05149	0 09179	0 99497	5 25923	57 008	12 00
-506 25	7219 74	5072 93	6198 71	1777426 85	-2053364 31	-0 04816	0 07975	1 01642	4 56940	58 236	12 25
-516 38	7281 30	5250 58	6431 78	1792167 73	-2053364 31	-0 04559	0 06835	1 03493	3 91642	59 297	12 50
-526 50	7338 48	5429 68	6668 43	1803559 32	-2053364 31	-0 04360	0 05745	1 05066	3 29192	60 198	12 75
-536 63	7391 26	5610 12	6908 60	1812434 45	-2053364 31	-0 04205	0 04694	1 06371	2 68961	60 946	13 00
-546 75	7439 60	5791 81	7152 25	1819510 02	-2053364 31	-0 04081	0 03674	1 07417	2 10498	61 545	13 25
-556 88	7483 48	5974 63	7399 33	1825402 47	-2053364 31	-0 03979	0 02679	1 08211	1 53509	62 000	13 50
-567 00	7522 86	6158 47	7649 79	1830638 96	-2053364 31	-0 03887	0 01707	1 08759	0 97829	62 314	13 75
-577 13	7557 73	6343 21	7903 59	1835664 86	-2053364 31	-0 03800	0 00758	1 09067	0 43405	62 491	14 00
-587 25	7588 06	6528 76	8160 66	1840849 02	-2053364 31	-0 03709	-0 00170	1 09141	-0 09723	62 533	14 25
-597 38	7613 84	6714 99	8420 95	1846487 43	-2053364 31	-0 03611	-0 01072	1 08985	-0 61441	62 444	14 50

AIRCRAFT INTEGRATION

Appendix H

H.1 FINITE ELEMENT MODEL - GRYPHON/ECLIPSE INTERFACE

The finite element models for the Gryphon/Eclipse inteface requirements were run on SDRC I-DEAS. Using the finite element code, a model was constructed consisting of approximately 40 elements. Seven pin configurations were run, but only the one used is presented here (See Figure H.1). As seen in the picture, the Gryphon was modeled as a beam. This beam's properties were determined by conventional methods. For instance, the area moment of inertia and modulus of elasticity were found, at first, by assumptions then refined as a better model was constructed. Note, in the Figure H.1 there is a ninth attachpoint. This attachpoint was disconnected and was not part of the final model run. This ninth point was analyzed for dynamic stability purposes and was found not to be needed. The solution to the final run is presented next (See Table H.1). As seen in the table, the forces on the thirty-two nodes of the model are given. Note, the y-forces on nodes 18 thru 21 and 29 thru 32 are the attachment forces. The loading per pin came out to 402 kips in the "worst case" factor of four load. This determined the pin and hook sizes by conventional shearing calculations. Note also in the table that there are small 'x' and 'z' forces present. These forces are errors in the source program and are not relevant because they are essentially zero. Finally, the deformed geometry of the model was looked into (see Figure H.2). The only importance the deformed geometry plot gave was the fact that the load was actually present at the center of gravity. The maximum deflection of 0.78 inches is not relevenant due to the assumption of the point load opposed to a more realistic displaced load.

Table H.1 Loading Results of 8 Point Attachment Run

SDRC I-DEAS VI: FE_Modeling_&_Analysis 04-APR-93 17:18:45
final_attachpoint_run

Group ID : No stored PERMANENT GROUP
Analysis Dataset : 2 - CASE 2,LOAD 1,REACTION FORCES
Report Type : Arrow Plot Units : IN
Dataset Type : Reaction Forces Load Set : 1
Frame of Reference: Global Data Component: Magnitude

Node	Force-X	Force-Y	Force-Z
13	0.000E+00	0.000E+00	0.000E+00
14	0.000E+00	0.000E+00	0.000E+00
15	0.000E+00	0.000E+00	0.000E+00
16	0.000E+00	0.000E+00	0.000E+00
17	0.000E+00	0.000E+00	0.000E+00
18	-2.962E-13	4.020E+05	2.105E-14
19	-2.187E-12	4.020E+05	2.105E-14
20	-2.962E-13	4.020E+05	-2.546E-12
21	7.745E-12	4.020E+05	1.032E-11
22	0.000E+00	0.000E+00	0.000E+00
25	0.000E+00	0.000E+00	0.000E+00
26	0.000E+00	0.000E+00	0.000E+00
27	0.000E+00	0.000E+00	0.000E+00
28	0.000E+00	0.000E+00	0.000E+00
29	-2.962E-13	4.020E+05	-6.716E-13
30	-2.187E-12	4.020E+05	-6.716E-13
31	-2.962E-13	4.020E+05	-3.238E-12
32	-2.187E-12	4.020E+05	-3.238E-12
Total	4.337E-19	3.216E+06	4.337E-19
	21	18	21
Maximum	7.745E-12	4.020E+05	1.032E-11
	19	13	31
Minimum	-2.187E-12	0.000E+00	-3.238E-12
Average	2.409E-20	1.786E+05	2.409E-20

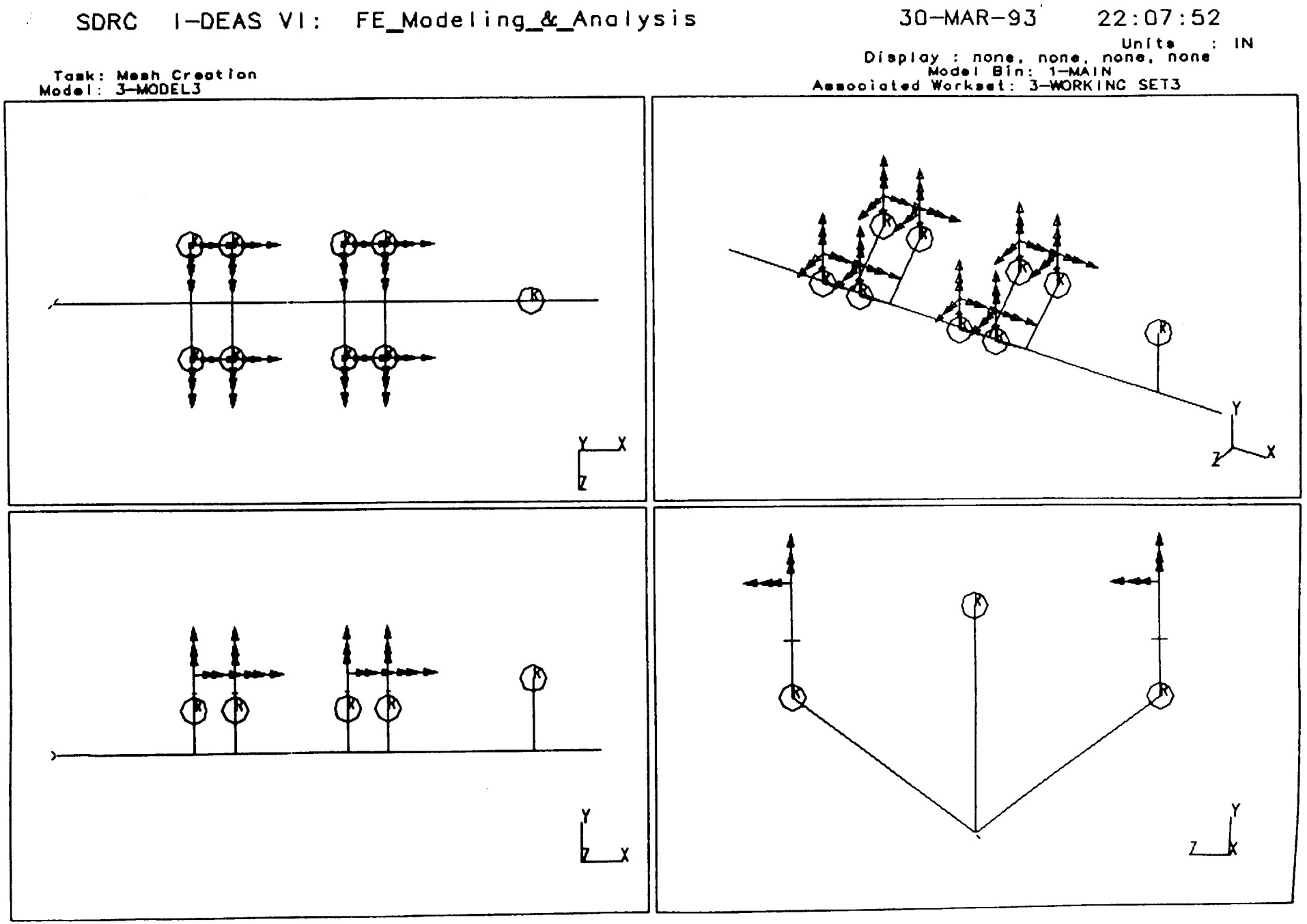

Figure H.1 Finite Element Model of Gryphon/Eclipse Attachment

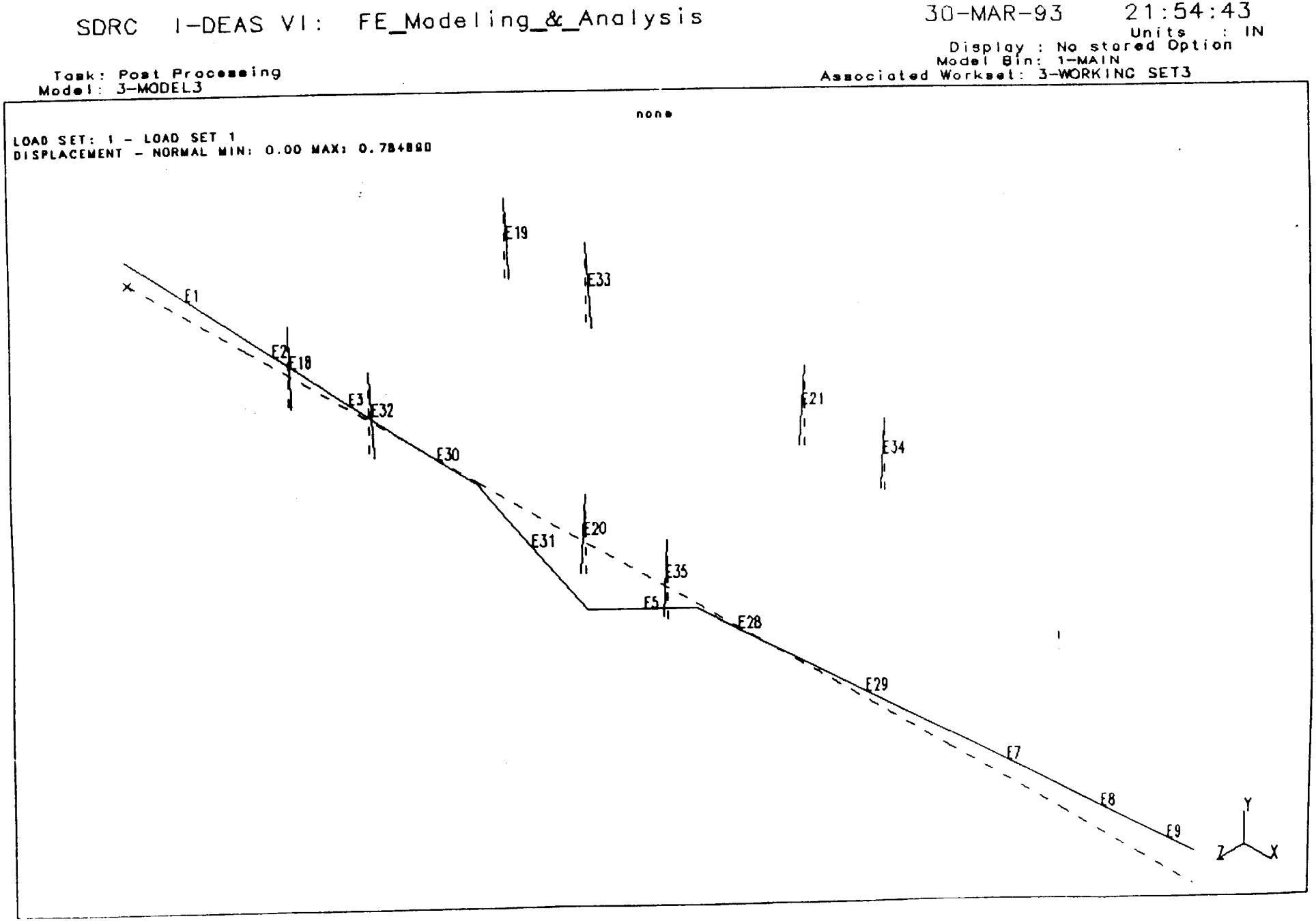

Figure H.2 Deformed Geometry Plot Showing Attachment Displacement